



National Library
of Canada

Bibliothèque nationale
du Canada

Canadian Theses Service

Service des thèses canadiennes

Ottawa, Canada
K1A 0N4

NOTICE

The quality of this microform is heavily dependent upon the quality of the original thesis submitted for microfilming. Every effort has been made to ensure the highest quality of reproduction possible.

If pages are missing, contact the university which granted the degree.

Some pages may have indistinct print especially if the original pages were typed with a poor typewriter ribbon or if the university sent us an inferior photocopy.

Previously copyrighted materials (journal articles, published tests, etc.) are not filmed.

Reproduction in full or in part of this microform is governed by the Canadian Copyright Act, R.S.C. 1970, c. C-30.

AVIS

La qualité de cette microforme dépend grandement de la qualité de la thèse soumise au microfilmage. Nous avons tout fait pour assurer une qualité supérieure de reproduction.

S'il manque des pages, veuillez communiquer avec l'université qui a conféré le grade.

La qualité d'impression de certaines pages peut laisser à désirer, surtout si les pages originales ont été dactylographiées à l'aide d'un ruban usé ou si l'université nous a fait parvenir une photocopie de qualité inférieure.

Les documents qui font déjà l'objet d'un droit d'auteur (articles de revue, tests publiés, etc.) ne sont pas microfilmés.

La reproduction, même partielle, de cette microforme est soumise à la loi canadienne sur le droit d'auteur, S.R.C. 1970, c. C-30.

THE UNIVERSITY OF ALBERTA

APPLICATION OF FULLY GROUTED BOLTS IN YIELDING ROCK

by

BUDDHIMA INDRARATNA

A THESIS

SUBMITTED TO THE FACULTY OF GRADUATE STUDIES AND RESEARCH
IN PARTIAL FULFILMENT OF THE REQUIREMENTS FOR THE DEGREE
OF DOCTOR OF PHILOSOPHY

DEPARTMENT OF CIVIL ENGINEERING

EDMONTON, ALBERTA

FALL 1987

Permission has been granted to the National Library of Canada to microfilm this thesis and to lend or sell copies of the film.

The author (copyright owner) has reserved other publication rights, and neither the thesis nor extensive extracts from it may be printed or otherwise reproduced without his/her written permission.

L'autorisation a été accordée à la Bibliothèque nationale du Canada de microfilmer cette thèse et de prêter ou de vendre des exemplaires du film.

L'auteur (titulaire du droit d'auteur) se réserve les autres droits de publication; ni la thèse ni de longs extraits de celle-ci ne doivent être imprimés ou autrement reproduits sans son autorisation écrite.

ISBN 0-315-41110-4

THE UNIVERSITY OF ALBERTA

RELEASE FORM

NAME OF AUTHOR BUDDHIMA INDRARATNA
TITLE OF THESIS APPLICATION OF FULLY GROUTED BOLTS
IN YIELDING ROCK
DEGREE FOR WHICH THESIS WAS PRESENTED DOCTOR OF PHILOSOPHY
YEAR THIS DEGREE GRANTED FALL 1987

Permission is hereby granted to THE UNIVERSITY OF ALBERTA LIBRARY to reproduce single copies of this thesis and to lend or sell such copies for private, scholarly or scientific research purposes only.

The author reserves other publication rights, and neither the thesis nor extensive extracts from it may be printed or otherwise reproduced without the author's written permission.

(SIGNED) *B. Indraratna*

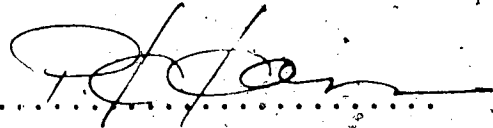
PERMANENT ADDRESS:

355 Park Road
(Colombo 5
SRI LANKA)

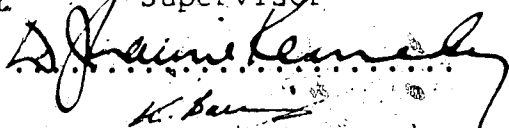
DATED *September 21* 1987

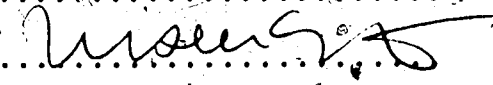
THE UNIVERSITY OF ALBERTA
FACULTY OF GRADUATE STUDIES AND RESEARCH

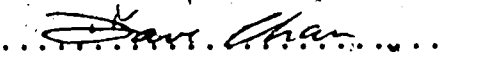
The undersigned certify that they have read, and recommend to the Faculty of Graduate Studies and Research, for acceptance, a thesis entitled APPLICATION OF FULLY GROUTED BOLTS IN YIELDING ROCK submitted by BUDDHIMA INDRARATNA in partial fulfilment of the requirements for the degree of DOCTOR OF PHILOSOPHY.

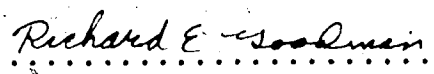


Supervisor









External Examiner

Date..... JULY 27, 1987

ABSTRACT

Presently, displacement monitoring plays an important role in the observational design approach for underground openings such as tunnels. In particular, tunnel convergence measurements are considered as the primary component of the design-as-you-go approach. Tunnel convergence is not only easily obtainable and hence, universally measured, but its magnitude constitutes a most useful parameter for the evaluation of tunnel stability. Consequently, the control of wall convergence by alternative support systems can be considered as a key component for the design of underground excavations.

The application of fully grouted bolts as a passive support system in underground openings is analyzed in this thesis. At present, design decisions related to fully grouted bolts are often empirical, based on experience, or are justified after an interpretation of convergence data. An analytical method based on the concepts of elasto-plasticity, has been developed to predict the displacement and strain field of the reinforced rock mass surrounding a circular tunnel opening. The method considers the influence of grouted bolts on the extent of yielding. Results from laboratory simulations and field measurements provide convincing evidence to support the theoretical predictions. In addition, it has been attempted to describe potential failure mechanisms associated with both unsupported and reinforced tunnels. The influence of

discontinuities on the tunnel behaviour has also been investigated by physical modelling. In the analytical model, reduced strength parameters describing the equivalent rock mass properties were chosen for comparison with the measurements. The practical application of the proposed displacement controlled design approach is discussed in detail and is illustrated by an analysis of one case history.

ACKNOWLEDGEMENTS

This research project was conducted under the supervision of Dr. Peter K. Kaiser, at the University of Alberta. His guidance, encouragement, and enthusiastic support throughout this research program are gratefully appreciated. I wish to extend my sincere thanks to Dr. D. Chan and Dr. D.J.L. Kennedy for their critical comments and advice with respect to some complex areas of this study. I am particularly grateful to Dr. N.R. Morgenstern for the encouragement and inspiration he provides for all of us engaged in graduate research in geotechnical engineering.

I would like to express my sincere gratitude to Christine Hereygers, a most dedicated and enthusiastic technician and to Sean Maloney, research engineer, for their assistance during the very intensive laboratory test program. My thanks are also due to Gerry Cyre, Steve Gamble, Jay Khajuria, Scotty Rogers, Heinz Friedrich and Ken Ellis of the Civil Engineering technical staff, for their efforts in many different ways which enabled this research study to be successful.

I am grateful to all my fellow graduate students especially in Room 103, for their friendship and understanding during the last four years. My special thanks are extended to Patrick Collins, Tai Wong and Fabrizio Pelli.

The financial support provided by the Department of Civil Engineering, University of Alberta and the National

Science and Engineering Research Council of Canada during the period of this research project is gratefully acknowledged.

Finally, I wish to express my sincere gratitude to my dear wife Manori and my parents for their continuing love and support. I would not have achieved this goal without their patience, understanding and encouragement. To them, I dedicate this thesis.

Table of Contents

Chapter	Page
1. INTRODUCTION	1
1.1 General Description	1
1.2 Time-independent Convergence Modelling	5
1.3 Organization of the Thesis	6
2. REVIEW OF ROCK BOLTING PRACTICES	8
2.1 Untensioned UngROUTED Reinforcements (Friction Dowels)	8
2.2 Untensioned Grouted Reinforcement (Grouted Bolts)	8
2.3 Tensioned Grouted Bolts	12
2.4 Tensioned Mechanical Bolts	12
2.5 Rock Anchors	12
2.6 Use of Weldmesh and Shotcrete in Rock Bolting Practice	13
2.7 Failure Modes of Rock Reinforcement Systems	13
2.7.1 Fall Out of Bolted Segments	13
2.7.2 Failure of Anchorage	15
2.7.3 Shear Deformation of Bolts	16
2.7.4 Improper Tensioning of Bolts	18
2.8 Localized Failure of the Bolt-Grout Composite ..	18
2.9 Comparison of Grouted and Mechanical Bolts	19
2.10 Selection of Rock Bolts for Various Rock Types ..	21
2.11 Summary of Interactive Factors Influencing the Design of Reinforcement Systems	23
2.12 Improvement of Rock Mass Shear Resistance by Joint Reinforcement	25
2.13 Reinforcement of a Single Plane of Weakness	29
2.14 Theories of Rock Reinforcement by Bolting	33

2.14.1	Suspension and Frictional Stabilization of Individual Blocks	33
2.15	Keyblock Bolting to Prevent Ravelling	35
2.16	Beam Building Theory	36
2.17	Arch Building Theory	39
2.18	Summary	41
3.	<i>THEORETICAL ANALYSIS OF FULLY GROUTED BOLTS IN UNDERGROUND EXCAVATIONS</i>	42
3.1	Application of Elasto-Plasticity in Tunnel Openings	42
3.1.1	Application to Physical Models	48
3.2	Assumptions and Analytical Considerations	50
3.2.1	Stress Distribution Along Fully Grouted Bolts	51
3.3	Influence of Bolting on Strength Parameters	55
3.4	Concept of Equivalent Strength Parameters	58
3.4.1	Determination of the Bolt Density Parameter	61
3.5	Influence of Bolt Length on Tunnel Wall Stability	63
3.6	Concept of Equivalent Plastic Zone	63
3.6.1	Determination of the Equivalent Plastic Zone Radius	64
3.6.1.1	<u>Zone 1</u> : $a < r < R$	66
3.6.1.2	<u>Zone 2</u> : $R < r < \rho$	66
3.6.1.3	<u>Zone 3</u> : $\rho < r < (a+L)$	67
3.6.1.4	<u>Zone 4</u> : $r > (a+L)$	67
3.7	Influence of Bolts on Tunnel Stability	74
3.7.1	Use of Displacement Control Approach for Design	75
3.7.2	Influence of Opening Size and Bolt Length on Tunnel Convergence	81

3.8	Normalized Convergence Ratio	81
3.9	Concept of Bolt Effectiveness	82
4.	FAILURE MECHANISMS NEAR TUNNELS	84
4.1	Failure Mechanisms of Intact Rock	84
4.1.1	Application of the Bifurcation Theory ...	86
4.2	Influence of Wall Curvature on Rupture Propagation	88
4.3	Influence of Bolting on Failure Mechanisms	89
4.4	Influence of Existing Joints on the Rupture Process	91
5.	LABORATORY SIMULATION	96
5.1	Fundamental Considerations in Physical Modelling	96
5.2	Dimensionless Analysis and Similitude Parameters	97
5.2.1	Geometric Similitude for a Reinforced Opening	97
5.2.2	Fundamental Material Similitude Parameters	97
5.2.3	Similitude Parameters for Discontinuities	98
5.3	Development of an Artificial Soft Rock	100
5.3.1	Selection of Model Materials	100
5.3.2	Mix Composition of a Synthetic Soft Rock	101
5.3.3	Technique of Manufacturing Gypstone	103
5.4	Engineering Properties of Gypstone	105
5.4.1	Uniaxial Compression Tests	105
5.4.2	Triaxial Compression Tests	106
5.4.3	Split Cylinder Tests	113
5.4.4	Poisson's Ratio Determination	113

5.4.5	Summary of the Properties of Gypstone ..	116
5.5	Selection of Model Rock Bolts	118
5.6	Influence of Bolts on the Behaviour of Intact Gypstone in Uniaxial Compression	119
5.6.1	Synthetic Smooth Joints and their Properties	122
5.7	Influence of Bolts on the Behaviour of Jointed Gypstone in Uniaxial Compression	123
5.8	Experimental Procedure: Bolted Tunnel Wall	127
5.8.1	Sample Preparation and Arrangement in Test Frame	127
5.8.2	Instrumentation and Monitoring	129
5.8.2.1	Plane Strain Condition	129
5.8.2.2	Applied Loads	130
5.8.2.3	Tunnel Convergence	130
5.8.2.4	Radial Strains near the Opening	131
5.8.2.5	Internal Radial Strains by Extensometers	133
5.8.2.6	Data Processing System and Presentation	133
5.8.3	Test Apparatus and Load Application	135
5.9	Simulation of Jointed Rock Masses	137
5.9.1	Frictional Properties	137
6.	<i>EXPERIMENTAL DATA AND INTERPRETATION</i>	141
6.1	Plane Strain Behaviour of Intact Samples	141
6.2	Behaviour of Reinforced Intact Samples	143
6.2.1	Bolt Patterns	143
6.2.2	Strain-Displacement Response of Reinforced Samples	145
6.2.3	Normalized Convergence Ratio as a Design Aid	152

6.2.4	Influence of Bolt Length on Tunnel Convergence	154
6.2.5	Strain Distribution	158
6.3	Influence of Bolts on the Behaviour of Reinforced Tunnels in Jointed Material	160
6.3.1	Simulation of a Tunnel Opening in a Jointed Medium	160
6.4	Observed Rupture Processes Around Tunnel Openings	167
6.4.1	Tunnel Openings in Intact Rock	167
6.5	Observed Rupture processes of Jointed Samples	168
7.	<i>ANALYSIS OF A CASE HISTORY AND COMPARISON WITH EMPIRICAL DESIGN METHODS</i>	174
7.1	Analysis of Enasan Tunnel	174
7.1.1	Geometry and Pattern of Bolts	175
7.1.2	Prediction of Tunnel Convergence	175
7.1.3	Application of Bolt Effectiveness	178
7.2	Comparison with Empirical Design Methods	179
7.3	Observations from the Kielder Experimental Tunnel	181
8.	<i>CONCLUDING REMARKS, IMPLICATIONS AND RECOMMENDATIONS</i>	186
8.1	Implications of the Equivalent Plastic Zone Theory	186
8.2	Implications of the advancing tunnel face	189
8.3	Implications of Geomechanical Modelling	192
8.3.1	Summary of Practical Guidance for Efficient Bolting	194
	<i>REFERENCES</i>	197
	APPENDIX A <i>GENERAL ELASTIC, BRITTLE-PLASTIC MODEL</i>	205
	APPENDIX B <i>DETERMINATION OF THE EXTENT OF YIELDING</i>	211

APPENDIX C	
REINFORCEMENT OF A SINGLE PLANE OF WEAKNESS	219
APPENDIX D	
EFFECTIVE STIFFNESS OF A REINFORCED COMPOSITE	222
APPENDIX E	
FEATURES OF THE LABORATORY TEST EQUIPMENT	226
APPENDIX F	
MATERIAL CHARACTERISTICS OF GYPSTONE	238
APPENDIX G	
BEHAVIOUR OF REINFORCED OPENINGS (LONG BOLTS) IN AN INTACT MEDIUM	254
APPENDIX H	
BEHAVIOUR OF REINFORCED OPENINGS (SHORT BOLTS) IN AN INTACT MEDIUM	262
APPENDIX I	
BEHAVIOUR OF REINFORCED OPENINGS (LONG BOLTS) IN A JOINTED MEDIUM	271

List of Tables

Table		Page
2.1	The Role of Bolting in Various Types of Rock	22
3.1	Summary of β/λ Ratios Determined from Several Case Histories	62
3.2	Influence of Bolt Density on Tunnel Wall Convergence, ($a/L=1.3$)	78
5.1	Properties of Gypstone Synthetic Soft Rock	117
7.1	Recommended Bolt Densities according to Geomechanics Classification (RMR)	183
7.2	Recommended Bolt Densities for Kielder Experimental Tunnel based on Geomechanics Classification	183
F.1	Physical Properties of Hydrocal Gypsum Cements (Data from U.S. Gypsum Company)	240

List of Figures

Figure	Page
2.1 Classification of Rock Reinforcement Systems	9
2.2 A Complete Operational Scheme for Rock Bolting	14
2.3 Shear Deformation of a Fully Grouted Bolt	17
2.4 Shear Strength of Reinforced Joints (modified after Bjurström, 1974)	27
2.5 Influence of Mobilized Friction Angle on Bolt Installation (modified after Barton and Bakhtar, 1984)	30
2.6 Reinforcement of a linear discontinuity	31
2.7 Stabilization of Unstable Individual Blocks	34
2.8 Prevention of Buckling and Sagging by Beam Building	38
2.9 Formation of a Compressive Rock Arch (modified after Lang, 1972)	40
3.1 Elastic, Brittle-Plastic Strength Model	44
3.2 Failure Criterion and the Flow Rule	44
3.3 Comparison of Model Tunnel with Reality	49
3.4 Stress Distribution Model for Grouted Bolts	52
3.5 Fully Reinforced Circular Excavation	53
3.6 Analysis of Bolt-Ground Interaction	56
3.7 Variation of the Equivalent Compressive Strength with β	59
3.8 Variation of the Equivalent Friction Angle with β	60
3.9 Categorization of the Extent of Yielding	65
3.10 Stress Field near the Tunnel Opening	71
3.11 Strain Field near the Tunnel Opening	72

Figure	Page
3.12 Displacement Field near the Tunnel Opening	73
3.13 Influence of Grouted Bolts on Tunnel Convergence	76
3.14 Effect of Grouted Bolts on the Failure Envelope	79
3.15 Effect of Grouted Bolts on the Ground Reaction Curve	79
4.1 Equilateral Spiral Slip Lines in the Plastic Zone	85
4.2 Unconfined Compression State at Tunnel Wall	87
4.3 Stability Curve for Potential Failure Mechanisms	87
4.4 Influence of Curvature on Rupture Propagation	90
4.5 Influence of Existing Joints on Rupture Surfaces (modified after Guenot, 1979)	93
4.6 Types of Rupture Initiation at a Tunnel Opening	94
5.1 The Stress-Strain Behaviour of Gypstone in Uniaxial Compression	107
5.2 Stress-Strain Behaviour of Gypstone in Triaxial Compression	108
5.3 Failure Envelope of Gypstone Simulated Rock	110
5.4 Comparison of Gypstone with Sedimentary Rocks in Triaxial Compression	111
5.5 Hoek and Brown Failure Representation of Gypstone and Various Rocks	112
5.6 Failure Strains of Gypstone and Sedimentary Rocks in Triaxial Compression	114
5.7 Variability of the Poisson's Ratio of Gypstone	115
5.8 Variation of Apparent Strength with Bolt Spacing for Intact Samples	120

Figure	Page
5.9	Variation of Apparent Strength with Bolt Spacing for Jointed Samples126
5.10	A Typical Reinforced Gypstone Test Sample128
5.11	Typical Extensometer Assembly (modified after Maloney, 1984)134
5.12	Transfer of Load to the Test Specimens136
5.13	Selected Joint Pattern for Physical Modelling138
5.14	Failure Envelope for Jointed Gypstone Medium140
6.1	Behaviour of Unsupported Opening in PST Apparatus142
6.2	Alternative Bolt Patterns in Test Samples144
6.3	Convergence of Reinforced Opening for $\beta=0.145$146
6.4	Radial Strain at Tunnel Wall for $\beta=0.145$ and $L=100$ mm148
6.5	Radial Strain in Elastic Zone for $\beta=0.220$ and $L=100$ mm149
6.6	Displacement at Field Boundary for $\beta=0.145$ and $L=100$ mm151
6.7	Variation of Convergence with Bolt Density for $L=100$ mm153
6.8	Variation of Convergence with Bolt Density for $L=50$ mm155
6.9	Radial Strain Response in the Elastic Zone for $\beta=0.145$ and $L=50$ mm159
6.10	Geomechanical Model of an Opening in a Jointed Medium161
6.11	Convergence Response of a Typical Jointed Sample163
6.12	Variation of Convergence with Bolt Density for Jointed Samples166
7.1	Effect of Bolts at the Enasan Tunnel Project176

Figure	Page
B.1 Influence of Tunnel Face and Excavation Sequence on Wall Convergence	190
D.1 Horizontal Bedding Planes Reinforced by Bolting	225
E.1 Details of the Mould - Part i	228
E.2 Details of the Mould - Part ii	229
E.3 Details of the Mould - Part iii	230
E.4 Details of the Test Frame - Part i	232
E.5 Details of the Test Frame - Part ii	233
E.6 Details of the Test Frame - Part iii	234
E.7 Details of the Test Frame - Part iv	235
E.8 A Schematic Diagram of the PST Apparatus	237
F.1 Grading Curve of Fine Ottawa Sand	241
F.2 Influence of Na_2HPO_4 on Setting Time of Gypstone	243
F.3 Drying Curve of Gypstone Synthetic Rock	244
F.4 Stress-Strain Behaviour of Intact Blocks	246
F.5 Shear Behaviour of Synthetic Joints	248
F.6 Failure Envelope of Synthetic Joints	249
F.7 Stress-Strain Behaviour of Jointed Blocks	251
F.8 Stress-Strain Behaviour of Jointed Blocks loaded in the PST apparatus	253
G.1 Behaviour of Reinforced Opening for $\beta=0.073$, $L=100$	255
G.2 Radial Strains near Tunnel Wall for $\beta=0.073$, $L=100$	256
G.3 Radial Strain in Elastic Zone for $\beta=0.073$, $L=100$	257
G.4 Convergence of Reinforced Opening for $\beta=0.220$, $L=100$	258

Figure	Page
G.5 Field Boundary Displacement for $\beta=0.220$, L=100	259
G.6 Radial Strain at Tunnel Wall for $\beta=0.220$, L=100	260
G.7 Behaviour of Reinforced Opening for $\beta=0.291$, L=100	261
H.1 Convergence of Reinforced Opening for $\beta=0.145$, L=50	263
H.2 Field Boundary Displacement for $\beta=0.145$, L=50	264
H.3 Radial Strain at Tunnel Wall for $\beta=0.145$, L=50	265
H.4 Radial Strain in Elastic Zone for $\beta=0.145$, L=50	266
H.5 Convergence of Reinforced Opening for $\beta=0.291$, L=50	267
H.6 Field Boundary Displacement for $\beta=0.291$, L=50	268
H.7 Radial Strain at Tunnel Wall for $\beta=0.291$, L=50	269
H.8 Radial Strain in Elastic Zone for $\beta=0.291$, L=50	270
I.1 Field Boundary Displacement (Jointed) for $\beta=0$	272
I.2 Radial Strain at Tunnel Wall (Jointed) for $\beta=0$	273
I.3 Radial Strain in Elastic Zone (Jointed) for $\beta=0$	274
I.4 Convergence of Opening in Jointed Medium for $\beta=0.073$, L=100	275
I.5 Field Boundary Displacement (Jointed) for $\beta=0.073$, L=100	276
I.6 Radial Strain at Tunnel Wall (Jointed) for $\beta=0.073$, L=100	277
I.7 Radial Strain in Elastic Zone (Jointed) for $\beta=0.073$, L=100	278

Figure	Page
I.8 Convergence of Opening in Jointed Medium for $\beta=0.145$, $L=100$	279
I.9 Field Boundary Displacement (Jointed) for $\beta=0.145$, $L=100$	280
I.10 Radial Strain at Tunnel Wall (Jointed) for $\beta=0.145$, $L=100$	281
I.11 Radial Strain in Elastic Zone (Jointed) for $\beta=0.145$, $L=100$	282
I.12 Convergence of Opening in Jointed Medium for $\beta=0.220$, $L=100$	283
I.13 Field Boundary Displacement (Jointed) for $\beta=0.220$, $L=100$	284
I.14 Radial Strain at Tunnel Wall (Jointed) for $\beta=0.220$, $L=100$	285
I.15 Radial Strain in Elastic Zone (Jointed) for $\beta=0.220$, $L=100$	286

List of Plates

Plate	Page
5.1 Typical Intact Sample Before and After its Failure	121
5.2 Typical Jointed Sample Before and After its Failure	124
5.3 Measurement of Radial Strains and Displacements near the Tunnel	132
6.1 Failure Around Openings with Minimum Reinforcement	169
6.2 Failure Around Intensely Reinforced Openings	170
6.3 Influence of the Critical Joint Plane on Rupture	172

LIST OF SYMBOLS

a = tunnel radius

r = distance from tunnel center to point of interest

t = thickness of a given structural body

k_0 = ratio of horizontal to vertical stress in situ

σ_0 = field stress for $k_0=1$ (hydrostatic loading)

σ_r = radial stress field

σ_θ = tangential stress field

σ_c = uniaxial compressive strength

$\sigma_{cr} = s \cdot \sigma_c$ = equivalent post peak compressive strength

s = post-peak strength reduction factor

σ_t = tensile strength from split cylinder test

σ_b = tensile strength of a bolt

σ_1 = major principal stress

σ_3 = minor principal stress

σ_n = normal stress across a joint plane

τ_2 = shear stress distribution

τ_f = shear strength of intact material

τ_j = shear strength of joint

τ_{bf} = shear strength of bolt

ϵ_r = radial strain field

ϵ_θ = tangential strain field

ϵ_f = failure strain in uniaxial compression

$\epsilon_c = \sigma_c/E$ = critical strain

ϕ = friction angle of Mohr-Coulomb material

ϕ_j = friction angle of joint

ϕ_g = friction angle of grout

m = internal friction parameter
 c = cohesion intercept of Mohr-Coulomb material
 c_j = Cohesion intercept of joint
 a = dilation coefficient
 E = Young's modulus
 G = shear modulus
 ν = Poisson's ratio
 A_j = area of joint per unit width
 A_b = cross section area of bolt
 L = length of bolts
 d = diameter of bolts
 S_T = circumferential (tangential) bolt spacing
 S_L = longitudinal bolt spacing
 T = tension developed on bolt
 z_n = distance from tunnel wall to the neutral point
 $\rho = a + z_n$ = radial distance to the neutral point
 λ = friction factor for bolt-ground interaction
 β = bolt density parameter
 R = radius of the yielded (plastic) zone
 R^* = radius of the equivalent plastic zone
 u_r = radial displacement field
 u_a = convergence of the unsupported opening
 u_e = elastic response of the total convergence
 u_p = plastic response of the total convergence
 u_a^* = convergence of the reinforced opening
 u_a^*/u_a = normalized convergence ratio
 i = bolt effectiveness

1. INTRODUCTION

1.1 General Description

Rock bolts can be classified as being either active or passive. Active support means that a pre-specified load is applied to the rock surface during installation. Tensioned bolts fall into this category. Active bolts are most advantageous for stabilizing loosened, individual blocks in non-yielding ground (support of gravity loads). Furthermore, active bolts are required in situations where they are installed late and cannot be activated by ground displacements.

Passive, untensioned, grouted bolts or friction bolts develop load as the rock mass deforms. Relatively small displacements (4 to 5 mm) are normally sufficient to mobilize axial bolt tension by shear stress transmission from the rock to the bolt surface. These bolts or dowels need not be pre-loaded and fall into the category of passive support. They have been successfully applied in yielding ground, and found to be often more economical and more effective than active bolts. For example, at the Washington D.C. Metro, fully grouted bolts have shown to reduce two-day displacements from 7.6-15.2 mm to 2.5-5.0 mm (Van Sint Jan, 1982). Grouted bolts are also widely used in mining for the stabilization of drifts and shafts. Simplicity of installation, versatility and lower cost of rebars are further benefits of grouted bolts in comparison to their

alternative countermeasures

The main objective of any support system should be to assist the rock mass in supporting itself by building a ground arch and by mobilizing the optimum shear strength of the rock. Grouted bolts become an integral part of the rock mass, thereby restricting the rock mass displacements by internal strengthening. The New Austrian Tunneling Method (NATM) adopts these concepts to combine grouted bolts with steel sets, shotcrete and weldmesh to provide a most efficient and economical support system that can be installed soon after excavation.

Tunnel convergence measurements are frequently recorded as the primary component of the observational design approach, because, wall convergence is a readily recordable indicator of the overall response of the ground. It is often not dominated by localized processes. Alternative displacement measurements by extensometers or load measurements by load or pressure cells are certainly informative, but often give results that are difficult to interpret due to their sensitivity to installation procedures and localized rock mass failure processes. Therefore, the effectiveness of grouted bolts can best be assessed in terms of convergence reductions.

The analytical solution presented in this thesis constitutes an extension of the application of elasto-plasticity to the design of underground excavations. It considers the influence of bolt/ground interaction,

opening geometry and the pattern of bolts on yielding and the tunnel convergence. A bolt density parameter, β , has been introduced as a dimensionless quantity to describe the dependence of the mobilized shear stress along the bolt surface, the bolt diameter, the tunnel radius, and the longitudinal and tangential (circumferential) bolt spacing. The influence of β on tunnel convergence is considered to be of prime importance for the design of grouted bolts. The shear stress distribution along the fully grouted bolts was chosen (semi-empirical) to satisfy equilibrium of the bolt relative to the surrounding ground. The mobilized shear stress along the bolt surface and, hence, the axial stress has been regarded as a function of the bolt/grout interaction.

In order to verify the analytical predictions, laboratory experiments have been performed with an artificial rock consisting of gypsum cement, fine sand and water. Similitude criteria relevant for physical modelling were carefully considered for the laboratory program and test specimens were subjected to plane strain condition and external loading using the Process Simulation Test apparatus developed by Kaiser and Morgenstern (1981). The behaviour of intact and jointed samples has been studied, and the measured displacements and strains have been compared with predictions. The observed data convincingly support these theoretical predictions.

A critical evaluation of the observed failure mechanisms constitutes another important aspect of this study. Observations confirm that isotropic, time-independent, elasto-plastic analysis for hydrostatic stress condition ($K_0=1$), can explain the equiangular spiral slip lines observed as the dominant failure mechanism around the circular opening. The presence of joints in the vicinity of the opening influences the rupture process by intersecting and shortening the plastic slip lines. However, a rock mass with four or more joints with the same properties seems to behave similar to an isotropic, homogeneous rock mass with reduced strength and deformation characteristics.

To date, the design of fully grouted bolts in underground excavations is largely based on either semi-empirical or simple force-equilibrium methods (Lang, 1972; U.S. Army, 1980). However, they cannot properly assess the influence of bolting on rock mass displacements. The analysis presented here provides an alternative design method for fully grouted bolts, based on a displacement control approach. The application of the proposed method in practice has been emphasized with particular reference to field conditions and rock mass classification. Its use as a practical design tool is demonstrated on data from the Enasan Tunnel in Japan (Ito, 1983).

1.2 Time-independent Convergence Modelling

Time-dependent deformations are due to both the face advance effect and the creep properties of the rock mass. The initial displacement response depends primarily on the rate of face advance (distance to the face from the point of interest) and the time-independent rock mass parameters. However, the ultimate convergence (unaffected by three-dimensional face effects) may be significantly influenced by the creep properties of the rock. The magnitude of time-dependent convergence is further influenced by the field stress level. At relatively low stress levels, displacements associated with creep are often negligible, and hence, the ultimate convergence response can be accurately predicted by time-independent elasto-plastic models.

Barlow (1986) has pointed out that the installation of supports has a dramatic effect in curtailing this time-dependent deformation. In this study, the NATM concept of excavation followed by immediate stabilization is emphasized. Delayed installation of grouted bolts can often be unsuccessful because the displacements created during propagation of the yielded zone are often insufficient for bolt activation. The Anasan Tunnel case history (Ito, 1983) which elucidates this situation is discussed later.

The proposed analytical solution is capable of predicting the ultimate tunnel convergence (at least two tunnel diameters behind the face), where three-dimensional

face effects are ignored. It is assumed that the excavated tunnel face is immediately supported by fully grouted bolts, such that the time-dependent behaviour and loosening can be neglected. However, materials such as coal, claystone, rock salt and other evaporites may exhibit considerable creep deformation even after immediate support is provided at the face. The analytical model developed in this thesis is not applicable to such rocks. The influence of grouted bolts on the time-dependent deformation of rock remains to be investigated.

1.3 Organization of the Thesis

The scope of this thesis is to examine, both analytically and experimentally, the influence of fully grouted bolts on the behaviour of underground openings in yielding rock.

A review of alternative bolt systems is presented in Chapter 2, in order to highlight the main differences between fully grouted bolts and conventional mechanical bolts. It contains a brief examination of different stabilization mechanisms and failure modes of active and passive bolts. In an attempt to investigate the influence of bolts on the shear strength of a discontinuity, the 'single plane of weakness' theory (Jaeger, 1960) has been extended.

Chapter 3 presents the development of the analytical model. It introduces the concept of an 'equivalent plastic zone' associated with openings reinforced by fully grouted

bolts. The main assumptions and relevant details of the elasto-plastic analysis are given. Chapter 4 contains an examination of the potential failure modes around a tunnel opening and a discussion of the influence of grouted bolts on their stabilizing effect.

Detailed descriptions of the laboratory simulation test procedure, the development of an artificial rock and the relevant similitude considerations are given in Chapter 5. The Process Simulation Test apparatus (Kaiser, 1979) has been used in the laboratory tests in conjunction with a specially designed test frame as shown in Appendix E.

Chapter 6 presents an interpretation of the laboratory test data. The value of the analytical approach as a reliable design tool is illustrated in Chapter 7, where an analysis of a case history is presented and other practical implications are discussed.

Finally, the most important aspects of this thesis are summarized with conclusions and recommendations in Chapter 8.

2. REVIEW OF ROCK BOLTING PRACTICES

The objective of this chapter is to review the general aspects of both active and passive bolts, in order to facilitate the understanding of the behaviour of fully grouted bolts in comparison with the alternative reinforcement systems. The chart illustrated in Figure 2.1 summarizes the types of bolts commonly used in practice. Most of these reinforcements and their installation methods are diagrammatically illustrated by Hoek and Brown (1980) and Littlejohn and Bruce (1975).

2.1 Untensioned UngROUTED Reinforcements (Friction Dowels)

Wooden friction dowels, full contact mechanical anchors, split set friction anchors and swellex expandable bolts fall into this category. These reinforcements are activated as a result of friction between the bolt surface and the surrounding ground. Consequently, the efficiency of these friction dowels depends largely on the roughness of the bolt surface as well as the degree of contact (interlock) between the bolt and the ground.

2.2 Untensioned Grouted Reinforcement (Grouted Bolts)

This category contains the perforated bolt type and the grouted rebars. These full contact passive bolts are most suitable in weak or fractured rock (soft ground) where mechanical anchorage is unsatisfactory. The other main advantage of the grouted bolts is that even if local

ROCK REINFORCEMENT SYSTEMS

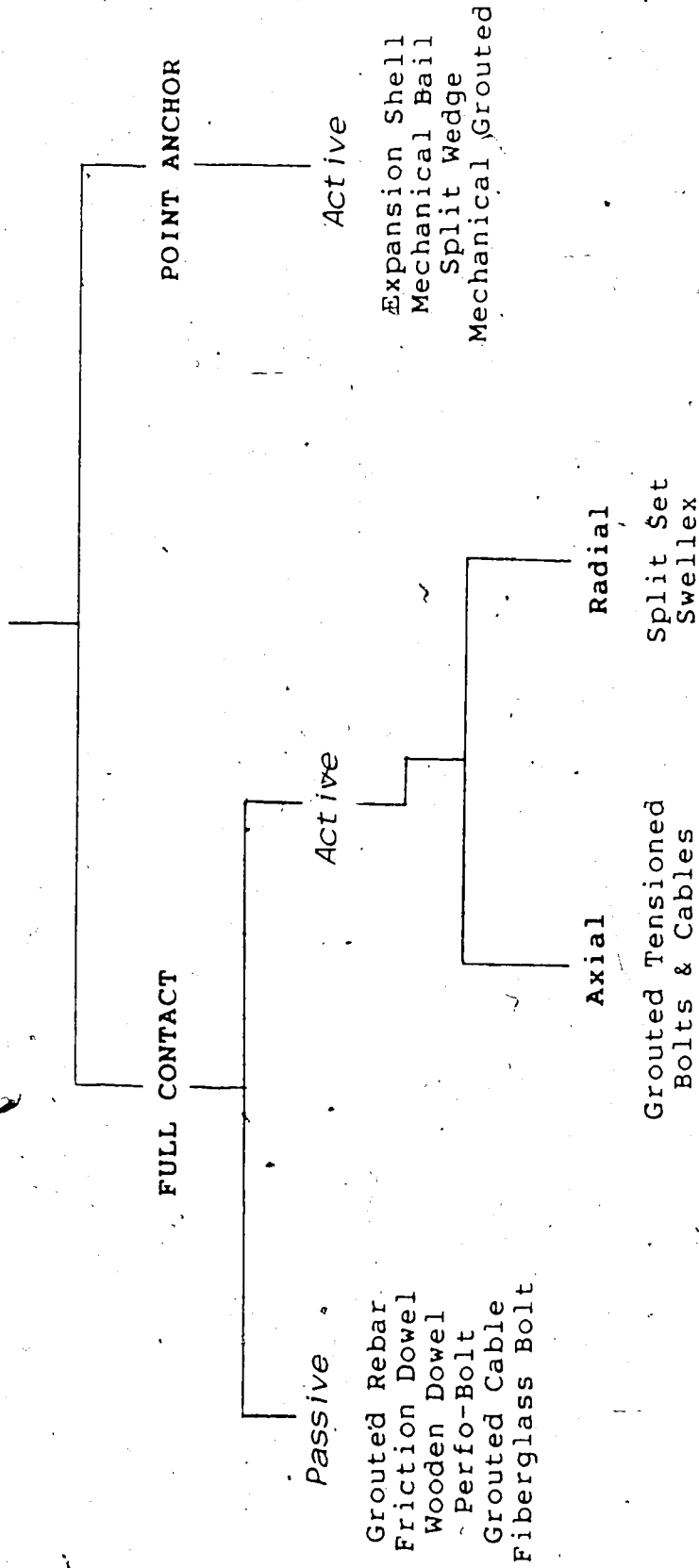


Figure 2.1 Classification of Rock Reinforcement Systems

yielding occurs at a position along the bolt length, total failure is prevented since the remaining intact parts will still carry load. In contrast, local failure of a mechanically anchored bolt will inevitably lead to instantaneous failure.

Grouting serves three major purposes:

- a) It bonds the bolt shank to the surrounding ground making the bolt an integral part of the rock mass itself,
- b) The grout acts as a protective cover for the bolt and prevents or reduces corrosion, and
- c) Low viscosity grouts can penetrate cracks that surround the drill hole and improve the rock mass further.

The efficiency of the grouted bolt depends on the shear strength of the bolt-grout interface and the grout-ground interface. Threaded rebars give an excellent bond with most grouts, and cement grouts and organic resin grouts establish a strong bond with most rocks.

In general most grouts are cement-water based. They should not contain ions that may lead to either corrosion of bolts or deterioration of the cement grout. Chloride ions are particularly harmful for steel bolts whereas sulphate ions can attack the cement grout. Chlorides, sulphides, sulphites, sulphates, carbonates and nitrates tend to lower the pH of the grout encouraging electrolytic action and hydrogen passage (Longbottom and Mallet, 1973; Caron, 1972). Therefore, it is very important that pure water is used for cement grouts. Rehm (1968) has shown that even a cover of 35

mm for bolts may not prevent corrosion if the grout is porous or cracked. In situations where the groundwater is contaminated (selenious or magnesian), organic resins are preferred to cement grouts for enhanced corrosion resistance. A review of the physical and chemical properties of commercially available organic resin grouts has been given by Indraratna (1983).

Grouts must have good workability for efficient injection into drill holes. However too high water contents may result in excessive shrinkage and reduced strength. Very fine sand or fly ash can be added to reduce shrinkage and increase plasticity. Fluidifiers and retarders are used to maintain workability especially in deep drill holes. Accelerators are used for rapid set under unfavourable groundwater conditions. The use of fluidifiers, air entraining agents and anti-bleed agents can effectively reduce the required water content for a given workability, thus producing a higher strength grout although at a higher cost. A typical mix composition of a cement grout (by weight) may consist of 55% of Portland cement, 19-22% of water and a fine sand content of 20-22% (water/cement ratio of 0.35-0.40). Further factors that affect the design and application of cement grouts and chemical resins have been discussed elsewhere (Indraratna, 1983 and 1984).

Grouting pressures are generally related to the type of rock, inclination and depth of drill holes. Minimum pressures (0.2 MPa) are more than sufficient for 3 - 5 m

drill holes in intact rock but are required for bolting in fissured rock. Grouting pressures must be carefully selected to avoid hydraulic fracture of rock, and for many types of rock they may typically lie in the range 0.3 - 0.7 MPa (Littlejohn and Bruce, 1975).

2.3 Tensioned Grouted Bolts

These bolts provide the best anchorage in poorer rocks. They can resist greater axial loads than mechanically anchored bolts. Anchorage in fractured rock can be tremendously improved by low viscosity chemical resins such as sodium silicates, acrylamides, chrome-lignin and some polyesters. Most modern systems use resin cartridges in drill holes.

2.4 Tensioned Mechanical Bolts

Expansion shell type anchors, slot and wedge type bolts all into this category. These systems consist of an anchor, a shank, a face plate, and a tightening nut. Mechanical anchorage may not be successful in soft rocks due to anchor slip, but very high loads can be achieved in good quality

2.5 Rock Anchors

Generally referred to bolts that are tensioned during installation, but are of much higher capacity than the normal tensioned bolts. They consist of high strength steel

tendons made up of several strands or bars fitted with a stressing anchorage at one end, and a means of transferring load to the rock at the other end. The study of pre-tensioned bolts and rock anchors is beyond the scope of this thesis.

2.6 Use of Weldmesh and Shotcrete in Rock Bolting Practice

Rock bolts themselves may not be able to support small blocks of loose rock on tunnel walls and rock slopes. It is normal practice to place a wire mesh (weldmesh) over the rock surface in addition to the bolts, and subsequently spray a layer of shotcrete to provide passive support to the rock surface. Shotcrete must cover the weldmesh completely especially when non-galvanized mesh is used in order to prevent corrosion. A typical weldmesh may consist of 100 mm x 100 mm squares composed of 4 mm diameter wires. Application of weldmesh and shotcrete has been discussed in detail by Hoek and Brown (1980).

A complete operational scheme for rock bolting is illustrated in figure 2.2.

2.7 Failure Modes of Rock Reinforcement Systems

2.7.1 Fall Out of Bolted Segments

Excessive tensioning of the bolts can sometimes generate shattered interface between bolt ends and virgin rock, leading to a separation of large volumes of rock

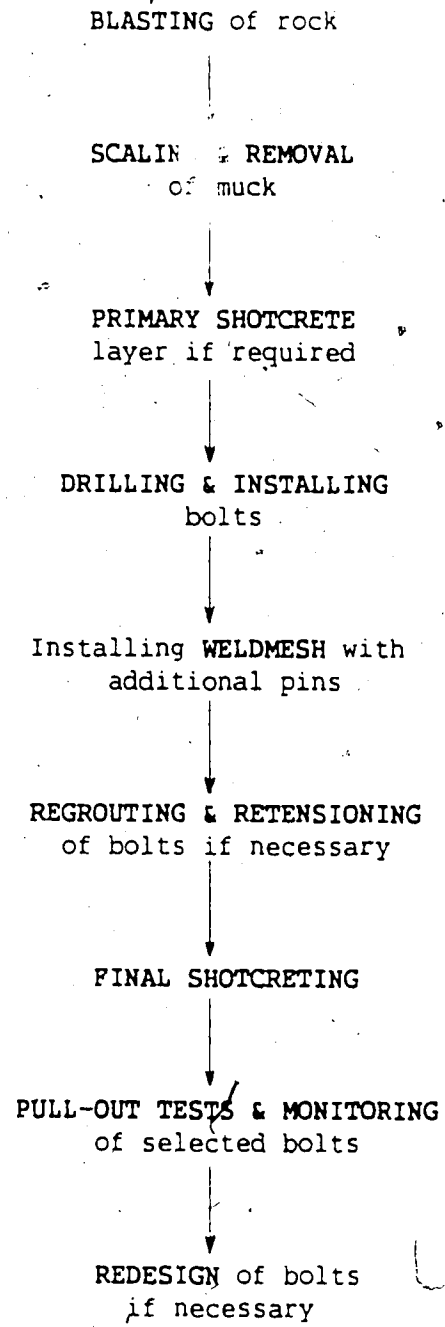


Figure 2.2 A Complete Operational Scheme for Rock Bolting

(segregation of blocks). Inadequate bolt lengths cannot prevent the failure of jointed weak strata. In rectangular mine openings, shear failure due to large bolt spacings or lack of inclined bolts at the ribs can also generate failure of bolted segments (Snyder, 1984). Fully grouted bolts in general are more efficient than tensioned bolts in preventing the above described failure modes, because they provide a greater shear and bending resistance at ribs and at weak interfaces. The use of different bolt lengths can be economically attractive and effective in reducing the risk of such failure in fractured rock (Maher, 1975; Douglas and Arthur, 1983).

2.7.2 Failure of Anchorage

Poor mechanical anchorage in weak rock or insufficient grouting can result in a reduction of the bolt load capacity, and this has been a major cause for occasional failure of spot bolted rock segments. The failure of a few bolts due to poor anchorage can lead to excessive load transfer on to the adjoining bolts, sometimes leading to progressive loosening, breaking and bending of bolts. Polyester resin anchorage has been found to be very successful with respect to this problem. It has been encouraged in recent times to avoid mechanical anchorage, where the rock is generally soft or where the rock is subjected to frequent blasting nearby (mining areas). Where mine openings are to remain in use for long periods of time,

it is certainly advisable to use full length grouted bolts instead of any mechanically anchored bolts.

Oversize drill holes can lead to poor anchorage where expansion shell type bolts are used, hence, such bolts must be installed in the smallest diameter holes that will accommodate them (Barry and McCormick, 1960). Anchorage strengths may vary widely between different bolts in the same rock. Consequently, pullout tests must be performed randomly to assess the anchorage efficiency of the proposed bolts.

2.7.3 Shear Deformation of Bolts

The deformation of layered and jointed rock can result in shear displacements along weak planes such as joints and bedding planes. Of course, one main purpose of bolting is to minimize such shear displacements by reinforcing the discontinuities. However, if either the axial load developed in the bolt or the shear stiffness of the bolts is inadequate, large shear movements may be generated at the discontinuities. As a result, the bolts may deform and subsequently yield as illustrated by Figure 2.3 thereby reducing their effectiveness.

Fairhurst and Singh (1974) provide convincing evidence that, for fully grouted bolts, the shear reinforcement of each plane of weakness is essentially independent of the other. Even if a grouted bolt fails at one level, the shear stiffness of the same bolt at any other layer is unaffected.

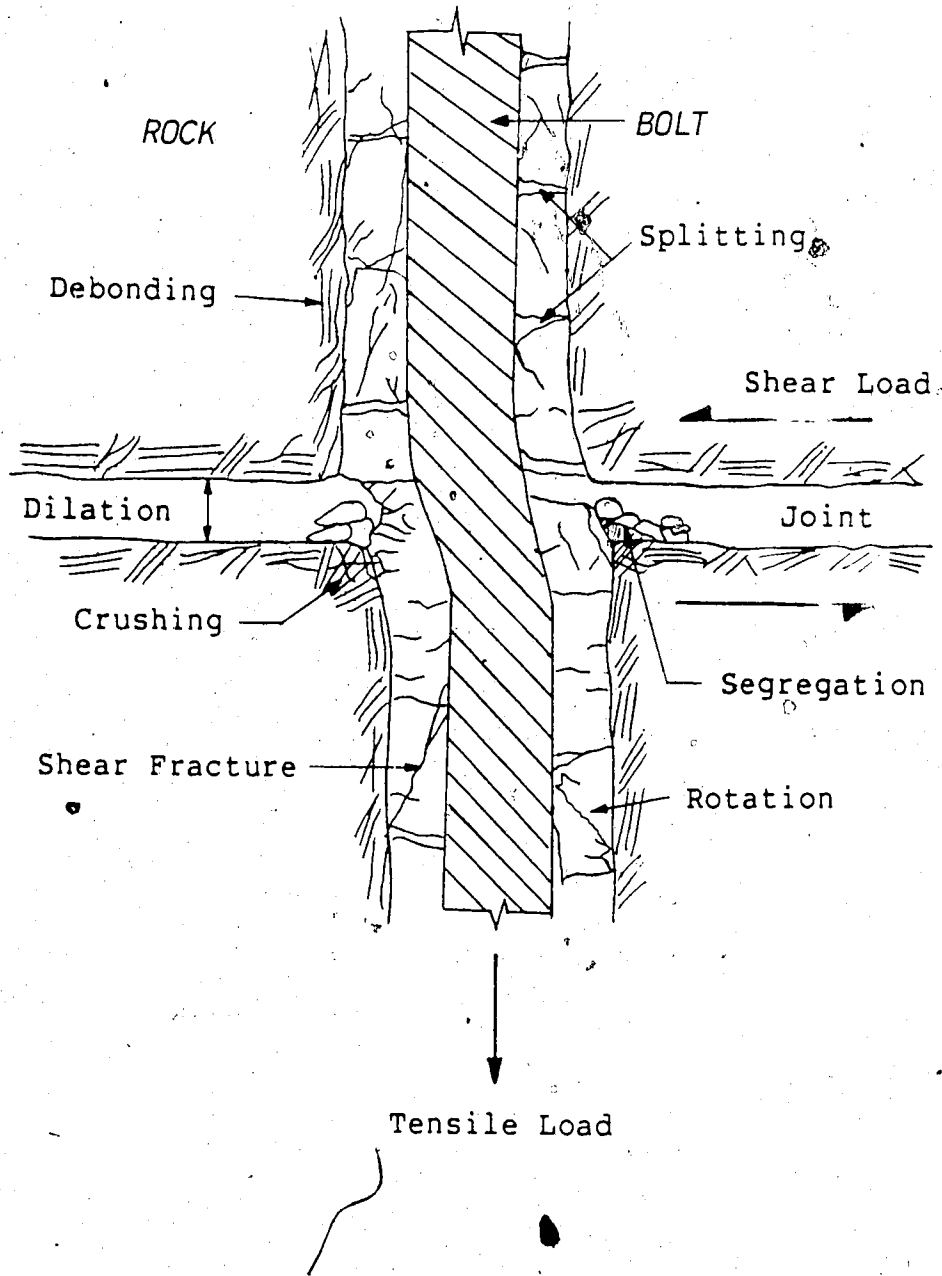


Figure 2.3 Shear Deformation of a Fully Grouted Bolt

In other words, local failure does not significantly affect the functioning of the overall bolted strata. In contrast, local yielding of a mechanical bolt will reduce the bolt tension considerably, thereby threatening the overall effectiveness of the bolted strata.

2.7.4 Improper Tensioning of Bolts

Inappropriate torque tension relationships, use of faulty torque wrenches or hydraulic jacks can either induce excessive or inadequate bolt tension. Excessive tension can either lead to slip at the anchorage, separation of blocks, or yielding of the bolt and its components. Overloading of grouted bolts can also occur due to strong shock wave pulses generated by nearby blasting. On the contrary, blasting can induce relaxation of pre-tensioned mechanical bolts (Stehlik, 1964). Insufficient tensioning assists in loosening and encourages shearing of bolts.

2.8 Localized Failure of the Bolt-Grout Composite

There are several ways in which a fully grouted untensioned bolt can malfunction:

- (a) Yielding of the bolt itself,
- (b) Failure along the bolt/grout interface,
- (c) Fracture within the grout annulus, and
- (d) Failure along the grout/rock interface.

Yielding of the bolt occurs when the maximum tensile stress at any position along the bolt exceeds the yield

stress of steel. If the shear stress developed along the bolt surface exceeds the bond strength (adhesion), 'pull-out' of the bolts occurs as generally observed in the case of smooth rebars. Such failure can be restricted or delayed by profiled bolt surfaces.

Fracture of the grout annulus or failure along the grout/rock interface can be regarded as pre-mature, if the load capacity of the bolt itself and the bond strength of the bolt/grout interface have not been reached. Excessive shrinkage cracking, high porosity and retarded strength development are some factors responsible for accelerated fracture propagation in the grout annulus. Impaired adhesion at the grout/rock interface can often be the result of inadequately cleaned boreholes, excessively smooth borehole walls or softened rock due to rock alteration.

2.9 Comparison of Grouted and Mechanical Bolts

The following important advantages of fully grouted bolts may be summarized:

1. In all ground types, grouted anchorage can be ensured, whereas mechanical anchorage is questionable in soft or fractured rock.
2. In grouted bolts, the effective bond or anchorage length is equal to the bolt length, whereas in tensioned bolts the effective length is limited to the fixed anchorage length.
3. Failure of rock at the mouth of the hole or local

yielding of bolt at any point can seriously affect the capacity of a mechanical bolts system.

4. Fully grouted bolts transmit shear stresses much more effectively in both lateral and axial directions, and have a greater axial, bending and shear stiffness. Once activated they are more effective than mechanical bolts, and also are more resistant to shock loads from blasting, and earthquakes.
5. Fully grouted bolts are more resistant to corrosion. In addition, the penetration of grout into cracks reduces permeability and discourages weathering or rock alteration processes in the surrounding rock.
6. Installation is more complex but the time and effort of manual tensioning is eliminated if fully grouted untensioned bolts are employed.

However, fully grouted bolts are not effective in the following adverse conditions:

1. Since grouted bolts depend on ground displacement for activation, tensioned bolts are preferred where displacements have to be readily curtailed. Tensioned grouted bolts can be installed by application of grouts (resins) with different setting times.
2. Setting time and strength properties of the grout are seriously affected where ground water continues to flow into the borehole.
3. Extreme temperatures affect the strength development of most grouts.

4. Grouted bolts may not be economical in situations where the presence of large cavities or fault zones in the near vicinity generate substantial loss of grout.

2.10 Selection of Rock Bolts for Various Rock Types

The following summary is intended as a guide for the selection of bolts. The role of bolting in strong and weak rock has been classified in Table 2.1.

A. Untensioned grouted dowels

i) Uses:

- (a) Stability of an exposed face or reinforcement prior to excavation (tension is quickly developed if installed close to an advancing face),
- (b) Permanent or temporary support of unstable rock strata, and
- (c) Principle support system in NATM to control yielding of rock mass, hence, tunnel convergence.

ii) Rock Type:

Generally advantageous in fractured or yielding rocks such as mudstone, coal, shale, weathered sedimentary or metamorphic rocks.

B. Tensioned Bolts (mechanical or resin grouted)

i) Uses:

- (a) Both for temporary and permanent support,
- (b) Particularly advantageous for stabilizing large unstable blocks (keyblocks), and
- (c) Suitable for excavations where displacements must be

Table 2.1 The Role of Bolting in Various Types of Rock

Rock Condition	Rock Strength	
	Strong	Weak
slightly jointed	A	A or/and B
stratified	B + C	B + C + D
highly fractured	B and/or E	B + E

ROLE OF BOLTING:

- A : prevent spalling and collapse of loosened blocks.
- B : increase cohesion & internal friction of rock mass.
- C : increase shear strength at interface.
- D : reduce vertical deflection by beam building.
- E : use of wire mesh & shotcrete for additional support as well as secondary and tertiary bolts to prevent spalling and squeezing.

severely curtailed.

ii) Rock Type:

In weak and fractured rock mechanical anchorage is inefficient. Resin grouted tensioned bolts are suitable for any type of rock, but purely mechanical bolts such as expansion shell are ideally suited for relatively hard rocks such as limestones, sandstones, marble, etc.

C. Tensioned Anchors or Cable Bolts

i) Uses:

Stabilization of tunnel intersections and other major excavations which require long bolt lengths and high support pressures (e.g. Diwidag or Macalloy anchors).

ii) Rock Type:

Not economical for weak rocks due to their high load capacity. Have been successfully used in unweathered stronger rocks such as blocky limestones and sandstones.

2.11 Summary of Interactive Factors Influencing the Design of Reinforcement Systems

1. Properties of Intact and Jointed Rock

Strength parameters ($\sigma_c, \sigma_t, c_u, s$), cohesion and friction (c_i, ϕ_i), Elastic constants (E, ν), permeability (k_w), properties of joints and bedding planes, and type of keyblocks must be known for design.

2. Groundwater and Associated Problems

Water pressures in tension cracks and weak planes, flow into excavation, feasibility of grouting and corrosion

potential also influence design and excavation procedures.

3. In-situ Field Stress

Overburden pressure and K_0 are required to predict the stress distribution (before and after excavation).

4. Geometry of Excavation

Circular, rectangular, horseshoe and other shapes affect the stress distribution and method of support.

5. Potential Failure Modes of Openings

The type and pattern of bolts required for stabilization are influenced by the potential failure modes or modes of yielding prior to bolt installation.

6. Excavation Procedure

Method of excavation (full face, part face etc.), type of equipment and rate of excavation not only affect the stress field but also the installation procedure of supports and, hence, the mode of bolt activation.

7. Properties of Bolts and Installation Procedure

Material and geometrical properties of bolts, torque-tension relationship, type of anchorage, method of drilling and grouting, type of wire mesh and shotcreting procedures influence the ultimate load capacity of the bolt.

8. Pattern of Bolting

Length and spacing (variable or uniform) of the bolts and their arrangement around the excavation directly influence the degree of stabilization.

9. Time Lapse

The time lapse between excavation and bolt installation influences the load development of a grouted bolt and, hence, the tunnel convergence.

10. Instrumentation

Load and displacement monitoring can provide very important data to assess bolt system performance and to establish more efficient designs for subsequent excavation work.

The recognition of most of the above mentioned interactive factors, in the development of an analytical method for the design of fully grouted rock bolts will be discussed in Chapter 3.

2.12 Improvement of Rock Mass Shear Resistance by Joint

Reinforcement

The presence of a major discontinuity with unfavourable dip can be catastrophic in underground openings unless such joints can be stabilized soon after excavation. Both active and passive bolts may prevent dilation and also minimize the shear displacement along a weakness. Conventional mechanical bolts immediately provide a direct normal stress and restrict dilation. Fully grouted bolts also provide shear resistance against the direction of sliding (shear displacement). However, the development of the optimum axial load (tension) in a fully grouted bolt requires a small amount of deformation of the rock mass which is quickly

attained in yielding rock. The shear resistance provided by mechanical bolts is purely due to an increase in normal stress that stimulates greater friction at the joint interface. Experiments conducted by Haas *et al.* (1975) on limestones and shales have revealed that the increase in shear resistance offered by grouted bolts is considerably greater than the additional friction provided by mechanical bolts.

Bjurström (1974) has considered the shear strength of a bolted joint as an aggregation of the following three constituents (Figure 2.4):

a) Shear resistance due to reinforcement effect:

$$T_b = P(\cos\theta + \mu \sin\theta)$$

where: P = bolt tension, θ = angle between the bolt and the joint and $\mu = \tan\phi$;

b) Shear resistance due to dowel effect:

$$T_d = 0.67 d^2 (\sigma_s \cdot \sigma_c)^{0.5}$$

where: d = bolt diameter, σ_s = bolt yield strength
and σ_c = uni-axial compressive strength of rock ;

c) Shear resistance due to friction of joint itself:

$$T_f = A_j \cdot \sigma_n \cdot \tan\phi_j$$

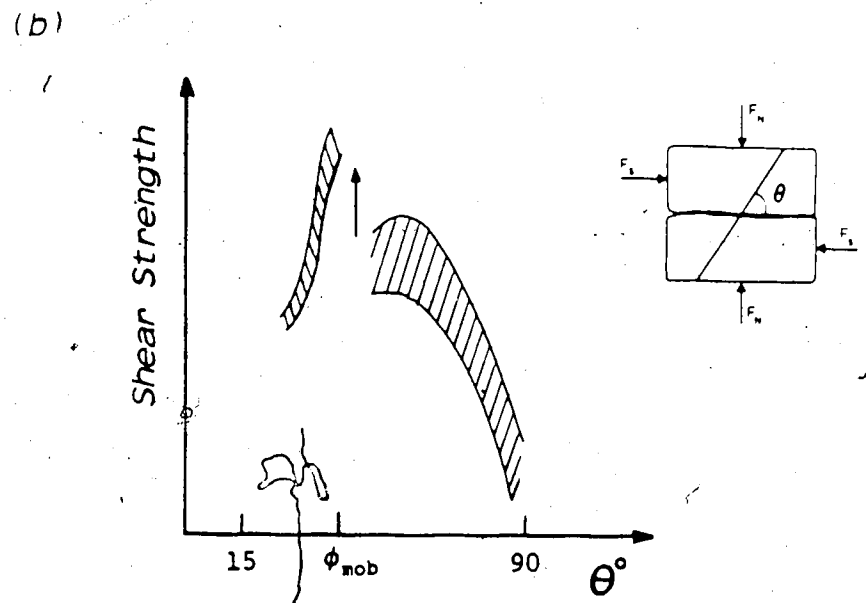
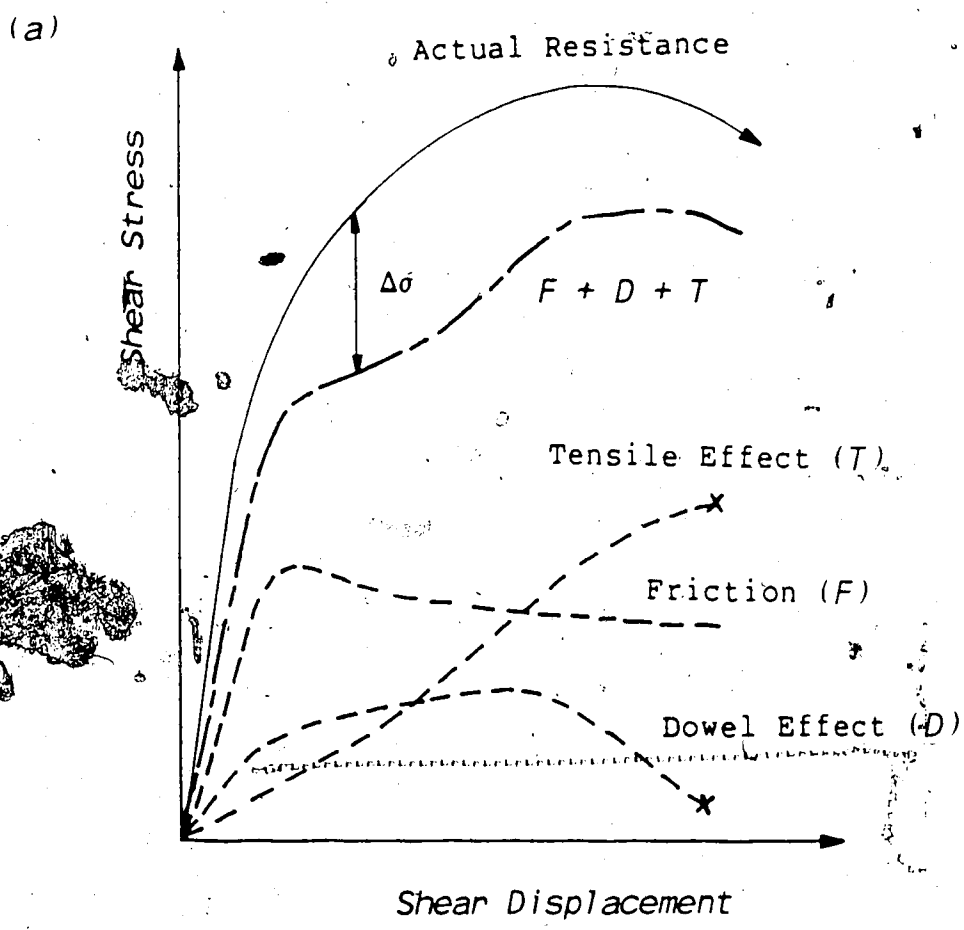


Figure 2.4 Shear Strength of Reinforced Joints (modified after Bjurström, 1974)

where: A_j = joint area, σ_n = normal stress on joint
and ϕ_j = joint friction angle.

Hence, the total shear resistance: $T_t = T_b + T_d + T_f$

Shear tests conducted by Bjurström (1974) also reveal that the optimum bolt capacity is achieved, when the inclination of the bolt to the joint (θ) equals the mobilized friction angle of the joint (Figure 2.4). As θ approaches ϕ_{mob} , the applied shear stress required to obtain a given shear displacement as well as the axial bolt stress rapidly increase. If the axial stress becomes excessive, yielding of the bolt may occur before the required shear displacement is attained. This is indicated by the discontinuity shown in Figure 2.4. Barton and Bakhtar (1984) and Haas (1981) have also published similar findings. The analysis of slopes and excavations by force-equilibrium methods (Barton, 1973) also suggests that the direction of the maximum bolt tension is inclined at an angle of ϕ (mobilized) relative to the joint plane.

A finite displacement of the joint is required for the mobilization of the shear strength. This mobilized shear strength is a function of the pre-peak, peak or post-peak displacements. Therefore, the appropriate bolt load and inclination angle depend on the corresponding strength envelope for peak or residual strength. Generally for practical purposes, the bolts are designed for post-peak displacements at the joints, hence, the optimal inclination angle of the bolt may be recommended as ϕ (mobilized) as

shown in Figure 2.5.

2.13 Reinforcement of a Single Plane of Weakness

Jaeger and Cook (1969) have analyzed, by application of the limit equilibrium, the behaviour of a linear discontinuity in a rock mass with the Mohr-Coulomb shear strength criterion. The analysis presented here is an extension of the latter approach to accommodate the influence of bolting on the joint. Figure 2.6 illustrates a single joint reinforced by a bolt inclined at an angle θ to the joint plane. The cross-section area of the bolt and the area of the joint per unit longitudinal length have been represented by A_b and A_j respectively. In the 'single plane of weakness' theory, Jaeger and Cook (1969) have proposed the following equations:

$$\tau_j = c_j + \sigma_n \tan \phi_j \quad (2.1)$$

$$\sigma_n = \frac{1}{2}(\sigma_1 + \sigma_3) - \frac{1}{2}(\sigma_1 - \sigma_3) \cos 2a \quad (2.2)$$

$$\sigma_1 = \sigma_3 + \frac{2(c_j + \sigma_3 \tan \phi_j)}{(1 - \tan \phi_j \tan a) \sin 2a} \quad (2.3)$$

where: τ_j = shear strength of the joint,

σ_n = normal stress across the joint,

σ_1, σ_3 = vertical and horizontal field stresses,

c_j, ϕ_j = cohesion and friction angle of the joint,

a = joint inclination to the minor principal plane.

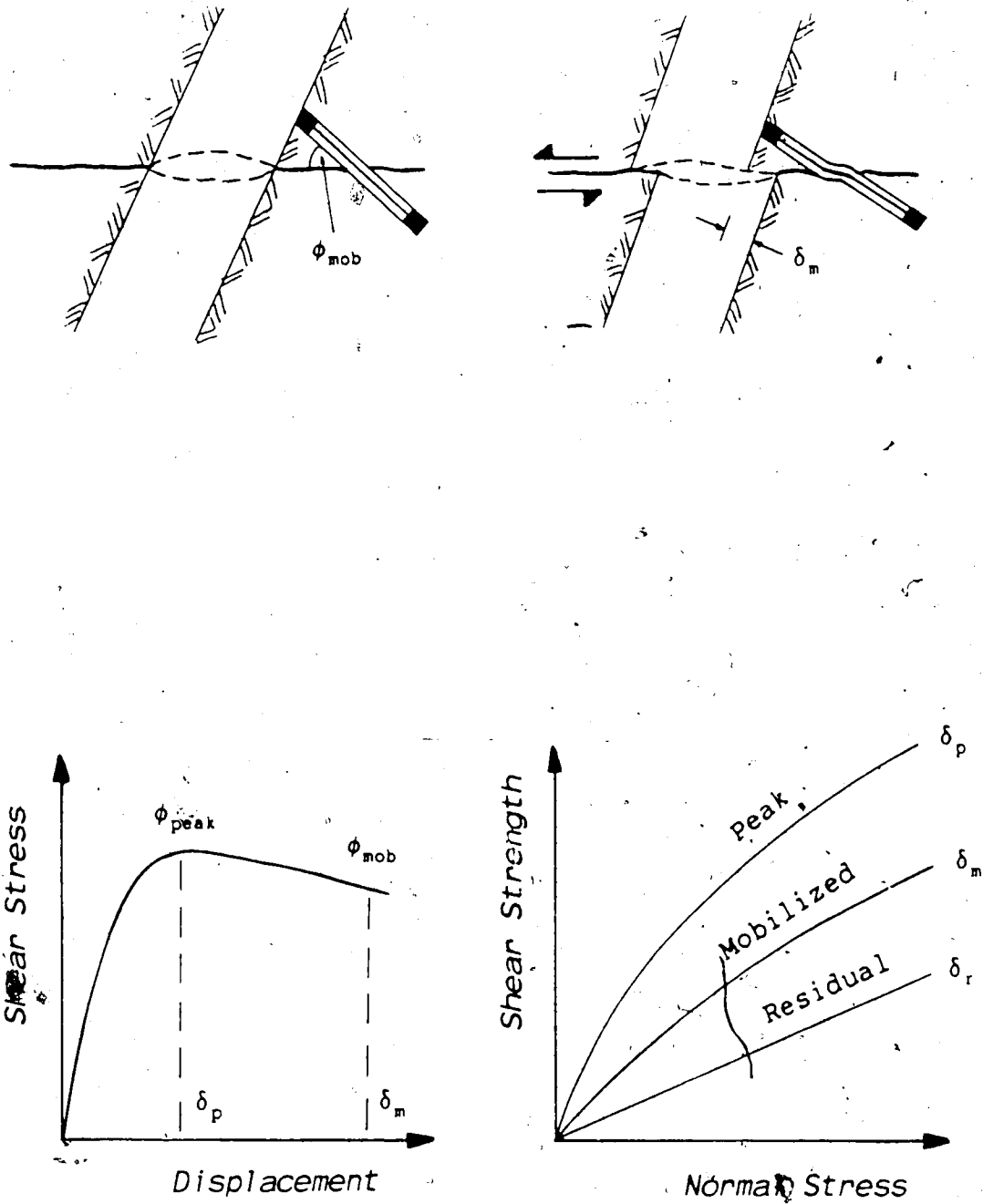


Figure 2.5 Influence of Mobilized Friction Angle on Bolt Installation (modified after Barton and Bakhtar, 1984)

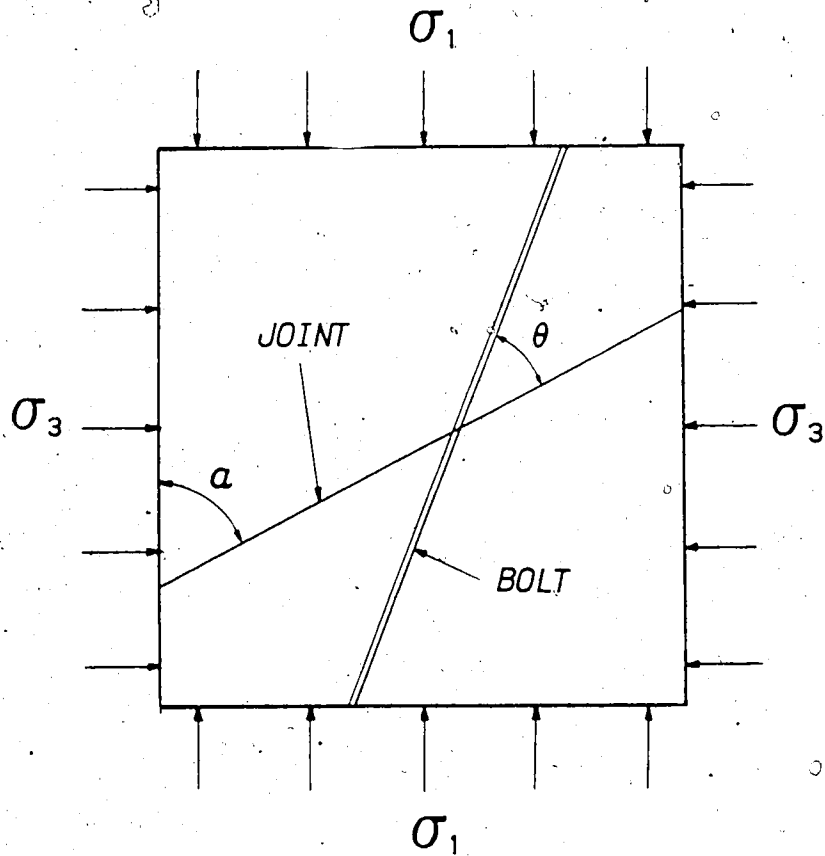


Figure 2.6 Reinforcement of a linear discontinuity

The development of load ($\sigma_b \cdot A_b$) along the bolt axis, provides additional normal stress and shear resistance to the joint. The equilibrium of the reinforced joint leads to the modification of Equations 2.2 and 2.3 as follows:

$$\sigma_n = \frac{1}{2}(\sigma_1 + \sigma_3) - \frac{1}{2}(\sigma_1 - \sigma_3)\cos 2a + \sigma_b \cdot A_b \cdot \sin\theta / A_j \quad (2.4)$$

$$\sigma_1 = \sigma_3 + \frac{2(c_j + \sigma_3 \tan\phi_j)}{(1 - \tan\phi_j \tan a)\sin 2a} + \frac{2(F_1 + F_2)}{(1 - \tan\phi_j \tan a)\sin 2a} \quad (2.5)$$

where: $F_1 = \sigma_b \cdot A_b \cdot \cos\theta(1 + \tan\phi_j \tan\theta) / A_j$

and $F_2 = \tau_{bf} \cdot A_b / (A_j \cdot \sin\theta)$

The mathematical derivation of the latter equations is summarized in Appendix C. The tensile stress (σ_b) and the shear strength (τ_{bf}) of a mechanical bolt should not exceed the yield stress of steel. However, fully grouted bolts have a larger effective cross-section area as a result of the grout annulus. Consequently, much larger axial and shear loads can be tolerated by them prior to failure. However, because the axial load varies along the length of a grouted bolt, the degree of reinforcement also depends on the location of the joint relative to the bolt axis.

The expressions F_1 and F_2 reflect the influence of bolting on the additional normal stress and shear resistance provided to resist the joint displacements. Since the shear strength of a discontinuity is modelled by Equation 2.1, any

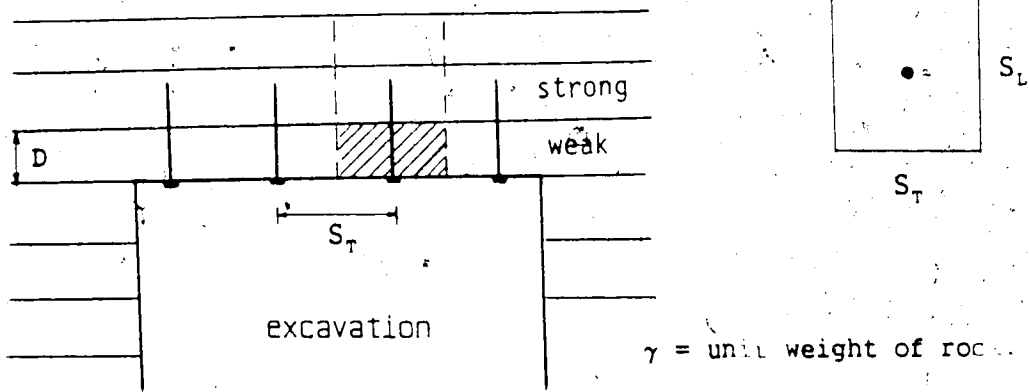
increase of the normal stress results in an enhanced shear strength of the joint. This analysis was extended further to include the effect of several bolts installed at different inclinations (Appendix C).

2.14 Theories of Rock Reinforcement by Bolting

2.14.1 Suspension and Frictional Stabilization of Individual Blocks

Bolting must attempt to strengthen the rock mass by preventing the detachment of loose blocks. The suspension theory is based on the fact that unstable individual blocks can be stabilized by suspension from the relatively stable rock beyond them. The bolt lengths must be adequate to penetrate sufficiently into the stable strata. Both active and passive bolts not only balance the weight of the unstable wedges, but may also increase the shear resistance of the joints which are intersected by the bolts. Figure 2.7 illustrates the above discussed stabilization concepts. The transverse resistance offered by the uncomparably high shear stiffness of the fully grouted bolts is greater than the shear resistance provided at a joint by a conventional mechanical bolt. A variety of simple analytical rock-bolt models have been developed for the stabilization of rectangular blocks and triangular wedges using the limit equilibrium technique (Lang, 1961; Cording and Deere, 1972; Hoek and Brown, 1980; Brady and Brown, 1985).

(A) A Simple Theory (for rectangular blocks)

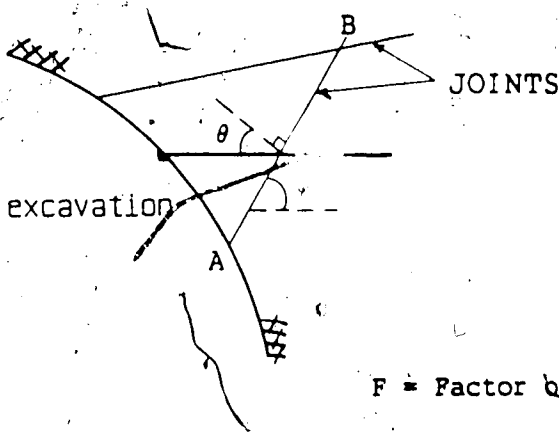


For simplicity, ignore shear on sides of the block,

Weight of block = $S_T \cdot S_L \cdot D \cdot \gamma =$ Tension of bolt (T)

(B) Resistance to Sliding of a Triangular Wedge

Hoek & Brown, 1980.



- AB = sliding surface
- W = weight of block
- A = area of sliding
- T = tension in bolt

F = Factor of safety for sliding

$$F = \frac{\tan\phi(cA + W \cdot \cos\psi + T \cdot \cos\theta)}{(W \cdot \sin\psi - T \cdot \sin\theta)}$$

Figure 2.7 Stabilization of Unstable Individual Blocks

Lang and Bischoff (1981) have proposed an analytical solution for the design of bolts in rectangular mine openings based on Terzaghi's limit equilibrium method. The latter 'Reinforced Rock Unit' approach reveals that the bolt length must be at least twice the spacing to prevent excessive loading of the bolt. The same criterion has been proposed earlier by Lang (1961) and the U.S. Army (1980) in semi-empirical design guides. The above discussed methods based on the theory of suspension may be employed successfully for spot or pattern bolting where the geometry of the unstable wedges can be determined by hemispherical projection or by other means.

2.15 Keyblock Bolting to Prevent Ravelling

Keyblock method is a lower bound approach that searches for all blocks that are potentially most critical. Any movable block must be finite and exposed at the opening wall. Keyblock bolting or spot bolting attempts to bolt all finite removable blocks such that no other potentially loose rocks are able to move. If a keyblock falls into the excavation, subsequent release of other blocks can follow and induce progressive ravelling. Given a particular excavation geometry, keyblock theory determines a complete set of joint planes that define keyblocks which can be extended to either individual joint blocks or multiple united blocks. Spot bolting should successfully stabilize a "potential keyblock area" by keying of rigid blocks to form

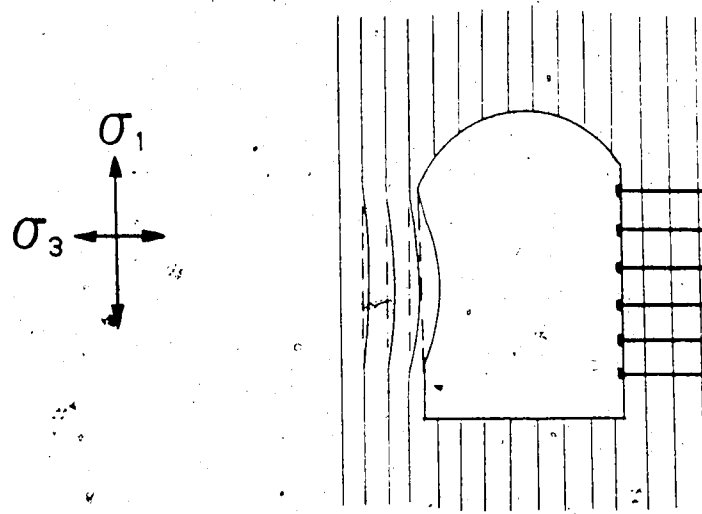
larger blocks. This in turn generates a compressive action that reduces the adverse effects of potential tension zone above the excavation. The theory and procedure for finding keyblocks and keyblock bolting are explained in detail by Shi Gen Hua and Goodman (1984).

2.16 Beam Building Theory

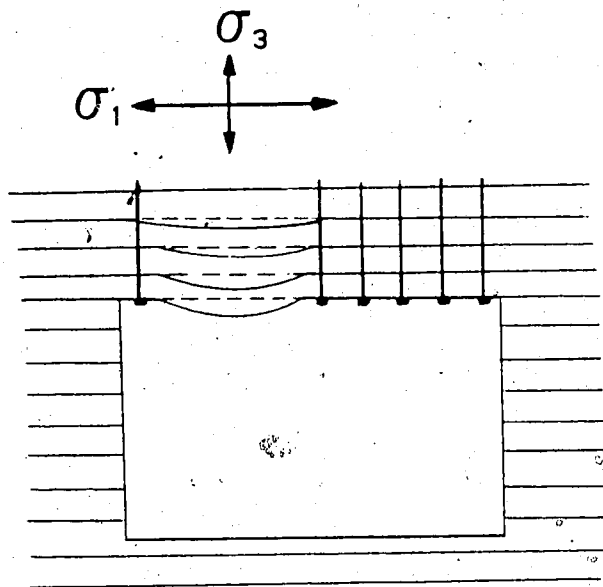
This theory can be explained in two ways. Firstly, one can consider the bolts as having the effect of laminating thin layers together, thereby forming a thicker monolithic system. Such a system will transmit horizontal shear from one layer to the other and minimize the relative horizontal displacements that will take place at the interfaces due to bending. Tensioned bolts can directly increase friction at interfaces by normal stress, whereas the grouted bolts can also transmit shear as a result of the shear stiffness of the bolt-grout system. The purpose of the bolts in producing a monolithic beam is the improvement of shear resistance between the layers and the reduction of deflections under the applied load. Snyder (1984) has shown that fully grouted bolts are more effective than mechanical tensioned bolts in reducing deflections due to their enhanced axial and shear stiffness. The increase in effective depth and flexural rigidity (EI) of the laminated composite is a function of the bolt spacing, the axial and shear stiffness of the bolts.

Sagging and buckling of laminations have often been observed in openings excavated in coal and thinly bedded sandstone/shale strata, as illustrated qualitatively in Figure 2.8. 'Beam building' provides protection against such failure modes. If the bottom layer immediately above the excavation is thinner or weaker than the other layers, it tends to sag more and separate at midspan from the layer above it. This process is common in rectangular coal mine openings. However, bolting at mid-span has been successful in restricting delamination. At the middle of the reinforced span, the bottom layers are mainly in tension, whereas the top most layers are mainly in compression. Consequently, the neutral axis of each layer tends to approach an imaginary neutral axis of a monolithic beam.

However, closer to the supports (ribs or pillars) the layers act independently, and separation tends to occur between supports and quarter-points of the span. The separation of layers at the ribs is mainly due to higher vertical shear and bending moments. Therefore, it is recommended to use smaller bolt spacing as well as angled bolts over the abutments (ribs). The mathematical analysis of the beam theory is given by Gerdeen *et al.* (1977) and Snyder (1984).



BUCKLING



SAGGING

Figure 2.8 Prevention of Buckling and Sagging by Beam Building

2.17 Arch Building Theory

Excavation creates a zone of loosened rock that can be effectively reinforced by bolting. Radial bolting leads to the concept of creating a structurally competent arch which is a fundamental approach used in many empirical designs. The geometry of the compressive arch has been predicted by assuming a dispersion angle of 45° (Figure 2.9), and its thickness is given by (Lang, 1972):

$$t_{\text{arch}} = L - S_T \quad (2.6)$$

where: L = bolt length and S_T = tangential bolt spacing.

The confinement provided by the tension in radial bolts creates a compressive arch around the opening with increased tangential stresses. For the arch to be structurally competent, bolts must not induce compressive stresses greater than the uniaxial strength of the rock. In addition, they must effectively control excessive deformations of the rock mass by stabilizing active joints.

The continuity of the artificial arch between the bolts is achieved, only if the ratio of the length/spacing of the bolts is greater than 2 (Lang, 1972). If the latter ratio is less than 2, the compressive zones will be confined to localized regions around individual bolts and will not intersect to form a continuous arch. Structural analysis of the reinforced arch are given by Lang, 1972; Bischoff and Smart, 1975 and Gerdeen *et al.*, 1977.

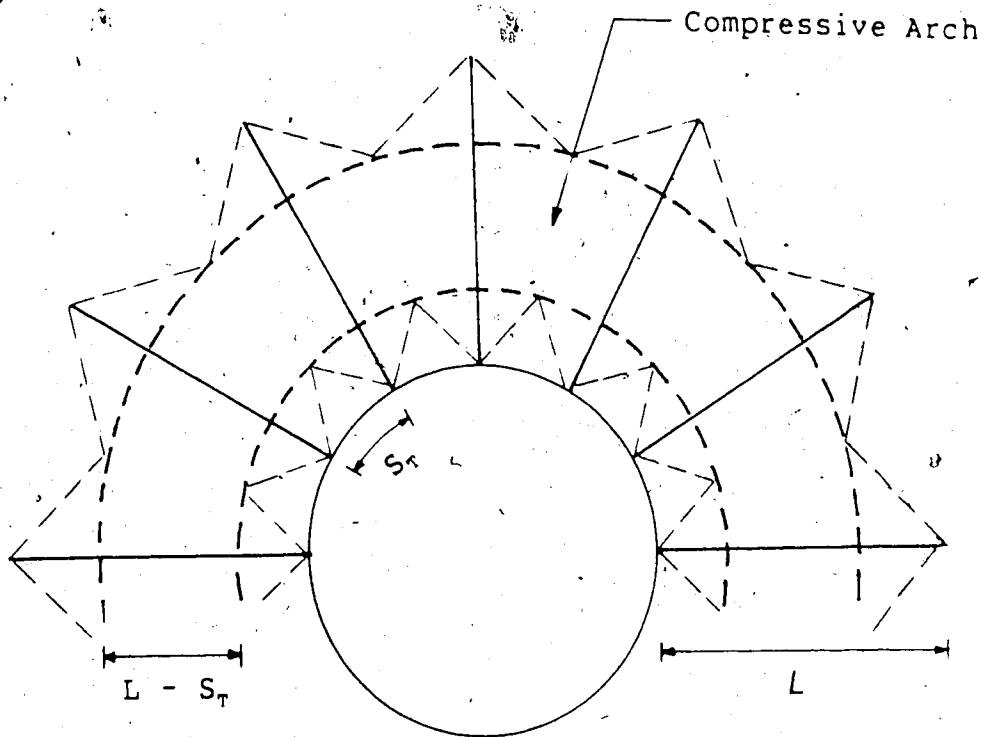


Figure 2.9 Formation of a Compressive Rock Arch (modified after Lang, 1972)

2.18 Summary

The comparative review of alternative bolt systems has emphasized the advantages of fully grouted bolts over the conventional mechanical bolts. Their enhanced shear stiffness and the effectiveness even in the weakest rocks have made fully grouted bolts economically attractive. A rational analytical model for the stabilization of underground excavations has been developed by Hoek and Brown (1980), employing the concepts of support confinement and ground reaction curves. Fully grouted rock bolts unlike other support systems cannot be modelled by a support confinement curve because they become an integral part of the rock mass, thereby restricting its deformations internally. The following chapter presents a rational analytical approach for the design of fully grouted rock bolts in tunnel openings.

3. THEORETICAL ANALYSIS OF FULLY GROUTED BOLTS IN UNDERGROUND EXCAVATIONS

3.1 Application of Elasto-Plasticity in Tunnel Openings

The assumptions of homogeneity, isotropy and linear elasticity before yielding occurs are made to simplify the analysis. The elastic behaviour of an opening in an infinite medium is well documented in the literature (e.g. Obert and Duvall, 1967). The application of Airy's stress functions and Hooke's law to determine the stress and strain fields constitutes the fundamentals of the elastic theory. Since tunnels are much longer than their diameter, it is reasonable to assume that the *plane strain* condition (longitudinal strain, $\epsilon_z=0$) prevails ultimately. The conditions at the face differ significantly and, hence, three dimensional effects should be considered. For the following, it is assumed that this transition does not affect the final *post-peak* behaviour.

Yield initiation is assumed to occur following a linear Mohr-Coulomb failure criterion. Post-peak behaviour is characterized by the flow rule that governs the plastic deformations. In the perfect plastic material model, there is no strength drop after yielding hence, yielding continues to occur at a constant peak stress level. However, a) strain weakening behaviour is generally observed in most rocks where the post-failure behaviour is strain-dependent.

The elastic, brittle-plastic model is a simplification of the above described behaviour, and is characterized by an instantaneous strength drop at peak as shown in Figure 3.1. The Mohr-Coulomb failure criterion is still applicable although the post-peak strength is reduced. The principal stresses in the plastic zone can now be related by:

$$\sigma_e = m \cdot \sigma_r + s \cdot \sigma_c \quad (3.1)$$

where: $m = \frac{1 + \sin\phi}{1 - \sin\phi} = \tan^2(\pi/4 + \phi/2)$ and $0 < s < 1$.

The parameter s is a measure of the degree of strength loss occurring immediately after the peak strength is reached. In uniaxial compression, s is almost zero, whereas it approaches unity if the perfectly elasto-plastic state is attained in triaxial compression. Further discussions on the application of different elasto-plastic models under various boundary conditions are given by Hendron and Aiyer (1972), Guenet (1979) and Goodman (1980).

At the boundary of an elastic excavation, the tangential stress is maximum, whereas the radial stress is minimum. The creation of such an unconfined stress state at a tunnel wall initiates yielding of the rock, if the tangential stress exceeds the unconfined compressive strength of the rock mass. In the case of isotropic yielding in a homogeneous material under a hydrostatic field stress, an axisymmetric plastic zone develops at the tunnel wall and

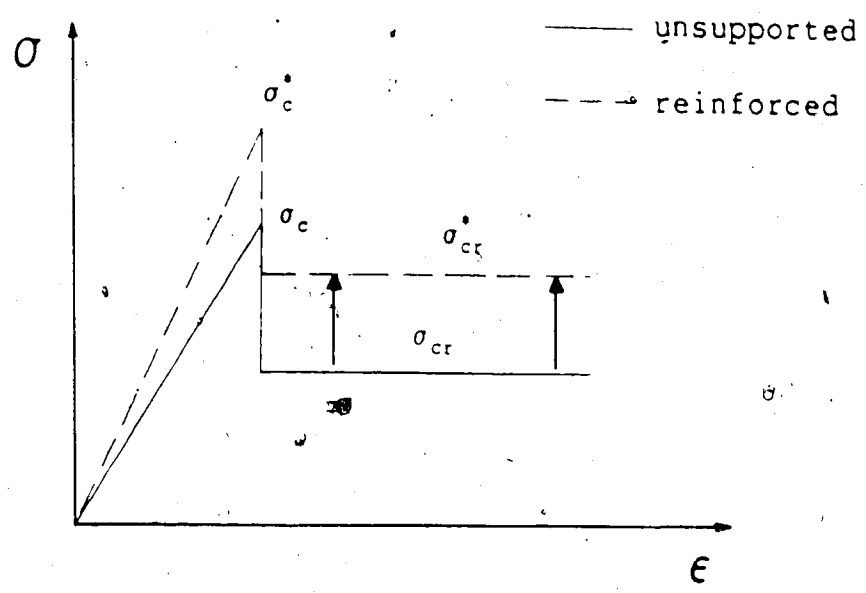


Figure 3.1 Elastic, Brittle-Plastic Strength Model

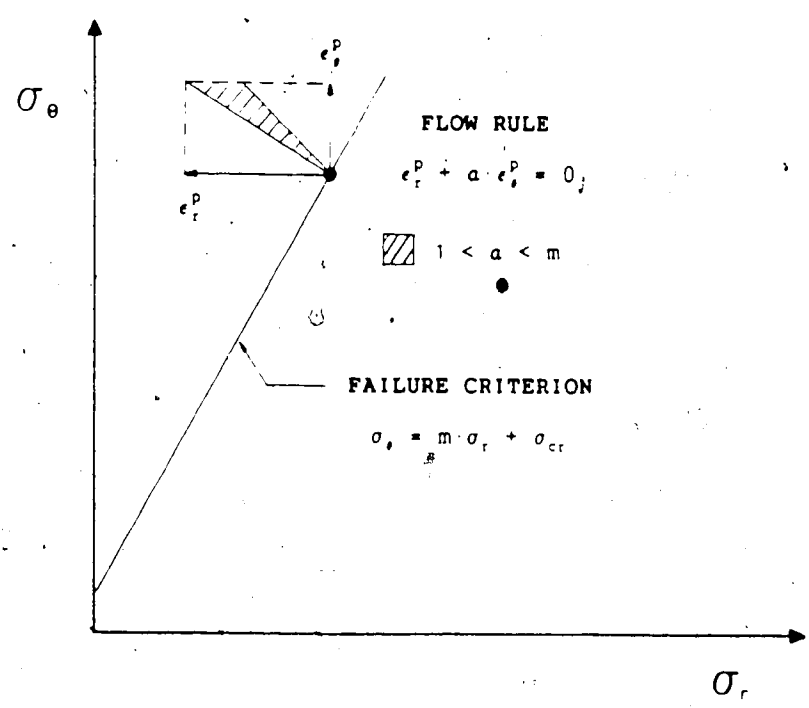


Figure 3.2 Failure Criterion and the Flow Rule

propagates away from the cavity. Since the radial or the confining stress increases from the opening, yielding is gradually inhibited with increasing distance from the tunnel wall. Where the tangential stress after redistribution is equal to or lower than the unconfined compressive strength of the rock, further yielding is prevented. Therefore, the yielded zone is always surrounded by an outer elastic zone.

Strain softening and creep properties of rocks are generally time-dependent. Furthermore, the presence of joints and fractures makes the rock mass anisotropic. Consequently, time-dependent stress redistribution with associated anisotropic yielding, generally induces localized failure, even if the in-situ stress field is hydrostatic ($K_0=1$). The process of modelling anisotropic, time-dependent behaviour by analytical techniques is mathematically complex or impossible, therefore, approximate solutions may have to be adopted, for example, by numerical methods. Analytical models based on elasto-plasticity (Goodman and Dubois, 1971; Hendron and Aiyer, 1972; Egger, 1973; Ladanyi, 1974; Hoek and Brown, 1980; Brown *et al.*, 1983; Kaiser *et al.*, 1985) have often assumed isotropic and time-independent material properties with relatively simple failure criteria.

The combination of equilibrium equations and a failure criterion provides the basis for the determination of stress distribution in the plastic zone. The assumption of the continuity of radial stress throughout the medium is necessary for the determination of the plastic zone radius.

The radial pressure at the elasto-plastic boundary can be regarded as an internal support, for the outer elastic zone. Consequently, the stress and strain fields of the outer elastic zone can be determined.

The strains in the plastic zone are the sum of elastic and plastic components. The elastic component of the strains and displacements in the plastic zone has been determined by assuming the same elastic constants (E , ν), and applying Hooke's laws. The plastic strains are governed by an appropriate flow rule postulated for the yielding behaviour. Since the extent of yielding is dependent on the dilation characteristics of the material, the flow rule must accommodate the influence of dilation. In the analysis presented here, the following flow rule applicable to linear Mohr-Coulomb failure has been adopted (Egger, 1973):

$$\epsilon_r^P + a \cdot \epsilon_\theta^P = 0 \quad (3.2)$$

where ϵ_r^P and ϵ_θ^P are the radial and tangential plastic strains, respectively.

The parameter a is the dilation coefficient characteristic of a given yielding material. Zero volumetric strain (no volume change) is represented by $a = 1$. If $a = m$, the associative flow rule for Mohr-Coulomb failure is obtained. For a material with a friction angle (ϕ) of 30° , a value of $a = 3$ is an upper bound for dilation. The associative law assumes that the plastic strain increments

are normal to the failure envelope (normality condition) and thereby generally over-estimates the plastic strains.

Therefore, a non-associative flow rule ($1 < a < m$) is more realistic as illustrated in Figure 3.2.

The compatibility equation for total strains can be written in the general form:

$$\frac{d\epsilon_r}{dr} + (\epsilon_r - \epsilon_t)/r = 0 \quad (3.3)$$

The combination of compatibility (plane strain) and the flow rule enables a solution for the strain field to be obtained.

Assuming a plane strain condition for axisymmetric stress field ($du_z/dr=0$), the following strain-displacement relationships can be derived to determine the radial displacements:

$$\epsilon_r^t = \frac{du_r}{dr} \quad \text{and} \quad \epsilon_t^t = \frac{u_r}{r} \quad (3.4)$$

where ϵ_r^t and ϵ_t^t are the total radial and tangential strains, respectively.

It can be assumed that the plastic strain components ϵ_r^p and ϵ_t^p are zero at the elasto-plastic boundary. The combination of strain compatibility and the flow rule enables the determination of the total strain and displacement fields. A summary of elasto-plastic solutions applicable to isotropic, axi-symmetric yielding is given in Appendix A.

3.1.1 Application to Physical Models

The main difference between a real tunnel and the physical model considered in this study is that in reality, a tunnel is excavated in a pre-stressed body subjected to in-situ stresses. Therefore, the deformation of the model is greater than that of the real tunnel by the initial elastic deformation of the intact plate (Figure 3.3).

The elastic convergence under hydrostatic field stress for the real and model tunnel are given by:

$$u_a(\text{real}) = \sigma_0 \cdot a(1+\nu)/E = \sigma_0 \cdot a/2G \quad (3.5)$$

$$u_a(\text{model}) = 2\sigma_0 \cdot a(1-\nu^2)/E = \sigma_0 \cdot a(1-\nu)/G \quad (3.6)$$

The shear modulus (G) is given by: $G = \frac{E}{2(1+\nu)}$

In other words, the elastic convergence of the model is $2(1-\nu)$ times greater than that of a real tunnel excavated in a pre-stressed body. However, under any field stress responsible for significant yielding, the magnitude of plastic strains generally dominate the total strains. This is particularly true for weak materials with a relatively low post-peak strength and a high dilation coefficient. Therefore, the difference in elastic convergence due to the initial pre-stress of a real tunnel can often be neglected.

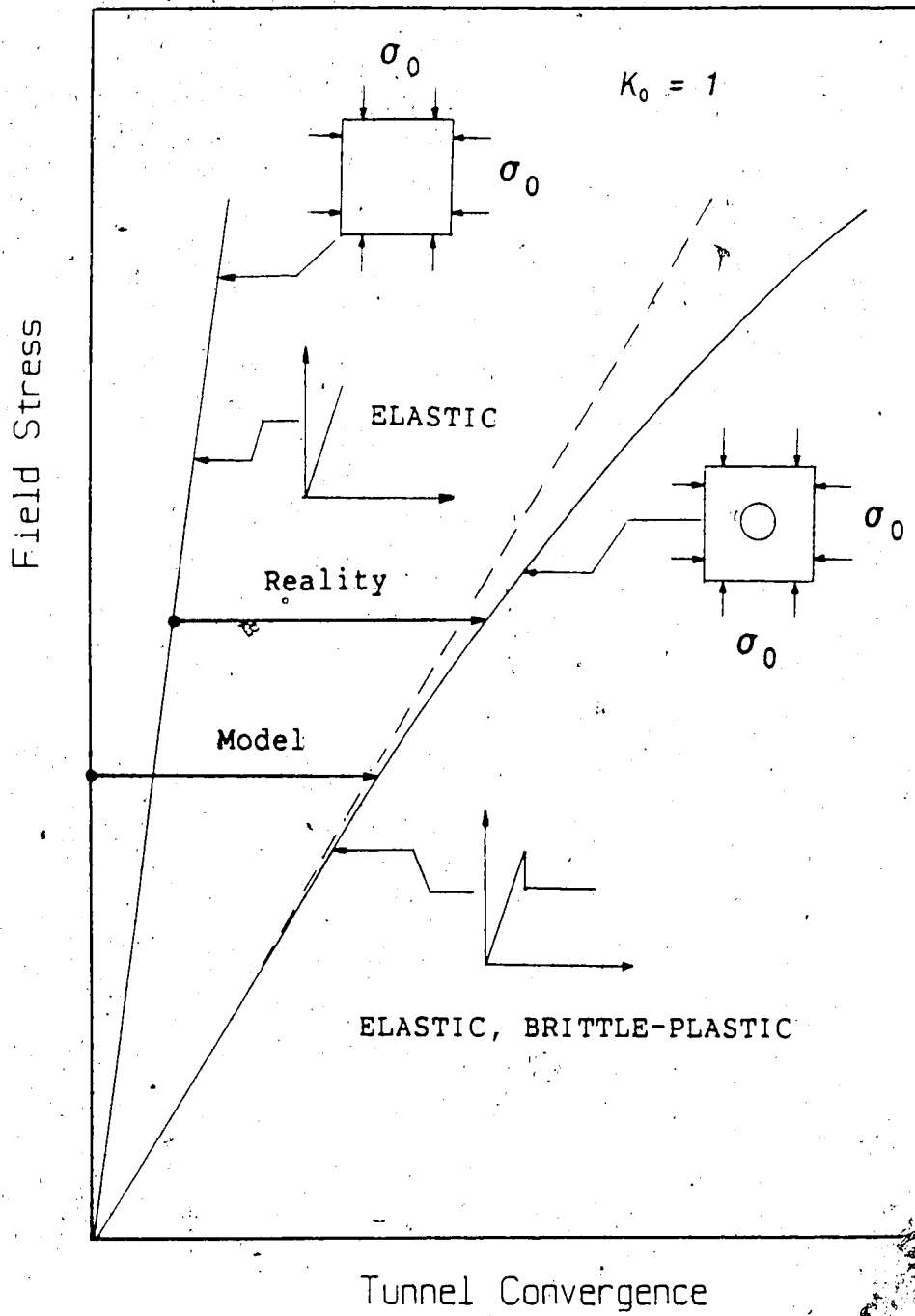


Figure 3.3 Comparison of Model Tunnel with Reality

3.2 Assumptions and Analytical Considerations

The extent of yielding (plastic zone radius) is dependent on the material properties of the rock, the in-situ field stress and the tunnel radius. Yielding may be followed by rupture of the wall if uncontrollable deformations occur in weak ground. It is the objective of bolting to minimize large displacements in order to maintain a coherent load bearing ring around the tunnel. The installation of bolts effectively improves the apparent material properties of the rock mass thereby reducing strains and displacements. The application of elasto-plasticity to the design of underground excavations has been introduced recently by Kaiser *et al.*, 1985. The analysis presented here constitutes an extension of this approach, to assess the influence of fully grouted (frictional) rock bolts on the tunnel behaviour.

The following major assumptions have been made:

1. Deep circular excavation in hydrostatic stress field ($K_0 = 1$).
2. Homogeneous, isotropic material with time-independent properties.
3. Elastic, brittle-plastic strength model (Figure 3.1) with a linear Mohr-Coulomb failure criterion (σ_c, ϕ). Plastic deformations follow a flow rule with a constant rate of dilation ($1 < a < m$).
4. Deformation pattern near the tunnel is properly described by plane strain condition. Three dimensional

- effects at tunnel face are neglected. Plastic deformations follow a non-associative flow rule with a coefficient of dilation, $1 < \alpha < m$, (Equation 3.1 and Figure 3.2).
5. Shear stress distribution along the fully grouted bolts is assumed by the model illustrated in Figure 3.4. The influence of the relatively thin grout annulus on rock mass deformation has been ignored.
 6. Axisymmetric bolt pattern around the excavation (Figure 3.5), consists of identical bolts with equal spacing along the tunnel axis and around the circumference. The tangential bolt spacing around the opening is defined by the product of the tunnel radius and the angle between two adjacent bolts (i.e. $S_T = a \cdot \theta$)
 7. The increase of the apparent elastic modulus (E) of the rock mass due to the presence of relatively stiff steel bolts around the tunnel is not modelled by the proposed analytical solution.

3.2.1 Stress Distribution Along Fully Grouted Bolts

A model for the stress distributions associated with grouted bolts has been proposed by Freeman (1978) and Sun Xueyi (1984), based on field observations (Figure 3.4). Tao and Chen (1984), have independently investigated the behaviour of grouted bolts in yielding rock and have supported the latter model with theoretical verification. Observations from the Kielder tunnel (Freeman, 1978) and the

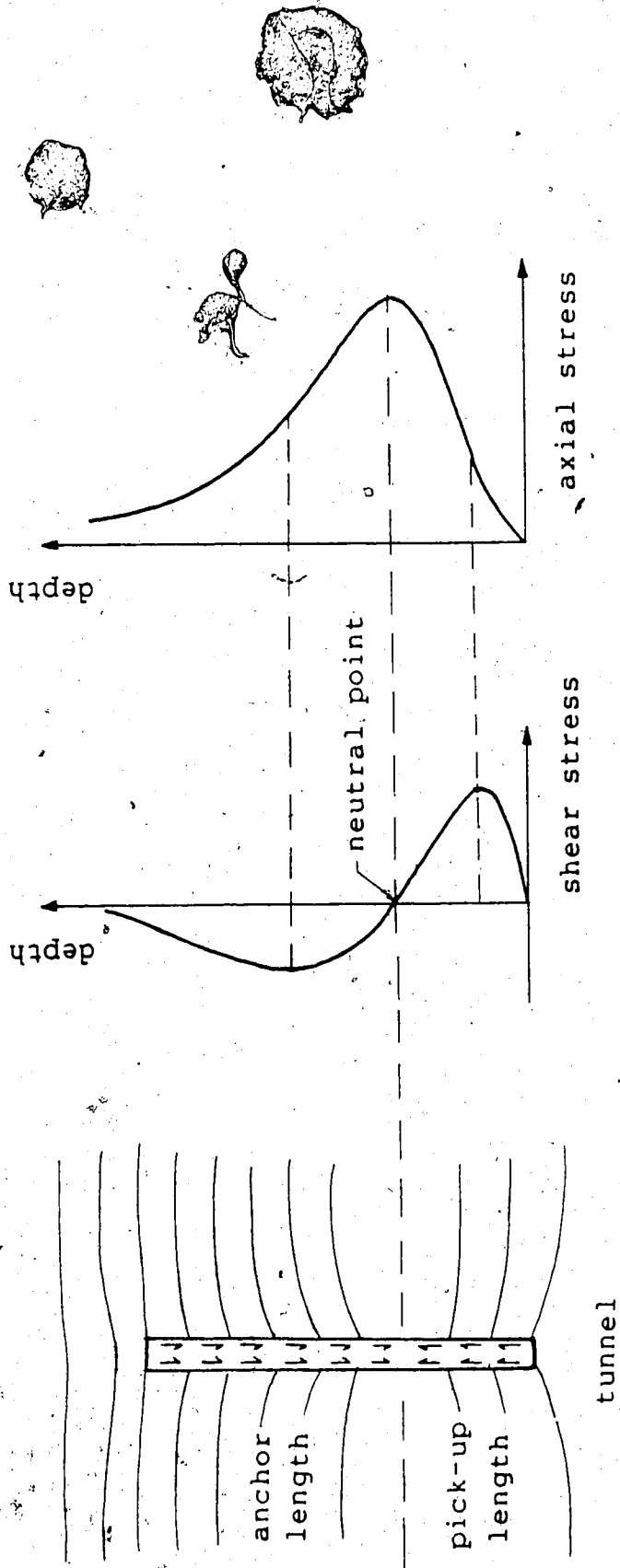
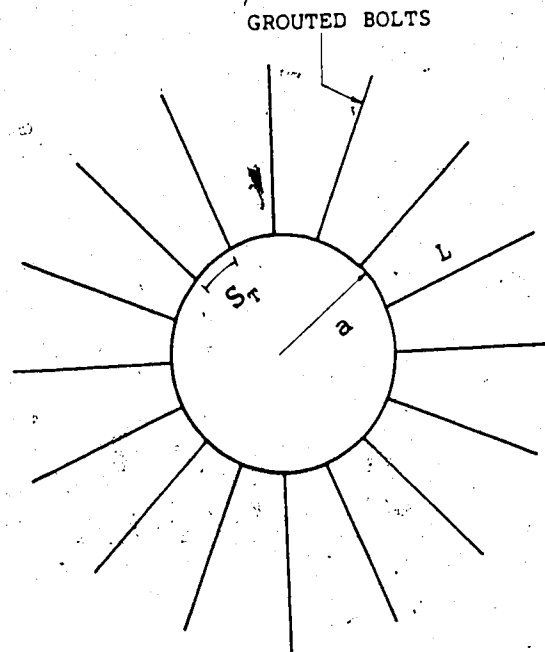
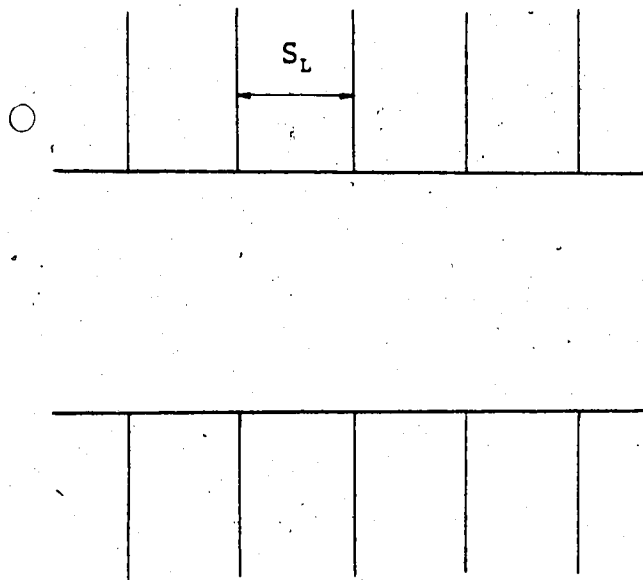


Figure 3.4 Stress Distribution Model for Grouted Bolts



(A) THE TRANSVERSE SECTION



(B) THE LONGITUDINAL SECTION

Figure 3.5 Fully Reinforced Circular Excavation

Kiirunavaara Mine (Björnfot and Stephansson, 1984) have provided most convincing evidence in support of the fact that in yielding ground, a fully grouted bolt is essentially divided into a pick-up length and an anchor length. The pick-up length restrains the rock from deforming, whereas the anchor length is restrained by the rock. The positive shear stresses developed on the pick-up length oppose the displacement of rock towards the excavation. The equilibrium of the grouted bolt relative to the ground is ensured by the negative shear stresses acting along the anchor length. The change in direction of the shear stresses creates a neutral point on the bolt, where the relative displacement between the bolt and the surrounding ground is essentially zero.

The shear stress distribution (τ_z) is given by:

$$\tau_z = - \frac{1}{\pi \cdot d} \cdot \frac{dQ(z)}{dz} \quad (3.7)$$

where: d = bolt diameter and $Q(z)$ = axial stress distribution along the bolt.

The neutral point of the bolt has been determined theoretically by Tao and Chen (1984), as given by:

$$\rho = \frac{L}{\ln[1 + (L/a)]} \quad (3.8)$$

where: ρ = radial distance to the neutral point, L = bolt length and a = tunnel radius.

Tanimoto *et al.* (1981) have shown independently, that the neutral point occurs near the mid-point of the bolt in many instances. In fact, Equation 3.5 can be simplified by algebraic expansion to yield: $a + 0.45L$.

3.3 Influence of Bolted Element Length Parameters

The equilibrium of an unsupported opening (Figure 3.6a) can be represented by:

$$\frac{d\sigma_r}{dr} + (\sigma_r - \sigma_\theta)/r = 0; \quad \tau_{r\theta} = 0. \quad (3.9)$$

Combination of the linear Mohr-Coulomb failure criterion (Eqn. 3.1) with equilibrium leads to the following:

$$\frac{d\sigma_r}{dr} + (1-m)\sigma_r/r = \sigma_{cr}/r \quad (3.10)$$

where: $m = \tan^2(\pi/4 + \phi/2)$ and $\sigma_{cr} = s \cdot \sigma_c$.

In a bolted element (Fig. 3.6b), the additional radial force due to shear stresses along the bolt is assumed to be given by: $\Delta\tau = \pi \cdot d \cdot \sigma_\theta \cdot \lambda \cdot dr$. The equilibrium condition for this segment of longitudinal length S_L is given by the following equation:

$$\frac{d\sigma_r}{dr} + [1 - m(1+\beta)]\sigma_r/r = \sigma_{cr}(1+\beta)/r \quad (3.11)$$

where: $\beta = \frac{\pi \cdot d \cdot \lambda}{S_L \cdot \theta} = \frac{\pi \cdot d \cdot \lambda \cdot a}{S_L \cdot S_T}$ as $S_T = a \cdot \theta$.

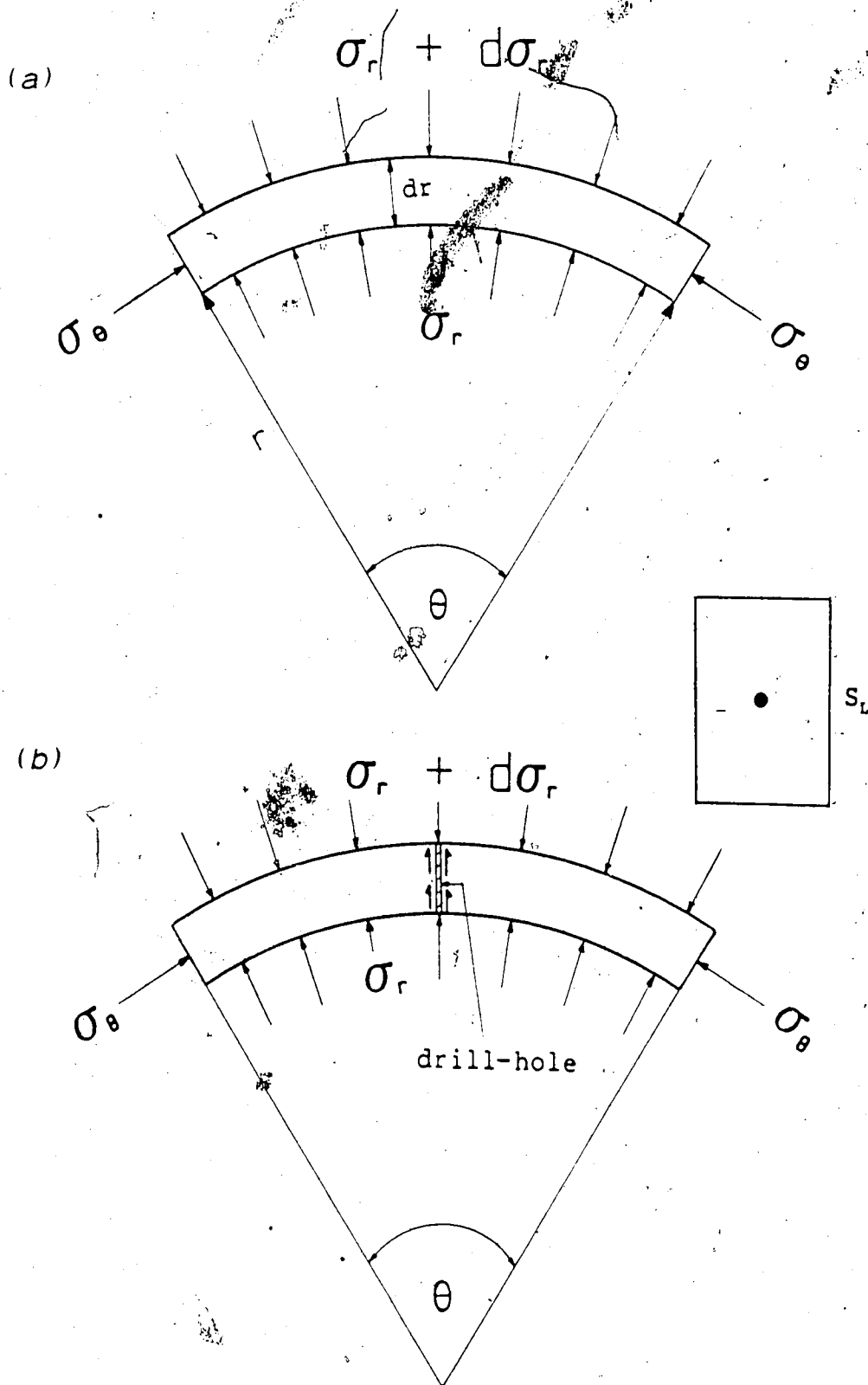


Figure 3.6 Analysis of Bolt-Ground Interaction

β is a dimensionless parameter, that reflects the relative density of bolts with respect to the tunnel perimeter. It takes into consideration the shear stresses on the bolt surface, which oppose the rock mass displacements near the tunnel wall.

The friction factor, λ , is analogous to the coefficient of friction or the bond angle. It relates the mean mobilized shear strength to the stress applied normal to the bolt surface. Theories of reinforced earth as well as the analysis of split sets and other friction bolts consider a similar parameter (Wijk and Skogberg, 1982; Bacot *et al.*, 1978; Schlosser and Elias, 1978). The magnitude of λ for smooth rebars falls in the range $\tan(\phi_g/2) < \lambda < \tan(2\phi_g/3)$ and for shaped rebars approaches $\tan\phi_g$, depending on the degree of adhesion (bond strength) at the bolt/grout interface. The friction angle of a hardened grout (cement or resin) is comparable to that of most intact rocks.

Failure of a bolt-ground composite takes place across the weakest interface unless the bolt itself yields. The product of the hole diameter and the bond strength of the grout/rock interface is higher than the product of the bolt diameter and the bond strength of the bolt/grout interface (i.e. $d_h \tau_{gr} > d_b \tau_{bg}$). Hence, failure generally occurs by the bolt 'pulling out' as often observed in the case of smooth rebars. Such failure of grouted bolts can be prevented by shaping of the bolt surface which increases the magnitude of λ . However, failure may initiate across the grout annulus or

at the grout/rock interface, due to impaired strength development of the grout or the poor adhesion between the grout and the borehole.

3.4 Concept of Equivalent Strength Parameters

By introducing $m^* = m(1+\beta)$ and $\sigma_{cr}^* = \sigma_{cr}(1+\beta)$, Equation 3.11 for the bolted composite can be simplified as follows:

$$\frac{d\sigma_r}{dr} + (1-m^*)\sigma_r/r = \sigma_{cr}^*/r \quad (3.12)$$

Comparison of the latter with Equation 3.10 for the unsupported case indicates that both equations have the same algebraic structure. Defining an *equivalent* friction angle and uniaxial compressive strength for the reinforced rock mass as ϕ^* and σ_c^* , the following expressions can be readily obtained:

$$\begin{aligned} \phi^* &= \sin^{-1} \left[\frac{\beta(1 + \sin\phi) + 2 \cdot \sin\phi}{\beta(1 + \sin\phi) + 2} \right] \\ &= \sin^{-1} \left[\frac{m(1+\beta) - 1}{m(1+\beta) + 1} \right] \end{aligned} \quad (3.13)$$

$$\sigma_c^* = \sigma_c(1 + \beta) \quad (3.14)$$

The above equations are graphically illustrated in Figures 3.7 and 3.8.

Grouted bolts create a zone of improved, reinforced rock in the region defined by the pick-up length of the

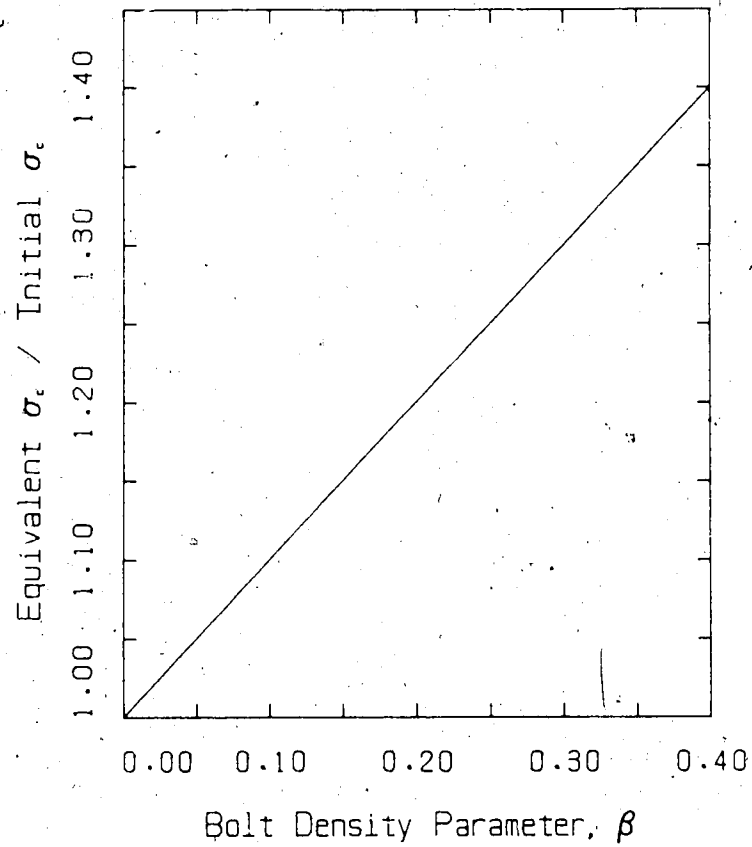


Figure 3.7 Variation of the Equivalent Compressive Strength with β

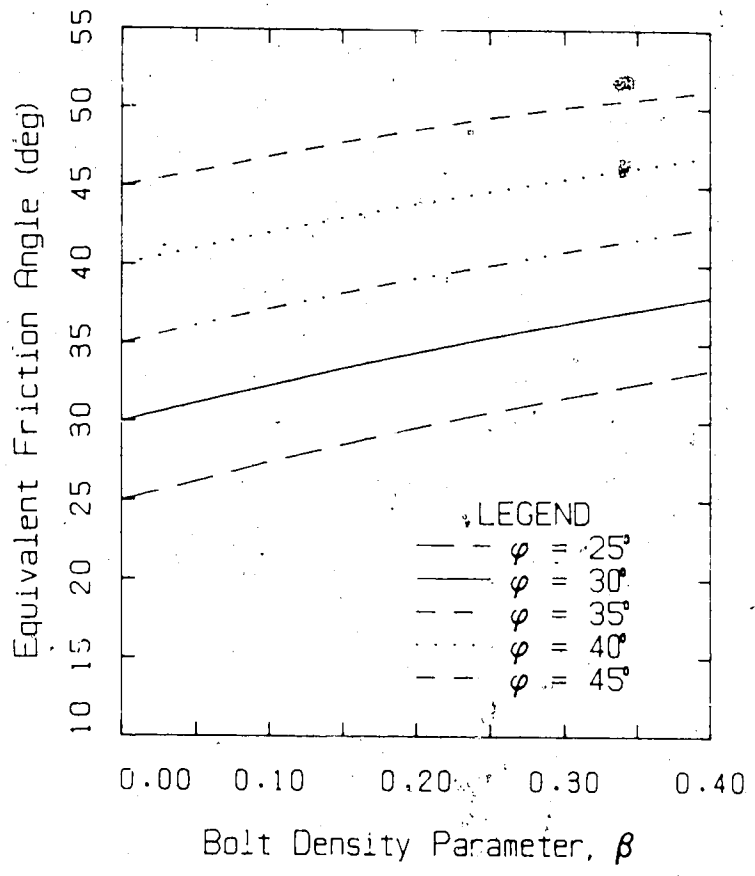


Figure 3.8 Variation of the Equivalent Friction Angle with β

bolts. Within this zone, the friction angle and the uniaxial compressive strength of the rock mass are increased. Therefore, the degree of stabilization around the tunnel wall is a function of the bolt density parameter β .

The magnitude of β can be increased by;

- a. decreasing the bolt spacing,
- b. increasing the bolt surface area,
- c. increasing the roughness of bolt surface.

John (1976) and Hoek and Brown (1980) have also recognized the increase in apparent strength parameters due to fully grouted bolts.

3.4.1 Determination of the Bolt Density Parameter

In practice, the value of β varies between 0.05 and 0.20 for most cases. In a few case histories such as at the Enhasan Tunnel (discussed later) very high values for β (greater than 0.40) were reached by very intensive bolting. Several examples documented in the literature are shown in Table 3.1. As an illustration for determining β , consider the following example, of a tunnel ($a = 5.1$ m) excavated in highly fractured rock ($\phi = 35^\circ$, $c = 0$), supported by bolts ($d = 32$ mm) at spacings of $S_L = 1.3$ m, $S_T = 1.0$ m. Assuming for shaped (rough) rebars, $\lambda = 0.6$, the bolt density parameter β becomes 0.118 or $\beta/\lambda = 0.20$.

Table 3.1 Summary of β/λ Ratios Determined from Several Case Histories

a (m)	d (mm)	S_L (m)	S_T (m)	β/λ	L (m)	Source
10.4	29	1.5	1.5	0.41	7.6	Bawa and Bumanis (1972)
4.5	27	1.5	2.0	0.12	3-6	John (1976)
1.65	25	0.9	0.9	0.16	1.8	Freeman (1978)
5.0	25	1.0	1.0	0.37	6-9	Ito (1983)
2.00	15	0.8	0.8	0.16	1.5	Sun (1984)
2.6	18	0.9	0.9	0.18	1.8	Sun (1984)
3.0	20	1.0	1.0	0.19	2.5	Liu and Huang (1984)

3.5 Influence of Bolt Length on Tunnel Wall Stability

One other important parameter for controlling displacements, i.e., the bolt length, is not included in the bolt density parameter because the effect of a bolt depends on its length relative to the radius of the yield zone. The shear stress distribution and, hence, the location of the neutral point are directly related to the bolt length, the extent of the plastic zone and the strength reduction in this zone. As it will be shown later, the extent of the yield zone and the tunnel wall displacements can be effectively reduced by increasing the bolt length.

3.6 Concept of Equivalent Plastic Zone

Grouted bolts have the effect of improving the weakened or loosened zone by increasing its apparent strength (σ_c and ϕ). The extent of the plastic zone is directly related to the rock mass properties and therefore, any improvement of the rock strength must reduce the extent of overstressed rock. Consequently, the plastic zone of a bolted tunnel is lower than that of an unsupported tunnel. It is termed 'Equivalent Plastic Zone' because it is the yield zone in a material of improved properties simulating a behaviour equivalent to the bolted rock mass. The following factors directly affect the magnitude of the 'Equivalent Plastic Zone':

- (a) Bolt density parameter β ;
- (b) Bolt length L ;

- (c) Radius to the neutral point of the bolt ρ ;
- (d) Tunnel radius a ; and
- (e) Field stress σ_0 .

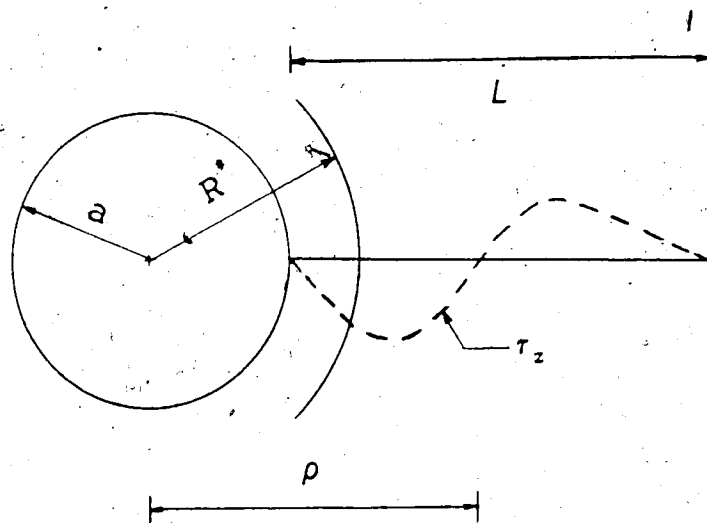
The determination of the equivalent plastic zone radius, R^* , must be divided into three categories depending on the boundary of the equivalent plastic zone relative to the neutral point and the bolt length:

- (I) $R^* < \rho < (a+L)$ (minimal yielding);
- (II) $\rho < R^* < (a+L)$ (major yielding);
- (III) $R^* > (a+L)$ (excessive yielding).

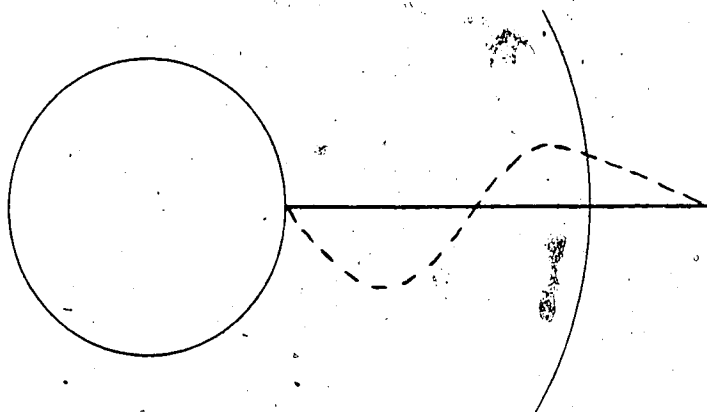
These three categories are diagrammatically illustrated in Figure 3.9.

3.6.1 Determination of the Equivalent Plastic Zone Radius

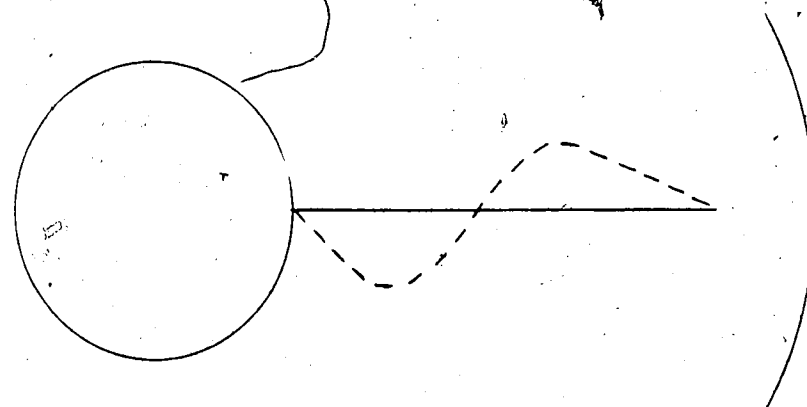
The condition of minimal yielding ($R^* < \rho < a+L$) occurs, either at relatively small field stresses or when the bolts are excessively long. In this situation, the extent of the plastic zone is confined within the pick-up length of the bolt. In addition, four distinct zones can be identified by the location of the plastic zone relative to the neutral point and the bolt ends.



(I) $R^* < \rho < (a+L)$ (minimal yielding)



(II) $\rho < R^* < (a+L)$ (major yielding)



(III) $R^* > (a+L)$ (excessive yielding)

Figure 3.9 Categorization of the Extent of Yielding

3.6.1.1 Zone 1: $a < r < R^*$

In this region of the pick-up length, the ground displacements towards the opening are resisted by the positive shear stresses. The equivalent stress fields in this zone are represented by:

$$\sigma_r = \left[\frac{s \cdot \sigma_c^*}{m^* - 1} \right] \left\{ (r/a)^{m^* - 1} - 1 \right\}$$

$$\sigma_\theta = m^* \cdot \sigma_r + s \cdot \sigma_c^* \quad (3.15)$$

where: $m^* = m(1 + \beta)$ and $\sigma_c^* = \sigma_c(1 + \beta)$

3.6.1.2 Zone 2: $R^* < r < \rho$

This part of the elastic zone is confined to the pick-up length of the bolt. The elastic stress fields in this zone are given by:

$$\sigma_r = \sigma_0 [1 - (R^*/r)^2] + \sigma_R \cdot (R^*/r)^2$$

$$\sigma_\theta = \sigma_0 [1 + (R^*/r)^2] - \sigma_R \cdot (R^*/r)^2 \quad (3.16)$$

The peak tangential stress at the elasto-plastic boundary is given by the following condition ($s=1$):

$$\sigma_\theta = m^* \cdot \sigma_r + \sigma_c^*$$

The radial stress at the elasto-plastic boundary σ_R is derived by substituting $r = R^*$ in the latter equations:

$$\sigma_R = \frac{2\sigma_0 - \sigma_c^*}{m^* + 1}$$

3.6.1.3 Zone 3: $\rho < r < (a+L)$

This part of the elastic zone is contained within the anchor length of the bolt. The radial and tangential stress fields are given by:

$$\begin{aligned}\sigma_r &= \sigma_0[1 - (\rho/r)^2] + \sigma_\rho \cdot (\rho/r)^2 \\ \sigma_\theta &= \sigma_0[1 + (\rho/r)^2] - \sigma_\rho \cdot (\rho/r)^2\end{aligned}\quad (3.17)$$

where: $\sigma_\rho = \sigma_0[1 - (R^*/\rho)^2] + \sigma_R \cdot (R^*/\rho)^2$

3.6.1.4 Zone 4: $r > (a+L)$

This is the outermost elastic region which is beyond the bolt, and can be regarded as virgin rock. The elastic stresses in this zone are given by:

$$\begin{aligned}\sigma_r &= \sigma_0\{1 - [(a+L)/r]^2\} + \sigma_L[(a+L)/r]^2 \\ \sigma_\theta &= \sigma_0\{1 + [(a+L)/r]^2\} - \sigma_L[(a+L)/r]^2\end{aligned}\quad (3.18)$$

where: $\sigma_L = \sigma_0\{1 - [\rho/(a+L)]^2\} + \sigma_\rho[\rho/(a+L)]^2$

The radial distance to the neutral point, ρ , is given by Equation 3.8 as discussed earlier.

At the elasto-plastic boundary, the assumption of the continuity of radial stress gives:

$$\sigma_R = \frac{2\sigma_0 - \sigma_c^*}{m^* + 1} = \left[\frac{s \cdot \sigma_c^*}{m^* - 1} \right] \{ (R^*/a)^{m^* - 1} - 1 \} \quad (3.19)$$

The solution of Equation 3.19 is given by:

$$\frac{R^*}{a} = \left[1 + \frac{1}{s} \left[\frac{m^* - 1}{m^* + 1} \right] \left[\frac{2\sigma_0}{\sigma_c^*} - 1 \right] \right]^{1/(m^* - 1)} \quad (3.20)$$

It is obvious that when β tends to zero, the parameters m^* and σ_c^* approach m and σ_c respectively. In other words, Equation 3.20 becomes identical to that of the unsupported case as derived by Kaiser *et al.* (1985). Expressions for the equivalent plastic zone radius can be derived for Categories (II) and (III) in the same manner (Appendix B). A summary is given below.

The condition of major yielding ($\rho < R^* < a+L$) occurs when the extent of the plastic zone has propagated beyond the neutral point. In this situation, the plastic zone itself is divided into two parts by the neutral point. Consequently, only the plastic zone region that falls within the pick-up length of the bolt is effectively stabilized by the positive shear stresses. The equivalent plastic zone radius is given by:

$$\frac{R^*}{a} = \frac{\rho}{a} \left[\frac{1 + B_1}{1 + A_1} \right]^{1/(m-1)} \quad (3.21)$$

where: $B_1 = \frac{1}{s} \left[\frac{m-1}{m+1} \right] \left[\frac{2\sigma_0}{\sigma_c} - 1 \right]$

and $A_1 = \left[\frac{m-1}{m'-1} \right] \left[\frac{1+\beta}{1-\beta} \right] \{ (\rho/a)^{m'-1} - 1 \}$

The condition of excessive yielding occurs ($R^* > a+L$) either due to large in-situ stresses in relatively weak rock or as a result of inadequate bolt lengths. In this situation the bolt is completely embedded in the yielded rock and no anchorage is provided from the outer elastic zone. The radius of the equivalent plastic zone is given by:

$$\frac{R^*}{a} = [1 + (L/a)] \left[\frac{1 + B_1}{1 + A_2 + A_3} \right]^{1/(m-1)} \quad (3.22)$$

where: $B_1 = \frac{1}{s} \left[\frac{m-1}{m+1} \right] \left[\frac{2\sigma_0}{\sigma_c} - 1 \right]$

$$A_2 = \left[\frac{m-1}{m'-1} \right] \left[[(a+L)/\rho]^{m'-1} - 1 \right]$$

$$A_3 = (1+\beta) \left[\frac{m-1}{m'-1} \right] [(a+L)/\rho]^{m'-1} \{ (\rho/a)^{m'-1} - 1 \}$$

$$m^* = m(1+\beta) \quad \text{and} \quad m' = m(1-\beta)$$

The terms A_2 and A_3 may be simplified by assuming that $m' \approx m$ at $r=a+L$ (bolt end). The derivations for Categories II and III are given in Appendix B. The strain and displacement fields are determined by the application of Hooke's law,

strain compatibility, flow rule and strain-displacement relationships as discussed earlier.

Evidence to support the analytical predictions has been obtained by laboratory simulations of a model tunnel (130 mm radius) and will be presented later. An artificial rock with the following properties was tested: $E = 1500$ MPa, $\nu = 0.25$, $\phi = 32^\circ$, $\sigma_c = 3.5$ MPa, $s = 0.90$ and $a = 2.0$. Elaborate details of the experimental procedure are summarized in Chapter 5. The predicted stress, strain and displacement fields for this model tunnel, reinforced with 100 mm brass bolts and subjected to a far field stress of 14 MPa are presented in Figures 3.10 to 3.12. Different bolt patterns ($\beta = 0$ to 0.291) are illustrated for comparison. A friction factor $\lambda = 0.36$ has been assumed for the smooth brass bolts. It can be seen from Figure 3.10 that as the bolt density parameter β increases, the radial and tangential stress fields approach those predicted for non-yielding, elastic rock, and the radius of equivalent plastic zone (R^*) approaches the tunnel radius. Further away from the tunnel, the stress field approaches the far field stress.

The strain field, illustrated in Figure 3.11, shows a similar trend. As β increases, the radial and tangential strains approach the elastic solution. The pronounced reduction of the total tangential strain (ϵ_θ) inside the overstressed zone at the elasto-plastic boundary, indicates 'strengthening' of the yielded material by the bolts. The accumulated effect of strain reduction is reflected in a

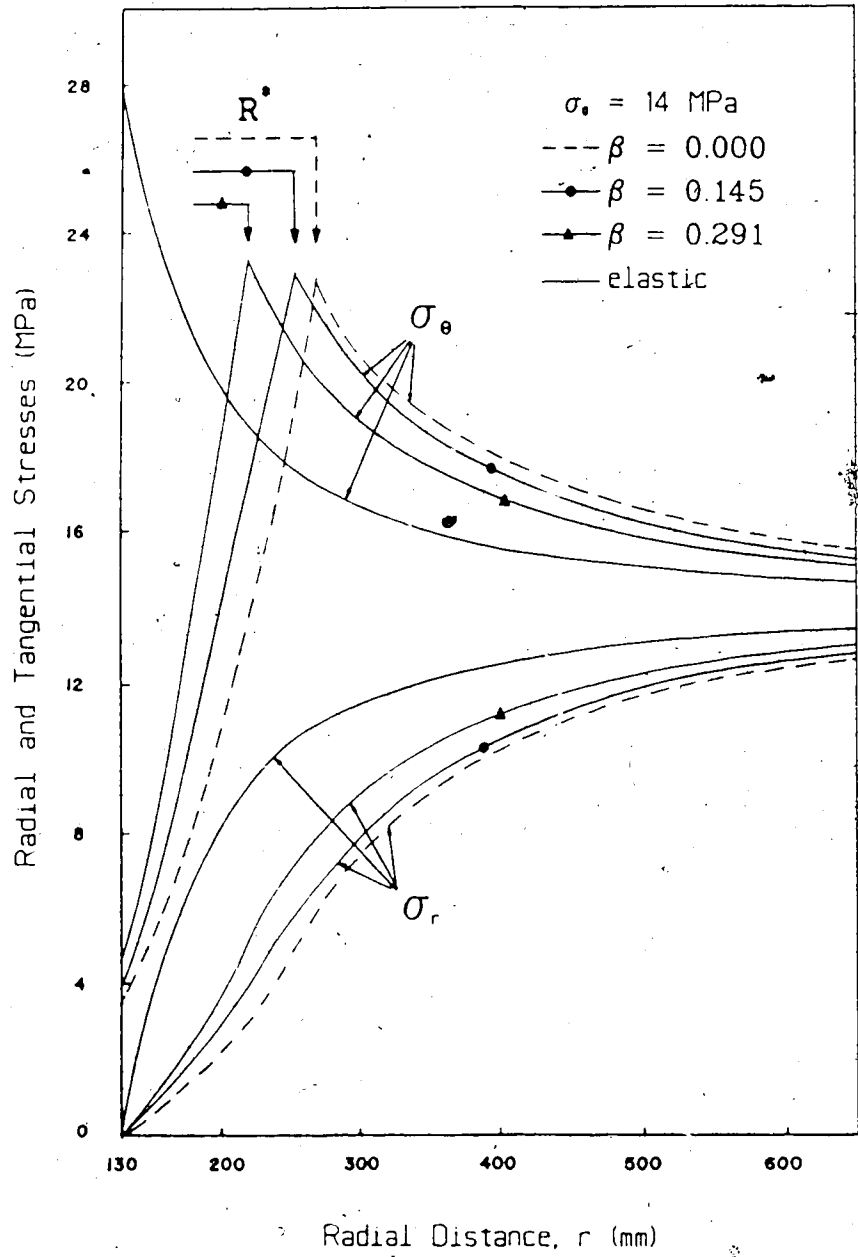


Figure 3.10 Stress Field near the Tunnel Opening

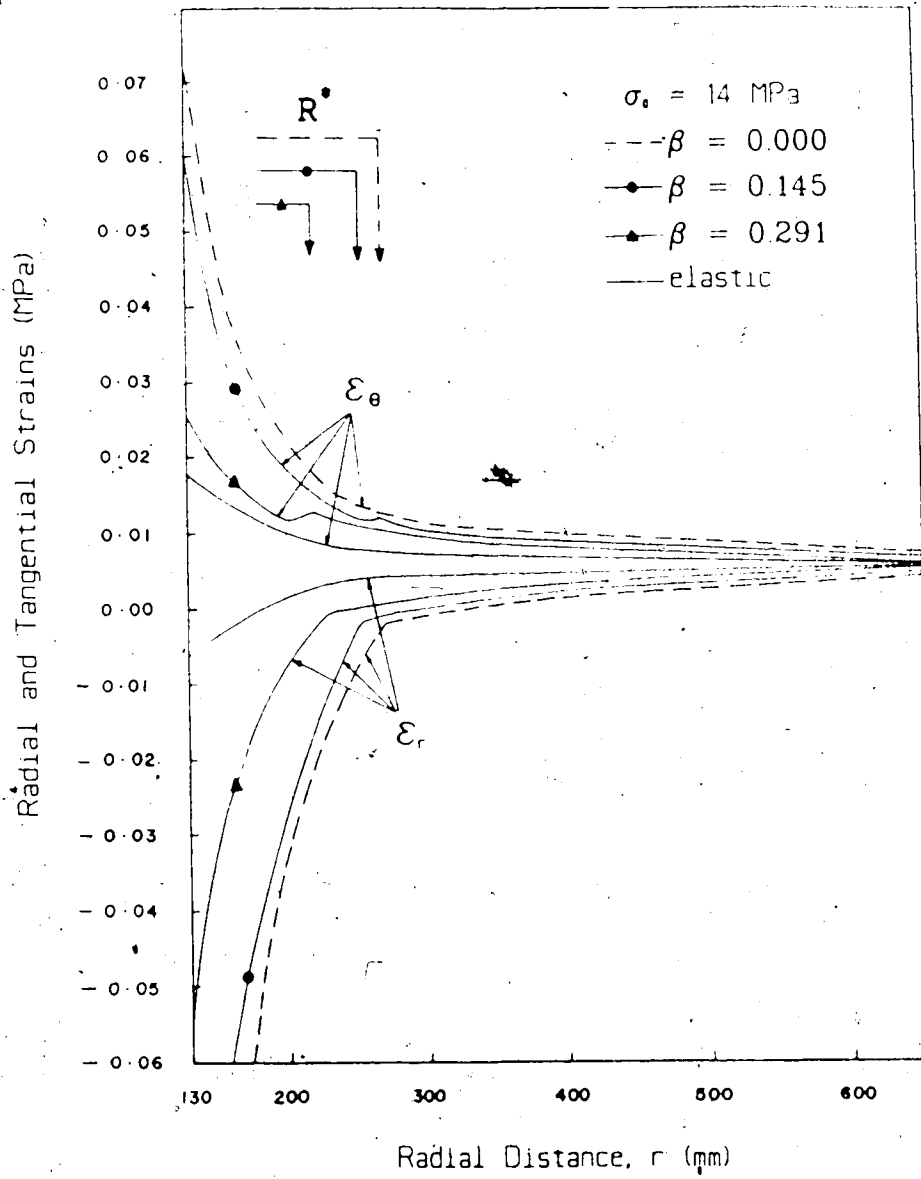


Figure 3.11 Strain Field near the Tunnel Opening

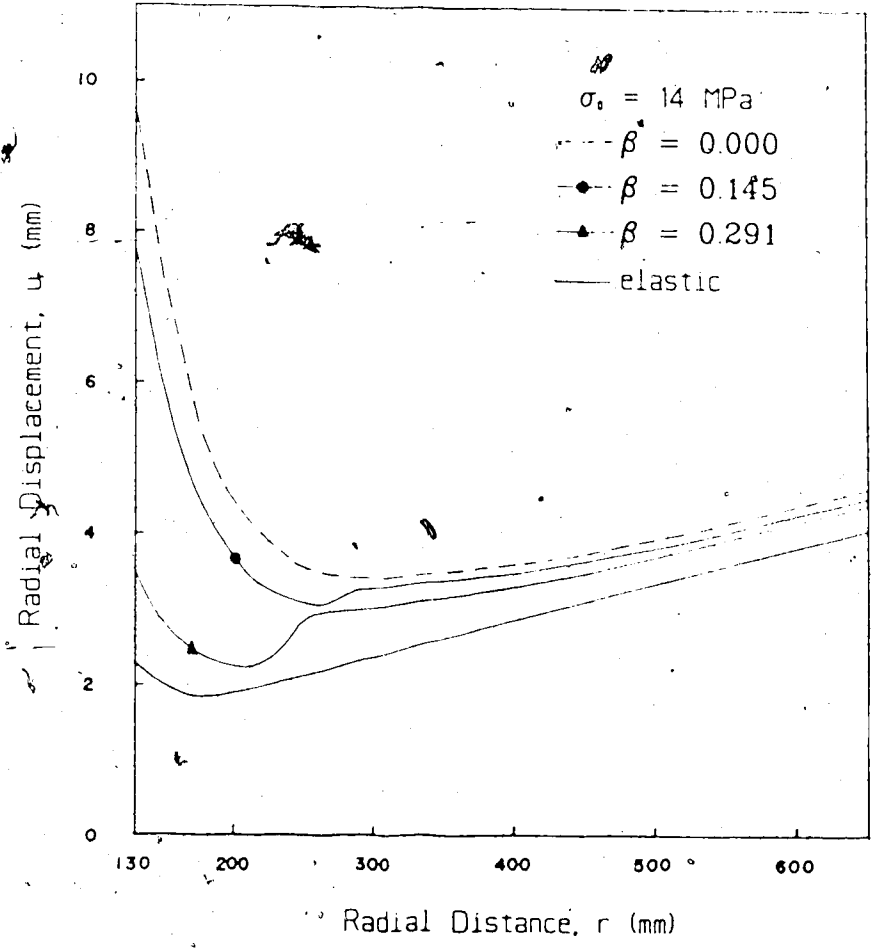


Figure 3.12 Displacement Field near the Tunnel Opening

shift of the radial displacement field (Figure 3.12). As the distance from the tunnel wall increases, the effect of bolting diminishes rapidly and the far field conditions are approached. It is evident that the maximum decrease in strains and radial displacements occurs at the tunnel wall. Hence, the tunnel wall convergence can be considered as the most appropriate parameter for a displacement controlled design approach.

3.7 Influence of Bolts on Tunnel Stability

The radial strains and displacements at the tunnel wall are the most fundamental quantities required to evaluate the stability of a tunnel opening. In the field they are not only feasible to measure but are also generally reliable. The radial strain and convergence of the reinforced tunnel wall can be predicted from the following equations, after the magnitude of R^* has been determined (see Section 3.6) for the respective Categories I to III:

$$\begin{aligned} \epsilon_a^* &= - a(1-\nu)\sigma_{cr}[(m+1)/(m+a)]\{(R^*/a)^{m+a} - 1\}/2G \\ &\quad - a(1-\nu)\sigma_c(1-s)[(R^*/a)^{1+a}]/2G_s - \nu\sigma_c s/2G \end{aligned} \quad (3.23)$$

$$\begin{aligned} u_a^*/a &= (1-\nu)\sigma_{cr}\{1 + [(m+1)/(m+a)][(R^*/a)^{m+a} - 1]\}/2G \\ &\quad + (1-\nu)\sigma_c(1-s)[(R^*/a)^{1+a}]/2G \end{aligned} \quad (3.24)$$

Figure 3.13 illustrates the variation of the predicted convergence of the model tunnel for different bolt patterns (100 mm long brass bolts) and a range of field stresses up to 14 MPa. A sudden shift to the right or increase in convergence occurs in this stress range for bolt densities of 0.072 to 0.220. This transition is found when the radius of the equivalent plastic zone exceeds the bolt length, such that the entire bolt becomes completely embedded in the plastic zone (defined by the equation for Category III; $R^* > a+L$). However, if the rock mass loses its strength more gradually rather than instantaneously, as assumed in the elastic, brittle-plastic model, this shift will be less pronounced in reality and is not expected to be found in the model tests.

3.7.1 Use of Displacement Control Approach for Design

The following example explains the use of the displacement control approach for design. Consider a tunnel of 5 m radius excavated at a depth of 500 m in a relatively weak sedimentary rock with the following representative material properties: $\phi = 35^\circ$, $\sigma_c = 15$ MPa, $E = 6000$ MPa, $\nu = 0.25$, $s = 0.4$ and $a = 2.0$. The predicted convergence of the unsupported tunnel wall is 31.6 mm with a plastic zone radius of 6.42 m. If fully grouted bolts ($\lambda = 0.6$, diameter 32 mm and length 2.5 m) were selected for stabilization of the tunnel wall, with a bolt density parameter $\beta = 0.075$, the extent of the equivalent plastic zone would be reduced

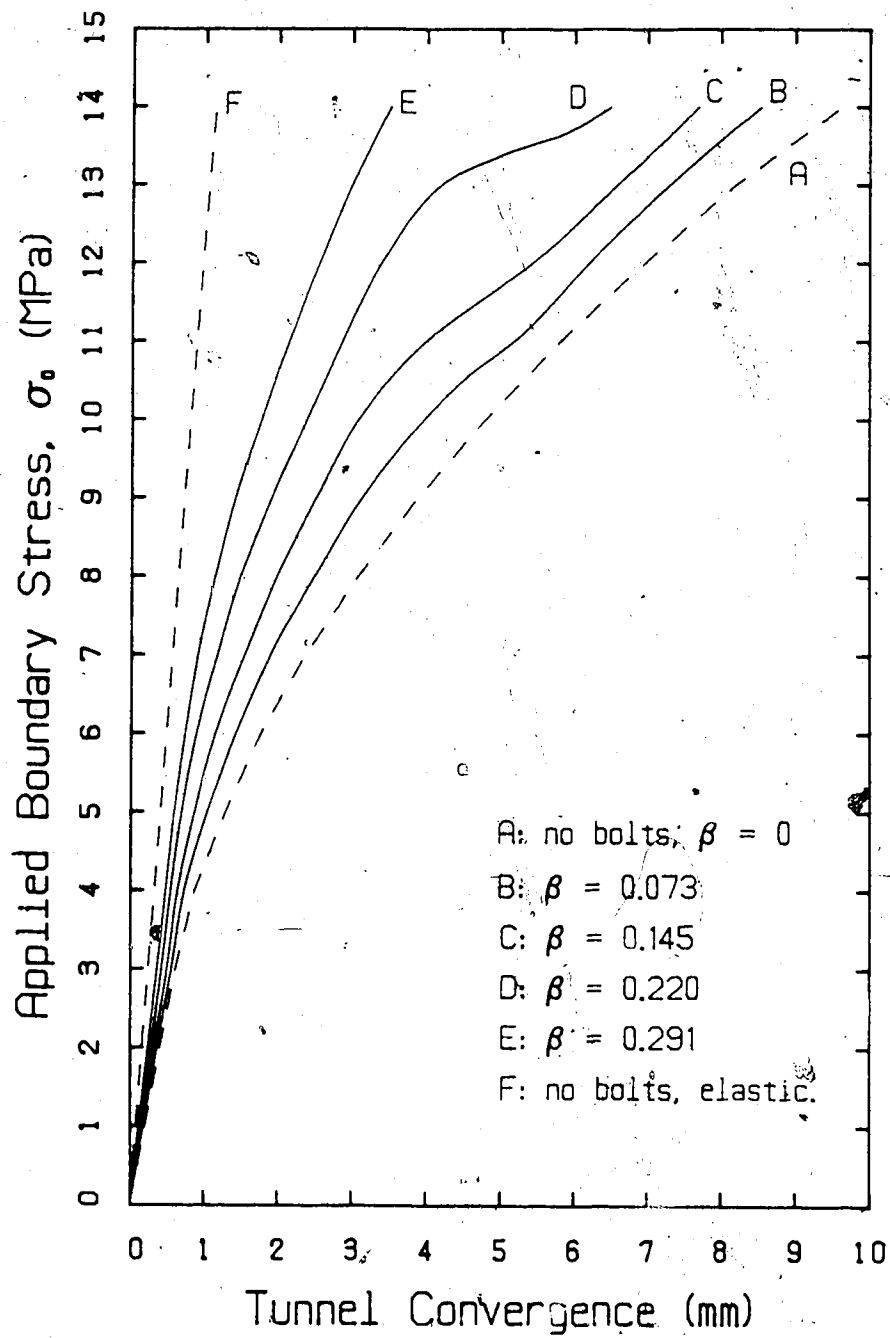


Figure 3.13 Influence of Grouted Bolts on Tunnel Convergence

by 3.1% and the tunnel convergence by 12.0%. However, a greater bolt density of $\beta = 0.17$ would reduce the extent of the plastic zone by 8.0% and the tunnel convergence as much as 29.2%. In this manner, the benefit of increased bolt density can be assessed in a rational manner.

Table 3.2 summarizes typical percentages of reduction of tunnel convergence with respect to the bolt density, for a tunnel excavated in a yielding material with the properties: $\phi = 32^\circ$, $\nu = 0.25$, $E/\sigma_c = 425$, $s = 0.90$, $a = 2.0$, for an excavation with grouted bolts (a/L ratio of 1.30), $\lambda = 0.36$ (smooth rebars) and $\sigma_0 = 14$ MPa. It shows that when relatively short bolts are used in a yielding rock, a high density is required to effectively reduce tunnel wall displacements.

The development of load on a grouted bolt has the effect of providing additional confinement (increased radial stress) in the yielded zone. As a result the tangential stress at the same point is increased more than proportionately, where: $\Delta\sigma_\theta > m \Delta\sigma_r$. The original failure envelope is thereby shifted upwards, indicating an improvement of the apparent strength (σ_c , ϕ), as represented by the Mohr diagram in Figure 3.14. This enables the rock mass to behave as a stronger material with a corresponding reduction in tunnel convergence at a given field stress.

Since fully grouted bolts effectively improve the apparent strength and stiffness of the rock mass, the behaviour of the reinforced opening can be ideally

Table 3.2 Influence of Bolt Density on Tunnel Wall
Convergence, ($a/L=1.3$)

S_T/L	S_L/L	β	% Reduction of convergence
Unsupported		0.000	0.0
0.50	1.00	0.073	10.9
0.50	0.50	0.145	19.8
0.50	0.33	0.220	32.3
0.50	0.25	0.291	63.5

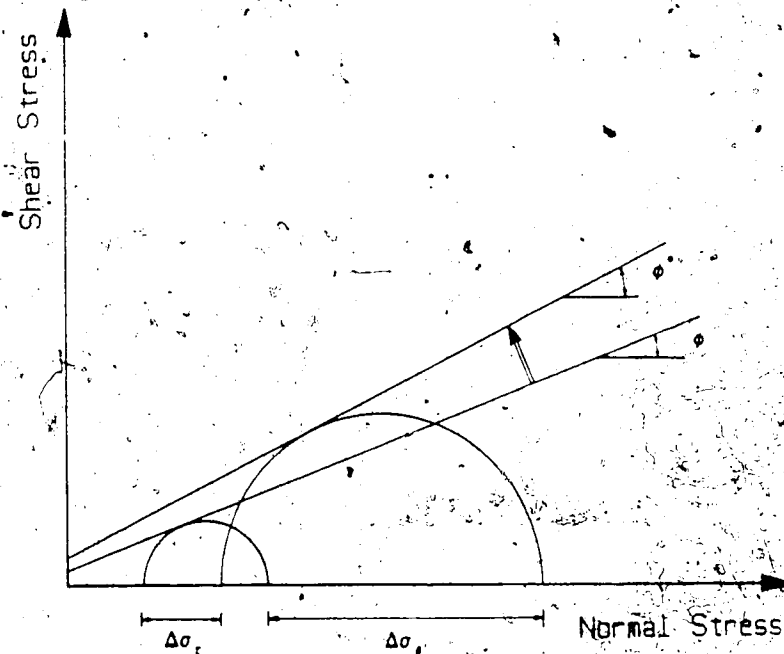


Figure 3.14 Effect of Grouted Bolts on the Failure Envelope

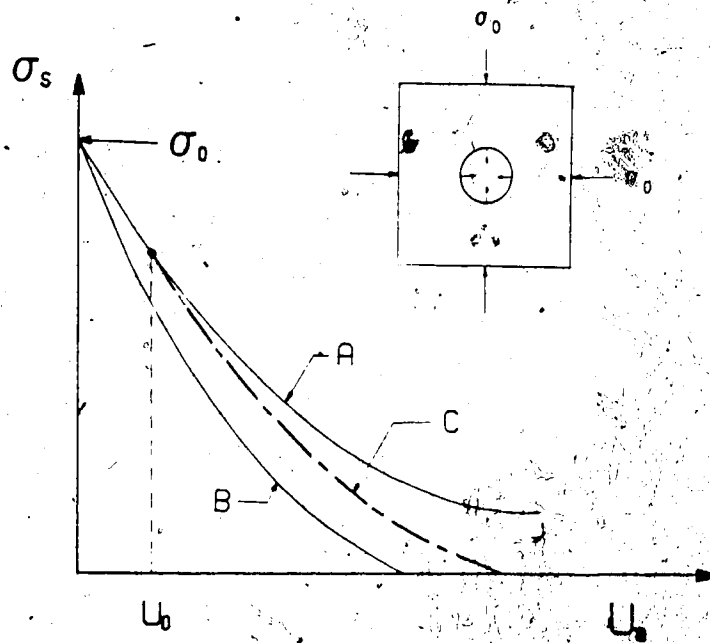


Figure 3.15 Effect of Grouted Bolts on the Ground Reaction Curve

represented by a change in slope of the ground reaction curve. The vertical axis of the ground reaction curve (Figure 3.15) represents the radial stress (σ_r) required at the tunnel boundary to prevent further convergence. The horizontal axis represents the tunnel convergence (u_a). The ground reaction curve is unique for every point along the tunnel boundary for the condition of axisymmetric yielding under hydrostatic field stress.

The response of an unsupported opening in yielding rock is given by Curve A. Curve B represents an imaginary ground reaction curve of the opening, where bolts would have been installed before any displacements could have occurred. Incidentally, Curve B represents a rock mass with a greater stiffness (slope) than Curve A. In reality, an initial displacement (u_0) of the tunnel wall cannot be prevented due to the time lag between excavation and the activation of grouted bolts. The magnitude of convergence after bolting is dependent on the stiffness of the bolt/ground composite (Appendix D), and is reflected by a 'downward shift' of the ground reaction curve from Curve A to C. In contrast to fully grouted bolts, pre-tensioned mechanical bolts provide direct radial pressure (active support) against the tunnel wall, but do not become an integral part of the deforming rock mass. Consequently, their performance is best represented by a support confinement curve with a specific stiffness (Hoek and Brown, 1980) and its interaction with the original ground reaction curve.

3.7.2 Influence of Opening Size and Bolt Length on Tunnel Convergence

It can be deduced from the analysis that the dimensionless ratios β and u_a^*/a are both directly dependent on bolt density parameter (β) and the normalized bolt length (L/a). If β is kept constant for a smaller tunnel excavated in the same homogeneous and isotropic rock, the ratio u_a^*/a is not affected if the bolt length is also reduced proportionately (i.e., scaled reduction). However, if the bolt length remains unchanged for a smaller tunnel radius (larger L/a ratio), the quantity u_a^*/a decreases for the same β . In contrast, for a larger opening the bolt length must be increased accordingly in order to maintain the same u_a^*/a ratio for a given β .

The above predictions may not be accurate for a tunnel excavated in a predominantly jointed medium. This is because, a larger opening intersects a greater number of discontinuities, thereby adopting a behaviour equivalent to that of an excavation in a weaker medium.

3.8 Normalized Convergence Ratio

The convergence of a reinforced tunnel opening can be presented by the dimensionless ratio u_a^*/u_a , where, u_a^* and u_a are the total convergences of the reinforced and unsupported tunnel openings respectively at the same stress level. The total tunnel convergence includes both the elastic and plastic displacements. For any given field stress, u_a is

less than u_a , but it approaches u_a when the bolt density parameter (β) or the bolt length (L) tends to zero (see later: Figure 6.8).

The normalized convergence ratio decreases as the intensity of bolting increases. It obtains a minimum value when u_a tends to u_e , the elastic portion of the total convergence. The latter condition may be approached at very intensive bolt densities such as $\beta > 0.30$, which is not only rare in practice but is economically unattractive. The convergence ratio is particularly useful in the design of grouted bolts, since it reflects the reduction in convergence that can be achieved by a given bolt pattern.

An important characteristic of the convergence ratio is that it is insensitive to moderate changes of the deformation and strength parameters. For instance, a change in Young's modulus affects both u_a and u_e equally, hence the ratio u_a/u_e remains unaltered. The latter characteristic of the normalized convergence ratio makes its use in design even more reliable, since the variations of in-situ geotechnical parameters can be tolerated without any significant error. The application of the convergence ratio in design is discussed in Chapter 6.

3.9 Concept of Bolt Effectiveness

In order to assess the efficiency of bolting, the tunnel convergence is selected as the appropriate evaluation criterion. Obviously, optimal efficiency of a bolt system

corresponds to minimal tunnel convergence that can be achieved within economic limitations. In reality, the total convergence of a yielding, reinforced tunnel wall (u_a) must be less than that of an unsupported opening (u_a^0), but more than the convergence predicted by the linear elastic solution (u_e). Considering these limitations the bolt effectiveness (i) for a given field stress is best defined as:

$$i = \frac{u_a - u_a^0}{u_a - u_e} \% \quad (3.25)$$

The application of the bolt effectiveness in practice will be highlighted by the analysis of one case history in Chapter 7. The bolt effectiveness (i) is sensitive to moderate changes in uniaxial compressive strength and the friction angle. Therefore, its use as a design tool is justified only if the geotechnical properties of the ground are accurately determined.

4. FAILURE MECHANISMS NEAR TUNNELS

4.1 Failure Mechanisms of Intact Rock

The purpose of this section is to predict the potential failure patterns of intact material which can subsequently be compared with actual observations. In the case of a circular opening excavated in a homogeneous, isotropic, material subjected to a hydrostatic field stress, an axisymmetric failure zone is anticipated. Elasto-plastic solutions propose a pattern of logarithmic spiral rupture surfaces for a Mohr-Coulomb material. The intersection of the above slip lines define unstable 'cherrystone' shaped wedges (Figure 4.1) that separate and tend to move into the opening. This phenomenon has been explained by Rabcewicz (1964) and Feder (1978). The locus of these equilateral slip lines is given by the following equation (Jumikis, 1979):

$$r = a e^{f(\phi)} \quad (4.1)$$

where: $f(\phi) = (1 - \sin\phi)/\cos\phi$

The slip lines make an angle of $(\frac{\pi}{4} - \frac{\phi}{2})$ with the tunnel wall, which is analogous to the Rankine stress state at a smooth boundary. They terminate at the boundary between the plastic and elastic zones. If the condition of isotropy is violated 'preferred' slip lines will be formed in directions dictated by weaknesses.

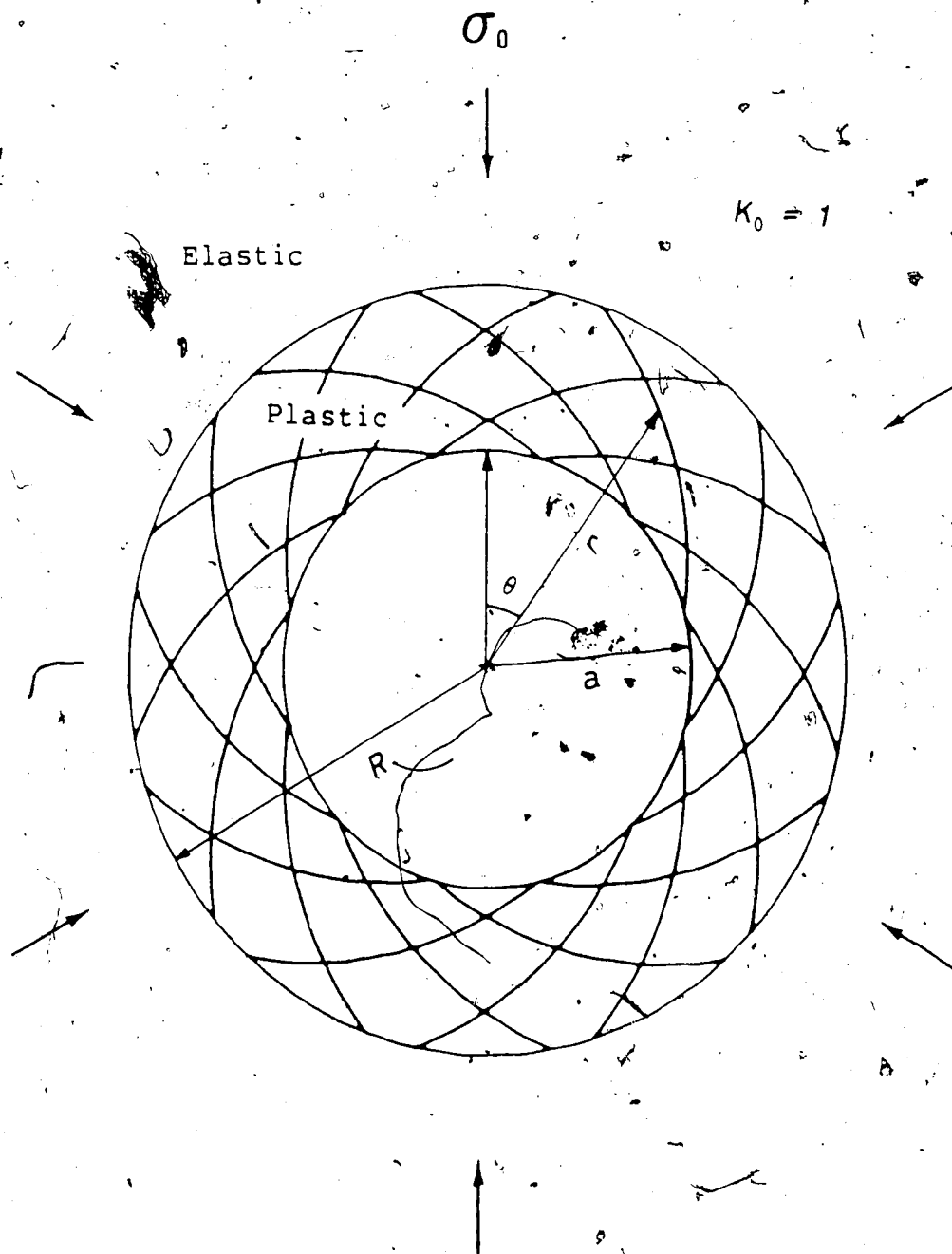


Figure 4.1 Equilateral Spiral Slip Lines in the Plastic Zone

Other rupture processes that have been observed are spalling and extensional slabbing, due to the propagation of tensile cracks near the tunnel wall. Since the radial stress at the tunnel wall is zero, the latter mechanisms can be explained by considering an element at the tunnel wall to be in a state of unconfined compression as shown in Figure 4.2. Both shear and tensile failure are observed in uniaxial compression test specimens. The propagation of equilateral spirals around a circular opening is comparable to the formation of shear planes in an uniaxial test specimen, at an angle of $(\frac{\pi}{4} - \frac{\phi}{2})$ to the direction of the applied stress. The occurrence of 'slabbing' of a tunnel wall is a magnification of the surface instabilities such as tensile splitting that are also observed in some test specimens.

4.1.1 Application of the Bifurcation Theory

The theory of bifurcation and the associated stability curve (Vardoulakis, 1984) can be used to predict the potential failure mechanism for a given material as illustrated in Figure 4.3. The vertical axis represents the ratio of tensile strength to compressive strength (η) of an uniaxial test specimen, and the horizontal axis represents the hardening parameter (N) which is determined from the stress-strain relationship. A linear Mohr-Coulomb material is characterized by $N = 1$. The stability curve separates distinct regions where shear failure predominates in Zone B, surface instability predominates in Zone S and only surface

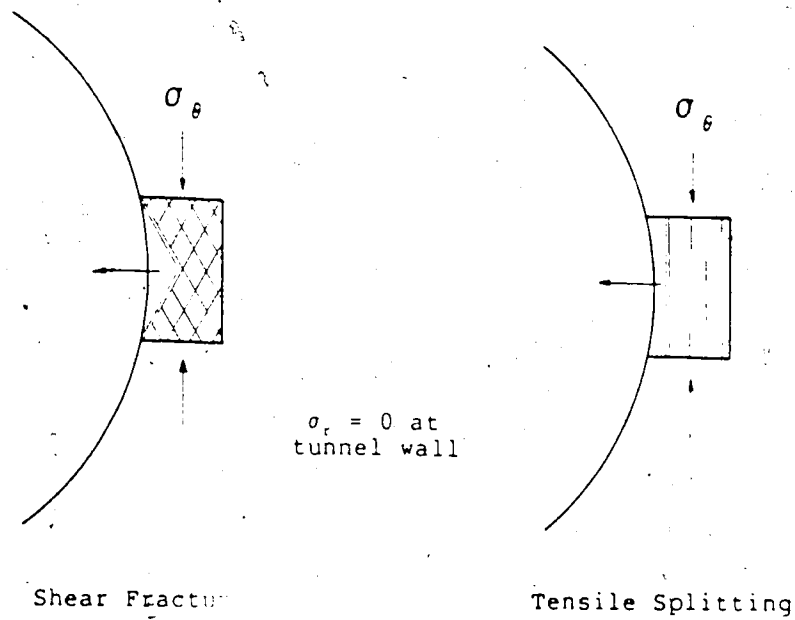


Figure 4.2 Unconfined Compression State at Tunnel Wall

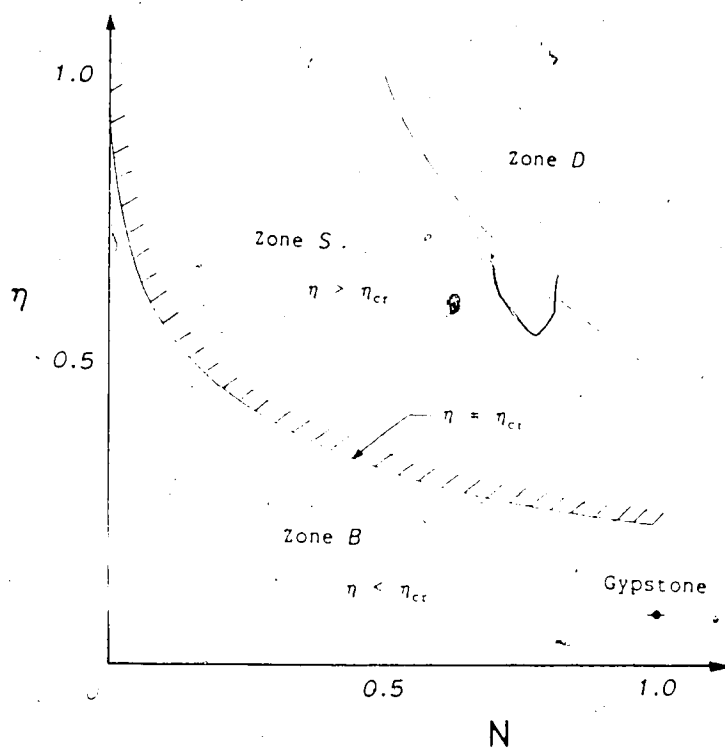


Figure 4.3 Stability Curve for Potential Failure Mechanisms

instability occurs in Zone D. Most rocks that exhibit a Mohr-Coulomb behaviour have a magnitude of η between 0.05 and 0.10, and a hardening parameter close to unity, hence, adopting a predominant shear failure character. Gypstone, the artificial rock developed for the purpose of geomechanical modelling (discussed in Chapter 5), was characterized by $N=1$ and $\eta=0.074$. Therefore, pronounced shear fracture can be expected during failure of this material.

4.2 Influence of Wall Curvature on Rupture Propagation

As the tangential stress at the boundary of a circular opening exceeds the compressive strength of the unconfined rock elements, failure is initiated and logarithmic slip lines propagate. The probability of failure is theoretically the same for all wedges nearest to the tunnel wall. However in reality, the nature of inhomogeneity and anisotropy dictates 'preferred' unstable wedges, creating localized cavities with reduced radii of curvature. For instance, an equivalent elliptical opening may be formed by the separation of two wedges either side of the same diameter, as often observed even in symmetric stress fields (Kaiser *et al.*, 1985).

The elements which are now exposed at the 'sharp' corners of the newly formed cavities will experience a tangential stress concentration (compressive). The smaller is the radius of curvature, the greater is the intensity of

stress concentration inducing progressive rupture. However, progressive rupture does not necessarily continue as expected. The height and volume of the elements at the boundary of a cavity are directly related to its radius of curvature as illustrated in Figure 4.4. Hudson *et al.* (1972) have shown experimentally, that larger or higher rock elements or samples exhibit lower uniaxial compressive strength and greater rate of post-peak strength reduction. Fairhurst and Cook (1966), and Guenot (1979) have also recognized the variation of the apparent strength with the shape of the opening. Therefore, it may be postulated that the over-stressed elements at a 'sharp' corner of a cavity may exhibit an increased apparent strength resisting subsequent rupture. Eventually, the opening may stabilize if the apparent compressive strength of the elements becomes greater than the current tangential stress at the tunnel boundary.

4.3 Influence of Bolting on Failure Mechanisms

The apparent friction angle of a material increases as a result of bolting. Therefore, the failure mechanisms around an opening should also be influenced by bolting. In the case of axisymmetric yielding under hydrostatic field stress, the formation of equilateral slip lines that make an angle of $(\frac{\pi}{4} - \frac{\phi}{2})$ at the tunnel wall has been predicted. Any improvement of the friction angle (ϕ) suggests, that the slip lines around a reinforced opening should make a smaller

SIZE OF ELEMENTS

$$\text{mean height} = 0.5(2r + dl)da$$

$$\text{mean volume} = 0.5(2r + dl)da \cdot dl$$

$$\Delta V = V_1 - V_2 = (r_1 - r_2)da \cdot dl$$

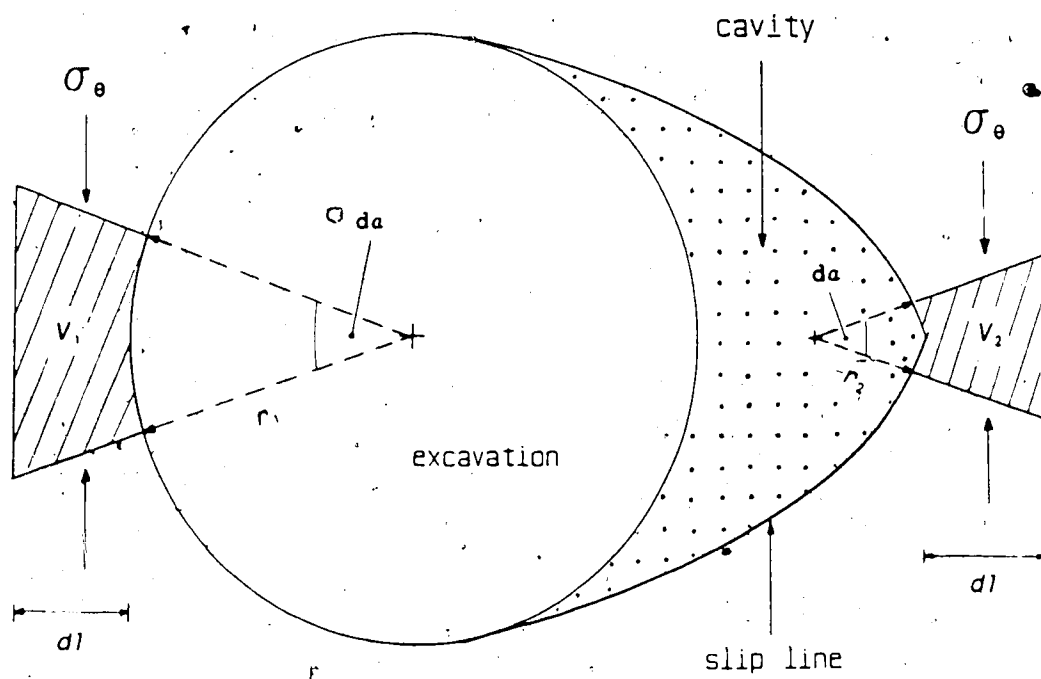


Figure 4.4 Influence of Curvature on Rupture Propagation

angle with the tunnel wall. In other words, the size (thickness) of the unstable wedges defined by the intersecting slip lines should become smaller as the intensity of bolting increases.

The installation of bolts normal to the direction of the maximum principal stress has the optimum effect of reducing the potential for tensile fracture. In an opening excavated in a bedded rock mass, failure mechanisms such as buckling of thin laminations or spalling can be suppressed by bolting. The application of confining pressure restricts surficial tensile splitting of a triaxial specimen. Installation of grouted bolts similarly controls the mechanisms of surface instability associated with a tunnel opening, as a result of the greater confinement provided by the increased radial and tangential stresses.

4.4 Influence of Existing Joints on the Rupture Process

Jaeger (1960), Patton (1966), Rechsteiner and Lombardi (1974) and Kaiser *et al.* (1985) have indicated that a joint may constitute a potential 'short cut' for a slip line. The existence of a joint can introduce random anisotropy on the material behaviour. Guenot (1979) describes in detail, how the equilateral spiral slip lines are directed from their general locus to alternative failure planes along existing discontinuities.

Discontinuities can influence the locus of fracture planes only if the friction angle or cohesion of the joints

is less than that of the intact material. In addition, the movement of a joint depends on the orientation of the joint relatively to the principal stress directions. Consequently, some joints initiate failure actively whereas the others remain inert. If the applied shear stress in the direction of a joint orientation exceeds the shear strength of that joint, the corresponding slip line will shear the rock along the joint, but otherwise, the failure will occur through the intact material. Figure 4.5 illustrates such a case, where the influence of joints on the failure of a tunnel wall is predominant at A, less significant at B and insignificant at C and D (Guenot, 1979).

Four types of rupture initiation around a tunnel wall can be predicted:

- (a) Splitting and buckling of a column of material between the tunnel wall and the adjoining discontinuity;
- (b) Slabbing of material between the tunnel wall and the adjoining discontinuity;
- (c) Sliding of wedges (separated by slip lines and joint planes) on their boundaries into the opening;
- (d) Sliding of a single 'Cherry-stone' shaped wedges where joint movements are insignificant, and slip lines propagate across the joints and intact material.

Figure 4.6 illustrates the above mentioned rupture processes around a tunnel opening. Splitting, buckling and slabbing are typical surface instability phenomena, whereas sliding of wedges are associated with shear failure as distinctly

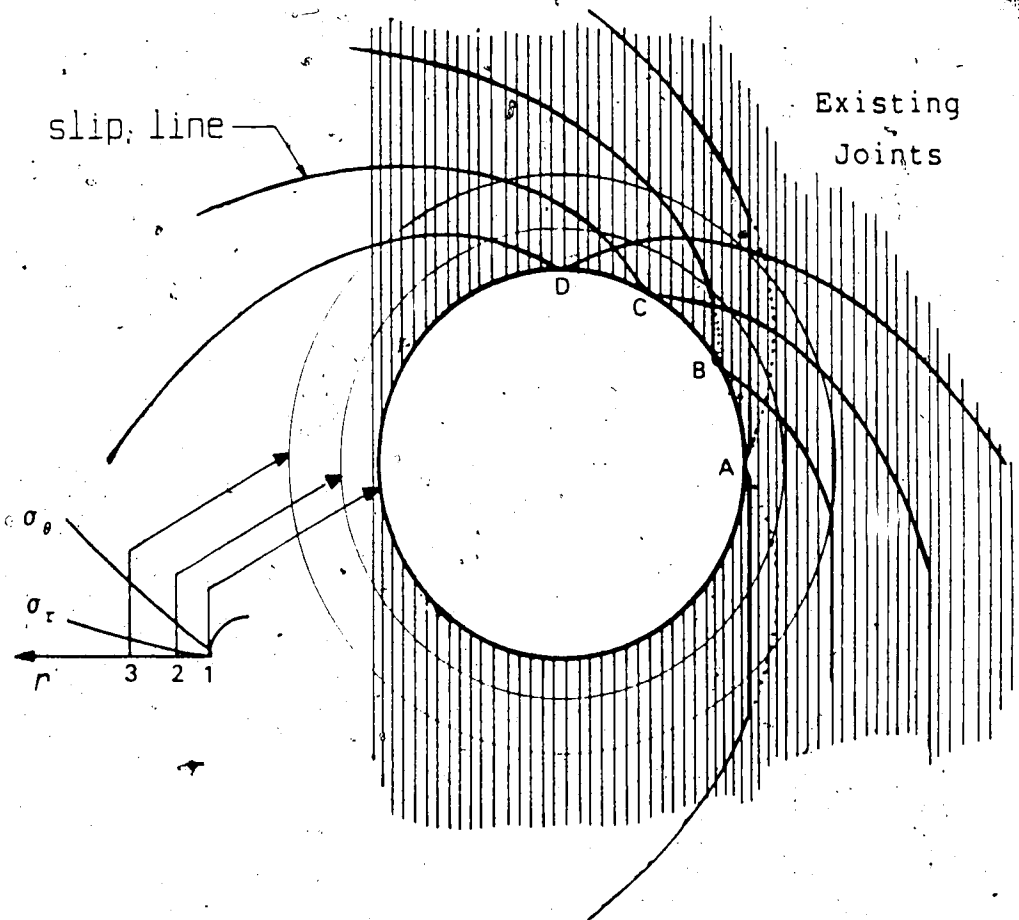
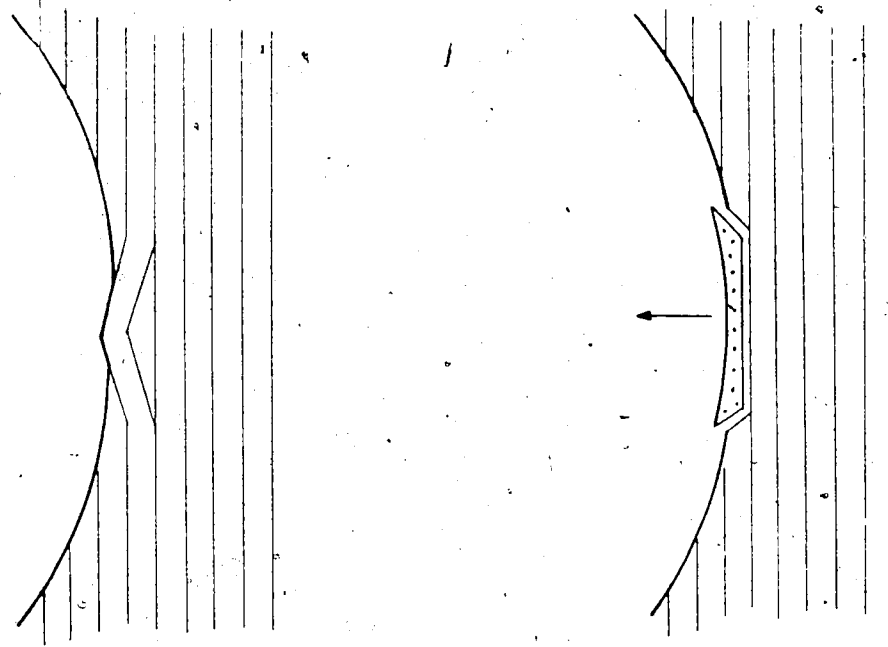
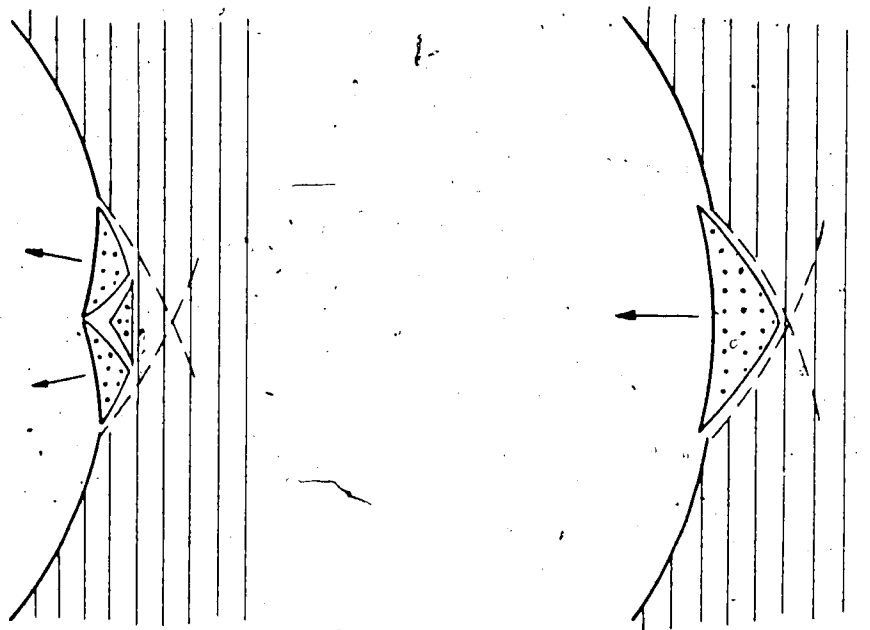


Figure 4.5 Influence of Existing Joints on Rupture Surfaces
(modified after Guenot, 1979)



BUCKLING

SLABBING



SLIDING

'CHERRYSTONE'

Figure 4.6 Types of Rupture Initiation at a Tunnel Opening

identified by the bifurcation theory (Vardoulakis, 1984).

A major objective of the grouted bolts is the improvement of the shear strength of existing joints. If the shear stiffness of the grouted bolts and the density of bolting are adequate, the apparent shear strength of the reinforced joint may be large enough to resist the applied shear stress in the direction of movement. Buckling and slabbing can be prevented by 'beam building', since such instabilities are applicable only to thin laminations (columns). Keyblock bolting can effectively restrict sliding of wedges. Consequently, the potential of any 'preferred' rupture mode propagation can be eliminated by systematic bolting.

5. LABORATORY SIMULATION

5.1 Fundamental Considerations in Physical Modelling

The behaviour of underground openings in rock is generally complex. A comprehensive understanding of the variables that determine the behaviour of large openings is important for rational design. In-situ field stresses, intact rock properties, joint characteristics and geometry of the opening are some of these variables. The use of simulated rock expands the scope of geotechnical research, since scaled models facilitate the investigation of the influence of specific variables on the behaviour of a rock structure. Furthermore, a great advantage of physical modelling is that lower capacity test equipment and less sophisticated cutting tools can be employed due to the lower strength and hardness of the artificial rocks. In addition, model materials can be readily made and reproduced in identical batches in the laboratory, thereby, eliminating the costs of excavation and transportation.

An acceptable geomechanical model must be constructed with a material that can accurately represent the properties of the real rock mass. In the case of a reinforced opening, the geometry and the material properties of the bolts must also be properly scaled. In order to reproduce the failure modes of the real opening exactly, the geometrical and material similitude criteria must be satisfied by the geomechanical model (Bureau *et al.*, 1972; Heuer and Hendron,

1971; Fumagalli, 1979; Clark, 1981; Kaiser et al., 1985).

5.2 Dimensionless Analysis and Similitude Parameters

Similitude laws are based on dimensionless analysis and are formulated by algebraic operations such as the Buckingham's π -theorem (Langhaar, 1951; Obert and Duvall, 1967). Dimensionless analysis is used to obtain a general form of equations common to both the model and the prototype, where the stress-strain behaviour is dependent on geometry, material properties, applied loads and gravity effects. The most relevant similitude parameters for geomechanical modelling are discussed below.

5.2.1 Geometric Similitude for a Reinforced Opening

The scale factor represents the ratio of any specific dimension (e.g. the radius) of the prototype to that of the model (l_p/l_m). The important specific dimensions common to both model and prototype are the tunnel radius (a), the spacing (S), the length (L) and diameter (d) of the bolts. Therefore, the geometric scale factor must be satisfied by all the following dimensionless ratios:

$$\frac{l_p}{l_m} = \frac{a_p}{a_m} = \frac{S_p}{S_m} = \frac{L_p}{L_m} = \frac{d_p}{d_m}$$

5.2.2 Fundamental Material Similitude Parameters

The following geotechnical parameters (dimensionless) must be accurately established for the artificial rock in

order to simulate the real behaviour:

(a) Poisson's ratio: $\nu_m = \nu_p$

(b) friction angle: $\phi_m = \phi_p$

(c) critical strain: $\left[\frac{\sigma_c}{E}\right]_m = \left[\frac{\sigma_c}{E}\right]_p$

(d) uniaxial strength ratio: $\left[\frac{\sigma_c}{\sigma_t}\right]_m = \left[\frac{\sigma_c}{\sigma_t}\right]_p$

The strain similitude for yielding and failure of bolts can be represented by the following equations:

yielding: $\left[\frac{\sigma_y}{E_b}\right]_m = \left[\frac{\sigma_y}{E_b}\right]_p$

failure: $\left[\frac{\sigma_f}{E_b}\right]_m = \left[\frac{\sigma_f}{E_b}\right]_p$

The comparison of relative deformation characteristics between the bolts and the rock yields the following similitude equation:

$$\left[\frac{E_b}{E_r}\right]_m = \left[\frac{E_b}{E_r}\right]_p$$

5.2.3 Similitude Parameters for Discontinuities

The behaviour of a tunnel opening is influenced by the joint structure of the surrounding rock mass. Therefore, the

joint properties are prudent in the simulation of anisotropic character. The friction-angle (ϕ_j), the spacing (t) and the orientation (θ) of the joints are the fundamental similitude parameters required for geotechnical modelling of a rock mass structure. The normal and shear stiffness as well as the joint roughness coefficient (Barton, 1973) should also be scaled but these are of secondary importance. The frictional properties of the model joints can be varied if necessary, by introducing various filler materials or by indentation or smoothing of the sliding surfaces. Friction angles for different filler materials and various simulated joints have been given elsewhere by Fumagalli (1979) and Stimpson (1979).

The similitude criteria for linear discontinuity modelling can be satisfied by the following equations:

(a) joint friction: $\phi_{j,m} = \phi_{j,p}$

(b) joint spacing: $\frac{l_p}{l_m} = \frac{t_p}{t_m}$

(c) joint orientation: $\theta_m = \theta_p$

If all the above similitude requirements can be fully satisfied, then the geomechanical model can be regarded as representative of the real prototype behaviour. However, all similitude parameters cannot be simultaneously established for any particular rock, especially with respect to the

material properties. Furthermore, the in-situ boundary conditions are rarely simulated perfectly in a laboratory model. Consequently, a perfect model (replica) of any particular prototype behaviour is impossible to achieve. However, realistic predictions of the rock mass behaviour can certainly be made for an acceptable range of material properties.

5.3 Development of an Artificial Soft Rock

A model material that uniquely obeys all the similitude laws simultaneously for a given rock is beyond the scope of practical limitations. However, the simulation of a general rock class or a range of different rocks is feasible. This chapter describes the development of a simulated rock that may represent a variety of sedimentary rocks such as limestones, sandstones and shales.

5.3.1 Selection of Model Materials

In the past, materials such as concrete, plaster of Paris, cork, rubber, plastics and gelatins have been used for physical modelling (Stimpson, 1970). In recent times, a natural material such as coal has been used to simulate jointed rock (Kaiser and Morgenstern, 1982; Kaiser *et al.*, 1985). However, the use of a natural material has the limitations of representing a prototype which has a similar joint structure, as well as being expensive in terms of excavation and transportation. Johnston and Choi (1986) have

explained the use of crushed mudstone, cement and water as constituents, to manufacture a model material that ideally simulates the consolidation behaviour of a real mudstone. The following considerations are respected and are intended as a general guide for the development of an appropriate artificial rock:

8. The constituents of the simulated rock must be universally obtainable, economical and should not be toxic;
9. One batch of specimens must be identical to another and easily prepared under laboratory conditions;
10. The physical properties of the synthetic rock must be time-independent and insensitive to variations in room temperature and humidity;
11. The deformation of the physical model under the specified laboratory loads must be adequately sensitive, in order to be monitored accurately with available strain and displacement measuring instruments;
12. The strength and deformation properties of the simulated rock must satisfy at least the basic similitude criteria required for the prediction of the prototype rock mass behaviour.

5.3.2 Mix Composition of a Synthetic Soft Rock

The development of an appropriate synthetic rock was aimed at representing a range of intact rocks with the following similitude parameters:

- (a) $25^{\circ} < \phi_1 < 40^{\circ}$
- (b) $0.25 < \nu < 0.35$
- (c) $0.2\% < \sigma_c/E < 0.4\%$
- (d) $10 < \sigma_c/\sigma_t < 20$

A simulated rock which satisfied the above criteria was prepared in the laboratory by mixing several constituents in the following proportions (by weight):

1. Hydrocal White gypsum cement - 10.0%
2. fine uniform Ottawa sand - 75.8%
3. water (25°C) - 14.15%
4. retarder (Na_2HPO_4) - 0.05%

Gypsum cements of different characteristics are produced by the U.S. Gypsum Corporation and their material properties are given in Appendix F1. Hydrocal gypsum cements are universally available and are inexpensive. They can be moulded into any shape when mixed with water, and their long term strength is time-independent after the hardening process (chemical hydration) is completed. Ottawa sand (type-7140) is a uniform fine silica sand distributed by the Ottawa Sand Company. Its grain size is characterized by D_{50} of 0.2 mm as indicated by the grading curve (Appendix F1). The latter constituents mixed with water give a setting time less than 10 minutes, hence, a retarding agent is necessary to delay hardening. Anhydrous Sodium Phosphate (Na_2HPO_4) is a soluble inorganic salt that does not affect the strength and deformation properties of the hardened compound. A very small amount of Na_2HPO_4 (0.05% by weight)

delays the initial setting time by approximately 6 hours measured by the Vicat apparatus. The variation of the setting time with the amount of retarder is illustrated in Appendix F2. This simulated rock thus prepared, will be referred to as *GYPSTONE* hereafter.

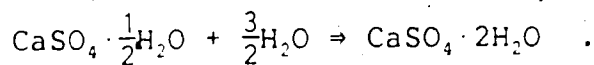
5.3.3 Technique of Manufacturing Gypstone

Mixing of the material constituents may be carried out in table mounted industrial mixers or in a standard concrete mixer, depending on the required volume of material. In order to ensure perfect homogeneity of the overall compound, gypsum cement and sand may be initially mixed together prior to the addition of water. Subsequently, water at room temperature with the retarder (dissolved) must be added to the dry constituents and thoroughly remixed.

Compaction of all specimens could be achieved by simultaneous vibration and tamping. In addition, systematic poking with a pointed steel rod was necessary to accelerate the expulsion of trapped air. Continuous vibration was achieved by firmly attaching the moulds on a vibrating table (500x500 mm²) of 200 Kg capacity with a maximum amplitude of 1.0 mm. The moulds were filled with thin layers (30-40 mm) of material, and the excess bleeding water was removed before the addition of the subsequent layer. During the process of hardening, this model material has a tendency to form a strong adhesive bond with most metal surfaces. Internally waxed cardboard moulds and aluminum moulds

treated internally with a thin coat of teflon spray or vaseline were found to be ideal for casting of small and large specimens.

The chemical name of gypsum cement is calcium sulphate hemihydrate. When mixed with water, it recrystallizes as the dihydrate forming a complex structure of monoclinic crystals with enhanced strength and deformation properties. This reaction can be represented by the following chemical equation:



The weight of water required for the above reaction is less than 19% of the weight of gypsum cement. However, a much greater quantity of water was employed in manufacturing the model material in order to obtain an adequately workable mix that could be readily compacted on the vibrating table.

Once the samples were cast, the moulds were removed from the vibrating table and kept at room temperature for about 42 hours until the initial setting was completed. Subsequently, the moulds were stripped and the samples cured between 45°C and 48°C for 4 weeks at 30% relative humidity. At the end of this curing period, a minimum dry unit weight of approximately 19.6 KN/m³ is attained for gypstone (Appendix F2). The curing temperature should not be allowed to exceed 50°C, because at this temperature excessive rate of evaporation of free water initiates shrinkage cracking on

the sample surface.

It has been explained by Raphael (1960), that beyond 54°C the bonded water of hydration dissociates from calcium sulphate dihydrates. Therefore, it may be deduced that at such temperatures disintegration of the crystallized structure begins to occur, adversely affecting its strength and deformation properties. In fact, gypstone samples cured at temperatures above 75°C were characterized by a reduction in uniaxial compression strengths by 25% to 50%.

5.4 Engineering Properties of Gypstone.

A series of uniaxial and triaxial compression tests and indirect tensile tests have been carried out to determine the following properties:

- (a) uniaxial compressive strength (σ_c) ;
- (b) Young's modulus (E) ;
- (c) critical strain (σ_c/E) ;
- (d) failure strain (ϵ_f) ;
- (e) Poisson's ratio (ν) ;
- (f) friction angle (ϕ) ;
- (g) tensile strength (σ_t) and
- (h) influence of confining stress (σ_3) .

5.4.1 Uniaxial Compression Tests

Standard cylindrical specimens (75mm x 150mm) were tested in uniaxial compression. The ends of the samples were smoothed and capped with a thin sulphur coating, in order

to prevent premature failure due to any stress concentrations. The large majority of the samples failed in shear generally separating into two cones. A handful of samples failed prematurely by tensile splitting which may have been caused by existing shrinkage cracks on the sample surface. The stress-strain behaviour of two typical samples is illustrated in Figure 5.1. The uniaxial compressive strength (σ_c) generally varied between 3.0 and 4.0 MPa and the elastic modulus (E) between 1350 and 1550 MPa, for the majority of samples in a batch of 43. The magnitude of E was measured at 50% of σ_c . The mean values of σ_c and E were determined at 3.44 MPa and 1463 MPa, respectively.

5.4.2 Triaxial Compression Tests

In order to ensure complete waterproofing, gypstone samples were jacketed in thin impermeable rubber membranes. The specimen ends were carefully smoothed, but to facilitate their enclosure inside the rubber membranes, sulphur caps were not installed. Several specimens were tested at confining stresses varying from 0.7 MPa to 5.2 MPa. The behaviour of a selected number of these triaxial specimens is illustrated in Figure 5.2. These stress-strain curves show that the deviator stress ($\sigma_1 - \sigma_3$) at failure, axial failure strain (ϵ_f) and the elastic modulus are dependent on the confining stress (σ_3). The failure envelope as a function of the principal stresses at failure (p-q plot) has been determined as illustrated in Figure 5.3. It

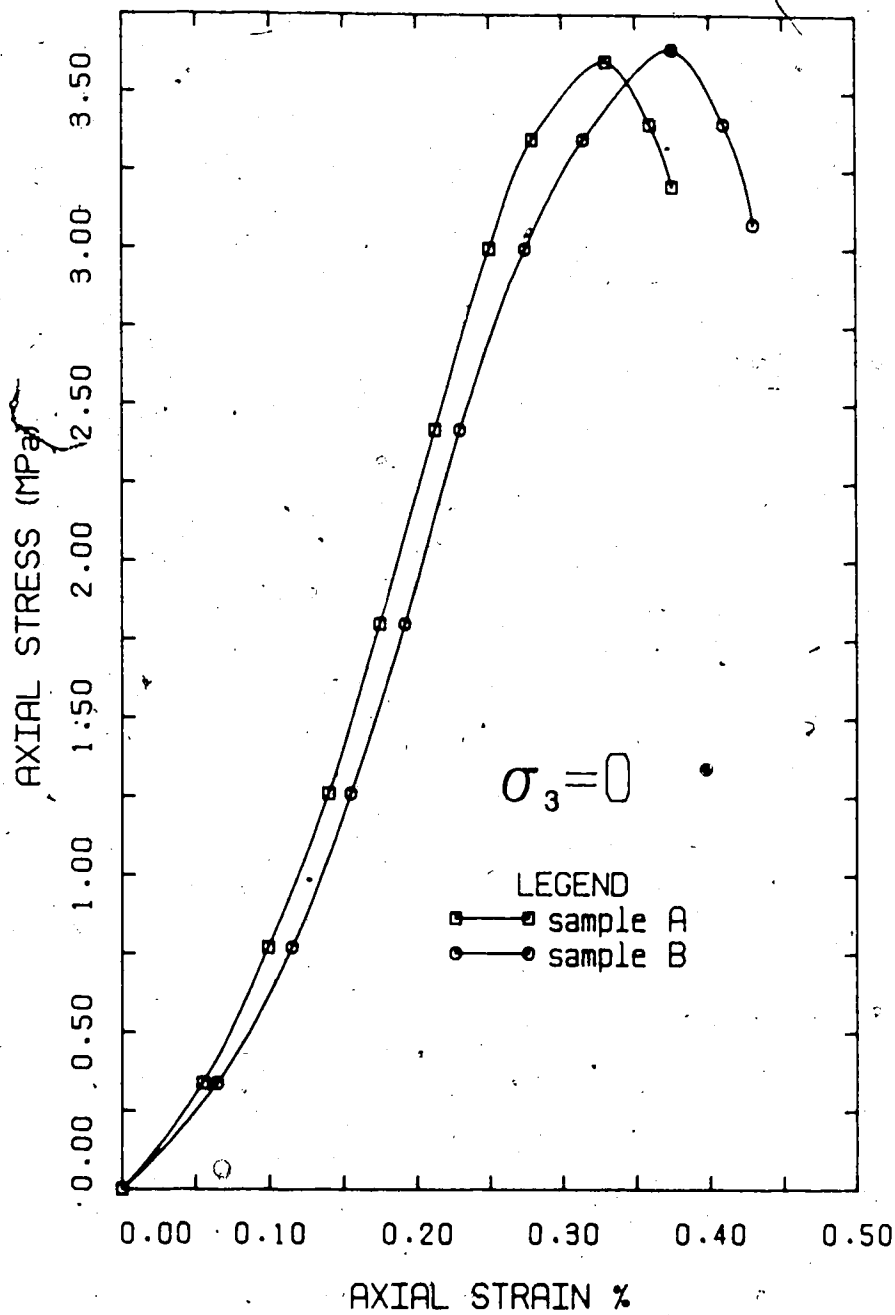


Figure 5.1 The Stress-Strain Behaviour of Gypstone in Uniaxial Compression

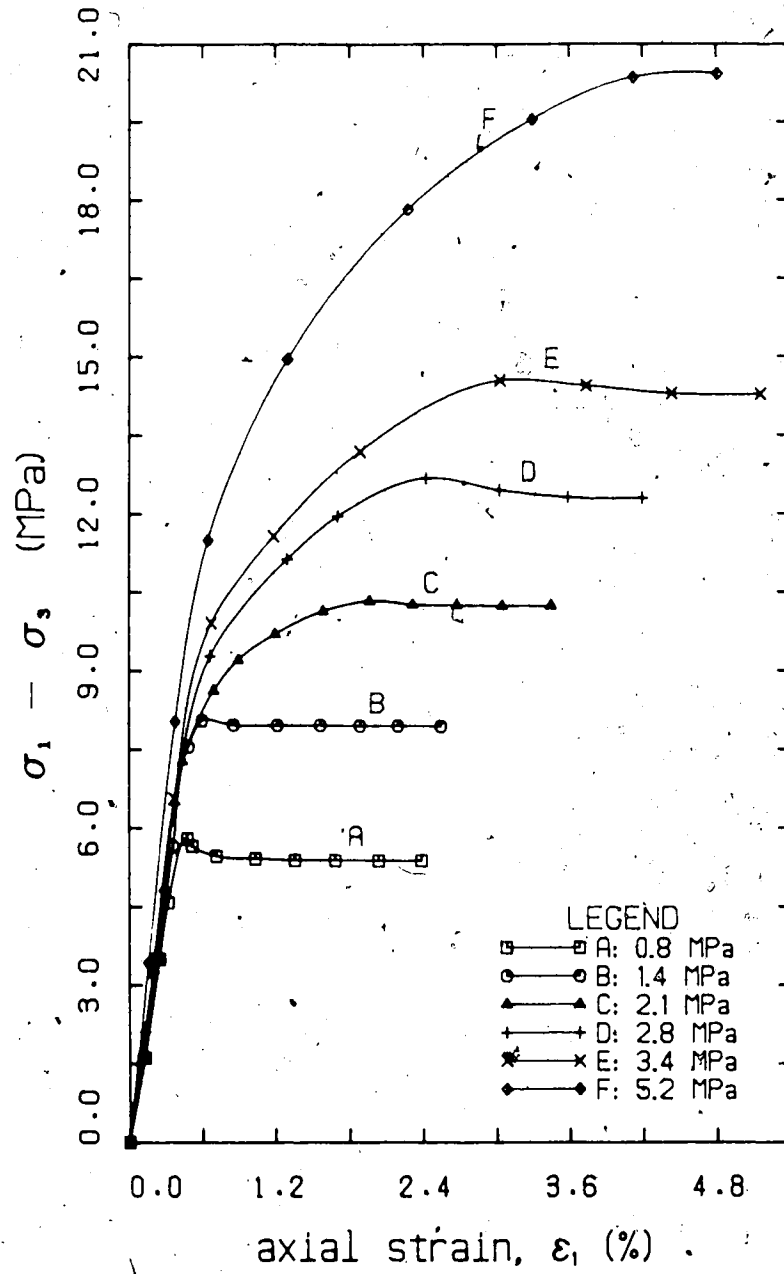



Figure 5.2 Stress-Strain Behaviour of Gypstone in Triaxial Compression

can be deduced from the failure envelope, that the behaviour of gypstone can be described by a linear, Mohr-Coulomb response, with a friction angle of 32° and a cohesion intercept of 0.92 MPa.

A generally observed phenomenon in many soft synthetic rocks is that the elastic modulus is highly sensitive to relatively small variations in confining stress (Rosenblad, 1968), in comparison with the associated change in deviator stress at failure. This may present difficulties in maintaining strain similitude requirements for triaxial compression. However, the elastic modulus of gypstone shows a gradual variation (1500-1900 MPa), as the confining stress is increased from 0 to 5.2 MPa, indicating a triaxial behaviour typical of most sedimentary rocks.

The increase in deviator stress at failure is a function of the applied confining stress. Similitude at failure in terms of stresses can be represented by normalizing the maximum deviator stress ($\sigma_1 - \sigma_3$) and the confining stress (σ_3) by the uniaxial compressive strength (σ_c). Figure 5.4 illustrates a comparison of gypstone with weak sedimentary rocks with respect to the normalized behaviour. Hoek and Brown (1980) failure criterion is, in fact, a similar normalized representation where the principal stresses at failure are normalized by the uniaxial compressive strength. Figure 5.5 illustrates this relationship for gypstone among a range of different rock types.



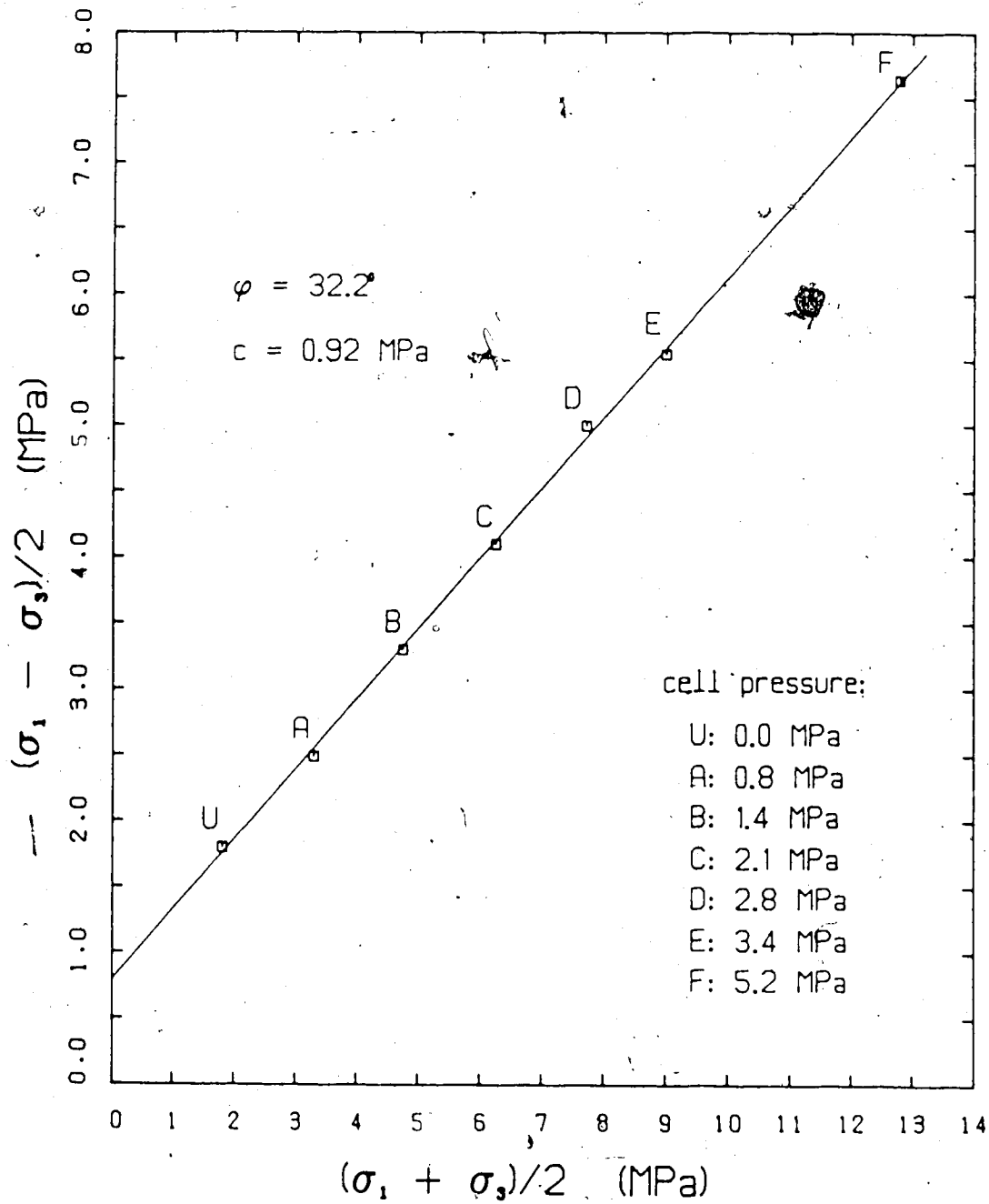


Figure 5.3 Failure Envelope of Gypstone Simulated Rock

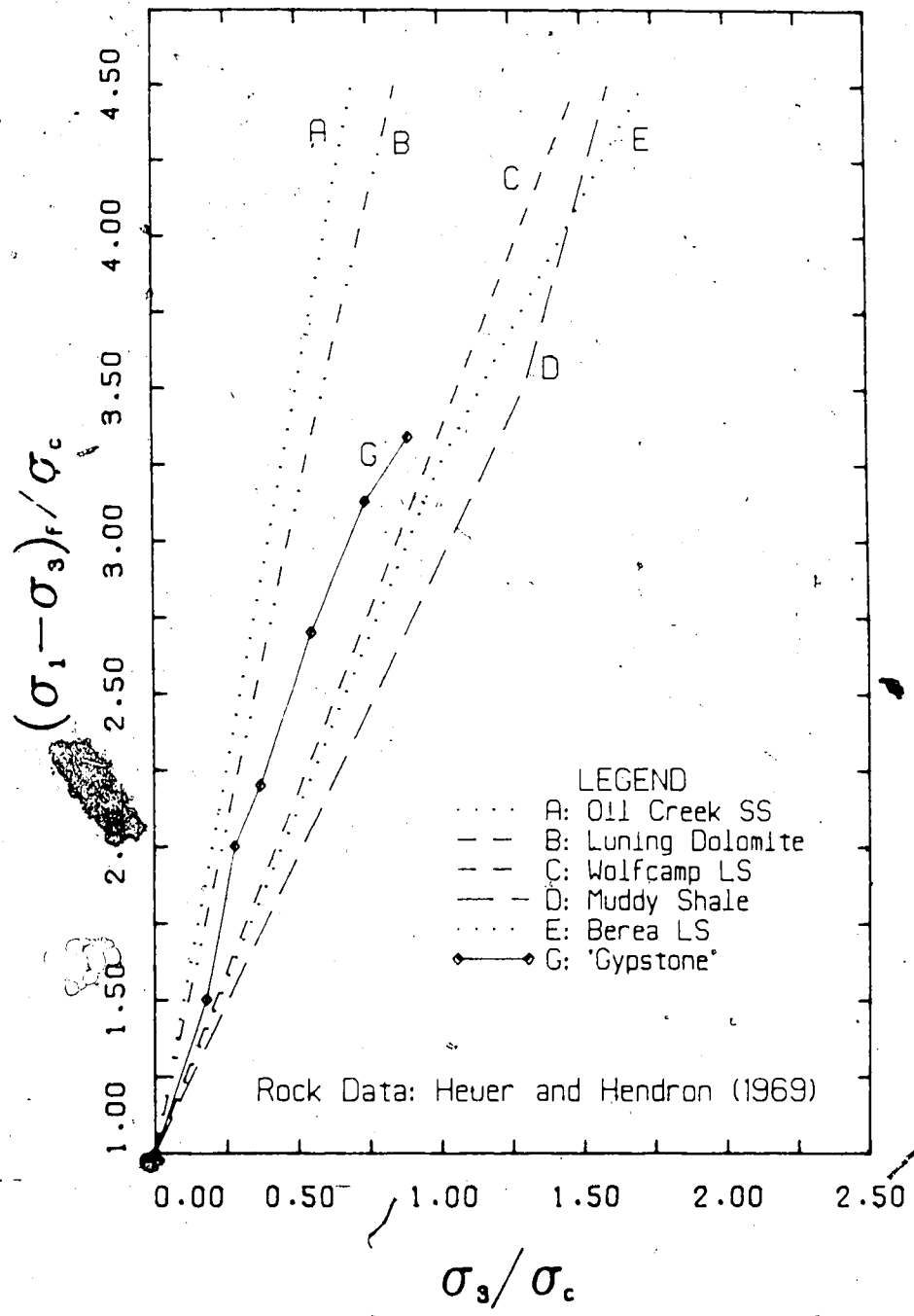


Figure 5.4 Comparison of Gypstone with Sedimentary Rocks in Triaxial Compression

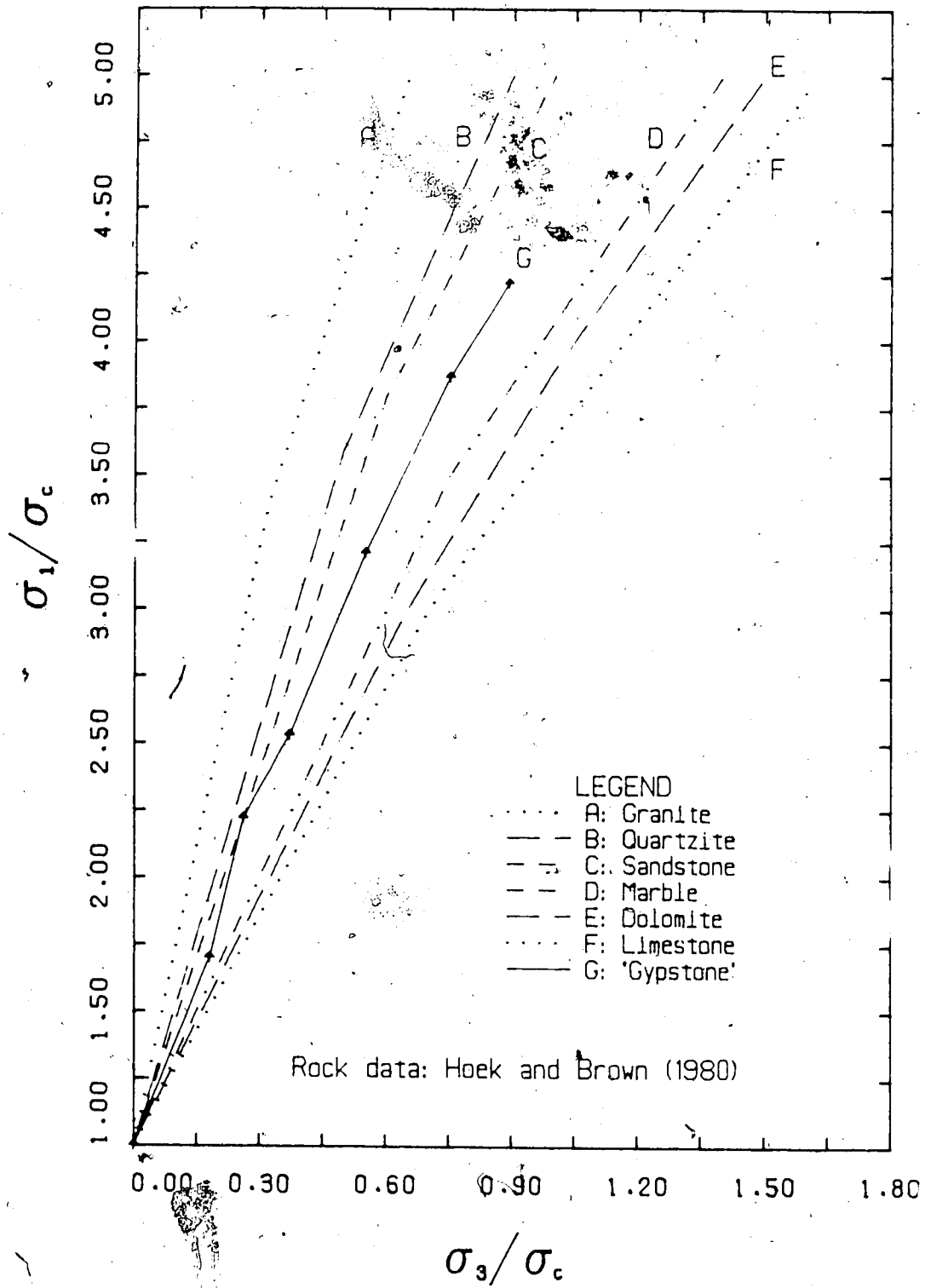


Figure 5.5 Hoek and Brown Failure Representation of Gypstone and Various Rocks

The failure strain (ϵ_f) is also dependent on the confining stress. An alternative comparison of stress-strain similitude in triaxial compression between the model and the prototype can be presented by a plot of failure strain against the normalized confining stress (σ_3/σ_c). Figure 5.6 illustrates the latter relationship for gypstone in comparison with the same sedimentary rocks presented in Figure 5.4. It is clear from the above discussed normalized failure representations, that gypstone obeys the fundamental triaxial stress-strain similitude requirements for modelling soft sedimentary rocks. The granular structure of gypstone actually resembles a typical sandstone.

5.4.3 Split Cylinder Tests

The tensile strength of gypstone was determined indirectly by split cylinder tests. The estimated tensile strengths varied between 0.20 MPa and 0.32 MPa, with a mean at 0.26 MPa and a standard deviation of 0.045 for a set of ten samples. The ratio of σ_t/σ_c was found to vary between 5.2% and 8.3%. It satisfies the required strength similitude criterion for sedimentary rocks. The uniaxial compressive strength was determined from samples of the same batch.

5.4.4 Poisson's Ratio Determination

Several specimens tested in uniaxial compression were instrumented with 'adhesive type' strain gauges in order to determine the Poisson's ratio. The system of instrumentation

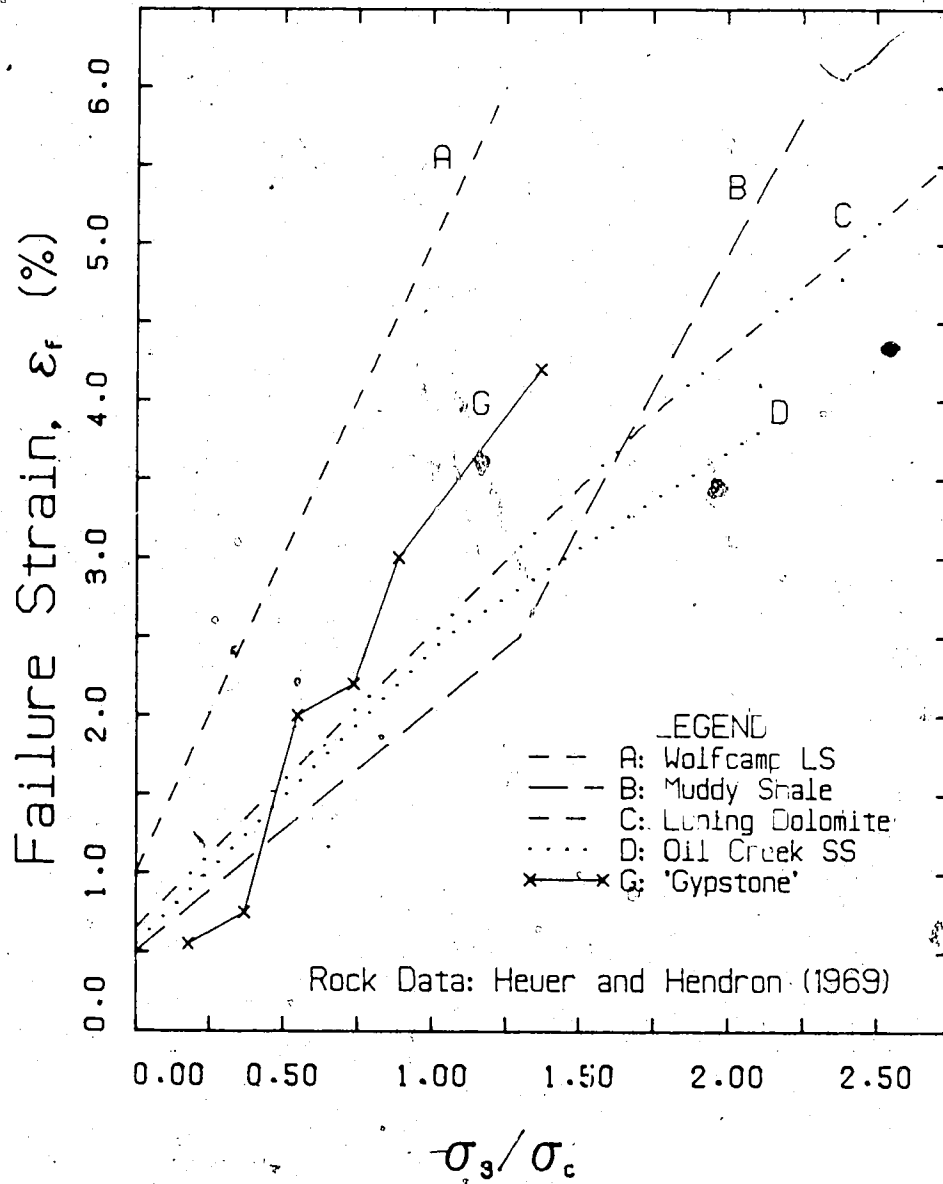
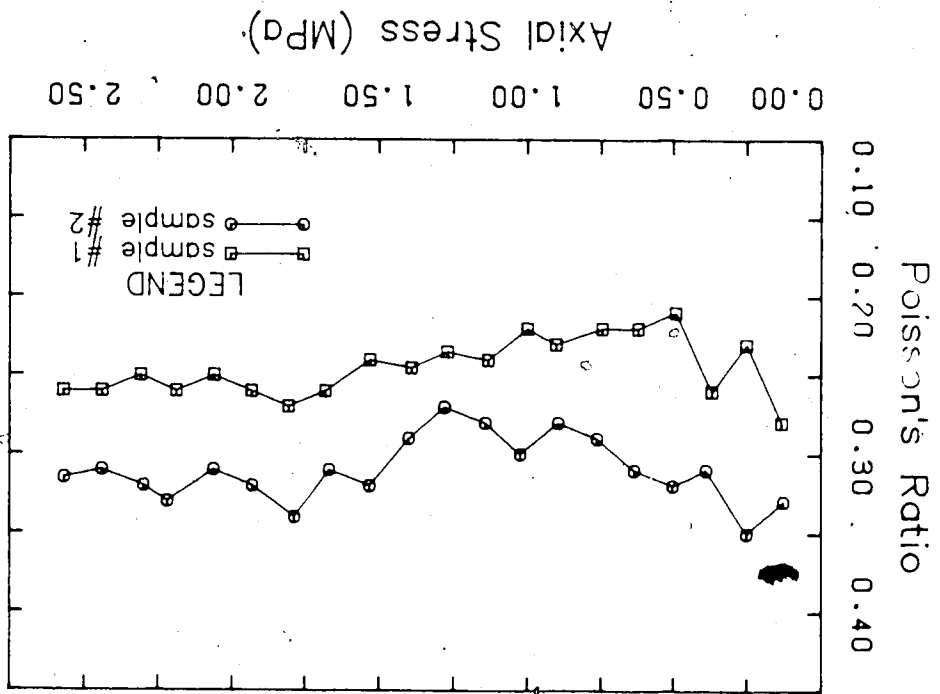


Figure 5.6 Failure Strains of Gypstone and Sedimentary Rocks in Triaxial Compression

Figure 5.7 Variability of the Poisson's Ratio of Gypstone



consisted of two pairs of axial and tangential strain gauges glued on to the sample surface, as well as two pairs of Linear Variable Differential Transformers (LVDT) mounted diametrically to monitor the lateral expansion of two orthogonal diameters. A vertically mounted LVDT was also installed to determine the average axial strain of the cylindrical specimen.

The measured Poisson's ratio varied erratically with the axial stress indicating a scatter of 0.20 to 0.35. The contrasting results of two samples are shown in Figure 5.7. A mean value for the Poisson's ratio (ν) of 0.26 was determined with a standard deviation of 0.4, for the elastic response of the stress-strain behaviour.

5.4.5 Summary of the Properties of Gypstone

Gypstone is a homogeneous and isotropic soft synthetic rock that can be reproduced readily under laboratory conditions with insignificant variation in properties from one batch to another. The initial wet mix gives an appropriate workability to facilitate compaction by vibration independent of the mould shape. The geotechnical similitude parameters of gypstone and its stress-strain behaviour in both uniaxial and triaxial compression, provides convincing evidence to support its suitability in modelling the behaviour of weak sedimentary rocks. Table 5.1 summarizes the relevant properties of gypstone.

Table 5.1 Properties of Gypstone Synthetic Soft Rock

Material property	Units (SI)	Mean	Standard deviation	Value used for analysis
γ_i (wet)	KN/m ³	21.81	0.10	-
γ_d (dry)	KN/m ³	19.56	0.05	-
e	-	0.329	0.004	-
w	%	24.76	0.22	-
σ_c	MPa	3.44	0.46	3.50
E	MPa	1463	95.3	1500
ν	-	0.256	0.056	0.25
ϵ_f	%	0.357	0.035	0.36
ϵ_c	%	0.238	0.028	0.23
σ_t	MPa	0.258	0.050	0.26
ϕ	deg	32.0	-	32.0
c	MPa	0.86	-	0.90
s	-	0.90	-	0.90
a	-	-	-	2.0

5.5 Selection of Model Rock Bolts

In reality, steel bolts are used as reinforcements for the stabilization of yielding rocks. The similitude parameter for yielding (σ_y/E_b) varies between 0.12% for mild steel and 0.21% for high yield steel. The similitude parameter for tensile failure (σ_t/E_b) varies in the range 0.19% - 0.38%, depending on the carbon content and the method of heat treatment. The elastic modulus of most sedimentary rocks varies considerably from 2000 MPa for weak mudstones to 20,000 MPa for relatively strong limestones and sandstones (Hoek and Brown, 1980). Therefore, the similitude parameter for relative deformation (E_b/E_r) may vary within the wide limits of 10-100, where, E_b and E_r are the elastic moduli of steel and rock respectively.

Annealed brass has an elastic modulus of approximately 110,000 MPa, a yield stress of 80 MPa and a tensile strength of 315 MPa. The similitude parameters evaluated for the brass/gypstone composite are summarized below:

$$(a) \sigma_{by}/E_{br} \approx 0.08\%$$

$$(b) \sigma_{bt}/E_{br} \approx 0.30\% \quad \text{and}$$

$$(c) E_{br}/E_g \approx 67$$

σ_{by} and σ_{bt} are the yield stress and the tensile strength of brass respectively. E_{br} and E_g are the elastic moduli of brass and gypstone respectively. After comparison with aluminum, copper, plastics and fibre glass, brass rods were considered as most appropriate for simulating prototype steel bolts.

5.6 Influence of Bolts on the Behaviour of Intact Gypstone in Uniaxial Compression

Gypstone samples (300x300x100 mm³) were prepared to study quantitatively the behaviour of reinforced composites. Brass bolts of 2.5 mm in diameter and 100 mm in length were installed normal to the 300mm x 300mm face, after drilling 3 mm holes and subsequent grouting with an organic resin. Different bolt patterns were selected by varying the horizontal and vertical spacing. These samples were tested in uniaxial compression and failure was promoted across the bolts. Plate 5.1 shows a typical reinforced sample and the associated failure across the plane of bolting.

The stress-strain behaviour (Appendix F3) shows that as the density of the bolts increases, the apparent strength and stiffness increase significantly, but with little effect on the failure strains. It was clear from these simple compression tests, that the grouted bolts support a significant proportion of the applied load, delaying the propagation of shear fracture. However, as the failure strain of the material is approached, brittle failure occurs inevitably by shear fracture propagation across the bolts. Figure 5.8 illustrates the variation of the apparent uniaxial strength of the reinforced sample normalized to that of the original sample. The horizontal axis represents I_b , the product of the quantities H/L and V/L , where H , V , and L are the horizontal spacing, vertical spacing and the length of bolts respectively. The parameter I_b is inversely

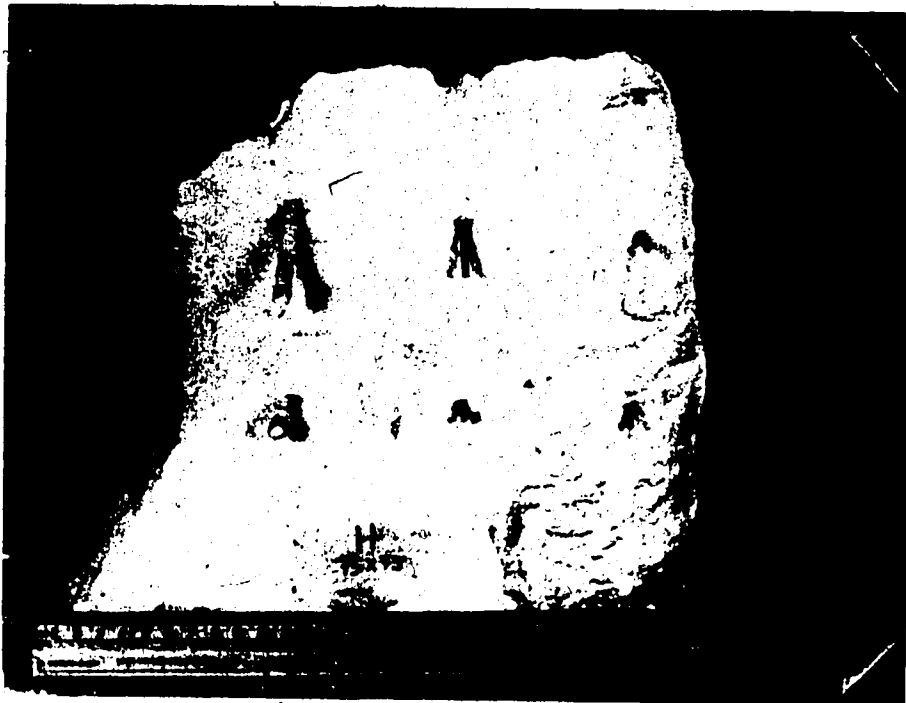
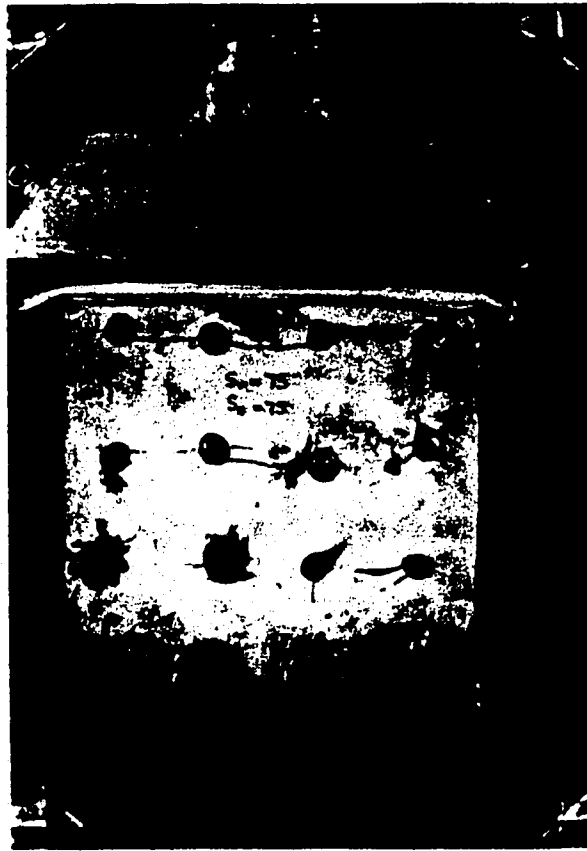


Plate 5.1 Typical Intact Sample Before and After its Failure

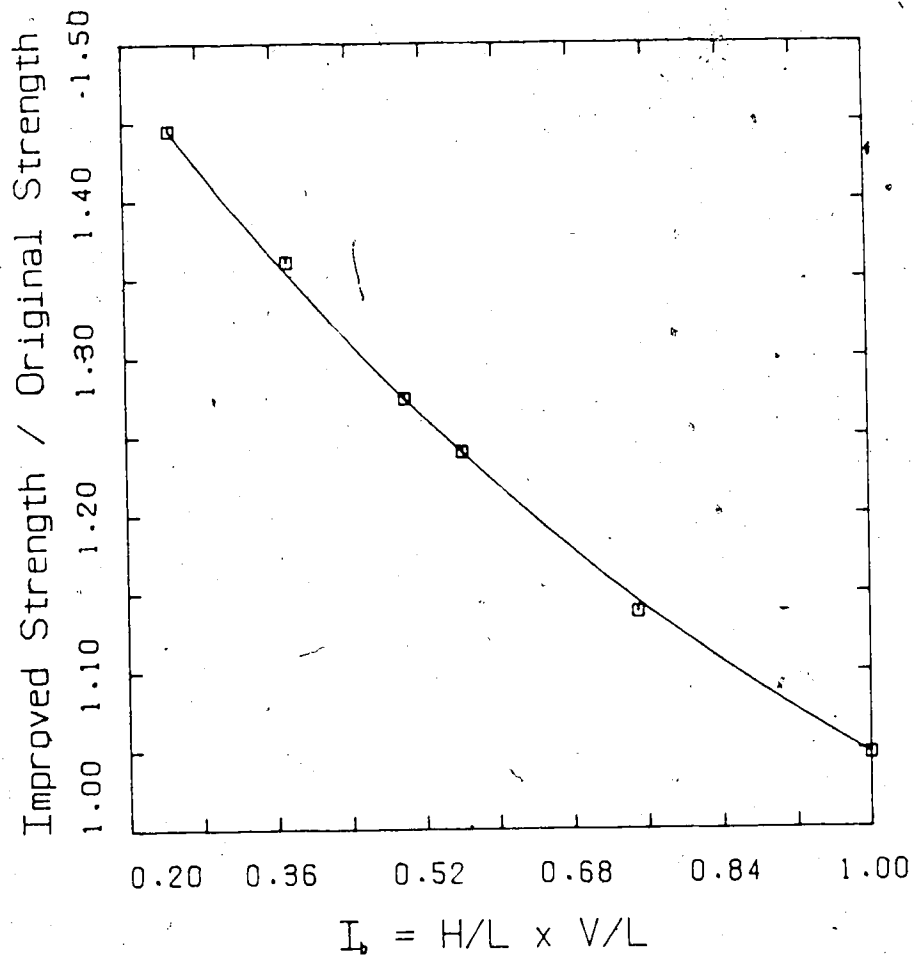


Figure 5.8 Variation of Apparent Strength with Bolt Spacing for Intact Samples

proportional to the bolt density, and is analogous to the bolt density parameter (β).

As the bolt density increases or I_b decreases, the apparent strength of the gypstone samples increases. This variation is not far from being linear, as predicted by the analytical model (Equation 3.14). The dominant failure mode of the resin grouted brass bolts was debonding at the bolt-resin interface, implying the phenomenon of 'pull-out' of bolts. In addition, yielding of a few bolts was occasionally observed in several samples, particularly after the failure load was reached.

5.6.1 Synthetic Smooth Joints and their Properties

A pair of hardened plaster surfaces can be utilized to simulate smooth joints. The synthetic joints (1.5 mm in thickness) were prepared by Hydrostone gypsum cement and water combined in the proportions of 5:2, and cured at a temperature of 40°C for one week. Shear box tests were conducted to determine their properties (Appendix F4). The joint frictional properties are summarized below:

- (a) mean friction angle (ϕ_j) = 21.9°
- (b) cohesion intercept (c_j) = 0.02 MPa
- (c) joint roughness coefficient (JRC) = 3.3 - 4.8
- (d) joint dilation angle = 4° - 9°

The joint roughness coefficient and the dilation angle have been determined from semi-empirical expressions (Barton, 1973). The above frictional properties are typical of smooth

rock joints slightly infilled with clay or silt.

In addition, the normal and shear stiffness of the joints were estimated from the monitored shear behaviour of the plaster joints. The normal stiffness was estimated at approximately 150 MPa/mm. The shear stiffness was not consistent, and fluctuated in the range 0.5 to 0.9 MPa/mm for the range of normal stresses varying from 0.094 to 0.370 MPa. This indicates a joint stiffness ratio (k_n/k_s) between 170 and 300, which is also typical of prototype smooth joints (Barton, 1973).

5.7 Influence of Bolts on the Behaviour of Jointed Gypstone in Uniaxial Compression

The Hydrostone joints were placed in three layers at vertical spacing of 75 mm, within 300x300x100 mm³ samples. The inclination of the joint layers was selected as 60° to the direction of the applied vertical load. Different bolt patterns were achieved by varying the horizontal and vertical bolt spacing (50, 75 and 100 mm), and by adjusting the location of the bolt rows relatively to the position of the three joint layers. The stress-strain curves of these samples in uniaxial compression are given in Appendix F5. Plate 5.2 illustrates a typically jointed sample and its failure in uniaxial compression.

The apparent strength of jointed materials is influenced by two major factors:

- (i) bolt density (spacing), and

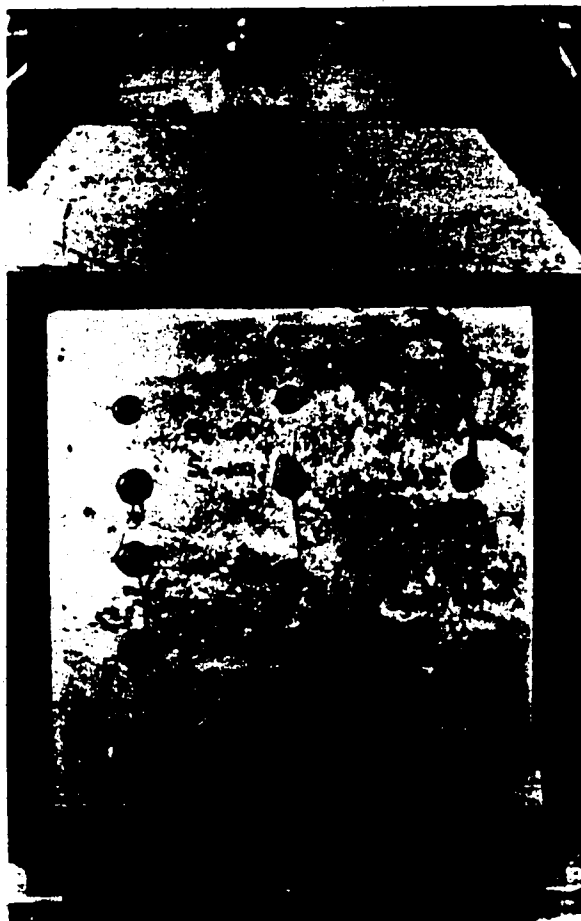


Plate 5.2 Typical Jointed Sample Before and After its Failure

(ii) degree of joint reinforcement.

Figure 5.9 illustrates the normalized apparent strength against I_b , the product of H/L and V/L . It shows that as the magnitude of I_b is reduced by decreasing the bolt spacing, the apparent strength is generally increased as expected. However, it is further observed that for a given bolt density (constant I_b), the apparent strength is considerably affected by the relative location of the bolt rows with respect to the joint planes. The latter variation in strength is depicted by the Curves A to D. For instance, both Curves A and D indicate vastly different strengths for the same bolt density. This is due to the fact that Curve D represents a pattern of bolts, where none of the bolts intersect with the joints to provide any stabilization. On the contrary, Curve A represents an alternative location of the bolts, such that the bolt rows and the joint planes intersect effectively to provide the optimum reinforcement effect for the samples.

The samples represented by Curve C also indicate a similar behaviour to those of Curve D, since only their middle joint layers are reinforced by bolting. Hence, failure occurs along one of the unreinforced joint planes. The addition of one row of bolts provides greater stability to the remaining joint planes, considerably improving the apparent strengths (Curve B). It can be concluded from Figure 5.9, that whatever the bolt density may be, the strength of a material cannot be improved significantly.

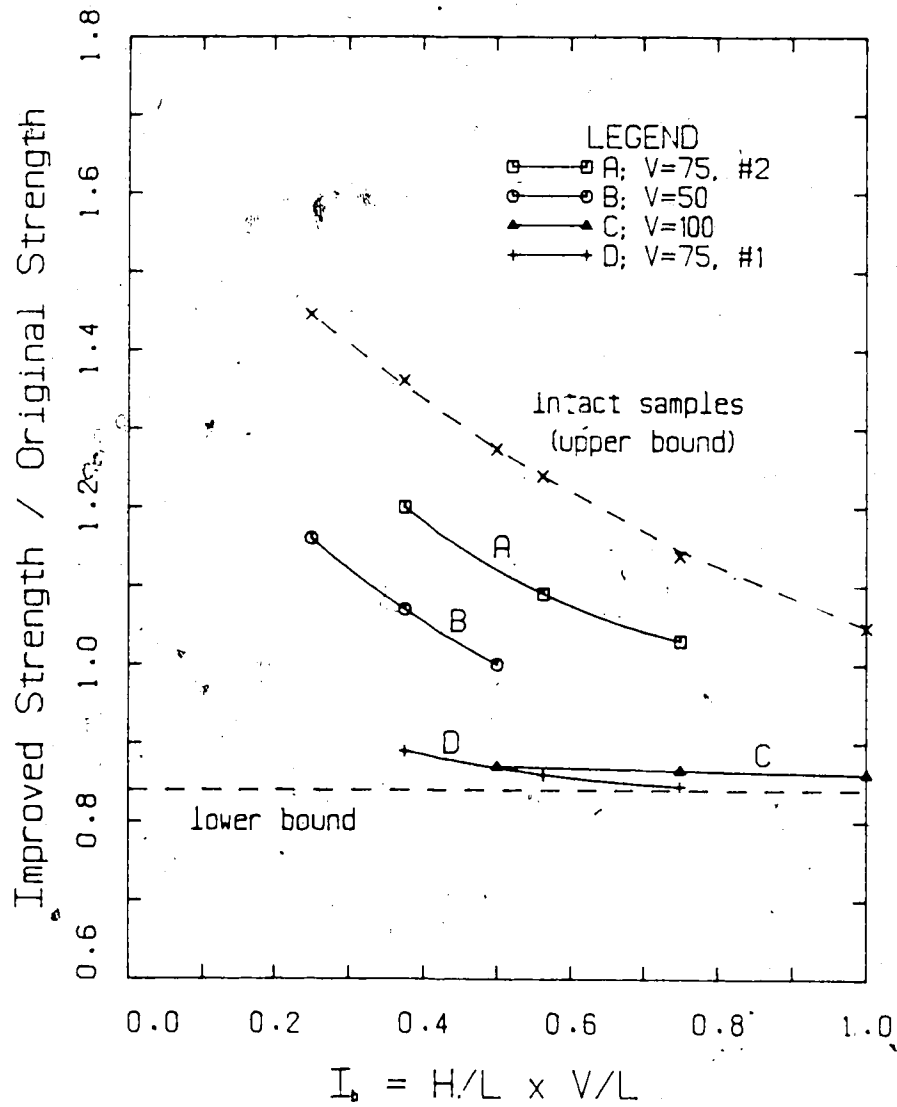


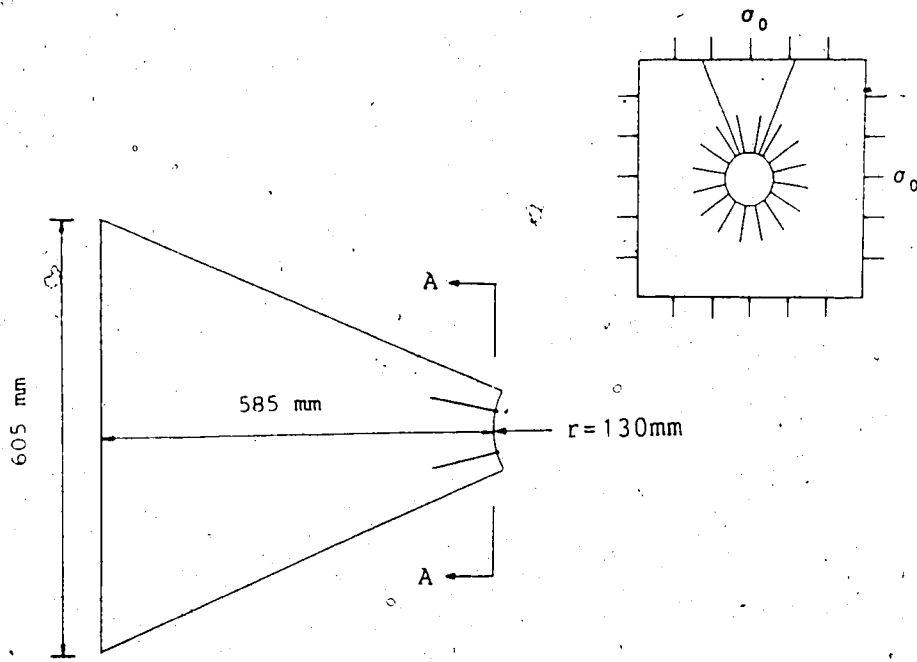
Figure 5.9 Variation of Apparent Strength with Bolt Spacing for Jointed Samples

unless the bolt pattern is carefully selected with respect to the existing joints, to provide the optimum reinforcement or dowel effect.

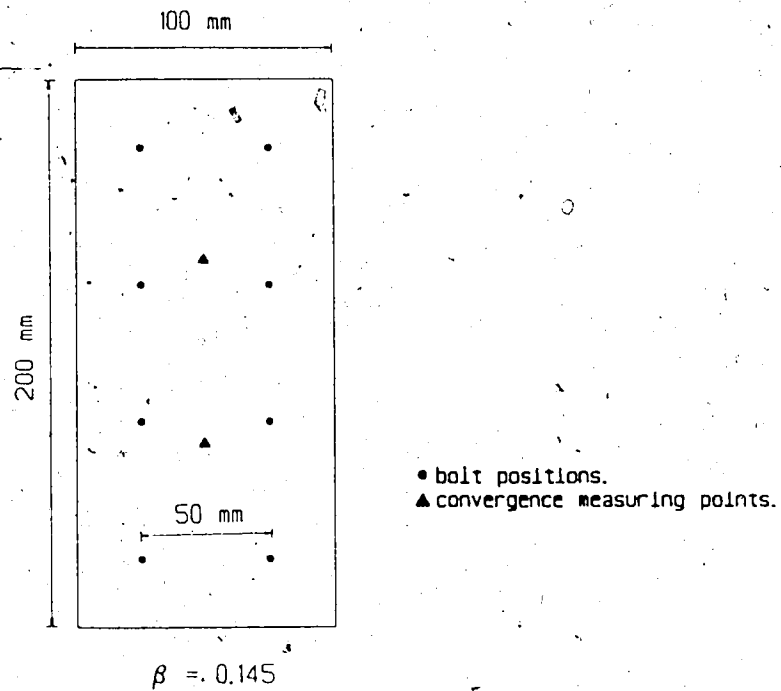
5.8 Experimental Procedure: Bolted Tunnel Wall

5.8.1 Sample Preparation and Arrangement in Test Frame

The geometry of the gypstone test samples defines a dispersion angle of 45° at the tunnel centre (130 mm radius). The general dimensions of the samples are indicated in Figure 5.10. This particular shape was selected to exaggerate the scale of the geomechanical model, since the complete tunnel opening is defined by the radial arrangement of eight such identical segments. Therefore, in the case of hydrostatic field stress, the axisymmetric deformation around the tunnel opening can be represented by one segment. A special mould (Appendix E1) was built to cast these samples. The compaction technique and curing procedure of gypstone have been described earlier. After curing was completed, the specimen sides were carefully smoothed where warranted, and any voids on the surface were filled with fresh gypstone prior to testing. The application of load to the samples requires a rectangular boundary. Therefore, the particular geometry of the samples dictated the design of a test frame with two triangular wedges as shown in Appendix E2.



(A) PLAN: GEOMETRY OF A TYPICAL TEST SAMPLE



(B) ELEVATION A-A: REINFORCED TUNNEL SECTION

Figure 5.10 A Typical Reinforced Gypstone Test Sample

Hydrostatic load condition ($K_0=1$) requires zero shear stress along any radial plane. Consequently, it is prudent to provide minimum friction at the sample boundaries during testing. In order to fulfill this requirement as practically as possible, a pair of teflon sheets (0.5 mm in thickness) was inserted between the specimen surfaces and the test frame. The friction angle at the interface of two sliding teflon surfaces was found to be less than 2° , hence, was adequate for the purpose of minimizing friction at all contact boundaries.

The installation of bolts required the drilling of 100 mm long, 3 mm diameter holes normal to the tunnel boundary, and carbide tipped drill rods were employed for this purpose. Compressed air was used to clean the drill holes prior to injection of the organic resin. Brass model bolts (smooth) were subsequently inserted into the drill holes and the overflowing resin was removed quickly from the tunnel surface. The samples were kept overnight to permit complete hardening of the resin before the installation of extensometers. Figure 5.10 illustrates a typical sample after the installation of bolts.

5.8.2 Instrumentation and Monitoring

5.8.2.1 Plane Strain Condition

A set of four LVDTs and four dial gauges were located at the corners of the top loading head above the test frame, in order to measure the vertical

displacements of the sample. The vertical stress (σ_z) was adjusted as necessary to arrest any significant vertical displacements.

5.8.2.2 Applied Loads

The magnitude of the applied stresses was measured by a total of 12 aluminum load cells placed at the end of each ram piston. Strain gauges were firmly attached to the interior surface of these hollow cylindrical load cells. The load cells were provided with spherical seating at the contacts with the loading platens to prevent eccentric load transmission. Further details of these load cells are given by Maloney (1984).

5.8.2.3 Tunnel Convergence

The wall convergence of the opening at different points could be measured by an assembly of two or three LVDTs mounted on a vertical stand. Similarly, the displacements at the far field boundary were also measured. Two LVDTs were mounted beside the test frame on either side of the tunnel to indicate any sample rotations, which were in fact found to be insignificant. The LVDTs were of the type HP-24DCDT-500 with a measuring range of ± 12.7 mm to a linearity accuracy of at least 0.5%.

5.8.2.4 Radial Strains near the Opening

The following procedure was adopted to measure the strains and displacements near the tunnel wall:

- (a) A 20 mm deep, 2 mm diameter hole was drilled and the measuring point of the LVDT rod (with core) was fixed (epoxy glue) at the bottom of the hole.
- (b) A cylindrical socket that can accommodate the LVDT barrel was then attached to the tunnel wall concentric with the protruding LVDT core.
- (c) The LVDT barrel was inserted into the socket with the core enclosed within the barrel.
- (d) The pair of screws provided on the socket was tightened to hold the LVDT barrel firmly inside the socket.

The fixed end of the LVDT rod directly measures the displacement of the material at that point, whereas the LVDT barrel with the socket is displaced by the same amount as the tunnel wall. Consequently, the data logger records the relative displacement between the tunnel wall and the bottom of the drill hole, which divided by the depth of the hole (20 mm) determines the average radial strain. The tunnel convergence was directly measured by mounting additional LVDTs behind the former LVDT barrels. This arrangement is shown in Plate 5.3.

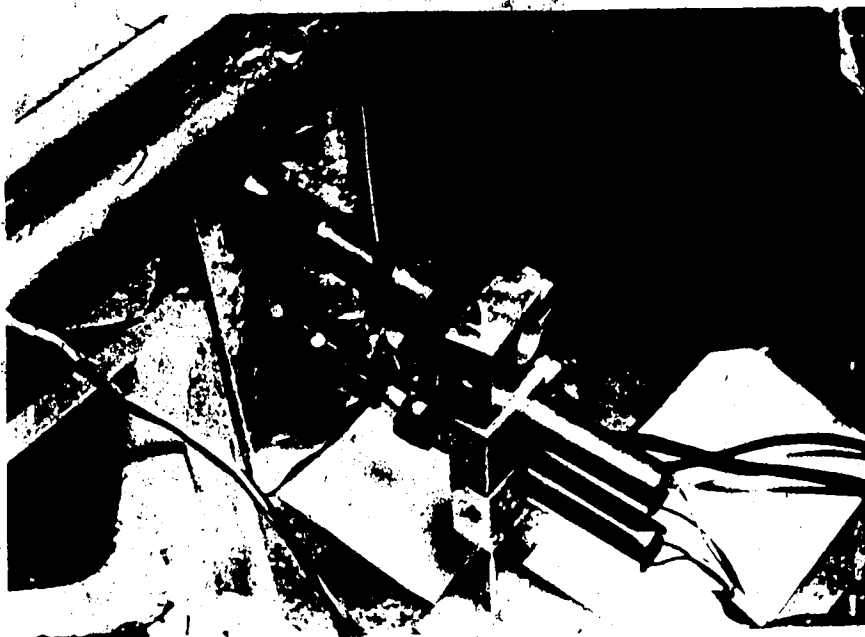


Plate 5.3 Measurement of Radial Strains and Displacements
near the Tunnel

5.8.2.5 Internal Radial Strains by Extensometers

The average internal strains are calculated from the measurement of relative displacement between two points separated by a known gauge length. The assembly of a system of laboratory extensometers is discussed in detail by Maloney (1984), and a diagrammatic illustration is given in Figure 5.11. In brief, two coaxial rods are grouted at their tips separated by a known gauge length. A LVDT core is attached to the inner rod, whereas a socket which holds the LVDT barrel is attached to the end of the outer rod. Therefore, the reading of the data logger indicates the relative displacement between the two grouted points, which divided by the gauge length determines the average radial strain between the grouted points.

5.8.2.6 Data Processing System and Presentation

The data logger scans the measurements of 12 load cells and 13 LVDTs at each load step. These readings are converted to loads and displacements using calibration charts and finally converted to stresses and strains. The displacement and strain response to variations in boundary stress (controlled variable) are discussed in detail in Chapter 6.

HP 24DCDT-250

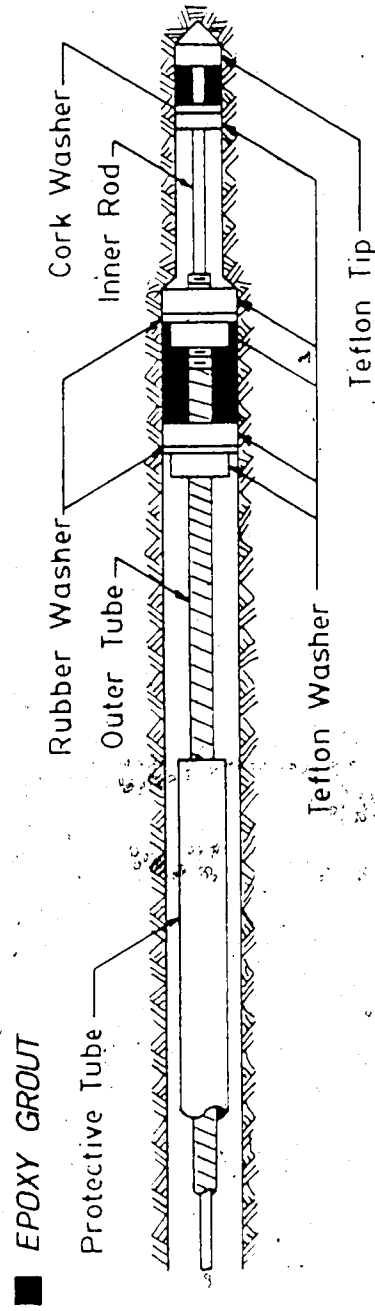
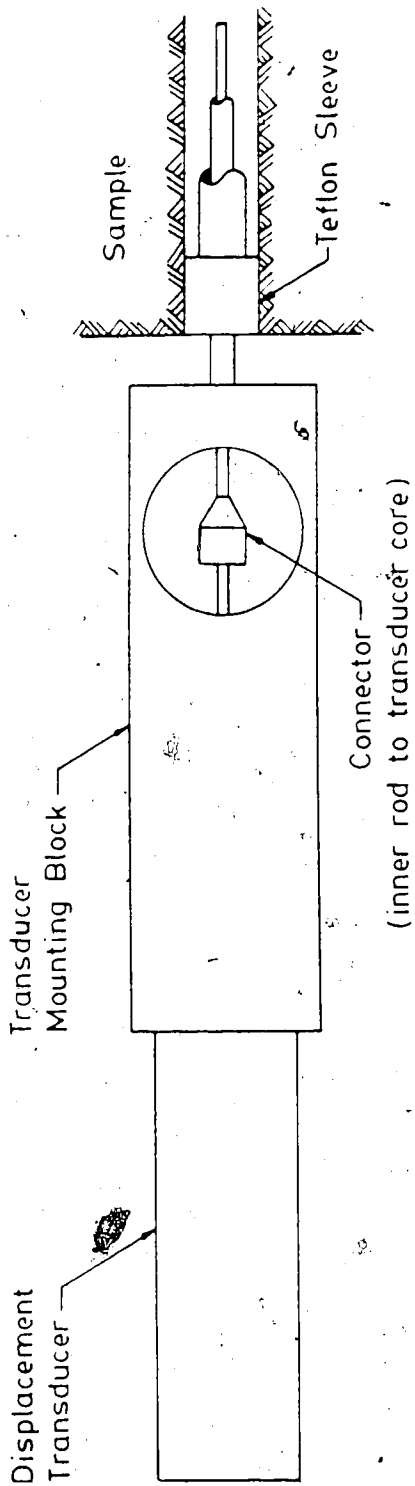


Figure 5.11 Typical Extensometer Assembly (modified after Maloney, 1984)

5.8.3 Test Apparatus and Load Application

The model study utilizes the Process Simulation Test (PST) apparatus developed by Kaiser and Morgenstern (1981), and only the essential aspects of the test machine and the loading procedure are discussed here. A schematic diagram of the PST apparatus is given in Appendix E3. After the test sample is arranged in the test frame, it is transferred on to the base plate of the PST apparatus. An assembly of twelve rams operated hydraulically can provide the required triaxial stress state. The rams in the vertical direction were used in this study to maintain plane strain conditions, whereas the horizontal rams were employed to simulate a lateral biaxial stress field.

The maximum pressure that can be applied to the sample in the lateral direction is 15 MPa, without significant load fluctuations. The applied load is uniformly distributed to the sample sides via the triangular steel wedges (test frame). The shear stress along the sample boundaries has been neglected due to the pair of teflon sheets inserted between the sample and the steel loading frame.

The application and transfer of load onto the sample is illustrated in Figure 5.12. The hydrostatic field stress (σ_0) was provided by the lateral stress applied in the Y-direction (σ_y) at the far field boundary. The tangential stress distribution (σ_c) applied normal to the remaining sides of the sample could be predicted by elasto-plastic analysis, which is a function of σ_0 and the material

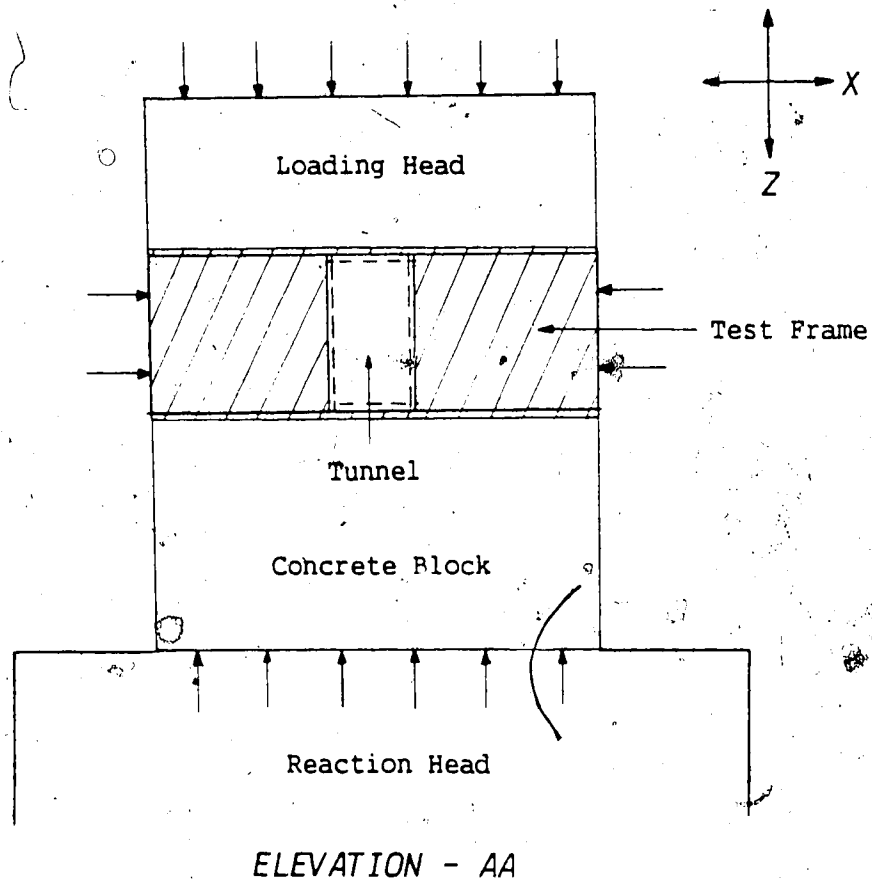
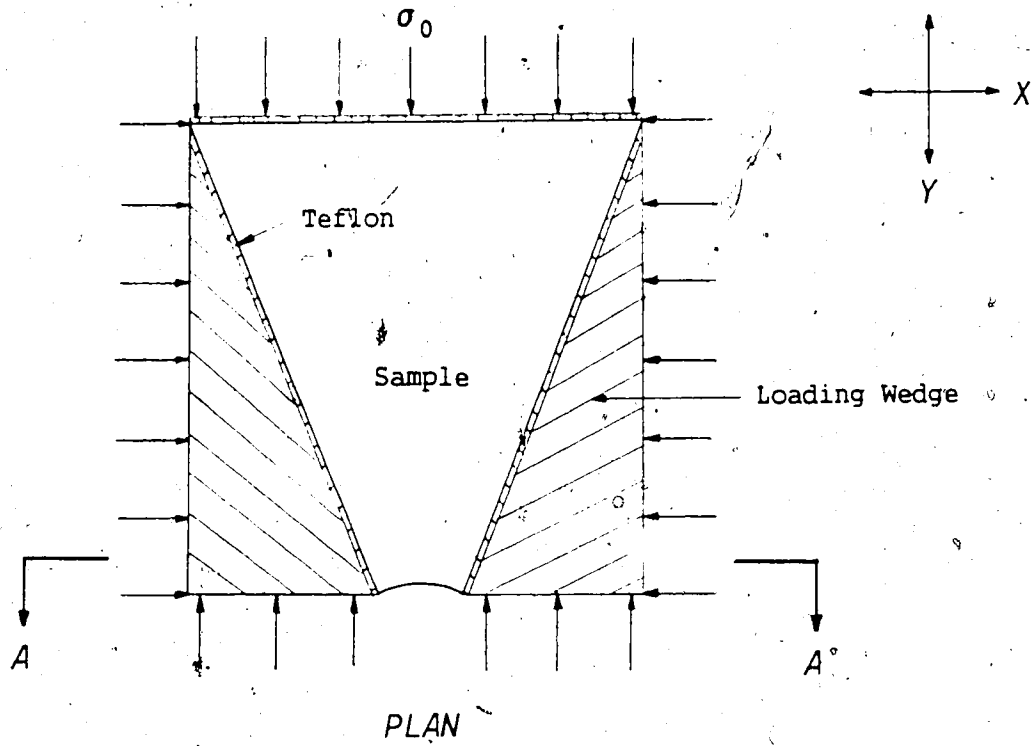


Figure 5.12 Transfer of Load to the Test Specimens

properties of gypstone. The lateral stress in the X-direction (σ_x) was determined by static equilibrium, to provide the mean resultant σ_0 , assuming zero shear stress along the sample sides. The magnitude of σ_0 was increased by increments of 1 MPa, and the vertical stress (σ_z) was adjusted accordingly to maintain plane strain conditions. The field stress was not increased beyond 14 MPa, so that σ_x would not exceed 15 MPa, which is the maximum load capacity of the apparatus.

5.9 Simulation of Jointed Rock Masses

5.9.1 Frictional Properties

In order to assess the behaviour of jointed rock masses in plane strain triaxial compression, a series of preliminary tests were conducted on 300x300x200 mm³ jointed samples. These gypstone samples were provided with Hydrostone joints (150x30x3 mm³), which were inserted from the sample top in an orderly arrangement to establish four sets of discontinuities as shown in Figure 5.13. The cured specimens were subsequently loaded to failure in the PST apparatus by increasing the major lateral stress (σ_1) for different confining stresses (σ_3), maintaining plane strain in the vertical direction.

The jointed samples failed by developing diagonal shear planes which propagated along the existing joint planes. The failure envelope in terms of principal stresses is shown in

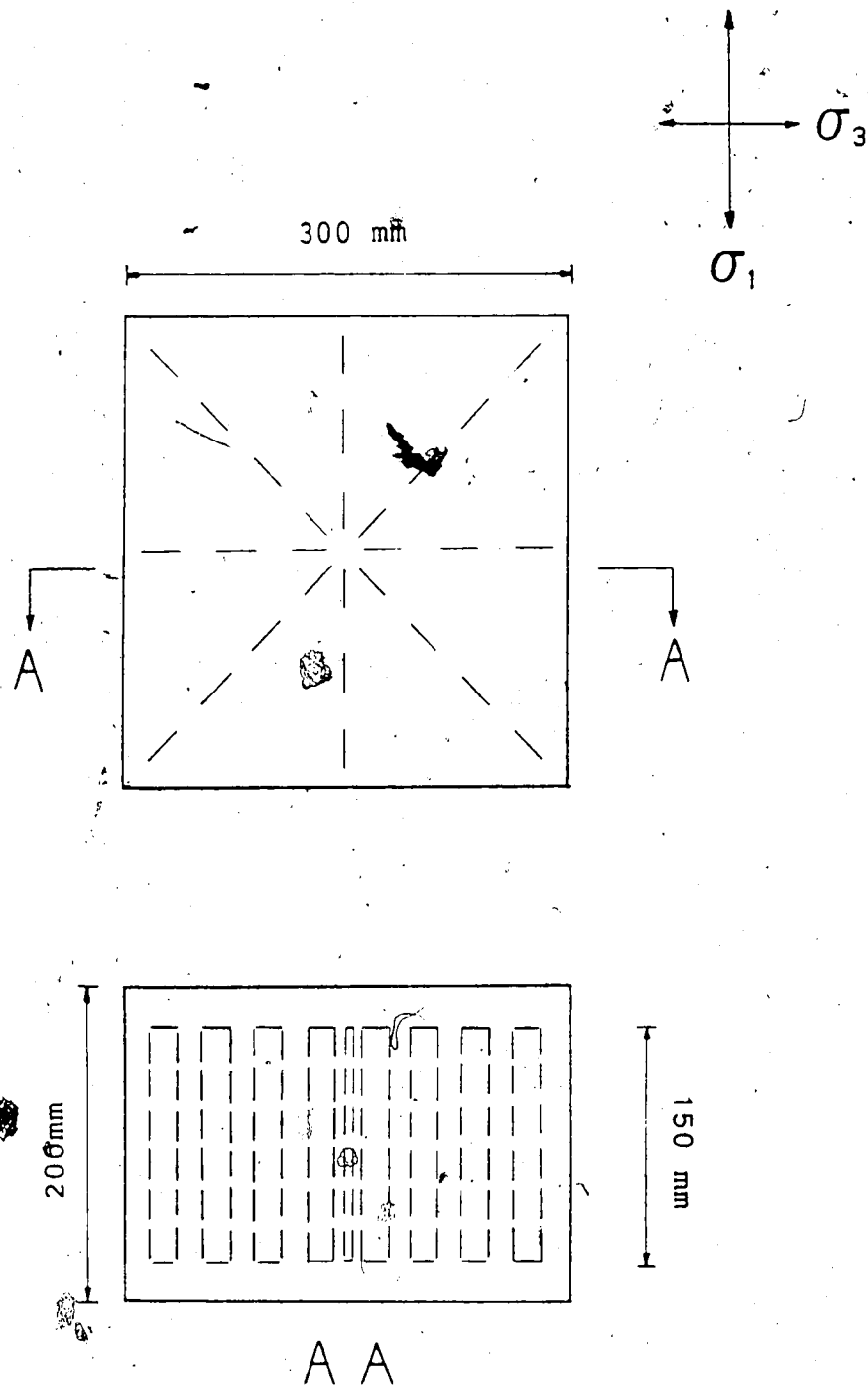


Figure 5.13 Selected Joint Pattern for Physical Modelling

Figure 5.14. The mean friction angle and the uniaxial strength determined by assuming a linear relationship were 27.9° and 3.36 MPa respectively. An elastic modulus of 1400 MPa and a Poisson's ratio of 0.25 were also estimated by the comparison of measured stress-strain data (Appendix F6) with theoretical predictions (plane strain Hooke's law).

It could be deduced from the observed stress-strain behaviour and the failure mode of these jointed samples, that four sets of discontinuities enable the material to adopt an equivalent near-isotropic behaviour with reduced strength properties. The only exception to this general statement is when one of the joints becomes much more pronounced (weaker) than the others (Hoek and Brown, 1980).

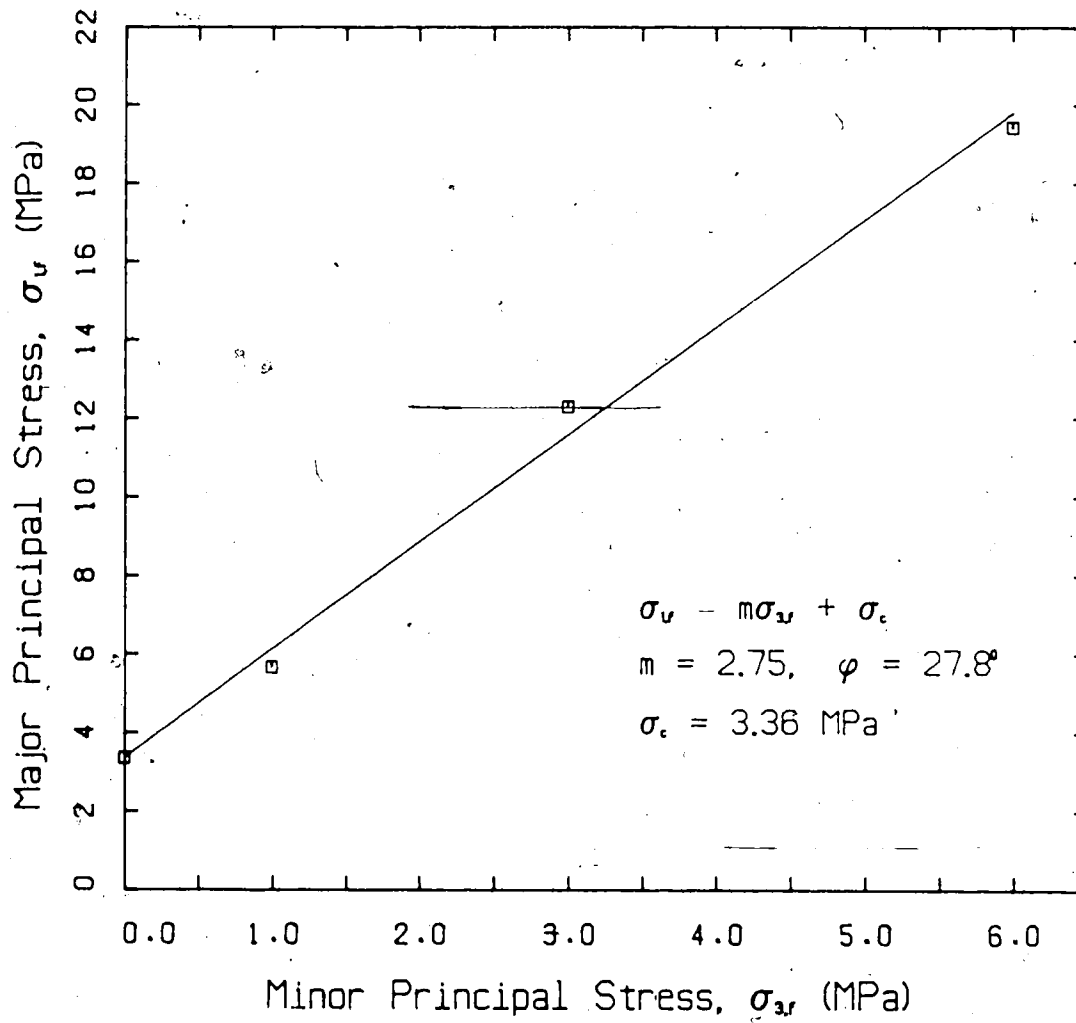


Figure 5.14 Failure Envelope for Jointed Gypstone Medium

6. EXPERIMENTAL DATA AND INTERPRETATION

6.1 Plane Strain Behaviour of Intact Samples

The material properties determined from laboratory tests have been used in the elasto-plastic analysis to predict the behaviour of gypstone samples under plane strain condition. Unfortunately, the dilation coefficient (α) cannot be determined reliably by laboratory tests. Hence, an assumed value of α in the range $1 < \alpha < m$ has been substituted in the analytical equations. The comparison of measured data and theoretical predictions (with an assumed α) provides a realistic method of evaluating the dilation characteristics of gypstone. In practice, α for an actual rock mass cannot be determined and must be estimated. For this purpose, an intact gypstone sample was tested in the PST apparatus, and the displacements of the tunnel wall and the far field boundary were carefully monitored at each stress increment. The radial distances to the tunnel wall and the far field boundary are 130 mm and 700 mm, respectively.

The measured displacements agreed well (within less than 10% deviation) with the predicted data for an assumed dilation coefficient of 2.0 as shown in Figure 6.1. It is evident from Figure 6.1 that the zero volume change condition ($\alpha=1$) underestimates displacements. In contrast, the associative flow condition ($\alpha=m$) overestimates displacements. The material properties of intact gypstone

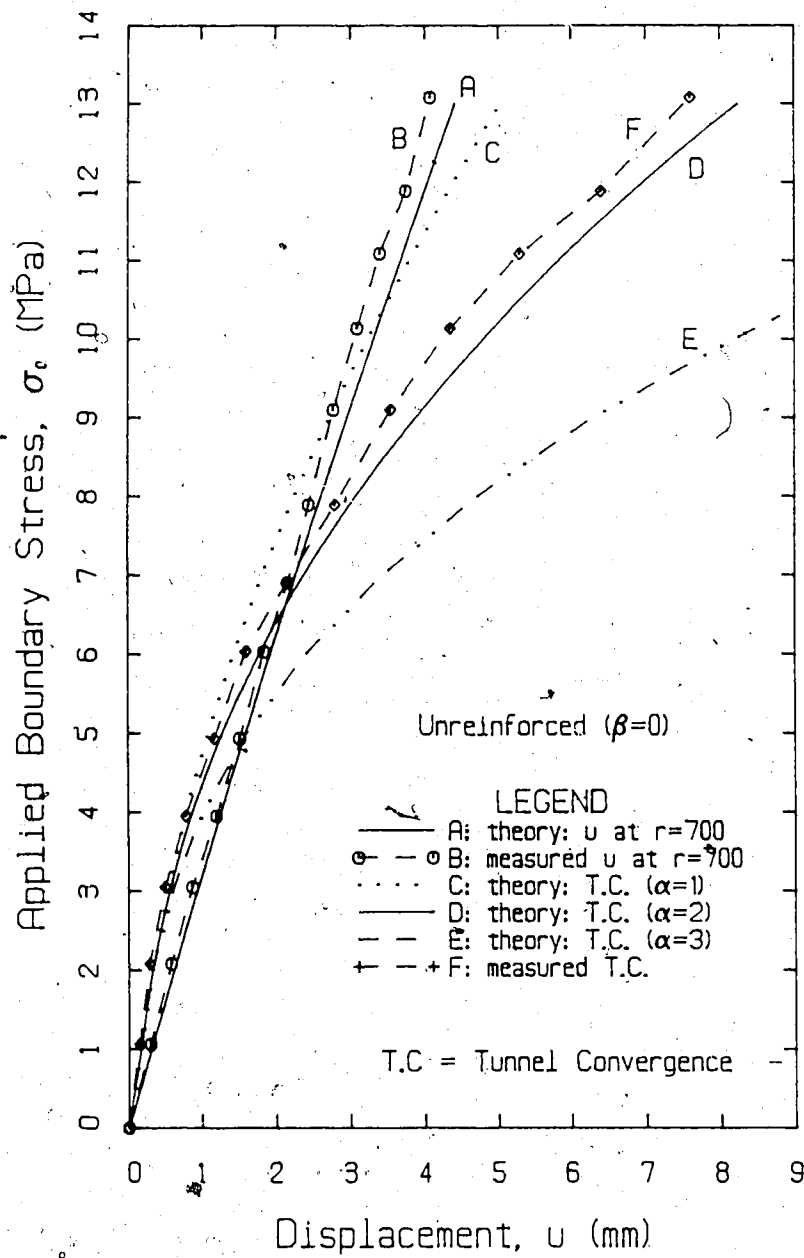


Figure 6.1 Behaviour of Unsupported Opening in PST Apparatus

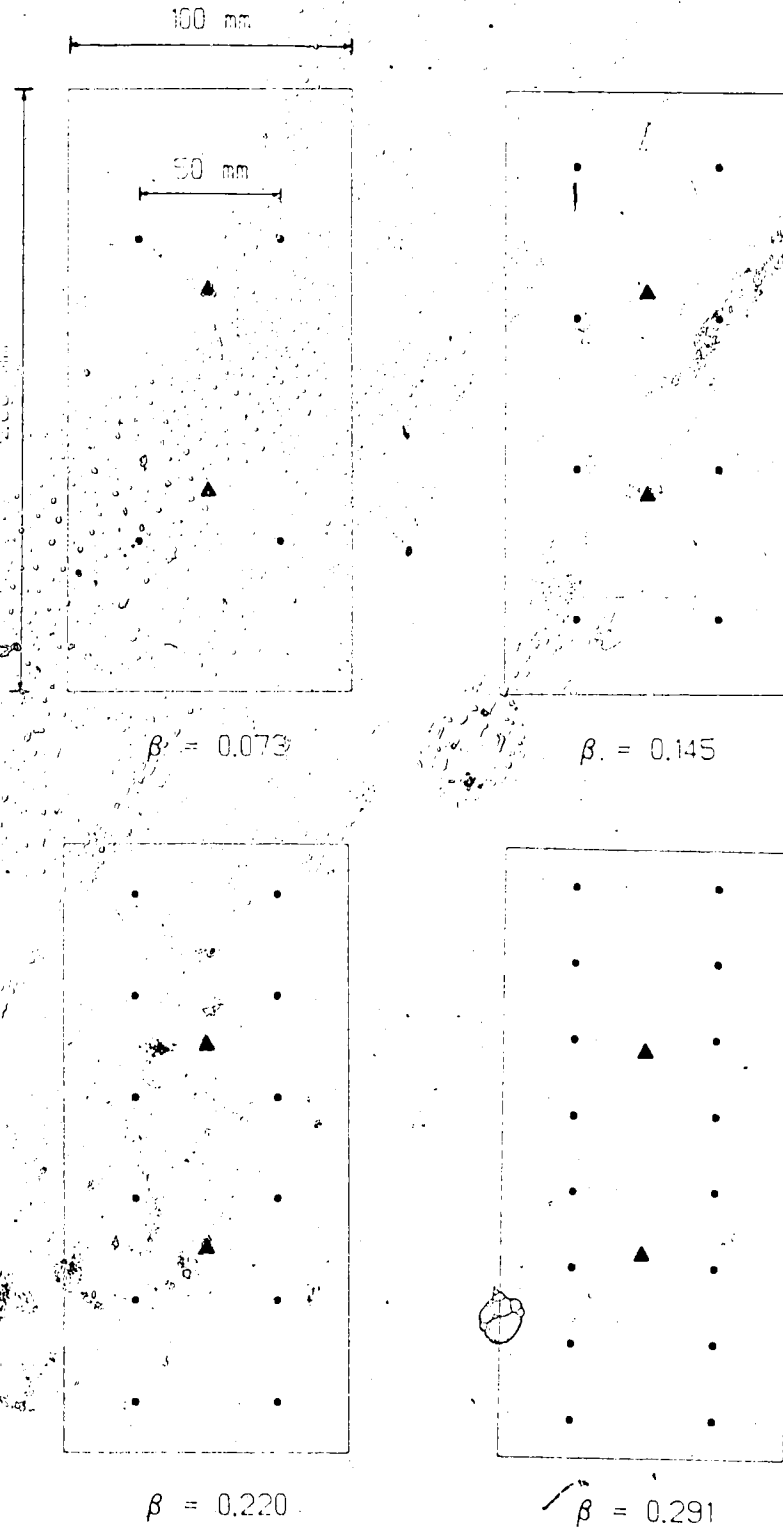
summarized earlier in Table 5.1 have been assumed in the analysis. The accuracy of the predictions made by the general elasto-plastic solutions depends largely on the material properties and the boundary stress conditions simulated by the PST apparatus (Guenot, 1979; Kaiser *et al.*, 1985).

6.2 Behaviour of Reinforced Intact Samples

6.2.1 Bolt Patterns

For the purpose of modelling different bolt patterns, the spacing and the length of bolts were varied. The vertical bolt spacing that represents the longitudinal bolt spacing in reality was varied from 25 mm to 100 mm, while keeping the transverse (tangential) spacing constant at 50 mm. This provides an array of bolt densities varying from $\beta=0.073$ to $\beta=0.291$ as illustrated in Figure 6.2. The installation of two rows of bolts in the transverse direction of the model tunnel section represents a pattern of 16 bolts around the circumference of a full circular opening.

In order to study the influence of bolt length on the behaviour of a tunnel opening, 100 mm and 50 mm long brass bolts (2.5 mm in diameter) were installed in different samples. A typical test sample reinforced by 100 mm long brass bolts at a density of $\beta=0.145$ may simulate a sector of a real tunnel of 5.2 m in diameter, reinforced by 2.0 m long



- typical bolt positions.
- ▲ convergence measuring points.

Figure 6.2 Alternative Bolt Patterns in Test Samples

steel bolts at a spacing of 1.0m x 1.0m.

6.2.2 Strain-Displacement Response of Reinforced Samples

Only one selected set of test data is discussed in detail here for the purpose of clarity. The remaining test results are given in Appendix G. Each test sample has been loaded incrementally to a maximum field stress of 14 MPa in the PST apparatus. The following material properties have been employed in the theoretical analysis of the model openings with bolt densities $\beta=0.145$ and $\beta=0.220$:

$E=1500$ MPa; $\nu=0.25$; $\sigma_c=3.5$ MPa; $\phi=32^\circ$; $s=0.90$ and $\alpha=2.0$.

Figure 6.3 presents an example of the measured and predicted tunnel convergence against the applied field stress for $\beta=0.145$ and $L=100$ mm. Both loading and unloading paths were followed, although one of the LVDT-mounts debonded prematurely (Curve c). The figure indicates excellent agreement of observed and theoretical convergence at lower load levels. Above 8 MPa, the tunnel wall experiences significantly larger convergence as spalling and dilation within the plastic zone become dominant. It is of interest to note that around 11.5 MPa, the radius of the equivalent plastic zone predicted by theory exceeds the bolt length, and the reinforcements become completely embedded in the plastic zone. This transition is reflected by a sudden shift in the theoretical curve, defined by the equation associated with $R' > a+L$. The experimental results do not show the same shift. This is expected, because the model

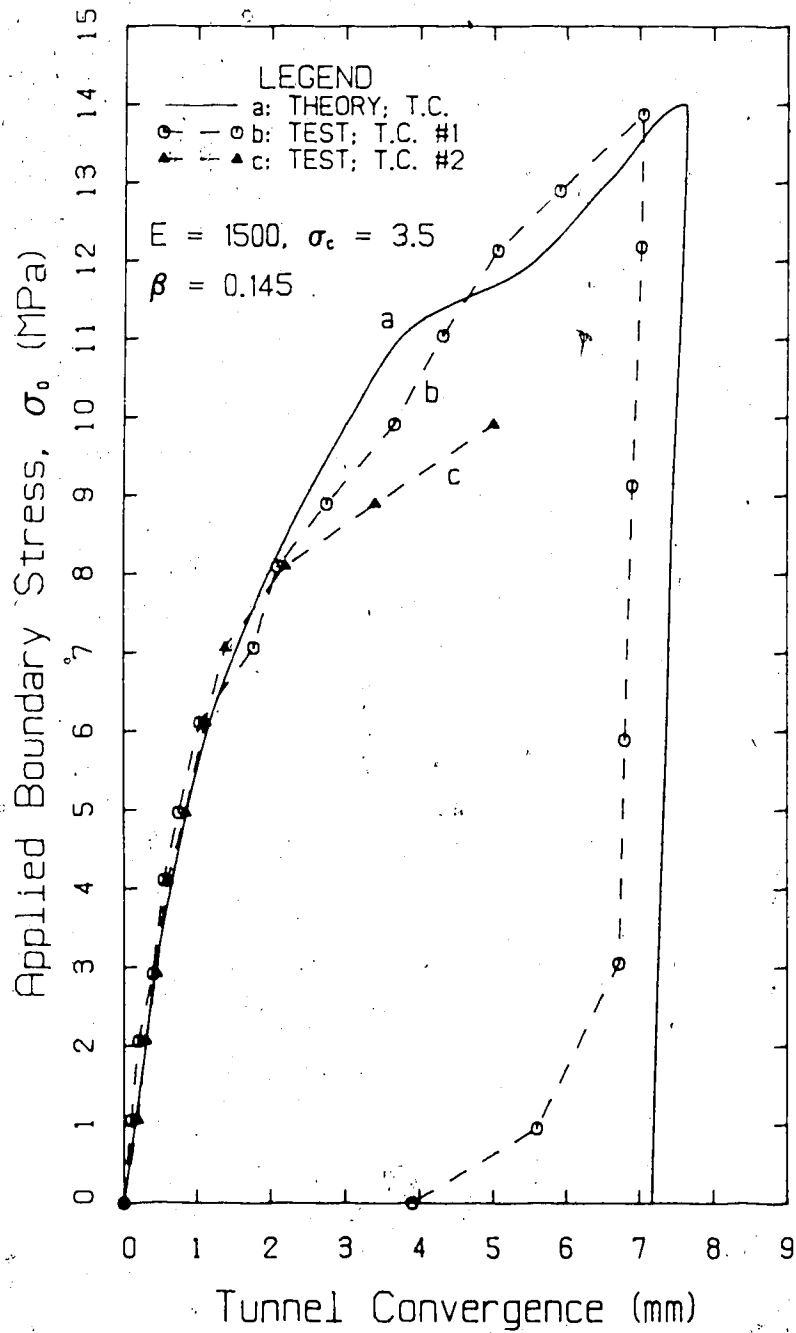


Figure 6.3 Convergence of Reinforced Opening for $\beta=0.145$

material loses its strength more gradually. The post-peak strength loss is not instantaneous as assumed in the elastic, brittle-plastic model. Considering these factors, the predictions and observations are in good agreement.

Figure 6.4 presents the variation of radial strains in close vicinity of the tunnel wall ($r=130$ to 150 mm) with the increase in applied boundary stress. Good agreement between the predicted and the measured strains was generally observed. However, at loads below 4 MPa, the relatively low measured strain response may suggest that the model had a somewhat higher than assumed strength near the tunnel wall, in the order of 4 MPa, due to sample preparation effects. The occurrence of a sudden shift in the theoretical curve associated with $R^* > a+L$ is not convincingly depicted by the test data, due to the same reasons as mentioned earlier with respect to tunnel convergence. In both Figures 6.3 and 6.4, the measured data illustrate a dramatic non-linearity of displacements and strains along the unloading paths at field stresses below 3 MPa. This behaviour is probably associated with the hysteresis phenomenon of crack opening which the analytical approach cannot model.

The radial strains monitored in the outer elastic zone of the sample with $\beta=0.22$ are illustrated in Figure 6.5. These strains were measured by extensometers installed in the positions $r=300/350$ mm and $r=400/450$ mm. The theory predicts a linear response at low applied stresses ($\sigma_0 < 3$ MPa), but with increasing field stress the enhanced

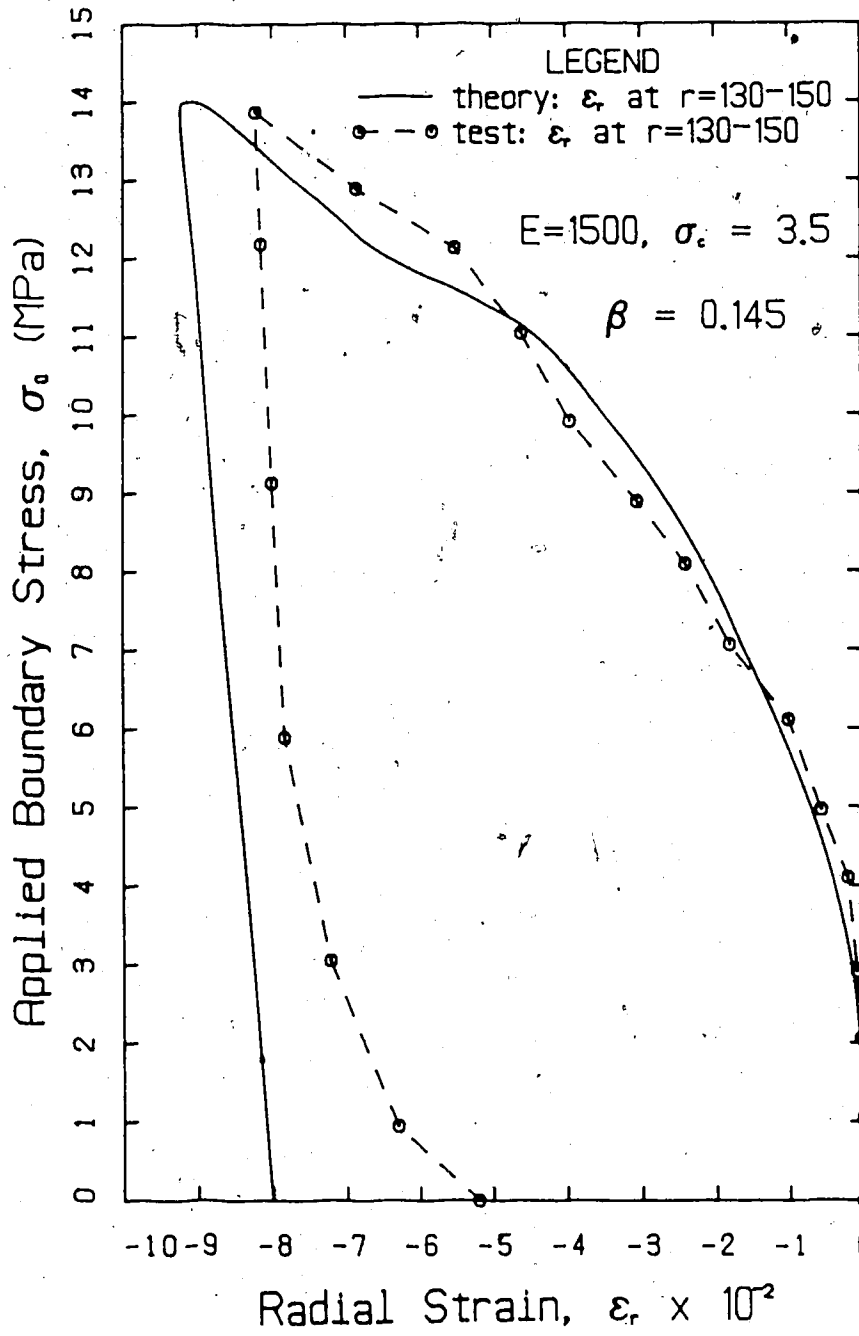


Figure 6.4 Radial Strain at Tunnel Wall for $\beta=0.145$ and $L=100$ mm

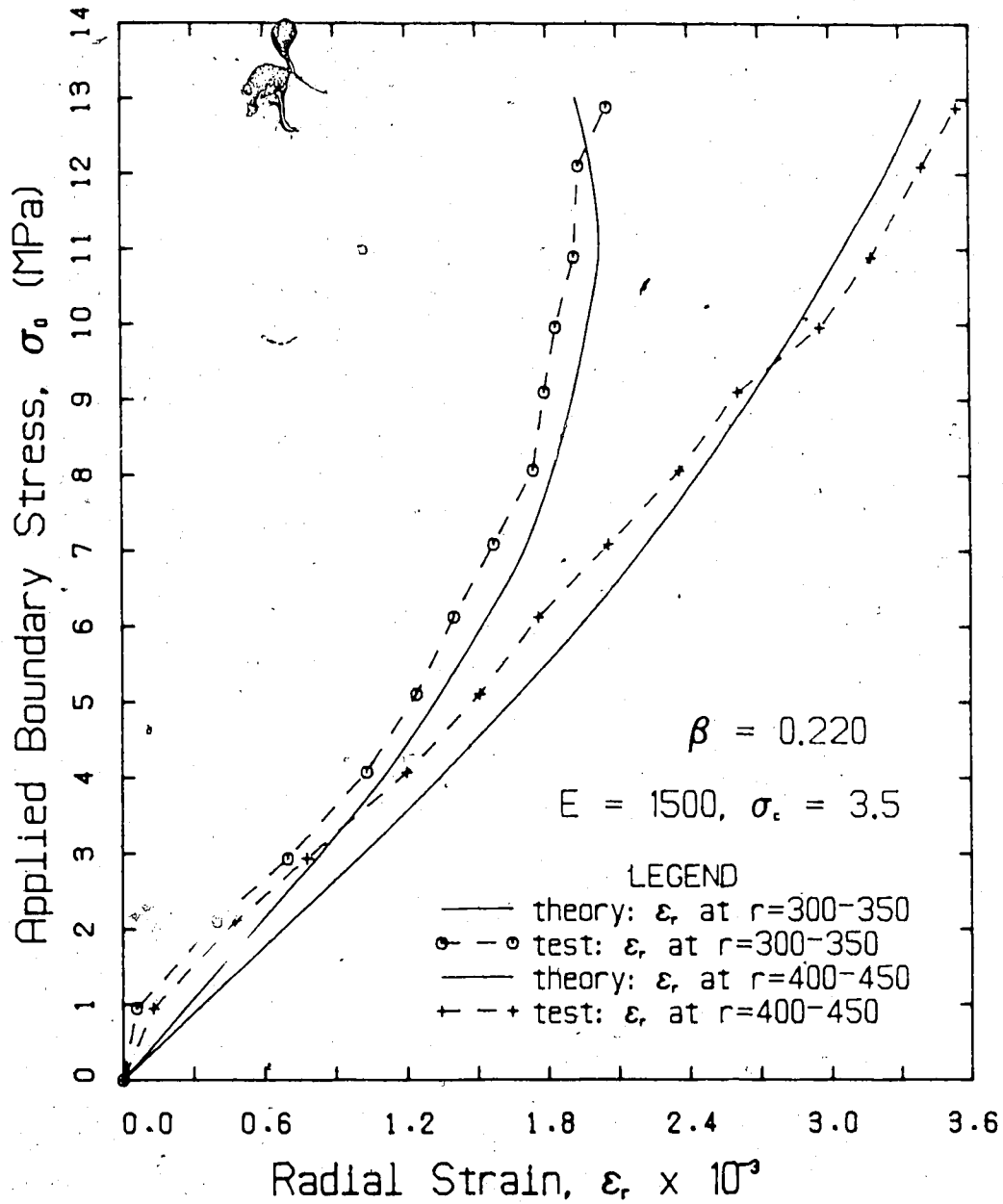


Figure 6.5 Radial Strain in Elastic Zone for $\beta=0.220$ and

$L=100$, mm

effect of plastic zone propagation is reflected by a change in curvature (anti-clockwise) of the radial strain response. The test data show excellent agreement with theory except that at very low field stresses below 2 MPa, the extensometer response is insensitive to small strains (most likely as a result of friction between the coaxial inner and outer rods). Unfortunately, the unloading path could not be followed due to unexpected bursting of an oil seal in one of the hydraulic rams above 13 MPa, preventing further testing.

Figure 6.6 illustrates the displacement of the far field boundary with the applied field stress. The far field boundary ($r=700$ mm) is away from the tunnel wall by more than four tunnel radii ($r=130$ mm). Therefore, the influence of plastic zone propagation on far field displacements is hardly noticeable for the range of applied stresses ($\sigma_0=1$ to 14 MPa), indicating an almost linear elastic response. However, at much higher field stresses, the extent of the plastic zone may become increasingly dominant, producing significant non-linearity. The theoretical predictions deviate from reality, when the plastic zone radius becomes considerably close to the far field boundary. Therefore, a larger geomechanical model would have to be used for accurate predictions at excessively high loads ($\sigma_0>15$ MPa). The measured displacements generally show good agreement with the theoretical predictions, but indicate a somewhat higher deformation modulus particularly along the unloading path.

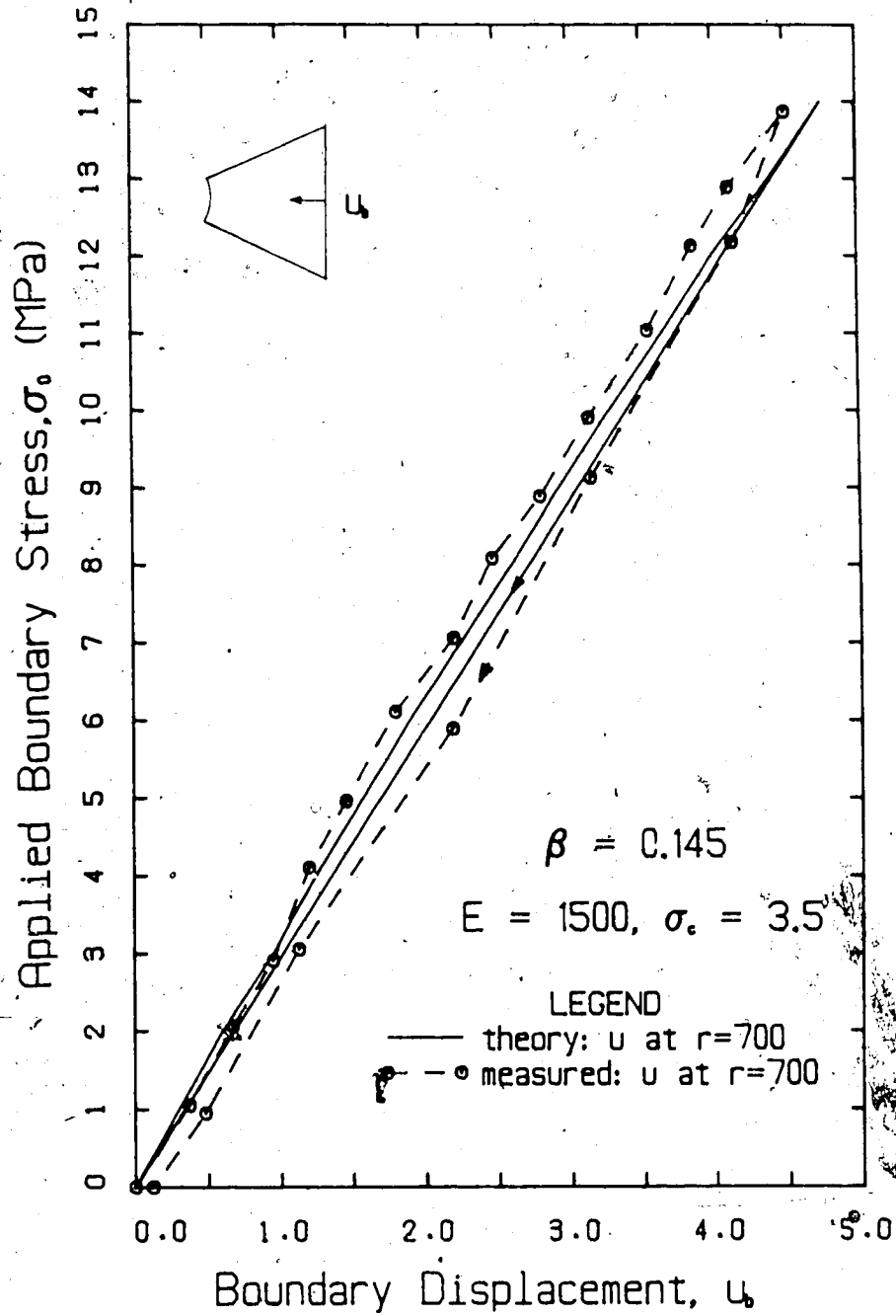


Figure 6.6 Displacement at Field Boundary for $\beta=0.145$ and $L=100$ mm

6.2.3 Normalized Convergence Ratio as a Design Aid

Figure 6.7 summarizes the measured and predicted results from tests with various bolt patterns (L/a constant at 0.7) at applied field stress levels between $\sigma_0 = 5$ to 14 MPa. The measured (dashed and vertically shaded) normalized convergence ratio, u_a^*/u_a , is plotted for these stress levels and five bolt density parameters, and compared with predictions (full lines and horizontally shaded). u_a^* is the total convergence of the reinforced tunnel wall and u_a is the convergence of the unsupported tunnel.

The observed convergence data convincingly support the theoretical predictions. The response of the tunnel convergence in elastic rock has also been plotted for comparison and for the same stress range. The normalized convergence ratio decreases as β increases (i.e., the tunnel convergence reduction is almost proportional to the bolt density). At bolt densities exceeding 0.25 to 0.45, the tunnel wall displacements converge towards the elastic response for stress levels of 5 to 14 MPa. Bolt density configurations where the tunnel wall displacements at a given field stress are less than the calculated elastic response are unrealistic. Therefore, theoretical predictions based on the proposed method of analysis beyond this point are meaningless. However, because the range of bolt densities normally employed in practice varies between 0.05 and 0.20, this does not limit the applicability of the predictive equations.

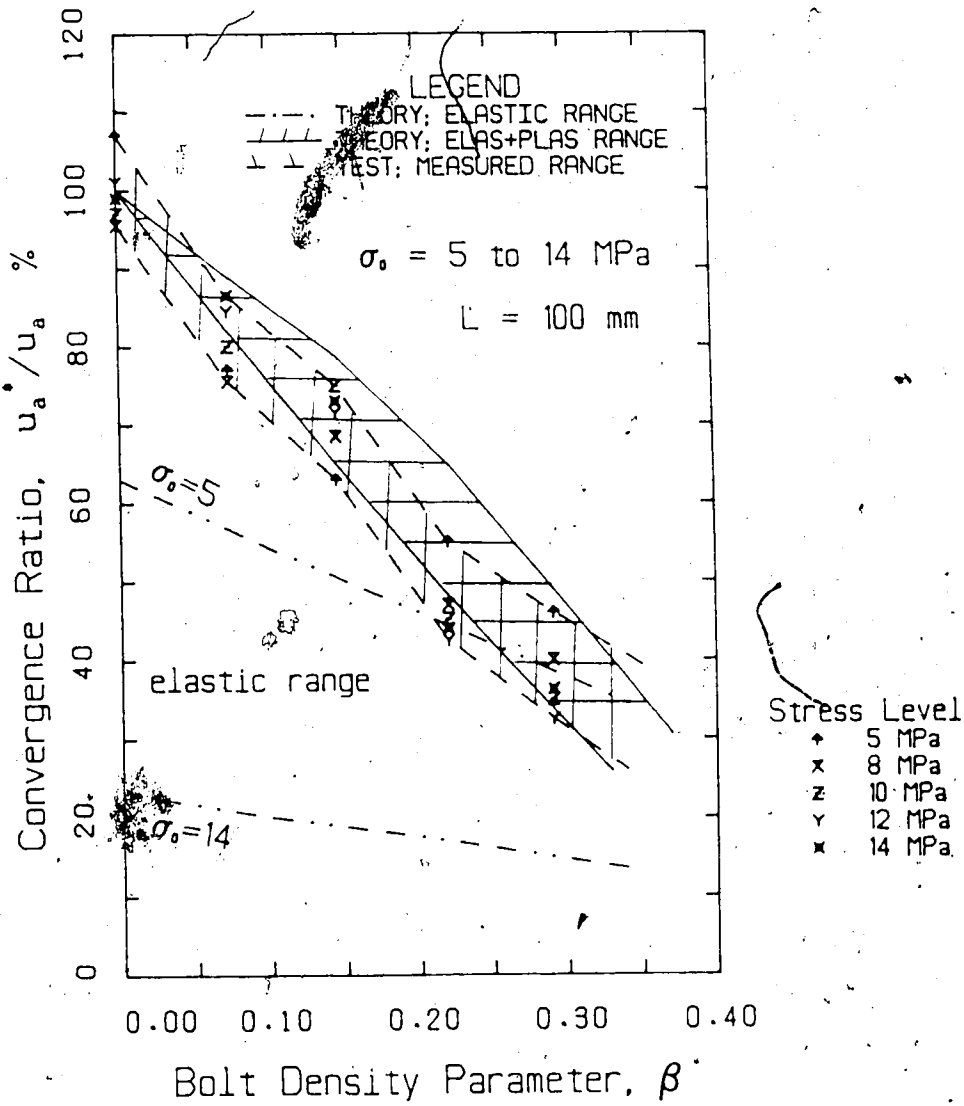


Figure 6.7 Variation of Convergence with Bolt Density for

L=100 mm

It can be shown that the normalized convergence ratio is independent of the elastic parameters and insensitive to moderate changes of the uniaxial compressive strength and the friction angle for a given configuration of reinforcement. Consequently, the relationship illustrated in Figure 6.7 for a given bolt length may be used for design purposes. For example, for a tunnel of 5 m diameter excavated in a yielding rock ($\phi = 35^\circ$; in a field stress of 10 MPa; 400 to 450 m deep) with 2 m long bolts ($L/a = 0.80$), the tunnel wall displacements would be reduced by 40% for a bolt density parameter (β) of 0.20. This could be achieved by installing 32 mm shaped rebars ($\lambda=0.60$) with a spacing of 0.85m x 0.85m.

6.2.4 Influence of Bolt Length on Tunnel Convergence

In order to assess the influence of the bolt length on tunnel convergence, 2 samples ($\beta=0.145$ and $\beta=0.291$) were reinforced by relatively short bolts of 50 mm in length. The measured and predicted strain-displacement response to the applied field stress is given in Appendix H. The agreement between the measured and the predicted data was generally within 10% for both samples.

Figure 6.8 summarizes the normalized convergence ratio against the bolt density parameter for 50 mm long brass bolts (2.5 mm in diameter). The measured results for $\beta=0$, 0.145 and 0.291 are plotted for comparison with the predictions, for the applied stress levels of 5 to 14 MPa. A

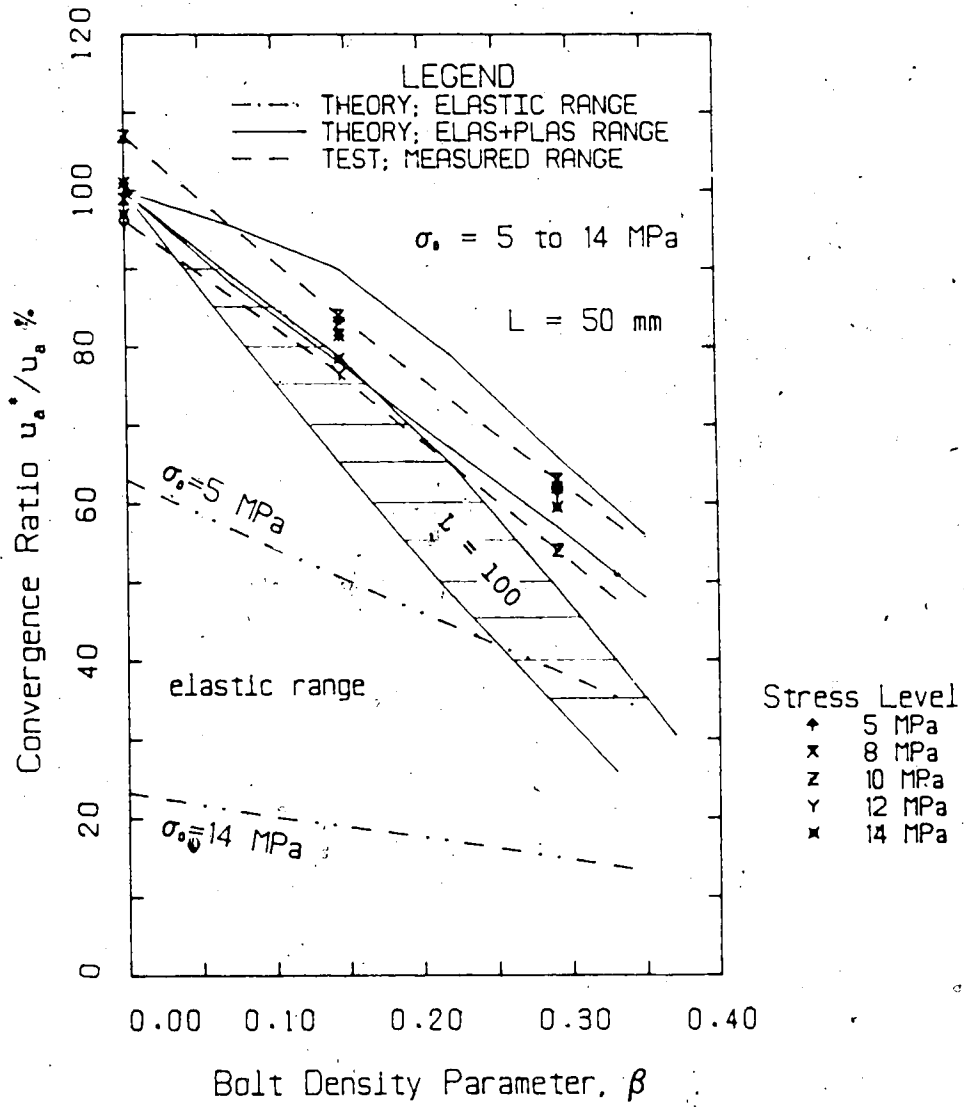


Figure 6.8 Variation of Convergence with Bolt Density for L=50 mm

comparison of Figure 6.7 with 6.8 clearly shows that the convergence reductions attained by 50 mm bolts ($L/a = 0.38$) are considerably less than those achieved by 100 mm bolts ($L/a = 0.76$), particularly at high bolt densities. The horizontally shaded range for 100 mm bolts has been repeated for ease of comparison. For instance at $\beta=0.25$, a convergence reduction of 42 to 58% is predicted for 100 mm bolts, whereas only a 26 to 37% reduction is expected for 50 mm bolts. The observed data generally indicate a very similar trend for the same applied stress levels.

At relatively low bolt densities ($\beta < 0.15$), the reduction in total convergence is less pronounced for any given bolt length, because the magnitudes of equivalent (improved) strength parameters (m^* , σ_c^*) decrease rapidly with the reduction of bolt density parameter (β). For instance, at $\beta=0.10$, a convergence reduction of 5 to 15% is predicted for 50 mm bolts, whereas the installation of 100 mm bolts curtails tunnel wall displacements only marginally predicting a convergence reduction of 15 to 23%. The measured test data verify these predictions with less than 10% deviation. In other words, the virtues of increasing the bolt length are less significant at low bolt densities, where yielding is considerable.

Figure 6.8 also indicates, that excessively high bolt densities ($\beta > 0.50$ to 0.60) are required for 50 mm bolts in order to limit tunnel wall displacements close to the elastic response. These densities would almost have to be

double the magnitudes of β required for the same convergence reduction by 100 mm bolts. Bolt density parameters of 0.50 to 0.60 are both impractical and uneconomical to be employed in the field. In such cases, where the required bolt densities are excessively high ($\beta > 0.25$), effective convergence reductions can only be attained by increasing the bolt lengths. It is obvious, that for a wide range of field stresses ($\sigma_0 = 5$ to 14 MPa), the bolt length/tunnel radius (L/a) ratio of 0.38 is certainly inadequate in obtaining acceptable convergence reductions. Based on the results of this study, it may be concluded that L/a ratios less than 0.75 cannot be recommended for efficient convergence control, even if acceptable bolt densities ($\beta > 0.15$) are employed.

The effect of increasing the bolt length on tunnel convergence is particularly emphasized, if as a result, the extent of the plastic zone becomes enclosed within the reinforced region ($R^* < a+L$). For example, at $\beta=0.291$ and at $\sigma_0=14$ MPa, a decrease in tunnel convergence from 9.6 mm to 3.5 mm (63.5% reduction) can be achieved by 100 mm bolts, because the plastic zone has not propagated beyond the bolted zone at this load. However, if 50 mm bolts are installed at the same field stress of 14 MPa, the plastic zone extends beyond the reinforced zone generating a much higher tunnel wall displacement of 6.2 mm (35.4% reduction). The measured convergence data verify this behaviour within an accuracy of 6 to 8%.

The influence of bolt length on tunnel convergence decreases significantly, if the plastic zone has propagated much beyond the reinforced zone ($R^* > a+L$). For example, for $\beta=0.145$ and at a field stress of 14 MPa, the convergence reductions associated with 100 mm and 50 mm bolts are 20.4% and 17.6% respectively, indicating a negligible effect of doubling the bolt length. Bolts of $L > 125$ mm would be more effective for this case.

6.2.5 Strain Distribution

The shorter the bolts are around an opening, the greater the extent of yielding and, hence, the tunnel wall displacements for a given field stress. The radial strains near the tunnel wall ($r=130$ to 150 mm) are affected in the same manner as the convergence. However, the influence of bolt lengths on the radial strains in the outer elastic zone depends on the radial distance to the point of interest. Figure 6.9 illustrates the radial strains measured in the regions $r=300$ to 350 mm and $r=400$ to 450 mm for $\beta=0.145$ and $L=50$ mm.

The continuous change in curvature of the predicted and measured data with increasing stress, particularly in the region $r=300$ to 350 mm, indicates significant influence of yielding associated with reduced bolt lengths. An increase in bolt lengths or the bolt density is reflected by a reduction in curvature (anti-clockwise) of the radial strain response as shown earlier in Figure 6.5 for $\beta = 0.22$ and

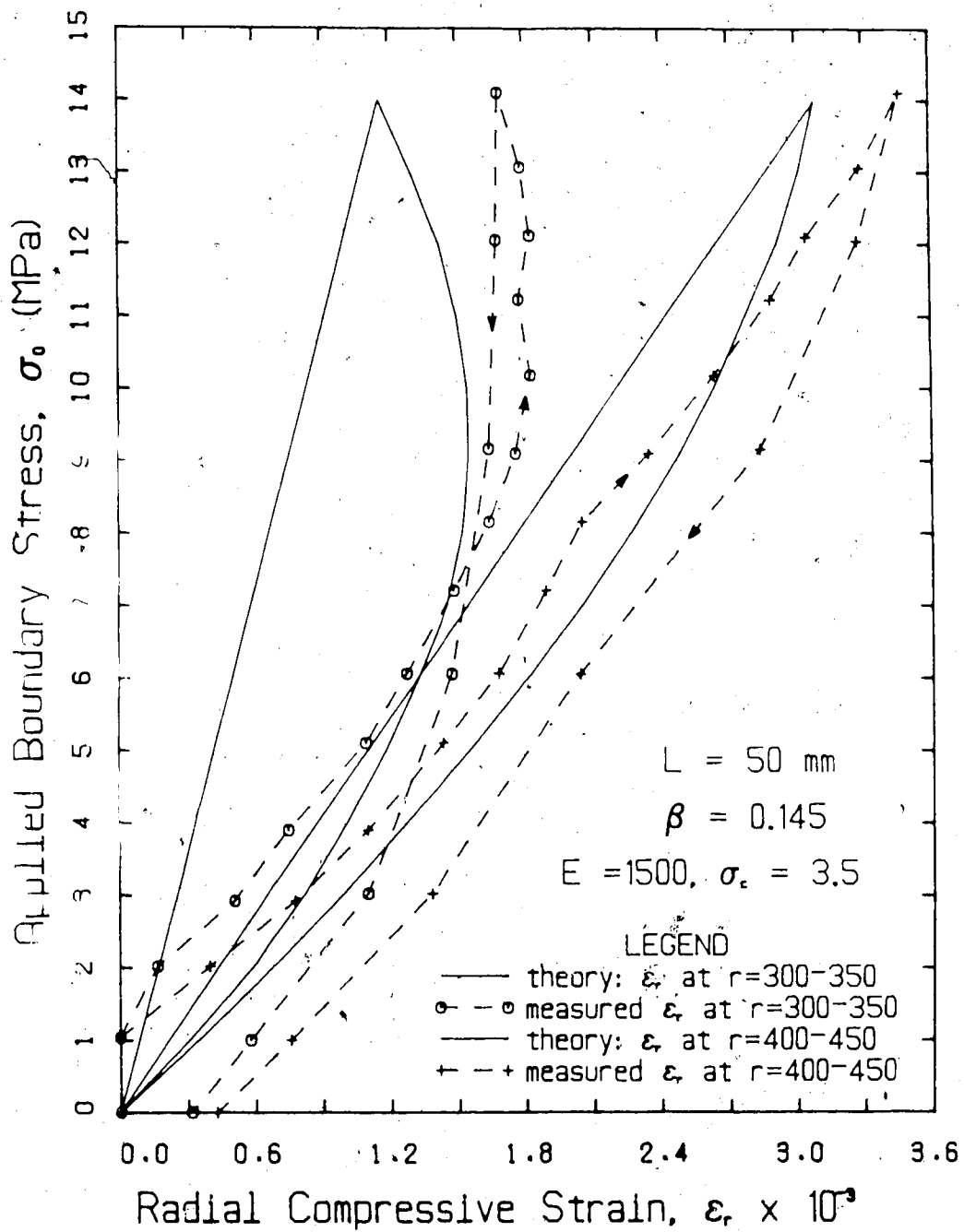


Figure 6.9 Radial Strain Response in the Elastic Zone for $\beta=0.145$ and $L=50 \text{ mm}$

$L = 100$ mm. The observed strain data (Figure 6.9) imply the possibility of a higher apparent strength of the material. The insensitivity of the strain response below 2 MPa is probably due to the frictional resistance between the coaxial measuring rods of the extensometers.

Neither the bolt length nor the bolt density can significantly influence the displacement response of the far field boundary to the applied stress. This is to be expected because the radial distance to the far field boundary is more than five tunnel radii, thereby making the elastic boundary displacements nearly independent of yielding around the opening.

6.3 Influence of Bolts on the Behaviour of Reinforced Tunnels in Jointed Material

6.3.1 Simulation of a Tunnel Opening in a Jointed Medium

The dimensions of the jointed test samples were identical to those of the intact samples described earlier (Figure 5.10). However, four sets of joint planes were introduced to represent a jointed medium as illustrated by a typical test sample in Figure 6.10. For the purpose of testing convenience, the density of the joints has been reduced beyond a distance greater than 275 mm from the tunnel wall, because this outer region remains elastic for the range of field stresses applied by the PST apparatus. Each test sample represents any one of the eight segments

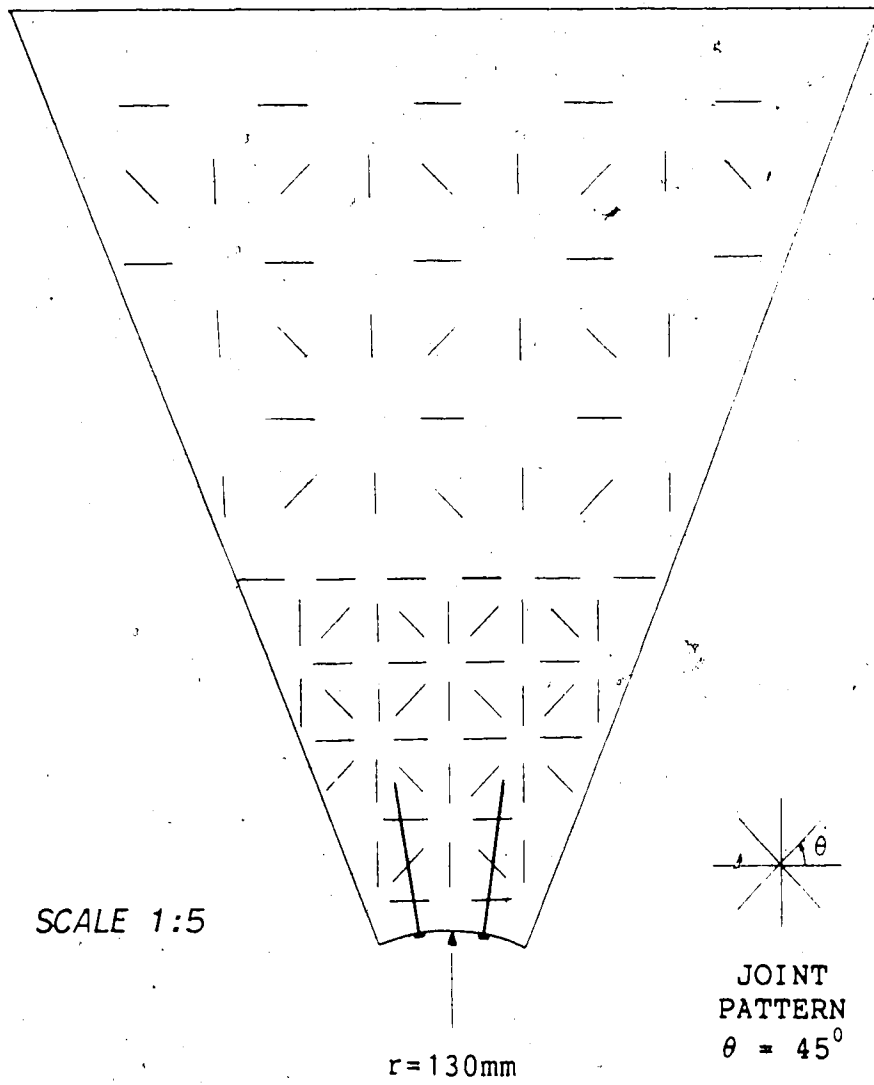


Figure 6.10 Geomechanical Model of ~~Failure~~ in a Jointed Medium

which constitute the complete tunnel opening when assembled circumferentially. The selected pattern of four closely spaced joint sets is not only expected to maintain nearly isotropic behaviour of the jointed rock mass (Hoek and Brown, 1980), but is also arranged to establish the same joint directions around the opening by symmetry between adjacent segments. In order to study the effect of grouted bolts on the strain and displacement response of this jointed medium, several bolt densities were simulated with $\beta=0.073$, 0.145 and 0.220 . The geometry of the brass bolts installed was kept constant at 100 mm in length and 2.5 mm in diameter.

Initially, a jointed sample without bolts ($\beta=0$) was tested (plane strain) in the PST apparatus. This preliminary test was necessary to verify accurately the properties of the jointed medium for comparison with those determined earlier in Section 5.9.1 for the same joint pattern. Figure 6.11 shows the variation of tunnel convergence ($\beta=0$) with the applied field stress in the jointed medium. The measured data agree well with the predicted data (Curve C) with a maximum deviation of 12% for the applied stress range of 0 to 14 MPa. The comparison of predicted and measured strain-displacement response of the unreinforced sample verifies, that the equivalent parameters $\phi = 27.5^\circ$, $\sigma_c = 3.4$ MPa, $E = 1400$ MPa, $\nu = 0.25$ and $a = 2.0$ are realistic in modelling the behaviour of heavily jointed gypsum as an apparently isotropic medium. A comparison

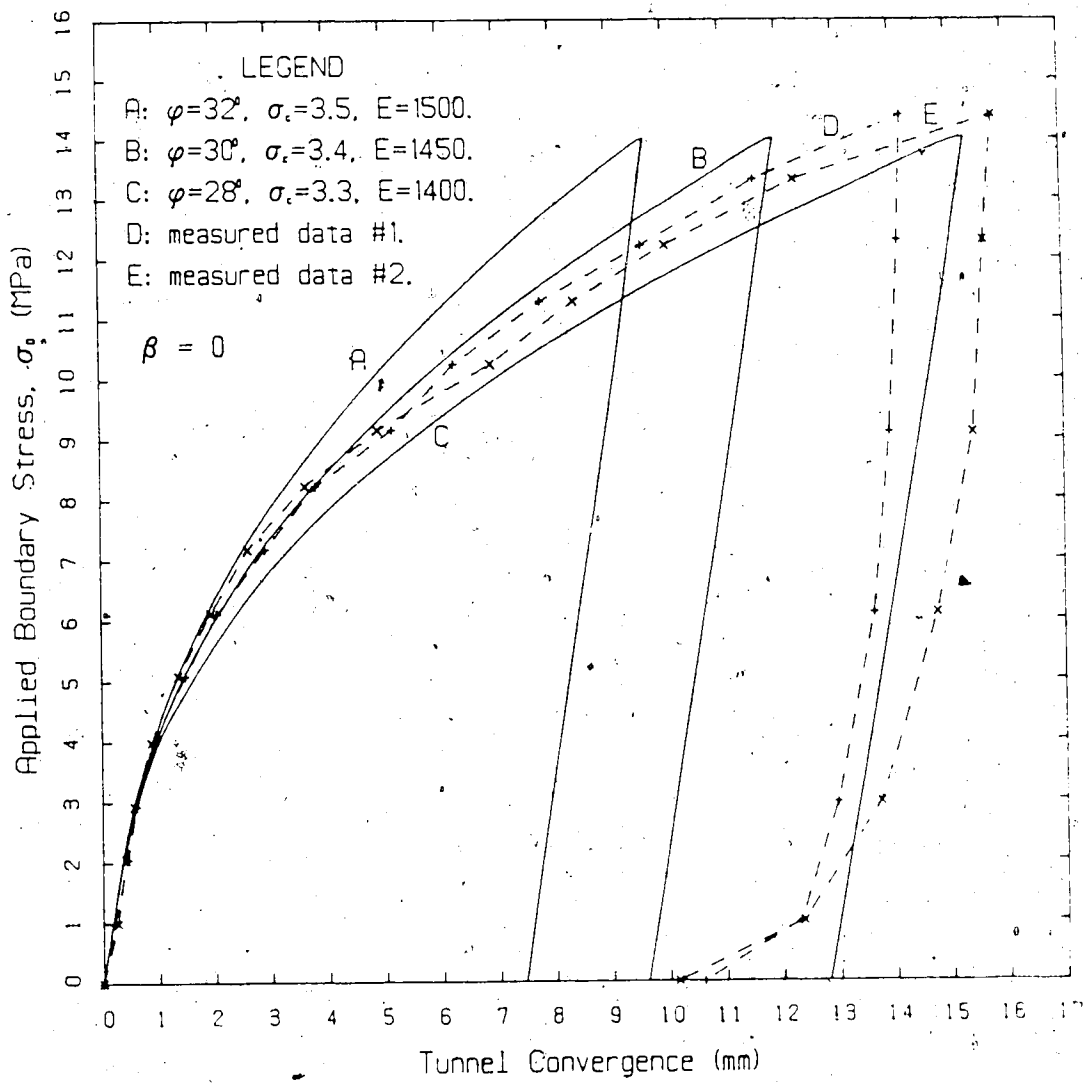


Figure 6.11 Convergence Response of a Typical Jointed Sample

with Table 5.1 shows that the jointed mass properties are slightly less than those of the intact material. The variation of strains and displacements with the applied field stress of all jointed samples is illustrated graphically in Appendix I. They support the extension of the analytical model in predicting the behaviour of an opening excavated in a medium with four relatively closely spaced joints.

However, there are a few limitations of the analytical model in the application to jointed rock. For example, if either the number of the joint sets is less than four (i.e., not axisymmetric around the tunnel) or if some joints are much weaker than the others, then the effects of anisotropy dictate the behaviour of the rock mass around the tunnel. On the contrary, if a large number of joints with similar properties exist randomly in a rock mass, nearly isotropic behaviour can be expected as explained by Hoek and Brown (1980).

As expected, the convergence response of the tunnel wall indicates higher magnitudes for the jointed sample. For example, at a field stress of 14 MPa, the behaviour of the reinforced opening with $\beta=0.145$ in the jointed medium indicates a convergence increase of 54%, with respect to the corresponding opening in the intact medium at the same stress level. Particularly at field stresses in excess of 7 MPa, the observed convergence increases at a higher rate than the predicted response of the intact medium. This is

expected as the joints are only affected when yielding propagates and considerable joint displacement is induced after weakening of the opening wall. Therefore, a gradual transition from the predicted behaviour of the intact to the discontinuous mass model is expected and observed with increasing field stress.

Figure 6.12 summarizes the convergence data for all the jointed samples tested in plane strain triaxial compression. The normalized convergence ratio (u_a^*/u_a) is plotted against the bolt density parameter (β) for the field stress levels of 5 to 14 MPa. u_a^* and u_a represent the convergences of the reinforced and unsupported tunnels in the jointed medium respectively. The test data indicate excellent agreement with the predictions assuming reduced rock mass properties. It is observed from Figure 6.12, that the tunnel convergence ratio decreases again almost linearly with bolt density, and approaches the elastic response for $\beta > 0.30$. In fact, a very similar trend was observed for intact samples reinforced with 100 mm bolts. The comparison of Figures 6.7 and 6.12 reveals that although a material with inferior strength and deformation parameters (jointed medium) results in larger tunnel wall displacements, the normalized convergence ratio (u_a^*/u_a) for a given bolt density (β) is insensitive to moderate changes of material properties. Therefore, the normalized convergence ratio against bolt density parameter relationships can be utilized as an useful tool in the displacement controlled design approach for a

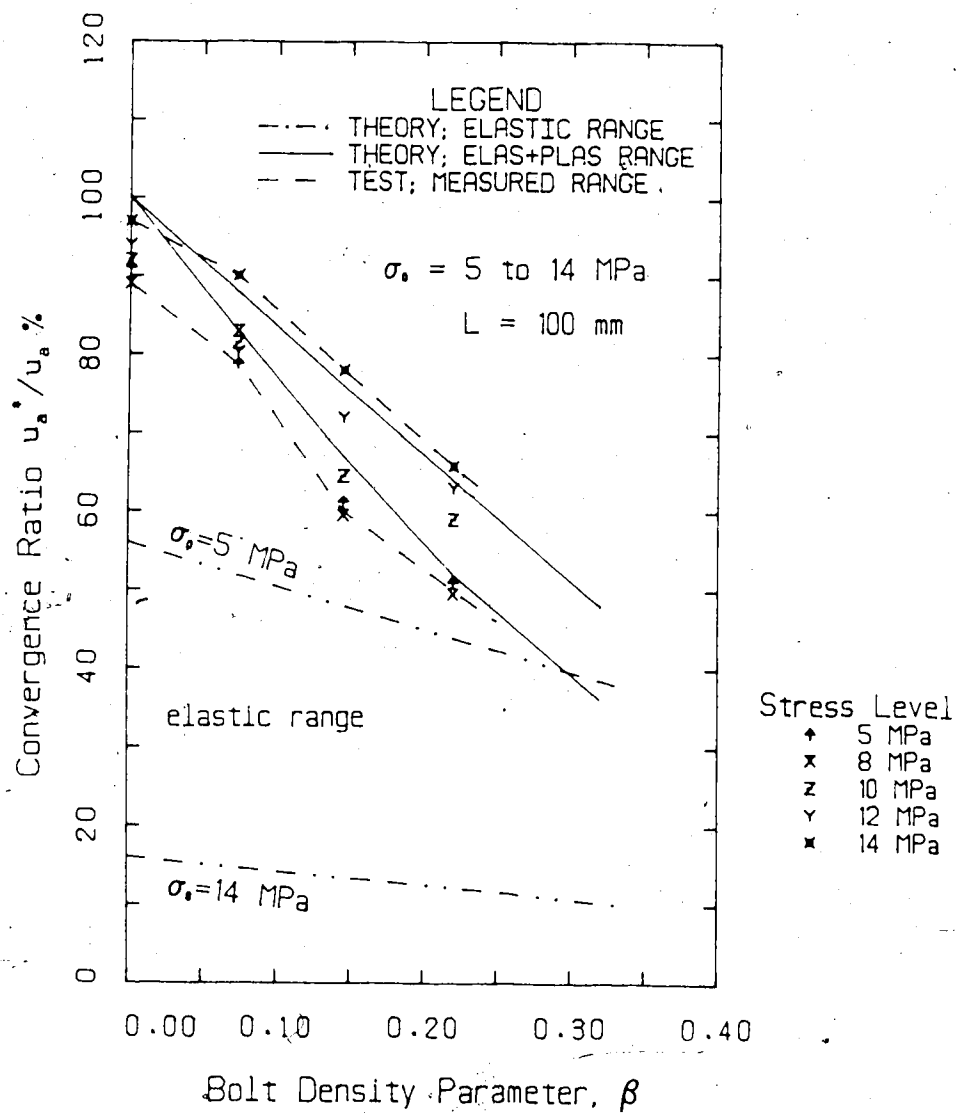


Figure 6.12 Variation of Convergence with Bolt Density for Jointed Samples

range of yielding rocks.

6.4 Observed Rupture Processes Around Tunnel Openings

6.4.1 Tunnel Openings in Intact Rock

As discussed in Chapter 4, two major types of potential failure mechanisms could be predicted theoretically. Shear failure of a tunnel excavated in a hydrostatically loaded Mohr-Coulomb material is associated with disintegrating wedges that are defined by intersecting spiral rupture surfaces. In addition, surface instabilities are associated with tensile splitting, spalling and slabbing of the tunnel wall. The synthetic material gypstone falls within the zone of predominant shear failure ($\eta < \eta_{cr}$), as indicated by the stability curve (Figure 4.3). Localized spalling (slabbing) of the unsupported tunnel wall was initiated beyond a field stress of 7 MPa, followed by extensive shear fracturing at loads above 12 MPa. The observed slabbing at lower stress levels has to be attributed to the existence of a thin skin of stronger rock at the tunnel wall. This skin is a result of the model preparation procedure.

The experimental observations consistently verified the analytical predictions that ultimate failure around circular openings reinforced with grouted bolts also occurs by disintegrating wedges associated with the intersection of multiple slip lines (shear). Plate 6.1 illustrates the multiple slip lines and associated wedge failure after

unloading from a field stress of 14 MPa, for two reinforced model tunnels ($\beta=0.073$ and 0.145) in intact gypstone medium.

In fact, the bolt density had a significant effect on the rupture propagation. As the bolt density was increased ($\beta > 0.145$), the extent of shear failure associated with the intersection of spiral slip lines was diminished dramatically, even at the maximum applied field stress of 14 MPa. The analytical model predicts a reduction of the angle subtended between the slip lines and the corresponding tangent at the tunnel wall, as a result of the increased apparent friction angle due to the grouted bolts. This in turn implies a reduction in extent (depth) of the failure zone. The observed shear failure around heavily reinforced model openings supports these analytical predictions.

Localized spalling of the tunnel wall continued to occur in the regions where the influence of rock reinforcement was minimum, but less pronounced. Plate 6.2 illustrates the failure pattern around openings associated with dense bolt patterns ($\beta=0.220$ and $\beta=0.291$). A comparison of Plates 6.1 and 6.2 clearly indicates a reduction in depth of the failure zone (segregating wedges) with increasing bolt density.

6.5 Observed Rupture processes of Jointed Samples

Failure initiation in the jointed samples differed from that of intact samples. The failure around the opening, without doubt, was influenced by the plane of joints nearest

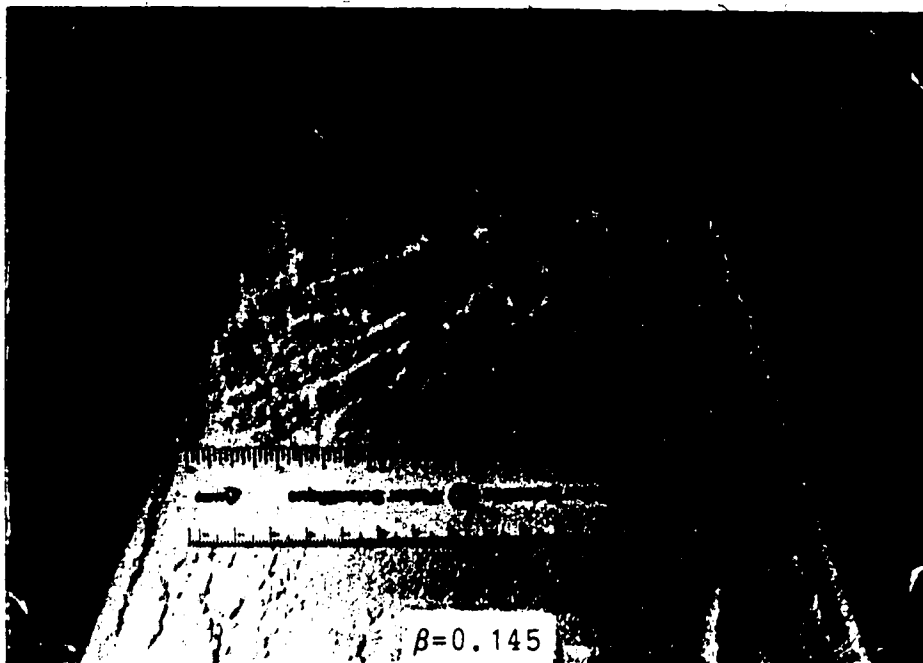
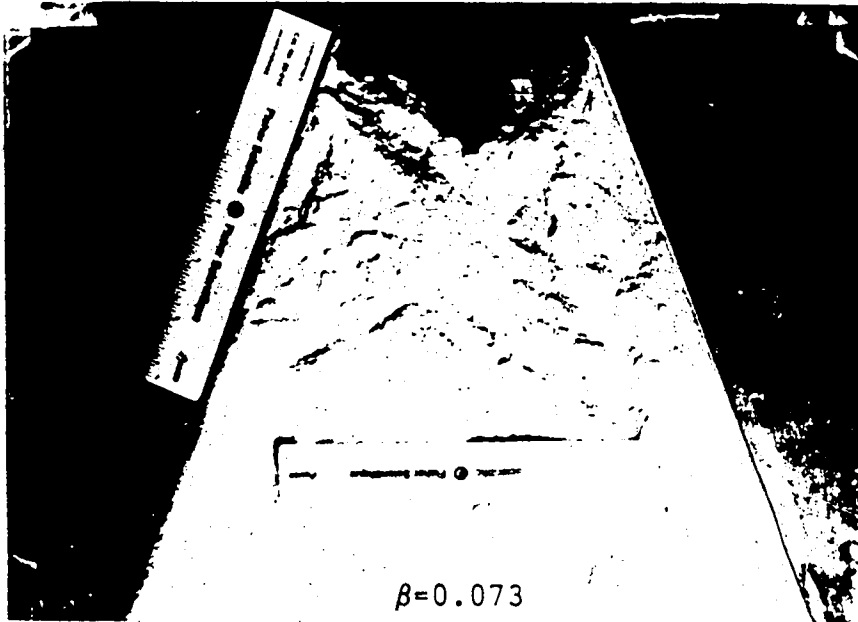


Plate 6.1 Failure Around Openings with Minimum Reinforcement

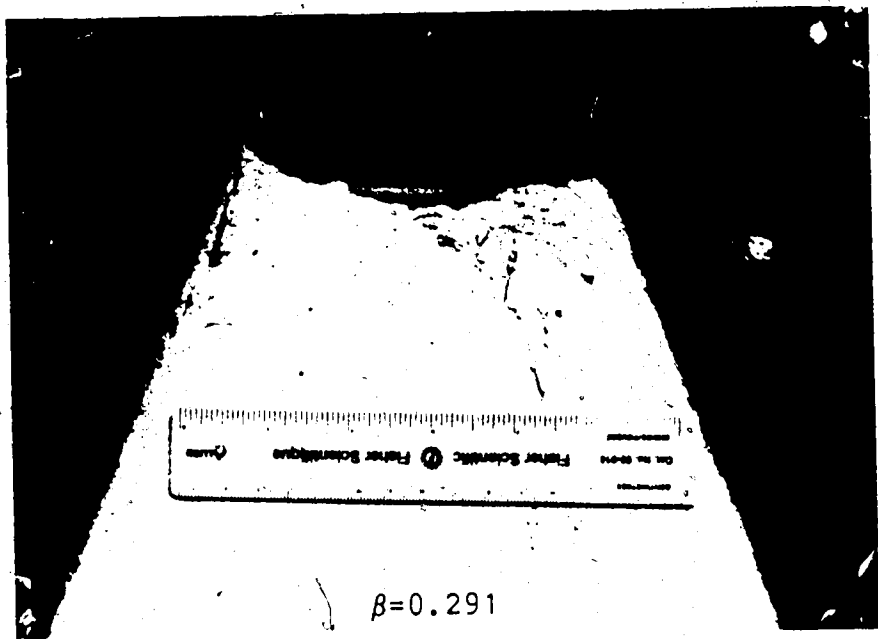


Plate 6.2 Failure Around Intensely Reinforced Openings

to the tunnel boundary. At low bolt densities (e.g. $\beta=0.073$), the zone of failure extended from the tunnel boundary to the plane of the nearest joints. In other words, the direction of the failure lines has been dictated by the critical plane of joints in the vicinity of the opening. However, the occurrence of surface instabilities (spalling and splitting) on the tunnel wall was similar to that of intact samples. Again, it is attributed to a thin skin of stronger rock at the tunnel wall. Plate 6.3 illustrates in both plan and elevation, the failure of a typical unsupported model tunnel in jointed rock after a field stress level of 14 MPa.

The effect of bolting on the jointed medium is very encouraging. The increase in bolt density ($\beta > 0.145$) has the effect of dramatically curtailing joint movements, with the result of decreasing the tunnel convergence (e.g. Figure I.12). Furthermore, failure initiation was postponed until the application of relatively high field stresses in excess of 9 to 10 MPa. For instance, at a bolt density of $\beta=0.22$, both shear fracture around the opening and surface instability of the tunnel wall were considerably restricted. The failure mode in fact resembled the one of a heavily reinforced opening in an intact medium. The zone of failure around the opening associated with shear planes (at $\sigma_0=14$ MPa) was confined to the immediate vicinity of the tunnel boundary, and was prevented from extending towards the nearest joint plane.

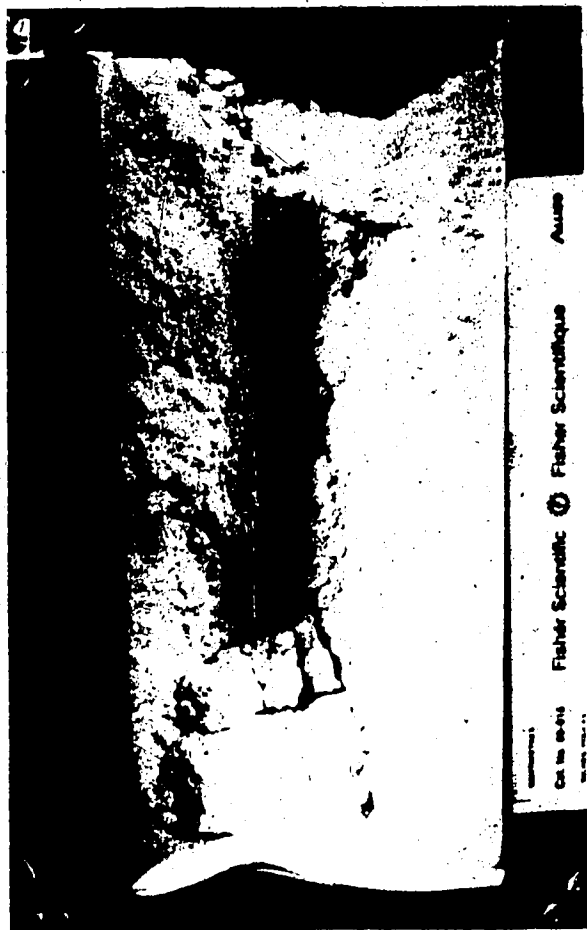


Plate 6.3 Influence of the Critical Joint Plane on Rupture

It may be concluded from these observations, that the behaviour of an opening in a jointed medium can be improved by employing an intensive bolt density, which can minimize joint displacements in the vicinity of the opening. The greater the bolt length, the larger the number of joints stabilized. However, the joints further away from the tunnel boundary (2 to 3 radii) do not experience the same magnitude of displacements typical of the joints in the weakened plastic zone near the tunnel wall. Consequently, increasing the bolt length beyond a certain depth from the plastic zone boundary implies rapidly diminishing economic returns.

7. ANALYSIS OF A CASE HISTORY AND COMPARISON WITH EMPIRICAL DESIGN METHODS

7.1 Analysis of Enasan Tunnel

The application of the elasto-plastic analytical solution to the Enasan tunnel project in Japan (Ito, 1983) will be demonstrated here. In this project, two parallel highways were constructed through Mount Enasan in the vicinity of the active Andrea fault of the central Alps in the Japanese island of Honshu. These highways are 8.6 km in length and are separated by 60 m center to center. The tunnel sections (North Enasan Highway) considered in this study have a radius of approximately 5.1 m, and they are subjected to a mean overburden depth of 450 m.

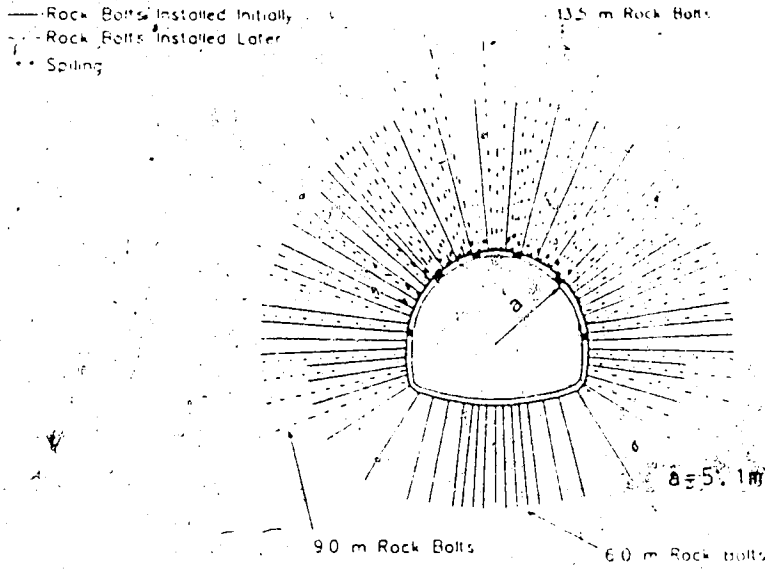
The Enasan Tunnel was constructed in three sequential excavation stages (heading, bench and invert) by the New Austrian Tunnelling Method. It was driven through heavily folded and fractured granite characterized by the following material properties: $E=245$ MPa, $\nu=0.4$, $\phi=35^\circ$, $c=0.49$ MPa, $\sigma_c=1.32$ MPa and $\gamma=25$ KN/m³ (Ito, 1983). Since the peak and ultimate strength parameters were found to exhibit nearly the same magnitudes, the post-peak behaviour could be modelled by a perfectly plastic stress-strain response with $s \approx 1.0$. The dilation properties of the rock were represented by a dilation coefficient (a) of 1.5, which was assumed to be typical for highly overstressed rock.

7.1.1 Geometry and Pattern of Bolts

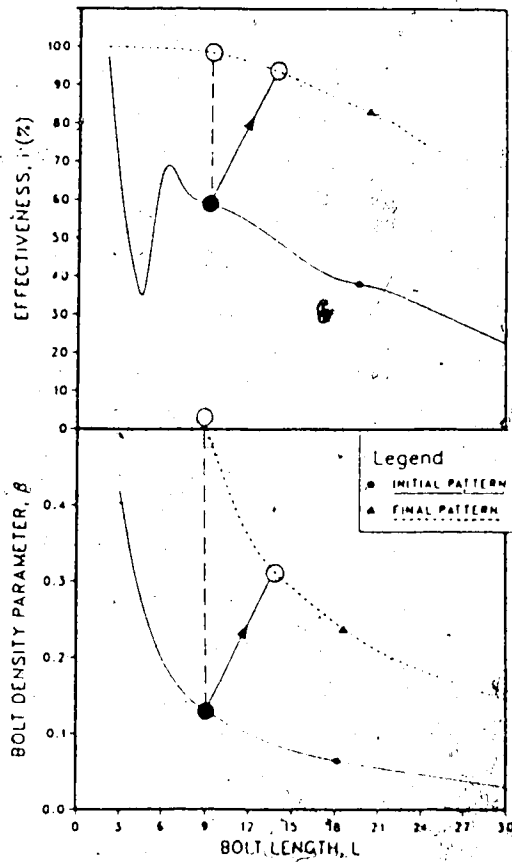
Figure 7.1a illustrates a typical transverse section of station B of the North Enasan Highway (Barlow, 1986). The initial support system consisted primarily of 9 m long grouted bolts (24 mm in diameter) installed at a spacing of 1.0 m x 1.05 m. A friction factor (λ) in the order of 0.35 to 0.40 can be regarded as typical of smooth grouted rebars installed in heavily fractured rock. A longitudinally slotted shotcrete liner was also installed. Supplemental reinforcement with 9 m and 13.5 m long bolts was employed when unacceptable convergences continued to occur, resulting in a mean circumferential bolt spacing of 260 mm. In fact, this corresponds to an increase in bolt density from $\beta=0.13$ to $\beta=0.52$.

7.1.2 Prediction of Tunnel Convergence

An unsupported tunnel section excavated in the same heavily fractured rock mass would present a predicted yield zone of 12.4 m in radius, with a corresponding convergence in excess of 2.0 m (i.e. total collapse). The linear elastic solution predicts a convergence of 350 mm which is in close agreement with the elastic convergence of 369 mm estimated by Barlow (1986) with an alternative convergence solution. Both elasto-plastic and elastic solutions indicate the necessity for intensive support for the control of these unacceptable displacements.



(A) SUPPORT SYSTEM - STATION B



(B) ANALYSIS OF STATION B

Figure 7.1 Effect of Bolts at the Enasan Tunnel Project

For the initial bolt pattern ($\beta=0.13$, $L=9$ m), a tunnel convergence of 1070 mm ($R^*=10.9$ m) is predicted by the analytical solution. The ultimate measured convergence at the roof after supplemental bolting (increase in β from 0.13 to 0.52) at a much later stage was 920 mm. In comparison with the tunnel convergence predicted for the initial bolt pattern, the convergence reduction attained due to supplemental bolting does not seem to be very considerable. However, a much greater convergence reduction could have been achieved if these supplemental bolts had also been installed initially. Barlow (1986) has in fact highlighted the same finding. This was to be expected, since bolts installed inside an already existing large plastic zone have much less effect than if they had been installed before or during the propagation of the yielded zone.

Station A of the North Enasan Highway is separated by a distance of 35 m to the west from Station B. The roof of the tunnel at Station A was reinforced primarily with alternating 6 m and 9 m long bolts with a bolt density parameter of 0.27. The invert was reinforced by the same bolt pattern as in Station B. A maximum convergence of 710 mm was measured at the roof at Station A. The predicted roof convergence for 9 m long bolts alone and 6 m long bolts alone were 480 mm ($R^*=9.33$ m) and 650 mm ($R^*=9.89$ m) respectively, for the given bolt density ($\beta=0.27$). These magnitudes slightly underestimate the convergence as compared to the measurements. This discrepancy may be

attributed to the variation in material properties between Stations A and B, which can be expected in a heavily folded and fractured rock mass. Considering these factors the tunnel convergences predicted by the analytical solution are indeed realistic. Furthermore, it shows that convergence could be reduced effectively by increasing the bolt density.

7.1.3 Application of Bolt Effectiveness

Figure 7.1b illustrates the calculated variation of bolt effectiveness as a function of bolt length at Station B. Keeping the total quantity of steel constant, the corresponding bolt density changes with bolt length are also shown in the lower diagram. A total steel quantity of 90m/m tunnel length was initially used at the roof (solid circle), whereas the final steel quantity was as much as 315m/m tunnel length after supplemental bolting (open circle). This, in fact, corresponds to an increase of β from 0.13 to 0.52 (at $L=9$ m). If 9 m long bolts with the final bolt density had been installed immediately, an effectiveness of almost 100% could have been achieved (dashed line). Alternatively, if 13.5 m long bolts had been installed at the beginning (full line) with a lower bolt density parameter of $\beta=0.32$, the bolt effectiveness would have been as much as 95% instead of 58% (full line, upper graph). In reality, because of delayed installation, a much lower effectiveness of approximately 65 to 70% was actually reached. This highlights the importance of installing

grouted bolts as early as possible near the tunnel face.

It is of interest to note that at a bolt length less than 6 m, the bolt effectiveness (initial pattern) drops dramatically. This is to be attributed to the fact that the extent of the plastic zone propagates beyond the bolts. However, for bolt lengths less than 4.5 m, the effectiveness increases again because of the dramatic increase in β . In this region, the bolt density β dominates over the effect of the bolt length. The corresponding bolt densities are however unrealistic.

7.2 Comparison with Empirical Design Methods

Barton *et al.* (1975) have provided a support design guide based on the rock mass quality (Q). For many ground classes, particularly in poor, yielding ground, they do not generally advocate the application of untensioned grouted bolts. Hence, it is not meaningful to compare the proposed method with the Q-system. However, Bieniawski (1976) based upon his Geomechanics Classification or Rock Mass Rating (RMR) system has discussed the applicability of fully grouted bolts in all classes of rock. His design tables and recommendations are intended for tunnel openings of the order of 10 m width, excavated at depths less than 1,000 m by drill and blast method, reinforced by 25 mm diameter grouted bolts. Supplemental support by shotcrete, wire mesh and steel sets are suggested for poorer ground.

The recommended bolt lengths (L) and grid spacings (S_L & S_T) for the different rock classes are tabulated in the first three columns of Table 7.1. The ratio β/λ for these rock classes can be deduced from the latter information and is tabulated in the fourth column of Table 7.1. The magnitude of λ can be estimated from the friction angle of the excavated rock to determine β . Corresponding bolt density parameters for an assumed $\lambda=0.5$ are given in the last column of Table 7.1.

Several interesting aspects evolve from this table. The recommended bolt densities for poor to very poor rock are insensitive to rock quality changes and the recommended range is very wide. Furthermore, the magnitude of the recommended bolt densities seems to be too low particularly for very poor ground at $RMR < 20$. The fact that only a change in bolt length is recommended to control poorer ground does not agree with the findings from this study and practical experience (Golser, 1987). It can be seen that the bolt density parameter varies significantly as the spacing is decreased from 1.5 m to 1.0 m. Therefore, a further reduction of the bolt spacing for the weakest rock class could assure a sufficiently high bolt density parameter to curtail displacements more effectively.

Laubscher and Taylor (1976), on the basis of their experience have proposed a bolt spacing of not more than 0.75 m for poor ground at $RMR < 30$, for support of mine excavations. This corresponds to β -values of about 0.28 for

$\lambda=0.5$, and seems to be in good agreement with the densities required for effective convergence reduction. The influence of bolt friction as a very important design parameter, is also ignored in this empirical method. From these observations we conclude that the RMR system does not provide a sufficiently sensitive guide to properly designed grouted bolts in yielding rock ($RMR < 40$). For poor and very poor rock, a rational design method for grouted bolts should be based on the proposed analytical approach, which provides a sound basis for effective convergence control.

7.3 Observations from the Kielder Experimental Tunnel.

The behaviour of different support systems has been studied in the Kielder experimental tunnel (Ward *et al.*, 1976; Freeman, 1978). The excavation of this tunnel was specifically selected to be in a weak mudstone layer (8 m thick), since the adjacent rocks consisted of competent limestone and sandstone which require relatively less support. In this project, rock movements were measured particularly above the roof of the 3.3 m diameter opening. The influence of fully grouted resin bolts on ground displacements was investigated mainly in the portion of the tunnel excavated by the drill and blast method (NATM).

The four fathom mudstone was extremely fissured with multi-directional fractures and abundant mica partings. It was characterized by a rock quality designation (RQD) of less than 8% indicating its highly fissured nature. Houghton

(1976) describes this mudstone as a material which when exposed is prone to rapid deterioration, quickly forming a soil-like mass. On the basis of Geomechanics Classification (RMR system), support recommendations for fully grouted bolts have been compiled for the different rocks surrounding the experimental tunnel and the access adits (Hoek and Brown, 1980).

Table 7.2 summarizes the calculated β/λ ratios for the RMR recommendations, which incorporate the effects of the relatively small size (1.65 m radius) of the experimental tunnel. According to Table 7.2, the recommended bolt pattern indicates a β/λ ratio of 0.05 to 0.10 and a bolt length of 3 to 4 m. For this tunnel with a diameter of 3.3 m, the recommended bolt length necessitates the coupling of two bolts together for feasibility of installation. The recommended bolt density parameter (β) for an assumed friction factor (λ) of 0.5 varies between 0.025 and 0.05. On the basis of the knowledge acquired from geomechanical modelling and the analysis of the Enasan Tunnel, one can deduce that the latter bolt density is insufficient for effective control of tunnel convergence. Furthermore, in comparison with the relatively competent limestones and sandstones, only a marginal increase in bolt density and bolt length has been recommended for much weaker mudstone. This justifies the conclusion drawn earlier (Section 7.2), that the RMR system does not provide a sufficiently sensitive guide for the design of fully grouted untensioned

Table 7.1 Recommended Bolt Densities according to Geomechanics Classification (RMR)

Rock Class RMR	L (m)	S_L & S_T (m)	β/λ	β (at $\lambda = 0.5$)
81-100	Generally	No Support	Required	0.00
61-80	2.0-3.0	2.5	0.05	0.10
41-60	3.0-4.0	1.5-2.0	0.08-0.14	0.04-0.07
21-40	4.0-5.0	1.0-1.5	0.14-0.31	0.07-0.16
below 20	5.0-6.0	1.0-1.5	0.14-0.31	0.07-0.16

Table 7.2 Recommended Bolt Densities for Kielder Experimental Tunnel based on Geomechanics Classification

Rock Type	L (m)	S_L & S_T (m)	β/λ	β (at $\lambda = 0.5$)
Great Limestone	2.0	1.5	0.046	0.023
Four Fathom Limestone	2.0	1.5	0.046	0.023
Four Fathom Mudstone	3.0-4.0	1.0-1.5	0.05-0.10	0.02-0.05
Natras Gill Sandstone	3.0	1.5-2.0	0.03-0.05	0.01-0.02

bolts in poor quality rock.

The recommended bolt pattern by Geomechanics Classification had not been followed during the stabilization of the experimental tunnel. The actually installed bolt pattern consisted of 1.8 m long fully grouted bolts (25 mm in diameter) at a spacing of 0.9m x 0.9m. This provides a β/λ ratio of 0.16 or a bolt density parameter (β) of 0.08 for an assumed λ of 0.5. However, the findings from this research study have revealed that a bolt density parameter of at least 0.15 to 0.20 is required, in order to obtain effective convergence reductions for bolt lengths approaching the magnitude of the tunnel radius. Therefore, it may be concluded that the Kielder experimental tunnel has not been sufficiently reinforced with fully grouted rock bolts for optimum ground control.

The field measurements have indicated the inadequacy of the bolt density. For an unsupported tunnel section, radial displacements in excess of 20 mm at a point 0.3 m above the roof have been observed. The installation of grouted untensioned bolts did not on average achieve convergence reductions greater than 20%. As a result, a thick layer of shotcrete (140 mm) was sprayed in order to maintain the tunnel wall displacements at an acceptable level of a few millimeters. Alternatively, a similar bolt effectiveness could have been achieved, for example, if 2.0 m long bolts had been installed at a β/λ ratio in the order of 0.2, i.e., at a spacing of 0.6m x 0.6m. The validity of this

recommendation cannot be verified as it was not investigated at the Kielder experimental tunnel.

8. CONCLUDING REMARKS, IMPLICATIONS AND RECOMMENDATIONS

8.1 Implications of the Equivalent Plastic Zone Theory

The theoretical analysis presented in this thesis has introduced a convergence controlled approach for the design of fully grouted bolts. The effectiveness of fully grouted bolts should be assessed on the basis of convergence reduction, which in turn should assist the designer in selecting the optimum reinforcement configuration. The extensive geomechanical model study and the analysis of the Enasan Tunnel case history have verified the reliability of the analytical solution in the convergence prediction of reinforced deep tunnel openings in poor ground conditions ($RMR < 40$).

The influence of the bolt density parameter (β) on the apparent strength of the rock mass, profoundly reflects the importance of the bolt spacing and bolt-grout interaction (frictional) in design. In poor ground, the use of shaped (rough) rebars with a relatively dense bolt configuration is recommended in practice. The evaluation of the equivalent plastic zone radius (R^*) as a function of the bolt density parameter and bolt length, provides a fundamental basis for the determination of tunnel wall convergence. Due to the algebraic structure of the pertinent mathematical equations, an accurate estimate of the dilation coefficient (α) is prudent in predicting the correct displacement field.

The normalized convergence ratio and the resulting bolt effectiveness are the fundamental design aids introduced in this analysis. The normalized convergence ratio is most appropriate in design, where the strength and frictional parameters are poorly defined. The bolt effectiveness, on the other hand, is a convenient design aid where the geotechnical parameters are well established. The study of the Enasan Tunnel shows that the installation of an optimum number of grouted bolts immediately on excavation near the tunnel face contributes to a much greater degree of stabilization than the provision of supplemental bolting at a later stage. It is indeed the initial bolt configuration that is predominant in controlling the extent of overstressing around the tunnel wall and the final tunnel convergence.

The mathematical treatment of the elasto-plastic analysis has been based on several simplifying assumptions. For instance, a circular opening reinforced with an axisymmetric bolt pattern, excavated in an isotropic, homogeneous medium, subjected to a hydrostatic field stress has been considered. The equivalent plastic zone, thus determined by the analytical method is axi-symmetric or circular in shape. Therefore, the accuracy of the analytical solution becomes questionable as the complexity of the geological conditions and geometry increases. Furthermore, since the behaviour of the rock mass is modelled by an elastic, brittle-plastic model with an associated linear

Mohr-Coulomb failure criterion, materials with a pronounced non-linear stress-strain behaviour or a strain-dependent plastic potential are not modelled accurately by the simplified analytical approach.

The presence of a major discontinuity is capable of introducing a predominant anisotropic element, which may itself dominate the rock mass behaviour around a tunnel opening. However, the geomechanical modelling of jointed rock masses in the laboratory has confirmed the fact that the presence of four sets of discontinuities causes the rock mass to behave in a nearly isotropic manner, albeit with reduced apparent strength and deformation parameters. Therefore, the theoretical solution can be extended to predict the behaviour of fractured rocks, if the rock mass geotechnical parameters can be determined.

The influence of time-dependent material properties on ground convergence has not been investigated in this study. Time-dependent loosening can be critical if an opening is left unsupported for a considerable period of time. However, time-dependent convergence of a tunnel opening can be minimized by the provision of supports at the face, immediately after excavation. Therefore, it may be deduced that the theoretical convergence predictions are realistic, if fully grouted bolts are installed soon after excavation. In this respect, the primary NATM design objective is also acknowledged.

The rational approach for the design of fully grouted bolts for underground excavations in yielding rock presented in this thesis clearly illustrates the capability of the fully grouted untensioned bolts in controlling rock mass displacements. Comparisons with empirical methods has demonstrated the superiority of the convergence controlled design method for very poor rock.

8.2 Implications of the advancing tunnel face

The proposed analytical solution predicts the ultimate convergence (more than two tunnel diameters behind the face). Three dimensional effects close to the face have been neglected. Therefore, the convergence ratio and the bolt effectiveness introduced in this analysis are related to a two dimensional solution. In reality, the observed convergence (u_r) is affected by the face effects, and is generally less than the predicted total closure (u_c) by the amount of displacement (u_f) which occurs ahead of the face or prior to initial measurement (Figure 8.1a).

Panet and Guenot (1982), Barlow (1986) and Sulem *et al.* (1987) have presented numerical analyses of the advancing face effect ($K_0=1$) for circular tunnels driven through elasto-plastic material. In their solutions, the prediction of the convergence profile behind the face requires a preliminary assessment of the ultimate time-independent closure and the final extent of the plastic zone. Alternatively, several in-situ convergence measurements

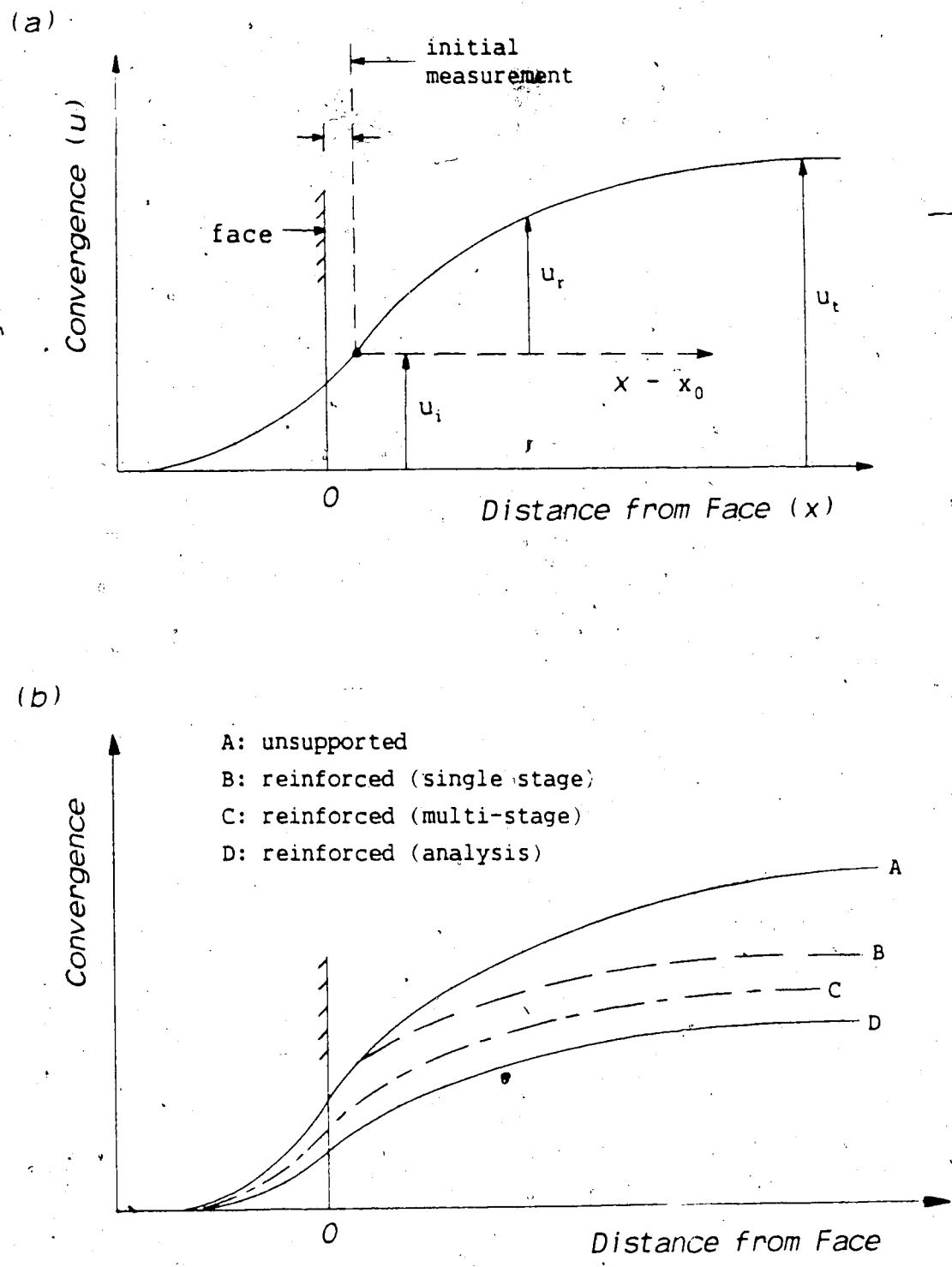


Figure 8.1 Influence of Tunnel Face and Excavation Sequence on Convergence

behind the face may be utilized for the purpose of semi-empirical solution. However, the ultimate convergence and the corresponding plastic zone radius for both unsupported and reinforced openings can be determined by the analytical solution proposed in this thesis. Consequently, the three-dimensional convergence response near the tunnel face may be extrapolated from the ultimate time-independent behaviour.

Figure 8.1b illustrates the influence of the excavation sequence on tunnel convergence. The closure of a reinforced tunnel predicted by the proposed analytical solution, as shown by Curve D (after consideration of the face effects) is expected to be less than the observed convergence of a single stage excavation (Curve B). This is because the analysis assumes instantaneous reinforcement at the face, in contrast to delayed installation of bolts behind the advancing face in the normal practice. However, multi-stage excavation with simultaneous reinforcement (Curve C) dramatically reduces the adverse effects of delayed support installation (time lag). The observed convergence response approaches the analytical solution as the number of headings and the speed of bolt installation are increased. For poor rock conditions, this construction sequence is very realistic and, hence, the analytical model is reasonably representative of reality.

8.3 Implications of Geomechanical Modelling

The present requirements for the excavation of underground openings in rock, of unprecedented size and complexity, require a more comprehensive understanding of the influence of the variables which determine their behaviour. A rational design requires a knowledge of the variables and their relative influence on the behaviour of underground excavations. Among these variables are the in-situ stresses, intact rock properties, discontinuity characteristics, the geometry of the structure and the construction and support techniques. The role of the above variables vary dramatically from one site to another. The cost and impracticality of obtaining data from construction sites to determine quantitative relationships between the pertinent variables and the opening response, suggest the need for alternative techniques.

Numerical analyses using finite element techniques can easily accommodate any opening shape in an elasto-plastic material with a given yield criterion. However, where the opening is reinforced with fully grouted rock bolts and where the rock mass contains several discontinuities in different directions, the development of a powerful numerical model becomes very complex. As a result, accurate prediction of failure modes and tunnel wall convergence may become unreliable.

A most promising technique to investigate experimentally, the influence of grouted bolts on the

behaviour of an opening excavated in a jointed medium is the development of geomechanical models. However, the similitude criteria for the fundamental geotechnical parameters must be carefully satisfied to reproduce the behaviour of the real opening in all respects, including the distribution of stresses, strains, displacements and failure modes. Generally, for any given model and prototype, it is very difficult to satisfy exactly all the material similitude parameters simultaneously, although perfect geometrical similitude (systematic scaling) can be easily achieved. However, this model study, as well as similar investigations (e.g. Kaiser *et al.*, 1979) has revealed that accurate predictions of the real behaviour can be made if, at least, the fundamental similitude requirements are satisfied to an acceptable degree of accuracy.

The major limitation of geomechanical modelling is the technical difficulties associated with similitude criteria, particularly encountered in simulating details of the geologic environment of the real structure and dynamic boundary loading conditions. For instance, the intact material properties and the joint or bedding characteristics (frequency, orientation and friction) can be accurately modelled, but the influence of folding, faulting and seismic disturbances are practically impossible to simulate reliably in a laboratory model.

This geomechanical model study has verified the analytical prediction that grouted bolts increase the

apparent strength and stiffness of both intact and jointed materials. In the case of jointed rock masses, the degree of joint reinforcement seems to be the fundamental factor which determines the strength of jointed materials. Although the apparent strength increases as a function of the bolt density, this effect is not obvious unless the critical joint planes are adequately reinforced to prevent further displacements and subsequent failure. In the case of a random pattern of joints, the failure may initiate along any critical discontinuity favourable to slip with respect to the applied load directions, and may even propagate across the intact material. Systematic bolting presents a pattern of 'stiff' elements around the opening which positively obstruct fracture propagation.

In the light of the knowledge gained from this research study and other investigations, the following general guide has been presented in an attempt to assist the design and installation of fully grouted bolts in underground openings.

8.3.1 Summary of Practical Guidance for Efficient Bolting

1. Install bolts close to the face soon after excavation.

Especially in weak fractured rock, installation of rough rebars that ensure a friction factor (λ) greater than 0.5 is essential. A dense bolt pattern with a bolt density parameter (β) greater than 0.15 ($\beta/\lambda > 0.30$) and a L/a ratio not less than 0.75 are recommended for effective curtailment of displacements.

2. Identify any critical joint planes in the vicinity of the tunnel opening. Effective reinforcement of the joint planes by grouted bolts inhibits premature failure around the opening and enable the rock mass to behave as an intact continuum.
3. Ensure integration of the bolt and the surrounding ground by sufficient grouting of the complete drill hole. Adequate frictional interlock at the bolt/grout interface and at the grout/rock interface is essential.
4. The axial and shear stiffness of the bolt-grout composite must be adequate to prevent excessive dilation and shear displacements of discontinuities.
5. The grouted bolt system must reduce further loosening or raveling of rock to satisfy acceptable design specifications (standards).
6. The bolt configuration must be feasible to install. It must provide the minimum obstruction at the working face.
7. Alteration of bolt lengths and spacing may be implemented for greater economy and efficiency, particularly where the rock properties are variable around the opening.
8. Minimum disturbance of the rock mass must be maintained. Hence, excavation, drilling and bolt installation must be carefully executed. Repeated drilling and regrouting, removal and replacement of bolts must be avoided as much as possible.

Selection of grouts must be carefully advocated to give the appropriate workability, short and long term strength. In areas where the rock is exposed to frequent blasting nearby or in seismic regions, grouts with greater plasticity may be considered.

REFERENCES

- Bacot, J., Iltis, M., Lareal, P., Paumier, T., and Sanglerat, G., 1978. Study of the soil reinforcement friction coefficient. Proc. ASCE Symp. on Earth Reinforcement, Pittsburgh, pp. 157-185.
- Barlow, J.P., 1986. Interpretation of Tunnel Convergence Measurements. M.Sc. Thesis, Department of Civil Engineering, University of Alberta, 235p.
- Barton, N., Lien, R. and Lunde, J., 1975. Estimation of support requirements for underground excavations. Proc. 16th Symp. on Rock Mechanics, Minneapolis, pp. 99-113.
- Barton, N., Lien, R. and Lunde, J., 1974. Engineering deformation of rock masses for the design of tunnel support. Rock Mechanics, 1974, Vol. 6, No. 4, pp. 189-236.
- Barton, N., 1973. Review of a new shear strength criterion for rock joints. Engineering Geology, Vol. 8, pp. 287-332.
- Barton, N., and Bakhtar, K., 1984. Bolt design based on shear strength. Int. Symp. on Rock Bolting, A.A Balkema, pp. 367-376.
- Barry, A.J., and McCormick, J.A., 1960. Evaluating anchorage testing methods for Expansion-Type mine roof bolts. U.S. Bureau of Mines, Report RI 5649.
- Bawa, K.S., and Bumanis, A., 1972. Design considerations for underground structures in rock. Proc. North American Rapid Excavation and Tunnelling Conference, Chicago, pp. 393-417.
- Bieniaski, Z.T., 1976. Rock mass classification in rock engineering. Proc. Symp. on Exploration for Rock Engineering, Johannesburg, Vol. 1, pp. 97-106.
- Bischoff, J.A., and Smart, J.D., 1975. A method of computing a rock reinforcement system which is structurally equivalent to an internal support system. 16th U.S. Symp. on Rock Mechanics, ASCE, New York, pp. 179-184.
- Björnsfot, F., and Stephansson, O., 1984. Interaction of grouted rock bolts and hard rock masses at variable loading in a test drift of the Kiirunavaara mine, Sweden. Int. Symp. on Rock Bolting, A.A Balkema, pp. 377-396.

- Bjurström, S., 1974. Shear strength of hard rock joints reinforced by grouted untensioned bolts. 3rd Congress of the Int. Soc. of Rock Mech., Denver, Vol. 11B, pp. 1194-1199.
- Brady, B.H.G. and Brown, E.T., 1985. Rock Mechanics for Underground Mining. George Allen & Unwin, London, 527p.
- Bray, J.W., 1967. A study of jointed and fractured rock. Rock Mech. Engng Geol., Vol. 5, Part 1: Fracture patterns and their failure characteristics, pp. 117-136. Part 2: Theory of limiting equilibrium, pp. 197-216.
- Brown, E.T., Bray, J.W., Ladanyi, B., and Hoek, E., 1983. Characteristic line calculations for rock tunnels. J. Geotech. Engng, ASCE, Vol. 109, pp. 15-39.
- Brown, E.T., 1970. Strength of models of rock with intermittent joints. J. Soil Mech. & Foundns. Div., ASCE Vol. 96, pp. 1935-1949.
- Bureau, G.J., Goodman, R.E., and Heuzé, F.E., 1972. Model studies of rock bolted tunnels in brittle and plastic ground. U.S. Corps of Engineers, Report No 12, Contract DACA45-71-C-0031, 88p.
- Caron, C., 1972. Corrosion et Protection des ancrages définitifs. Construction, pp. 52-56.
- Clark, G.B., 1981, Geotechnical centrifuges for model studies and physical property testing of rock and rock structures. Colorado School of Mines Quarterly, Vol. 76; No. 4, 51p.
- Cording, E.J., and Deere, D.U., 1972. Rock tunnel supports and field measurements. Proc. North American Rapid Excavation & Tunnelling conference. Chicago, Vol. 1, pp 601-622.
- Daemen, J., and Fairhurst, C., 1972. Rock failure and tunnel support loading. Int. Symp. on Underground Openings, Lucerne, pp. 356-369.
- Douglas, T.H., and Arthur, L.J., 1983. A guide to the use of rock reinforcements in underground excavations. CIRIA Report-101, 74p.
- Egger, P., 1973. Einfluss des Post-Failure-Verhaltens von Fels auf den Tunnel Ausbau. Veröffentlichungen des Institutes fuer Bodenmechanik und Felsmechanik, Universitaet Fridericiana Karlsruhe, Heft 57, pp. 1-83.
- Fairhurst, C., and Cook, N.G.W., 1966. The phenomenon of rock splitting parallel to the direction of maximum

- compression in the neighbourhood of a surface. Proc. 1st Congress of the Int. Soc. Rock Mech., Lisbon, Vol. 1, pp. 687-690.
- Fairhurst, C., and Singh, B., 1974. Roof bolting in horizontally laminated rock. Eng. Min. Journal, Vol. 175, pp. 80-90.
- Feder, G., 1978. Bergbau und tunnelbau-anregungen und ergaenzungen. Rock Mechanics, Supplementum 7, pp. 103-127.
- Freeman, T.J., 1978. The behaviour of fully bonded rock bolts in the Kielder Experimental Tunnel. Tunnels and Tunnelling, Vol. 10, pp.37-40.
- Fumagalli, E., 1979. Model simulations of rock mechanics problems. chapter 11, Rock Mechanics in Engineering Practice, Staag, K.G., and Zienkiewicz, O.C.(ed), John Wiley & Sons, pp. 353-384.
- Fumagalli, E., 1979a. Les Modeles geomecaniques de fondation aux grands barrages. Int. Colloquium on Physical Geomechanical Models, Bergamo, Italy, pp. 133-147.
- Gerdeen, J.C., Snyder, V.W., Viegelahn, G.L., and Parker, J., 1977. Design criteria for roof bolting plans using fully resin grouted non tensioned bolts to reinforce bedded mine roof. Vol. I-V, OFR 46(1)-80, U.S. Bureau of Mines, Contract J0366004.
- Golser, J., 1987. Personal Communication.
- Goodman, R.E., and Ewoldsen, H.M., 1969. A design approach for rock bolt reinforcement in underground galleries. Proc. Int. Symp. on Large Permanent Underground Openings, Oslo, pp 181-195.
- Goodman, R.E., and Dubois, J., 1971. Static and dynamic analysis of rock bolt support. U.S. Corps of Engineers, Report No. 6, Contract DACA45-67-C-0015, 130p.
- Goodman, R.E., 1976. Methods of Geological Engineering in Discontinuous Rocks. West Publishing Co., St. Paul, Minn., 472p.
- Goodman, R.E., 1980. Introduction to Rock Mechanics. John Wiley & Sons, 478p.
- Guenot, A., 1979. Tunnel Stability by Model Tests. M.Sc. Thesis, Dept. of Civil Engineering, University of Alberta, 217p.
- Haas, C., Clark, G.B., and Nitzsche, R.N., 1975. An

- investigation of the interaction of rock and type of rock bolts for selected loading conditions. Rock Mechanics and Explosives Research Centre, Report PB 267 673, University of Missouri-Rolla.
- Haas, C., 1981. Analysis of rock bolting to prevent shear movement in fractured ground. Mining Engineer, pp. 698-704.
- Hendron, A.J., and Aiyer, A.K., 1972. Stresses and strains around a cylindrical tunnel in an elasto-plastic material with dilatancy. U.S. Corps of Engineers, Omaha, Report No. 10, 72p.
- Heuer, R.E., and Hendron, A.J., 1969. Geomechanical model study of the behaviour of underground openings in rock subjected to static loads. U.S. Corps of Engineers, Report N-69-1, No. 1, Contract DACA39-67-C-0009, 209p.
- Heuer, R.E., and Hendron, A.J., 1971. Geomechanical model study of the behaviour of underground openings in rock subjected to static loads. U.S. Corps of Engineers, Report N-69-1, No. 2, Contract DACA39-67-C-0009, 370p.
- Heuzé, F.E., and Goodman, R.E., 1973. Numerical and physical modelling of reinforcement systems for tunnels in jointed rock. U.S. Corps of Engineers, Report No-16.
- Hoek, E., and Brown, E.T., 1980. Underground Excavations in Rock. Inst. Min. and Metall., London, 527p.
- Houghton, D.A., 1976. The role of rock quality indices in the assessment of rock masses. Proc. Symp. Exploration for Rock Engineering, Johannesburg, pp. 129-135.
- Hudson, J.A., Brown, E.T., and Fairhurst, C., 1972. Shape of the complete stress-strain curve for rock. Proc. 13th Symp. on Rock Mechanics, Illinois, pp. 773-795.
- Indraratna, B., and Kaiser, P.K., 1986. Control of Tunnel Convergence by Grouted Bolts. Rapid Excavation & Tunnelling Conference, New Orleans, Louisiana, 20p.
- Indraratna, B., Kaiser, P.K., 1986. Wall convergence in tunnels supported by fully grouted bolts. 28th U.S. Symp. Rock Mechanics, Tucson, Arizona, 10p.
- Indraratna, B., 1983. The Properties of Grouts and Application of Grouting. M.S. Thesis, Dept. of Civil Engineering, Imperial College, University of London, 235p.
- Indraratna, B., 1984. The factors that influence the design of cement grouts for the penetration of fine fissures in

- rock foundations. Engineer, Journal of the Inst. of Civil Engineering, Sri Lanka, pp. 14-17.
- Ito, Y., 1983. Design and Construction by NATM through Chogiezawa Fault Zone for Enasan Tunnel on Central Motorway (in Japanese). Tunnels & Underground, Vol. 14, pp. 7-14.
- Jaeger, J.C., 1960. Shear fracture of anisotropic rocks. Geology Magazine, Vol. 97, pp. 65-72.
- Jaeger, J.C., and Cook, N.G.W., 1969. Fundamentals of Rock Mechanics. Methuen and Company, London.
- John, M., 1976. Geotechnical measurements in the Arlberg tunnel and their consequences on construction (in German). Rock Mechanics, Supplementum 5, pp. 157-177.
- Johnston, I.W., and Choi, S.K., 1986. A synthetic soft rock for laboratory model studies. Géotechnique, Vol. 36, No. 2, pp. 251-263.
- Jumikis, A.R., 1979. Rock Mechanics. Trans Tech Publications, Germany, 365p.
- Kaiser, P.K., and Morgenstern, N.R., 1981. Time-dependent deformation of small tunnels-I, Experimental facilities. Int. J. Rock Mech. Min. Sci. & Geomech. Abstr., Vol. 18, pp. 129-140.
- Kaiser, P.K., and Morgenstern, N.R., 1981a. Time-dependent deformation of small tunnels-II, Typical test data. Int. J. Rock Mech. Min. Sci. & Geomech. Abstr., Vol. 18, pp. 141-152.
- Kaiser, P.K., and Morgenstern, N.R., 1982. Time-dependent and time independent deformation of small tunnels-III, Pre-failure behaviour. Int. J. Rock Mech. Min. Sci. & Geomech. Abstr., Vol. 19, pp. 307-324.
- Kaiser, P.K., Guenot, A., and Morgenstern, N.R., 1985. Deformation of small tunnels-IV, Behaviour during failure. Int. J. Rock Mech. Min. Sci. & Geomech. Abstr., Vol. 22, pp. 141-152.
- Kaiser, P.K., 1979. Time-Dependent Behaviour of Tunnels. Ph.D. Thesis, Dept. of Civil Engineering, University of Alberta, 395p.
- Ladanyi, B., 1974. Use of long term strength concept in the determination of ground pressure on tunnel linings. Advances in Rock Mechanics, Proc. 3rd congress, Int. Soc. Rock Mech., Denver, Vol. 2B, Washington D.C., pp. 1150-1156.

- Lang, T.A., 1961. Theory and practice of rock bolting. Trans. Soc. Min. Engineers, Am. Inst. Min. Metall. Petrolm. Engrs, Vol. 220, pp. 333-348.
- Lang, T.A., 1972. Rock reinforcement. Bull. Assoc. Eng. Geology, Vol. 9, pp. 213-219.
- Lang, T.A., and Bischoff, J.A., 1981. Research study of coal mine rock reinforcement. U.S. Bureau of Mines, contract J0295072, OFR 72-82.
- Langhaar, H.L., 1951. Dimensionless Analysis and Theory of Models. John Wiley & Sons, New York, 166p.
- Laubscher, D.H., and Taylor, H.W., 1976. The importance of Geomechanics Classification of jointed rock masses in mining operations. Proc. Symp. Exploration for Rock Engineering, Johannesburg, pp. 119-128.
- Littlejohn, G.S., and Bruce, D.A., 1975, 1976. Rock Anchors - State of the Art. Ground Engineering, Part 1- Design, May 1975, pp. 25-32; July 1975, pp. 41-48. Part 2- Construction, Sept. 1975, pp. 34-45; Nov. 1975, pp. 36-45. Part 3- Stressing and testing, March 1976, pp. 20-29; April 1976, pp. 55-60; May 1976, pp. 33-44.
- Liu, B., and Huang, J., 1984. State of the art of rock bolting in People's Republic of China. Int. Symp on Rock Bolting, A.A. Balkema, pp. 285-294.
- Longbottom, K.W., and Mallet, G.P., 1973. Pre-stressing steels. The Structural Engineer, Vol. 51, pp. 455-471.
- Maher, J., 1975. Comparisons of uniform four-foot length fully grouted resin roof bolts and alternating four and six foot length fully grouted resin roof bolts. U.S. Bureau of Mines, OFR 23-77.
- Maloney, S.M., 1984. An Assesment of Deformation Monitoring Practice in Underground Excavations in weak Rock by Model Tests. M.Sc. Thesis, Dept. of Civil Engineering, University of Alberta, 282p.
- Obert, L., and Duvall, W.I., 1967. Rock Mechanics and the Design of Structures in Rock. John Wiley & Sons, New York, 650p.
- Panet, M., 1976. La mécanique des roches appliquée aux ouvrages de génie civil. Association amicale des ingénieurs anciens élèves de L'Ecole Nationale des Ponts et Chaussées, Paris, 235p.
- Panet, M., and Guenot, A., 1982. Analysis of convergence

behind the face of a tunnel. Tunnelling 82., Inst. Min. and Metall., Brighton, pp. 197-204.

Patton, F.D., 1966. Multiple modes of shear failure in rock. Proc. 1st congress, Int. Soc. Rock Mech., Lisbon, Vol. 1, pp. 509-513.

Rabcewicz, L.V., 1964, 1965. The New Austrian Tunnelling Method (3 parts). Water Power (England); Nov. 1964, pp. 453-457; Dec. 1964, pp. 511-515; Jan. 1965, pp. 19-24.

Rabcewicz, L.V., 1969. Stabilities of tunnels under rock load. Water Power (England); June, pp. 225-229; July, pp. 266-273; Aug., pp. 297-302.

Raphael, J.M., 1960. Structural model investigations for Oroville Dam. Series 100, Issue 6, Institute of Engineering Research, University of California, Berkeley, 164p.

Rechsteiner, G.F., and Lombardi, G., 1974. Une méthode de calcul élasto-plastique de l'état de tension et de déformation autour d'une cavité souterraine. Proc. 3rd congress, Int. Soc. Rock Mech., Denver, Colorado, Vol. 2B, pp. 1034-1054.

Rehm, G., 1968. Corrosion of pre-stressing steel. Proc. Symp. on Pre-stressing. Madrid, Spain.

Rosenblad, J.L., 1968. Development of a rocklike model material. Proc. 10th U.S. Symp. on Rock Mechanics, Austin, Texas, pp. 331-361.

Schlosser, F., and Elias, V., 1978. Friction in reinforced earth. ASCE Symp. on Earth Reinforcement, Pittsburgh, pp. 735-762.

Shi Gen Hua and Goodman, R.E., 1984. Keyblock bolting. Int. Symp. on Rock Bolting, A.A. Balkema, pp. 143-168.

Snyder, V., 1984. Analysis of beam building using fully grouted roof bolts. Int. Symp. on Rock Bolting, A.A. Balkema, pp. 187-194.

Stehlik, C.J., 1964. Mine roof rock and roof bolt behaviour resulting from nearby blasts. U.S. Bureau of Mines, Report RI 6372.

Stimpson, B., 1970. Modelling materials for engineering rock mechanics. Int. J. Rock Mech. and Min. Sci., Vol. 7, pp. 71-121.

Stimpson, B., 1979. Technical note, A new approach to simulating rock joints in physical models. Int. J. Rock

- Mech. Min. Sci. & Geomech. Abstr., Vol. 16, pp. 215-216.
- Sulem, J., Panet, M., and Guenot, A., 1987. Closure analysis in deep tunnels. Int. J. Rock Mech. Min. Sci. & Geomech. Abstr., Vol. 24, pp. 145-154.
- Sun Xueyi, 1984. Grouted rock bolts used in underground engineering in soft surrounding rock or in highly stressed regions. Int. Symp. on Rock Bolting, A.A. Balkema, pp. 93-100.
- Tao Zhen Yu and Chen Jie Xian, 1984. Behaviour of rock bolts as tunnel support. Int. Symp. on Rock Bolting, A.A. Balkema, pp. 87-92.
- Tanimoto, C., Hata, S., and Kariya, K., 1981. Interaction between fully bonded bolts and strain softening rock in tunnelling. 22nd U.S. Symp. on Rock Mechanics, Cambridge, Massachusetts, pp. 367-372.
- U.S. Army Corps of Engineers, 1980. Engineering and Design, Rock Reinforcement. EM1110-1-2907.
- Vardoulakis, I., 1984. Rock bursting as a surface instability phenomenon. Int. J. Rock Mech. Min. Sci. & Geomech. Abstr. Vol. 21, No. 3, pp. 137-144.
- Van Sint Jan, M.L., 1982. Ground and Lining Behaviour of Shallow Underground Rock Chambers for the Washington D.C. Subway. Ph.D. Thesis, University of Illinois, Urbana.
- Ward, W.H., Coats, D.J., and Tedd, P., 1976. Performance of tunnel support systems in four fathom mudstone. Proc. Tunnelling '76, Inst. Min. and Metall., London, pp. 329-340.
- Wijk, G., and Skogberg, B., 1982. The Swellex rock bolting system. 14th Canadian Rock Mech. Symp., Vancouver, CIM Vol. 30, pp. 106-115.

APPENDIX A

GENERAL ELASTIC, BRITTLE-PLASTIC MODEL

(a) Failure Criterion

The linear Mohr-Coulomb criterion is applied with a reduction in post-peak strength, as given by the following relationships:

$$\sigma_r = m \cdot \sigma_r + s \cdot \sigma_c$$

$$0 < s < 1$$

The parameter s is a measure of the degree of strength loss occurring instantaneously after the peak (failure) stress.

(b) Stresses in the Yielded Zone

The combination of the equilibrium equation and failure criterion results in the following differential equation:

$$\frac{d\sigma_r}{dr} + (1-m)\sigma_r/r = \sigma_{cr}/r \quad (A.1)$$

where: $m = \frac{1 + \sin\phi}{1 - \sin\phi}$ and $\sigma_{cr} = s \cdot \sigma_c$

The shear stress ($\tau_{r\theta}$) at any given radial distance is zero for axisymmetric deformation under plane strain condition.

For an unsupported opening ($\beta=0$), the solutions of Equation A.1 are given by:

$$\sigma_r = \left[\frac{S \cdot \sigma_c}{m-1} \right] \left\{ (r/a)^{m-1} - 1 \right\}$$

$$\sigma_\theta = \left[\frac{S \cdot \sigma_c}{m-1} \right] \left\{ m(r/a)^{m-1} - 1 \right\} \quad (\text{A.2})$$

The above solution is the same for both the geomechanical model and the actual excavation.

(c) Stresses in the Outer Elastic Zone

The stress distribution in the elastic zone is equivalent to that of a larger opening of radius R , supported by a uniform internal stress σ_{r1} under the same external field stress. R is the radial distance to the outer limit of the yielded zone surrounding the tunnel.

At the elasto-plastic boundary ($r=R$), the internal stresses are given by:

$$\sigma_{r1} = \left[\frac{S \cdot \sigma_c}{m-1} \right] \left\{ (R/a)^{m-1} - 1 \right\}$$

$$\sigma_{\theta 1} = \left[\frac{S \cdot \sigma_c}{m-1} \right] \left\{ m(R/a)^{m-1} - 1 \right\} \quad (\text{A.3})$$

In the elastic zone, the stress distributions are given by:

$$\sigma_r = \sigma_0 \left[1 - (R/r)^2 \right] + \sigma_{r1} (R/r)^2$$

$$\sigma_\theta = \sigma_0 \left[1 + (R/r)^2 \right] - \sigma_{r1} (R/r)^2 \quad (\text{A.4})$$

where: $\sigma_r + \sigma_\theta = 2\sigma_0$

(d) Radius of the Yielded Zone

The plastic zone radius (R) can be determined by assuming continuity of radial stress at the elasto-plastic boundary. It is also assumed that the field boundaries are far enough from the tunnel, such that their influence on the solution for R is negligible.

Equating the expressions for σ_{r1} at $r=R$, obtained for the elastic and plastic zones respectively, the normalized plastic zone radius (R/a) can be derived as follows:

$$\frac{R}{a} = \left[1 + \frac{1}{s} \left[\frac{m-1}{m+1} \right] \left[\frac{2\sigma_0}{\sigma_c} - 1 \right] \right]^{1/(m-1)} \quad (\text{A.5})$$

(e) Strains in the Elastic Zone

Hooke's laws can be applied to determine the radial and tangential strains in the elastic region surrounding the plastic zone.

$$\begin{aligned} \epsilon_r &= \frac{1-\nu^2}{E} \left[\sigma_r - \left[\frac{\nu}{1-\nu} \right] \sigma_\theta \right] \\ \epsilon_\theta &= \frac{1-\nu^2}{E} \left[\sigma_\theta - \left[\frac{\nu}{1-\nu} \right] \sigma_r \right] \end{aligned} \quad (\text{A.6})$$

Substitution of the expressions for stresses (Equations A.4) in the above relationships provides the strain fields for the model test under plane strain conditions ($\gamma_{r\theta}=0$):

$$\epsilon_r = \frac{\sigma_0}{2G} (1-2\nu) - \frac{\sigma_0}{2G} \left[1 - (\sigma_{r1}/\sigma_0) \right] (R/r)^2$$

$$\epsilon_e = \frac{\sigma_0}{2G}(1-2\nu) + \frac{\sigma_0}{2G} \left[1 - (\sigma_{r1}/\sigma_0) \right] (R/r)^2 \quad (\text{A.7})$$

The term $\sigma_0(1-2\nu)/2G$ is the initial elastic deformation of the plate without the opening. The other term is the deformation due to excavation. The deformation of the laboratory model is the combination of both terms.

(f) Strains in the Plastic Zone

The total strains in the plastic zone are made up of both elastic and plastic strains ($\epsilon^t = \epsilon^e + \epsilon^p$). Hooke's law has been applied to calculate the elastic strains which are given by the following expressions:

$$\begin{aligned} \epsilon_e^e &= \frac{1}{2G} \left[\frac{s \cdot \sigma_c}{m-1} \right] \left[(m-m\nu-\nu)(r/a)^{m-1} + (2\nu-1) \right] \\ \epsilon_r^e &= \frac{1}{2G} \left[\frac{s \cdot \sigma_c}{m-1} \right] \left[(1-\nu-m\nu)(r/a)^{m-1} + (2\nu-1) \right] \end{aligned} \quad (\text{A.8})$$

The continuity of total strains across the elasto-plastic boundary requires a specific tangential plastic strain associated with strength loss after peak to occur immediately. The magnitude of this plastic strain at $r=R$ is given by:

$$\epsilon_e^R = \frac{\sigma_c}{2G} (1-\nu)(1-s) \quad (\text{A.9})$$

Clearly, the plastic strains become zero at the elasto-plastic boundary for perfectly plastic material with

$s=1$.

Substitution of Equation A.8 and the flow rule (Eq. 3.2) in the total strain compatibility condition (Eq. 3.3) provides the following differential equation:

$$\frac{d\epsilon_r^p}{dr} + \epsilon_r^p(1+a) = -\left[\frac{s\sigma_c}{2G}\right](1-\nu)(m+1)(r/a)^{m-1} \quad (\text{A.10})$$

The solution of the above equation with the boundary condition stated in Equation A.9 is given by:

$$\epsilon_r^p = s\sigma_c \left[\frac{1-\nu}{2G} \right] \left[\frac{m+1}{m+a} \right] \left[(R/r)^{m+a} - 1 \right] (r/a)^{m-1} + \epsilon_r^R (R/r)^{1+a}$$

and $\epsilon_r^p = -a \cdot \epsilon_r^p$. (A.11)

The addition of the corresponding Equations A.8 and A.11 gives the total strains in the plastic zone for the boundary conditions of the model test, where:

$$\epsilon_r^t = \epsilon_r^e + \epsilon_r^p \quad \text{and} \quad \epsilon_\theta^t = \epsilon_\theta^e + \epsilon_\theta^p \quad (\text{A.12})$$

(g) Radial Displacement Field

The displacement field can be obtained directly by the following strain-displacement relationships which satisfy the compatibility conditions:

$$\epsilon_r^t = \frac{\partial u_r}{\partial r} \quad \text{and} \quad \epsilon_\theta^t = \frac{u_r}{r} + \frac{1}{r} \frac{\partial u_\theta}{\partial \theta} \quad (\text{A.13})$$

The conditions of plane strain under axisymmetric deformation ($\gamma_{r\theta}=0$) imply that the total strains are independent of the tangential strain components. Therefore, the radial displacement field can be readily evaluated from any of the following expressions:

$$\frac{u_r}{r} = \epsilon_r^t \quad \text{or} \quad u_r = \int \epsilon_r^t \cdot dr \quad (\text{A.14})$$

Elasto-plastic tunnel convergence can be subsequently determined by substituting $r=a$ in the above expressions.

Further details of the general elasto-plastic models have been discussed by Kaiser *et al.* (1985), Guenot (1979), Panet (1976) and Bray (1967).

APPENDIX B

DETERMINATION OF THE EXTENT OF YIELDING

The Categories I to III of the equivalent plastic zones have been diagrammatically illustrated in Figure 3.9. A complete analysis of Category I and a general discussion of Categories II and III have been presented in Section 3.6.1. The mathematical treatment of Categories II and III is presented in detail here.

Category II: $\rho < R^* < a+L$

Zone 1: $a < r < \rho$

This is the inner yielded zone confined between the tunnel boundary and the neutral point. The equivalent stresses in this region are given by equations identical to those of Zone 1 of Category I:

$$\sigma_r = \left[\frac{s \cdot \sigma_c^*}{m^* - 1} \right] \left\{ (r/a)^{m^*} - 1 \right\}$$

$$\sigma_\theta = m^* \cdot \sigma_r + s \cdot \sigma_c^* \quad (\text{B.1})$$

$$\text{at } r = \rho, \quad \sigma_r = \left[\frac{s \cdot \sigma_c^*}{m^* - 1} \right] \left\{ (\rho/a)^{m^*} - 1 \right\}$$

where: $m^* = m(1 + \beta)$ and $\sigma_c^* = \sigma_c(1 + \beta)$.

Zone 2: $\rho < r < R^*$

This is the outer plastic zone beyond the neutral point. The plastic stresses in this zone are given by the following equations:

$$\sigma_r = \left[\frac{s \cdot \sigma_c'}{m' - 1} \right] \left\{ (r/\rho)^{m'-1} - 1 \right\} + \sigma_\rho \cdot (r/\rho)^{m'-1}$$

$$\sigma_\theta = m' \cdot \sigma_r + s \cdot \sigma_c' \quad (\text{B.2})$$

where: $m' = m(1 - \beta)$ and $\sigma_c' = \sigma_c(1 - \beta)$.

As r approaches R^* , m' and σ'_c approach m and σ_c respectively, where: $m > m'$ and $\sigma_c > \sigma'_c$.

Zone 3: $R^* < r < a+L$

This is the inner elastic zone within the reinforced region which surrounds the yielded zone. The equivalent elastic stresses in this zone are represented by the following equations:

$$\begin{aligned}\sigma_r &= \sigma_0 [1 - (R^*/r)^2] + \sigma_R (R^*/r)^2 \\ \sigma_\theta &= \sigma_0 [1 + (R^*/r)^2] - \sigma_R (R^*/r)^2\end{aligned}\quad (B.3a)$$

The peak tangential stress at the elasto-plastic boundary is given by the following condition ($s=1$):

$$\sigma_\theta = m \cdot \sigma_r + \sigma_c$$

The radial stress at the elasto-plastic boundary σ_R is deduced by substituting $r = R^*$ in the above equations:

$$\sigma_R = \frac{2\sigma_0 - \sigma_c}{m+1}\quad (B.3b)$$

Zone 4: $r > a+L$

This is the outer undisturbed elastic zone beyond the reinforced region. The elastic stress fields in this zone are given by:

$$\sigma_r = \sigma_0 \{1 - [(a+L)/r]^2\} + \sigma_L [(a+L)/r]^2$$

$$\sigma_\theta = \sigma_0 \{1 + [(a+L)/r]^2\} - \sigma_L [(a+L)/r]^2 \quad (\text{B.4})$$

where: $\sigma_L = \sigma_0 \{1 - [R^*/(a+L)]^2\} + \sigma_R [R^*/(a+L)]^2$

At the elasto-plastic boundary, the assumption of radial stress continuity yields:

$$\frac{2\sigma_0 - \sigma_c}{m+1} = \left[\frac{s \cdot \sigma_c}{m-1} \right] \left\{ (R^*/\rho)^{m-1} - 1 \right\} + \sigma_c (R^*/\rho)^m \quad (\text{B.5})$$

The plastic zone radius is then given by the equation:

$$\frac{R^*}{a} = \frac{\rho}{a} \left[\frac{1 + B_1}{1 + A_1} \right]^{1/(m-1)} \quad (\text{B.6})$$

where: $B_1 = \frac{1}{s} \left[\frac{m-1}{m+1} \right] \left[\frac{2\sigma_0}{\sigma_c} - 1 \right]$

and $A_1 = \left[\frac{m-1}{m-1} \right] \left[\frac{1+\beta}{1-\beta} \right] \left\{ (\rho/a)^{m-1} - 1 \right\}$

Category III: $R \rightarrow a+L$

Zone 1: $a < r < \rho$

The equivalent radial and tangential stress fields for this inner plastic zone (pick-up length region) are represented by the same equations corresponding to Zone 1 of Category II:

$$\sigma_r = \left[\frac{S \cdot \sigma_c}{m-1} \right] \left\{ (r/a)^{m-1} - 1 \right\}$$

$$\sigma_\theta = m \cdot \sigma_r + S \cdot \sigma_c \quad (\text{B.7})$$

at $r = \rho$, $\sigma_r = \left[\frac{S \cdot \sigma_c}{m-1} \right] \left\{ (\rho/a)^{m-1} - 1 \right\}$

where: $m = m(1 + \beta)$ and $\sigma_c = \sigma_c(1 + \beta)$.

Zone 2: $\rho < r < a+L$

This is the middle plastic zone which is confined to the anchor length of the bolted region. The stress fields are given by the same equations corresponding to Zone 2 of Category II:

$$\sigma_r = \left[\frac{S \cdot \sigma'_c}{m'-1} \right] \left\{ (r/\rho)^{m'-1} - 1 \right\} + \sigma_\rho \cdot (r/\rho)^{m'-1}$$

$$\sigma_\theta = m' \cdot \sigma_r + S \cdot \sigma'_c \quad (\text{B.8})$$

where: $m' = m(1 - \beta)$ and $\sigma'_c = \sigma_c(1 - \beta)$.

Zone 3: $a+L < r < R^*$

This is the outer plastic zone beyond the reinforced region and its equivalent stresses are represented by:

$$\sigma_r = \left[\frac{s \cdot \sigma_c}{m-1} \right] \{ [r/(a+L)]^{m-1} - 1 \} + \sigma_L \cdot [r/(a+L)]^{m-1}$$

$$\sigma_e = m \cdot \sigma_r + s \cdot \sigma_c \quad (B.9)$$

where: $\sigma_L = \left[\frac{s \cdot \sigma_c}{m-1} \right] \{ [(a+L)/\rho]^{m-1} - 1 \} + \sigma_\rho \cdot [(a+L)/\rho]^{m-1}$

Zone 4: $r > R^*$

This is the elastic region surrounding the plastic zone. The elastic stress fields are given by the same equations corresponding to Zone 3 of Category II:

$$\sigma_r = \sigma_0 [1 - (R^*/r)^2] + \sigma_R \cdot (R^*/r)^2$$

$$\sigma_e = \sigma_0 [1 + (R^*/r)^2] - \sigma_R \cdot (R^*/r)^2 \quad (B.10)$$

The radial stress continuity at $r = R^*$ yields:

$$\frac{2\sigma_0 - \sigma_c}{m+1} = \left[\frac{s \cdot \sigma_c}{m-1} \right] \{ [R^*/(a+L)]^{m-1} - 1 \} + \sigma_L \cdot [R^*/(a+L)]^{m-1} \quad (B.11)$$

The radius of the equivalent plastic zone can be determined from the following expression:

$$\frac{R^*}{a} = [1 + (L/a)] \left[\frac{1 + B_1}{1 + A_2 + A_3} \right]^{1/(m-1)} \quad (B.12)$$

where:
$$B_1 = \frac{1}{s} \left[\frac{m-1}{m+1} \right] \left[\frac{2\sigma_0}{\sigma_c} - 1 \right]$$

$$A_2 = \left[\frac{m-1}{m'-1} \right] \left[\left[(a+L)/\rho \right]^{m'-1} - 1 \right]$$

$$A_3 = (1+\beta) \left[\frac{m-1}{m^*-1} \right] \left[\left[(a+L)/\rho \right]^{m'-1} \left\{ (\rho/a)^{m^*-1} - 1 \right\} \right]$$

$$m^* = m(1+\beta) \quad \text{and} \quad m' = m(1-\beta)$$

At the far end of the grouted bolt ($r \approx a+L$), m' and σ'_c approach m and σ_c respectively, where: $m > m'$ and $\sigma_c > \sigma'_c$. Hence, modification of the terms A_2 and A_3 can be made accordingly. This procedure of updating parameters seems to result in a greater accuracy of convergence prediction (Category III) if β tends to be large.

SOLUTIONS OF THE EQUIVALENT PLASTIC ZONE RADIUS

i) Case 1: $R^* < \rho < a + L$ (minimal yielding)

$$\frac{R^*}{a} = \left\{ 1 + s^{-1} \left[\frac{(m^* - 1)}{(m^* + 1)} \right] \left[\left(\frac{2\sigma_0}{\sigma_c} \right) - 1 \right] \right\}^{1/(m^*-1)}$$

where $m^* = m(1 + \beta)$, $\sigma_c^* = \sigma_c (1 + \beta)$

ii) Case 2: $\rho < R^* < a + L$ (major yielding)

$$\frac{R^*}{a} = \frac{\rho}{a} \left\{ \frac{1 + s^{-1} \left[\frac{(m-1)}{(m+1)} \right] \left[\left(\frac{2\sigma_0}{\sigma_c} \right) - 1 \right]}{1 + A_1} \right\}^{1/(m-1)}$$

where $A_1 = \left(\frac{m-1}{m^*-1} \right) \left(\frac{1+\beta}{1-\beta} \right) \left[(\rho/a)^{m^*-1} - 1 \right]$

iii) Case 3: $R^* > a + L$ (excessive yielding)

$$\frac{R^*}{a} = \left(\frac{a+L}{a} \right) \left\{ \frac{1 + s^{-1} \left[\frac{(m-1)}{(m+1)} \right] \left[\left(\frac{2\sigma_0}{\sigma_c} \right) - 1 \right]}{1 + A_2 + A_3} \right\}^{1/(m-1)}$$

where $A_2 = \left(\frac{m-1}{m'-1} \right) \left\{ \left(\frac{a+L}{\rho} \right)^{m'-1} - 1 \right\}$

$$A_3 = (1 + \beta) \left(\frac{m-1}{m^*-1} \right) \left\{ (\rho/a)^{m^*-1} - 1 \right\} \left(\frac{a+L}{\rho} \right)^{m'-1}$$

$m^* = m(1 + \beta)$, $m' = m(1 - \beta)$

$\rho = L/\ln [1 + (L/a)]$

The terms A_2 and A_3 can be simplified by assuming that $m' = m$ at the boundary $r = a + L$.

APPENDIX C

REINFORCEMENT OF A SINGLE PLANE OF WEAKNESS

Modification of the single plane of weakness theory to accommodate the effect of bolting has been discussed in Section 2.15 with a diagrammatic illustration in Figure 2.4. The mathematical derivations of Equations 2.4 and 2.5 are presented here.

List of Symbols

A_j = area of the joint

A_b = cross-section area of the bolt

σ_b = axial stress (tensile) of the bolt

τ_{bf} = shear strength of the bolt

σ_n = normal stress across the joint

σ_1, σ_3 = vertical and horizontal field stress

c_j, ϕ_j = cohesion and friction angle of the joint

θ = angle between the bolt and the joint

α = inclination of the joint to the vertical axis.

Forces Normal to the Joint

The normal stress acting across the joint (σ_n) can be determined by resolving forces perpendicular to the joint direction. The equilibrium of these forces is represented by the following equation:

$$\sigma_n \cdot A_j = \sigma_1 \cdot A_j \cdot \sin^2 a + \sigma_3 \cdot A_j \cdot \cos^2 a + \sigma_b \cdot A_b \cdot \sin \theta \quad (C.1)$$

Substitution of $\cos 2a = 1 - 2\sin^2 a = 2\cos^2 a - 1$ and subsequent simplification gives:

$$\sigma_n = \frac{1}{2}(\sigma_1 + \sigma_3) - \frac{1}{2}(\sigma_1 - \sigma_3)\cos 2a + \sigma_b \cdot A_b \cdot \sin \theta / A_j \quad (C.2)$$

Forces Parallel to the Joint

If F_s and R_s are the applied shearing and resisting forces parallel to the joint, respectively, resolving forces in the direction of the joint yields:

$$F_s = \frac{1}{2}(\sigma_1 - \sigma_3)A_j \cdot \sin 2a \quad (C.3)$$

$$R_s = \sigma_n \cdot A_j \cdot \tan \phi_j + c_j \cdot A_j + \sigma_b \cdot A_b \cdot \cos \theta + \tau_{bf} \cdot A_b / \sin \theta \quad (C.4)$$

The condition of equilibrium ($F_s = R_s$) and subsequent algebraic manipulation result in the following equation:

$$\sigma_1 = \sigma_3 + \frac{2(c_j + \sigma_3 \tan \phi_j)}{(1 - \tan \phi_j \tan \alpha) \sin 2\alpha} + \frac{2(F_1 + F_2)}{(1 - \tan \phi_j \tan \alpha) \sin 2\alpha} \quad (C.5)$$

where: $F_1 = \sigma_b \cdot A_b \cdot \cos \theta (1 + \tan \phi_j \tan \theta) / A_j$

and $F_2 = A_b / (A_j \sin \theta)$

Reinforcement of the Joint by Several Bolts

In general, several bolts may be installed at different angles across the plane of weakness. If the number of bolts is represented by n , then the parameters σ_{b_i} , A_{b_i} and θ_i vary for $i = 1$ to n . Hence, Equations C.2 and C.5 can be modified as follows:

$$\sigma_n = \frac{1}{2}(\sigma_1 + \sigma_3) - \frac{1}{2}(\sigma_1 - \sigma_3) \cos 2\alpha + \frac{1}{A_j} \sum_{i=1}^n \sigma_{b_i} \cdot A_{b_i} \cdot \sin \theta_i \quad (C.6)$$

$$\sigma_1 = \sigma_3 + \frac{2(c_j + \sigma_3 \tan \phi_j)}{(1 - \tan \phi_j \tan \alpha) \sin 2\alpha} + \frac{2(P_1 + P_2)}{(1 - \tan \phi_j \tan \alpha) \sin 2\alpha} \quad (C.7)$$

where: $P_1 = \frac{1}{A_j} \left[\sum_{i=1}^n \sigma_{b_i} \cdot A_{b_i} \cdot \cos \theta_i + \tan \phi_j \cdot \sum_{i=1}^n \sigma_{b_i} \cdot A_{b_i} \cdot \sin \theta_i \right]$

and $P_2 = \frac{\tau_{bf}}{A_j} \sum_{i=1}^n A_{b_i} / \sin \theta_i$

APPENDIX D

EFFECTIVE STIFFNESS OF A REINFORCED COMPOSITE

List of Symbols

$\Delta\sigma$ = stress change after excavation

E_{IR}, E_J, E_{JR} = moduli of intact rock, joint and jointed rock

E_b = elastic modulus of the bolt

A_b = cross-section area of the bolt

A_r = longitudinal spacing \times transverse spacing

σ_b = axial bolt stress spread over the area A_r

$\sigma_{IR}, \sigma_J, \sigma_{JR}$ = stresses in intact rock, joint and jointed rock

ϵ_b = axial strain of the bolt

$\epsilon_{IR}, \epsilon_J, \epsilon_{JR}$ = strains of intact rock, joint and jointed rock.

Assumptions

(i) the joint is horizontal and the bolt is installed normal to the joint direction;

(ii) each bolt has an area of influence of A_r in plan,

where: $A_r = S_L \times S_T$;

(iii) effective bolt stress is averaged over the area A_r ;

(iv) the axial strain of the bolt at a given point is the same as that of the surrounding rock for small relative slip at their interface.

The total strain of the jointed rock is determined by the summation of the strain vectors of the intact rock and the joint as given below:

$$\epsilon_{JR} = \epsilon_{IR} + \epsilon_J$$

$$\Rightarrow \epsilon_{JR} = (\Delta\sigma - \sigma_b)/E_{IR} + (\Delta\sigma - \sigma_b)/E_J \quad (D.1)$$

Assuming that $\epsilon_b \approx \epsilon_{JR}$, the additional stress provided by the bolt can be given as follows:

$$\sigma_b = \frac{A_b}{A_r} \cdot E_b \cdot \epsilon_{JR} \quad (D.2)$$

The effective modulus of the composite (E') can be determined by re-arranging Equation D.1:

$$E' = \frac{\Delta\sigma}{\epsilon_{JR}} = \frac{1 + \sigma_b(1/E_{IR} + 1/E_J)/\epsilon_{JR}}{1/E_{IR} + 1/E_J} \quad (D.3)$$

Combination of Equations D.2 and D.3 results in:

$$E' = \frac{1}{1/E_{IR} + 1/E_J} + \frac{A_b}{A_r} \cdot E_b \quad (D.4)$$

The modulus of the unsupported jointed rock can be deduced by making $\sigma_b = 0$, which yields the following expression:

$$\frac{1}{E_{JR}} = \frac{1}{E_{IR}} + \frac{1}{E_J} \quad (D.5)$$

Substitution of the latter in Equation D.4 gives:

$$E' = E_{JR} + \frac{A_b}{A_r} E_b \quad (D.6)$$

This can be extended for the case of several parallel joints reinforced by bolting. The greater the number of joints is, the smaller the magnitude of the modulus E_{JR} is. The latter condition may be ideally represented in a rectangular mine opening, where the horizontal bedding planes are stabilized by vertical bolts (Figure D.1).

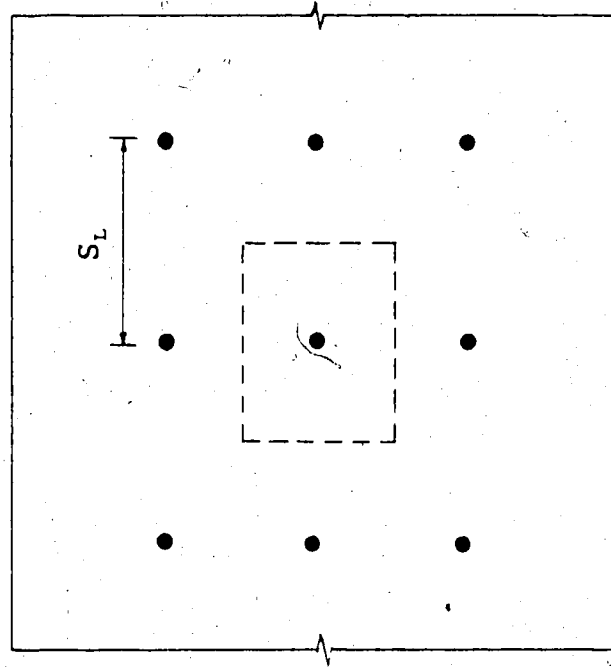
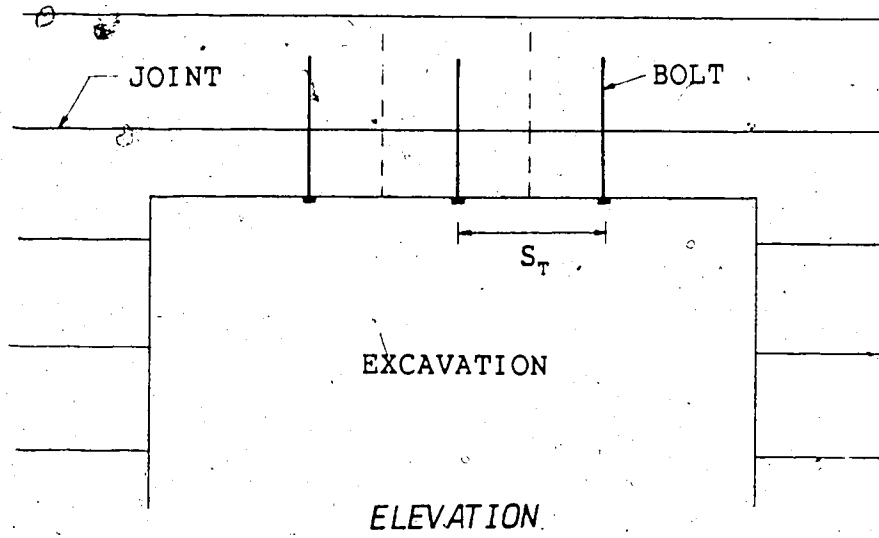


Figure D.1 Horizontal Bedding Planes Reinforced by Bolting

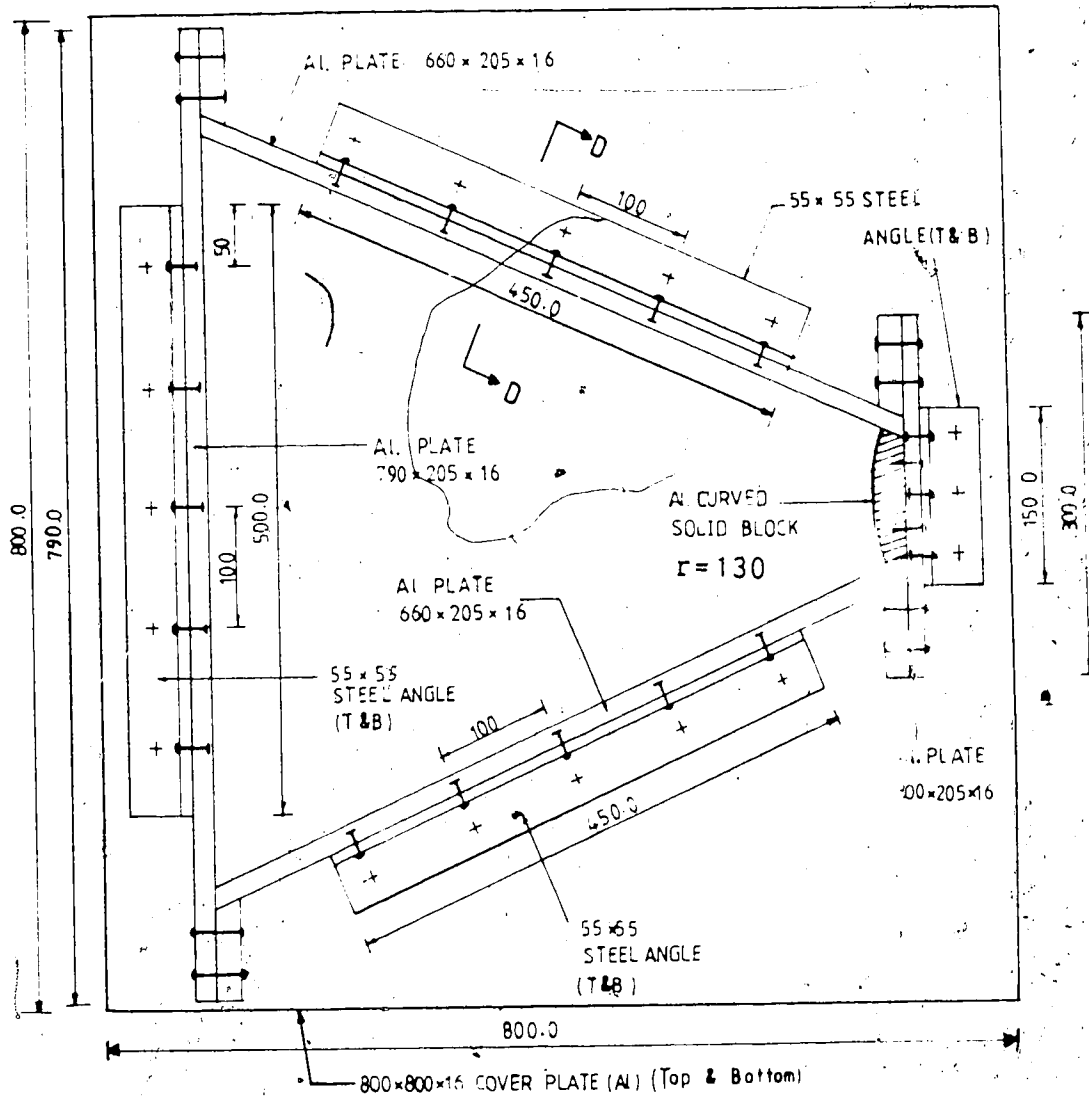
APPENDIX E

FEATURES OF THE LABORATORY TEST EQUIPMENT

In Appendix E1, the design details of the aluminum mould used for casting of gypstone samples are illustrated. In Appendix E2, the design features of the steel test frame used for loading of the samples are presented. These diagrammatic illustrations were utilized for manufacturing the mould and the test frame in the workshops at the University of Alberta. In Appendix E3, a schematic diagram of the Process Simulation Test (PST) apparatus is presented. Further details of the PST apparatus has been given by Kaiser (1979). The gypstone samples were loaded in plane strain using the latter test equipment.

APPENDIX E1

Design of the Aluminum Mould



PLAN

- NOTES - ONLY THE 55×55 ANGLE SECTIONS ARE STEEL. REST OF THE STRUCTURE IS ALUMINIUM.
 - THE EXACT REQUIRED DIMENSIONS OF THE SAMPLE SPACE ARE AS FOLLOWS →

Dimensions in mm

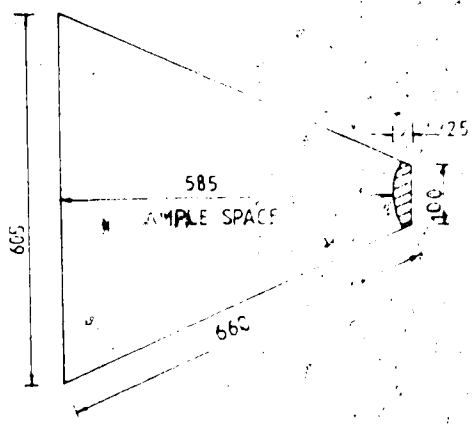


Figure E.1 Details of the Mould - Part i

TYPICAL CONNECTION BETWEEN STEEL ANGLES AND ALUMINIUM PLATES

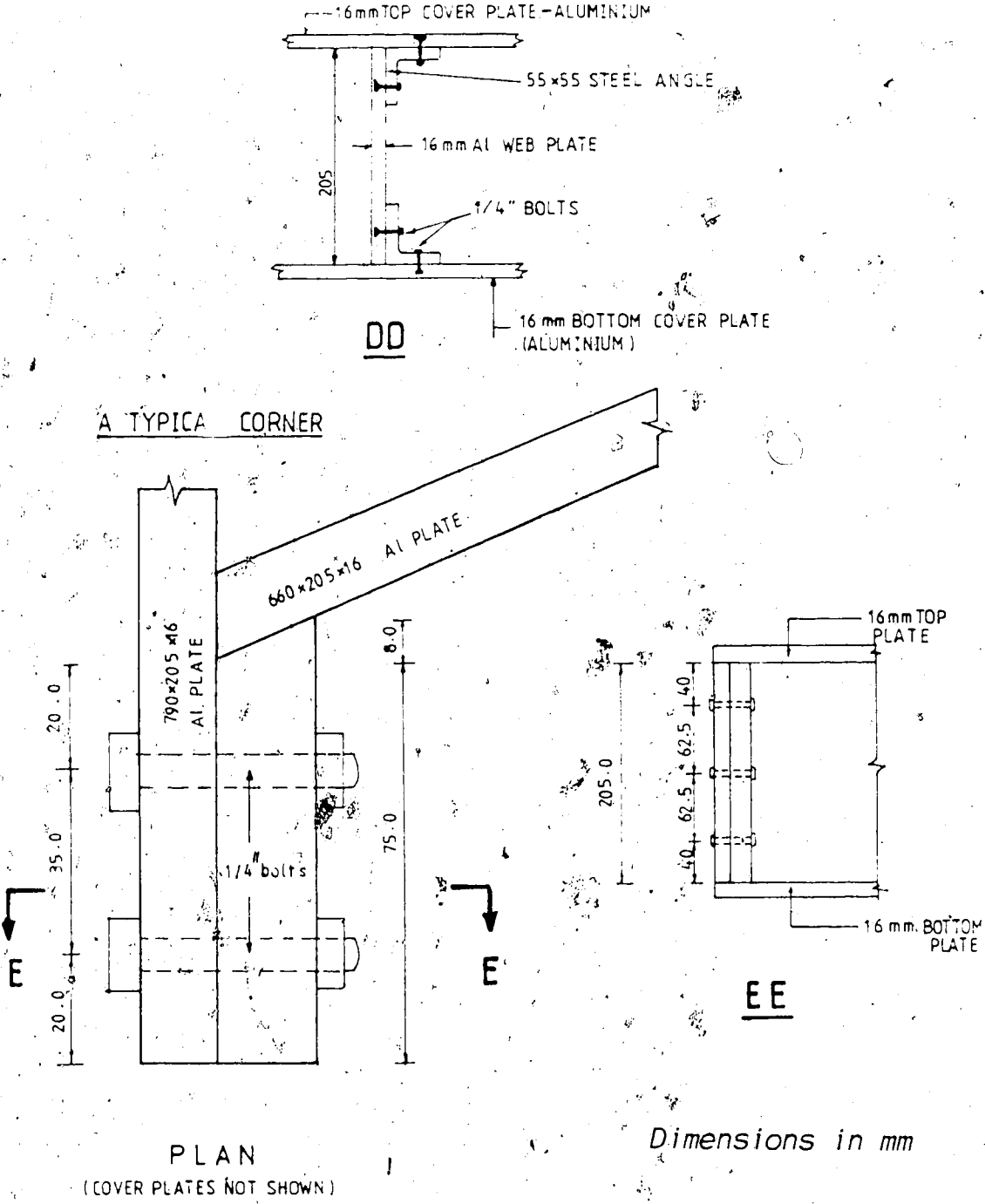


Figure E.2 Details of the Mould - Part ii

CONNECTION OF CURVED ALUMINIUM BLOCK - PLAN

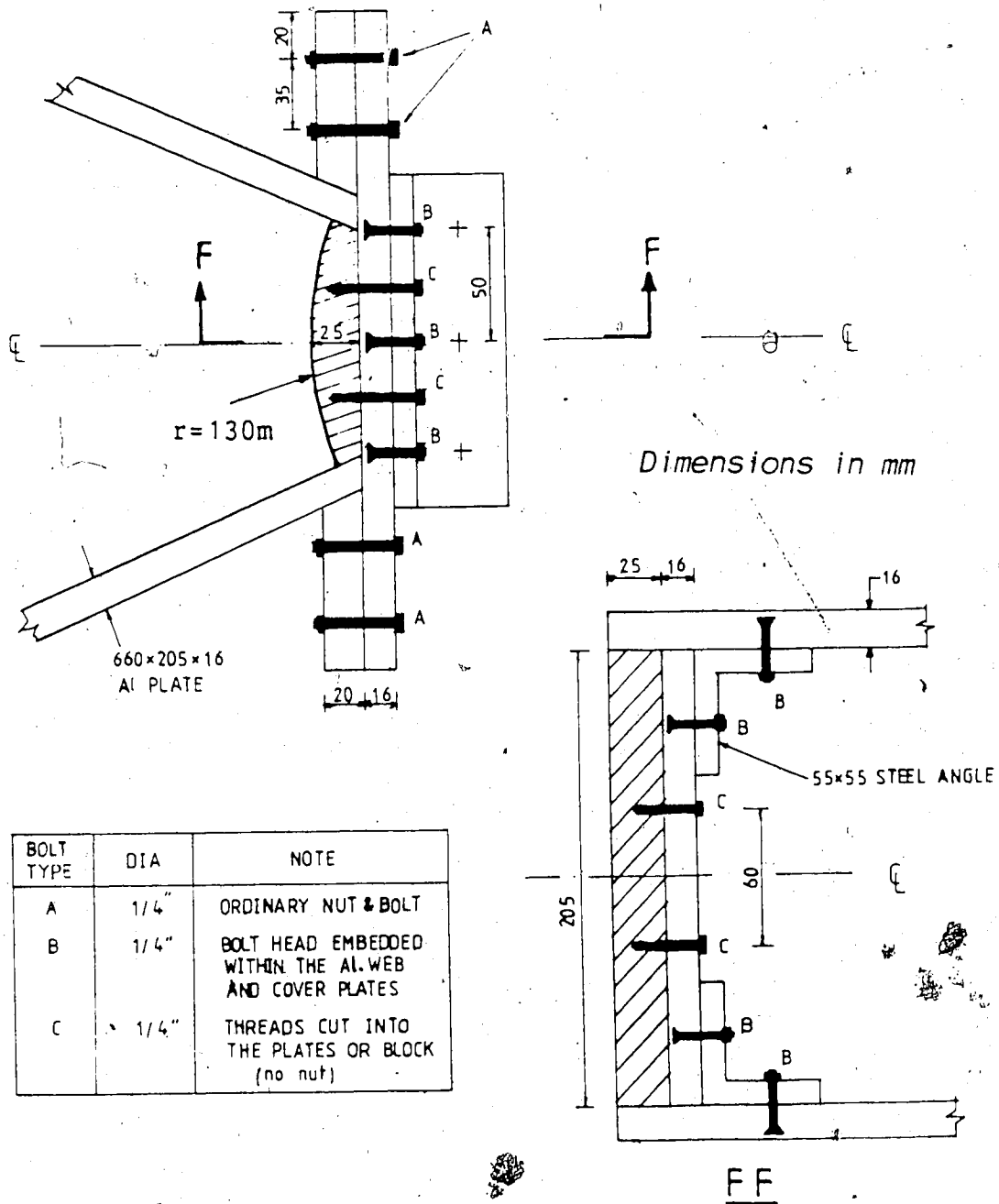
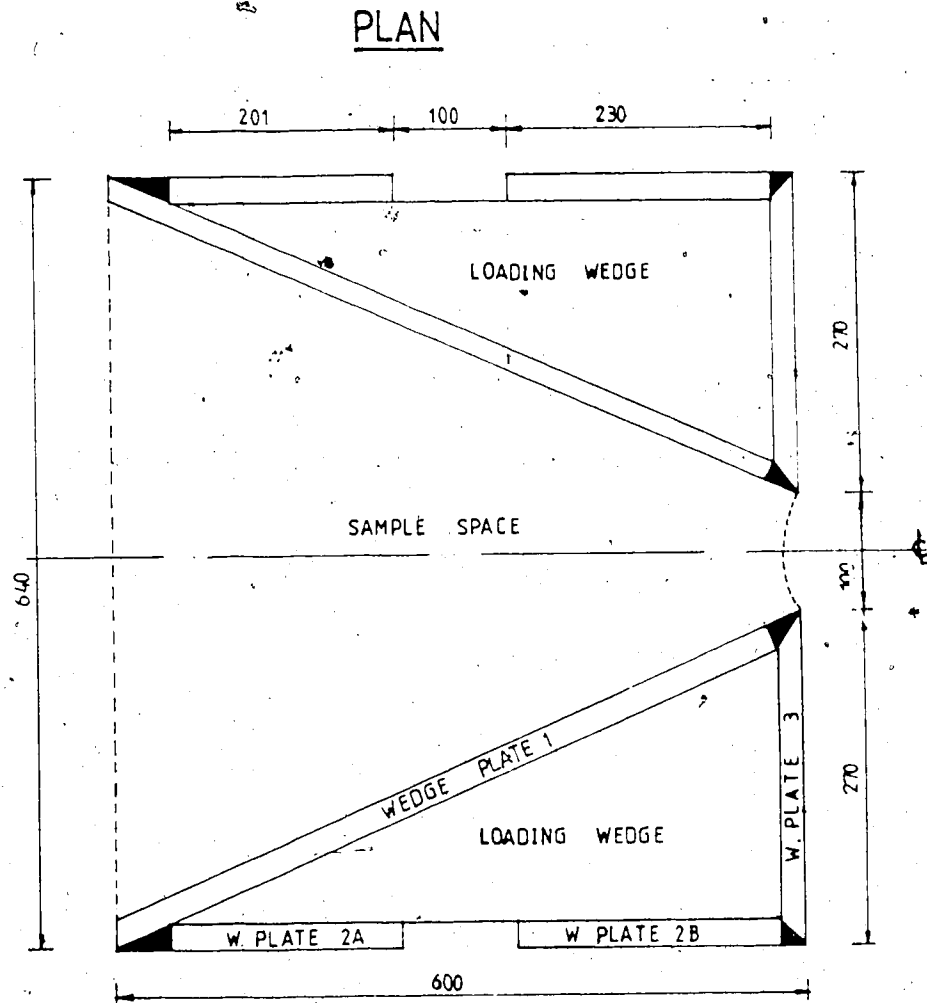


Figure E.3 Details of the Mould - Part iii

APPENDIX E2

• *Design of the Steel Test Frame*

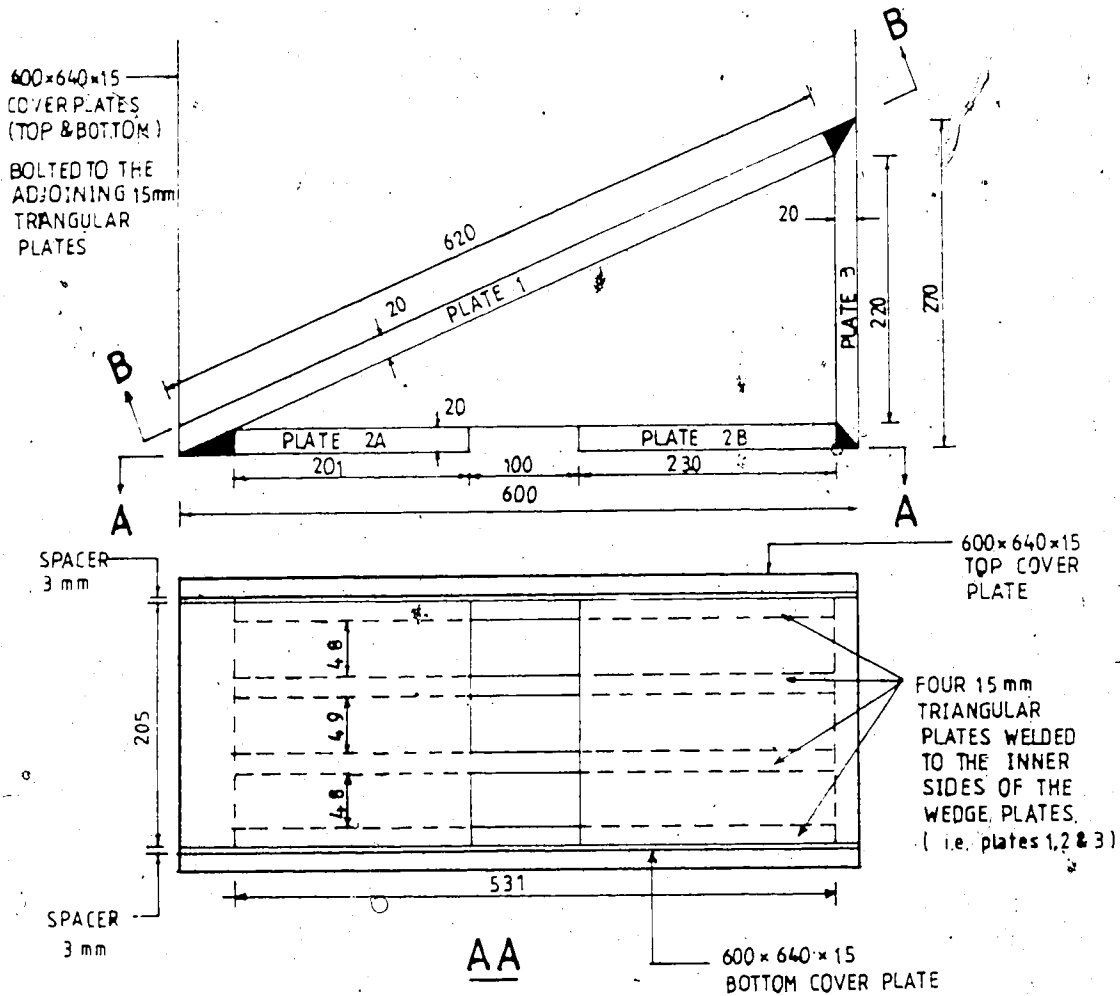
ARRANGEMENT OF SAMPLE AND THE LOADING WEDGES.



- NOTES
- THE ABOVE DRAWING DOES NOT SHOW THE CONSTRUCTION DETAILS OF THE WEDGES, THE TOP & BOTTOM COVER PLATES OR ANY BOLT DETAILS.
 - THE REQUIRED SAMPLE SIZE AND SHAPE ARE SHOWN IN THE MOULD DETAILS. THE DOTTED LINES SHOWN IN THE ABOVE DRAWING ARE ONLY FOR GENERAL GUIDANCE.
 - THE CONNECTIONS OF WEDGE PLATES AT THE CORNERS (WELDED) MUST BE CAREFULLY CARRIED OUT TO MAINTAIN A PERFECT TRIANGULAR BOUNDARY.

Dimensions in mm

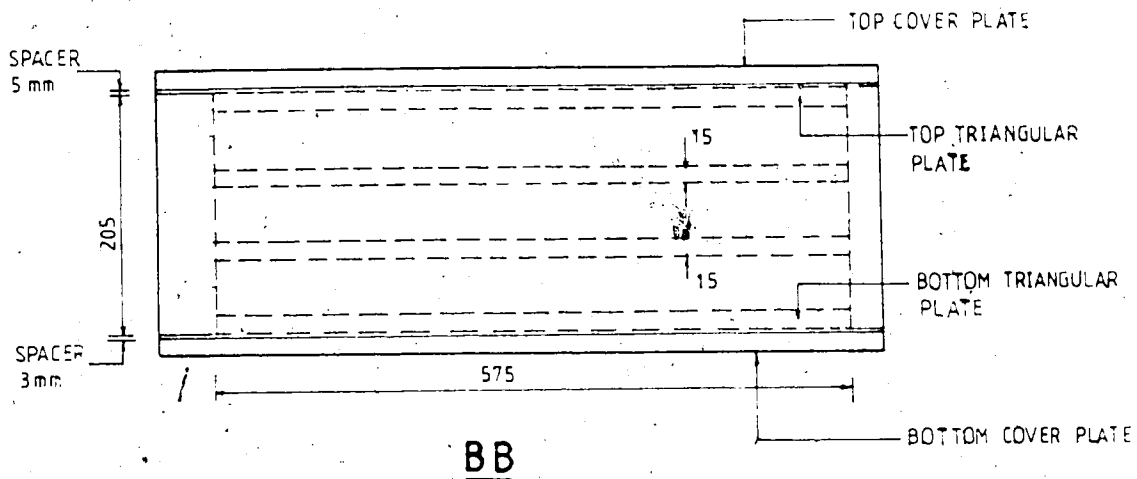
Figure E.4 Details of the Test Frame - Part i



- NOTES**
- THE TOP AND BOTTOM COVER PLATES (600 × 640 × 15) ARE BOLTED TO THE ADJOINING 15mm TRIANGULAR PLATES (T & B). BOLT DETAILS ARE SHOWN ON PAGE 235.
 - 3mm SPACER IS REQUIRED BETWEEN COVER PLATES AND ADJOINING TRIANGULAR PLATES, HENCE THE BOLTS INSTALLED ACCORDINGLY. SEE PAGE 235.
 - THE FOUR 15 mm TRIANGULAR PLATES (SIDES 531 × 220 × 575) ARE WELDED ALONG THE INNER BOUNDARIES OF THE WEDGE PLATES 1, 2 & 3 WITH AT LEAST 8 mm LEG LENGTH FILLET WELDS.
 - THE HEIGHT OF EACH WEDGE BEFORE THE BOLTING OF COVER PLATES MUST BE ACCURATE AT 205mm AS SHOWN ABOVE.

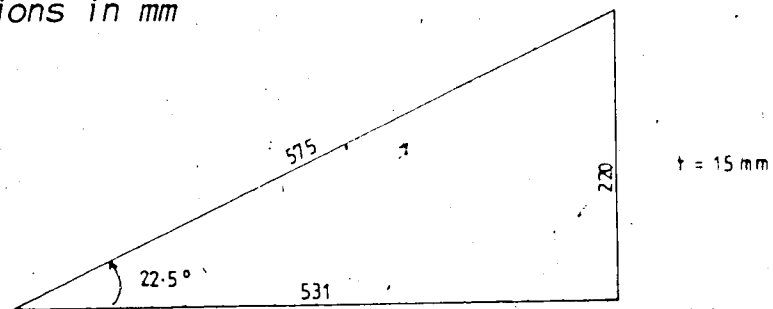
Dimensions in mm

Figure E.5 Details of the Test Frame - Part ii



- NOTES**
- BOLT DETAILS BETWEEN THE COVER PLATES (T & B) AND THE ADJOINING TRIANGULAR PLATES (T & B) ARE NOT SHOWN ABOVE (see page 235)
 - THE 15 mm THICK TRIANGULAR PLATES ARE WELDED AS DESCRIBED EARLIER, TO THE SURROUNDING WEDGE PLATES

Dimensions in mm

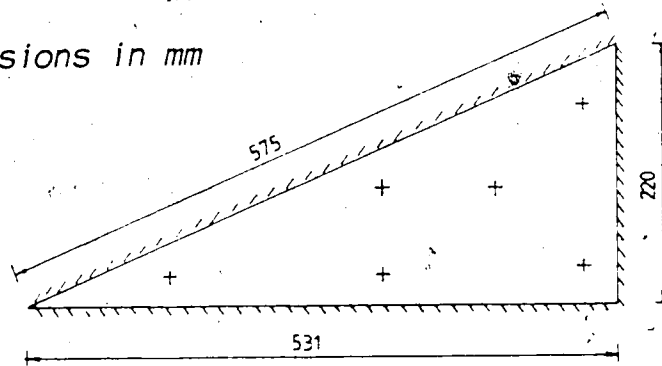


PLAN DIMENSIONS OF THE 15 mm TRIANGULAR PLATES

Figure E.6 Details of the Test Frame - Part iii

BOLTING OF COVER PLATE (TOP & BOTTOM) TO THE ADJOINING TRIANGULAR PLATE (TOP & BOTTOM)

Dimensions in mm

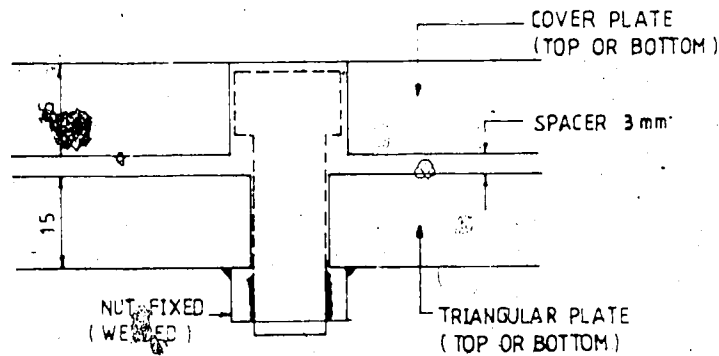


PLAN

NOTES - BOLTS, SIX 0.5" (12.7 mm) BOLTS
 THE PATTERN OF THE BOLTS IS AS INDICATED APPROX. TO SCALE
 BUT CAN BE VARIED SLIGHTLY.

—— T-ANGULAR PLATES WELDED TO THE INNER SIDES
 OF THE WEDGE PLATES (i.e. PLATES 1, 2 & 3)
 - 8 mm LEG LENGTH FILLET WELDS PREFERRED

A TYPICAL BOLT SECTION



NOTES - BOLT HEAD MUST BE WITHIN THE COVER PLATE

Figure E.7 Details of the Test Frame - Part iv

APPENDIX E3

Process Simulation Test Apparatus

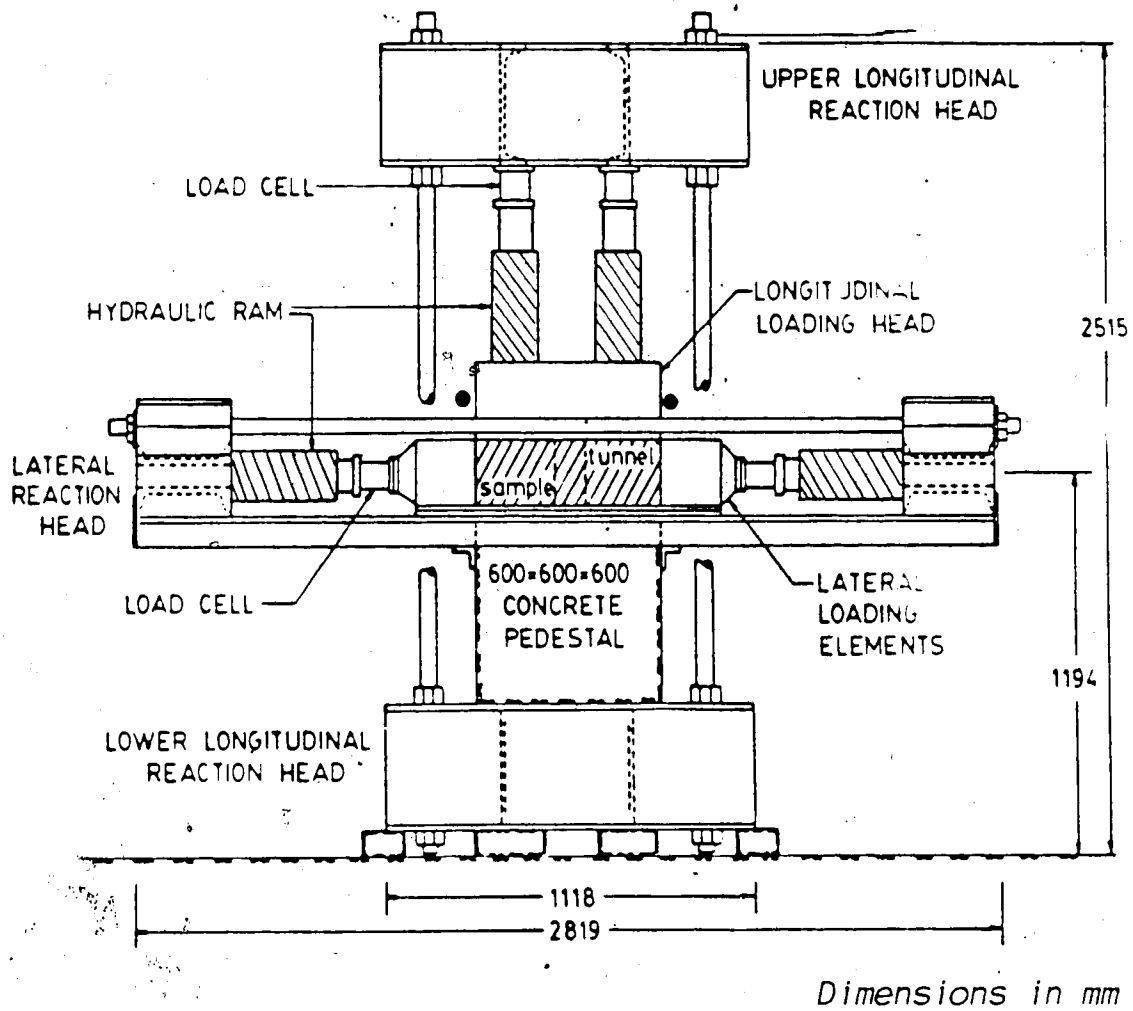


Figure E.8 A Schematic Diagram of the PST Apparatus
(modified after Maloney, 1984)

APPENDIX F

MATERIAL CHARACTERISTICS OF GYPSTONE

Properties of Hydrocal gypsum cement and fine Ottawa sand used in manufacturing gypstone synthetic rock are presented in Appendix F1. The variation of the density of gypstone during the curing period is illustrated in Appendix F2. The influence of the retarder anhydrous sodium hydrogen phosphate (Na_2HPO_4) on the initial setting time of gypstone is also shown in Appendix F2.

The stress-strain behaviour of intact, reinforced gypstone blocks in uniaxial compression is graphically illustrated in Appendix F3. The behaviour of Hydrostone joints in the shear box test and the uniaxial stress-strain characteristics of jointed, reinforced gypstone samples are presented in Appendices F4 and F5 respectively. The behaviour of the multi-directional jointed samples, loaded in triaxial compression (plane strain) by the PST apparatus is illustrated in Appendix F6.

APPENDIX F1

Properties of Gypstone Constituents

Table F.1 Physical Properties of Hydrocal Gypsum Cements
 (Data from U.S. Gypsum Company)

PRODUCT	USE CONSISTENCY (parts of water by weight per 100 parts of plaster)	VICAT SET (minutes)	DRY COMPRESSIVE STRENGTH (psi)	DRY IMPACT STRENGTH (g-cm)	SUGGESTED DRYING TIME (hrs.) (1"-2" thick cast)
White HYDROCAL Gypsum Cement	45	25-35	5,000	1,750	12-20 (at 120°F)
Statuary HYDROCAL Gypsum Cement	40	20-25	6,500	1,700	12-20 (at 120°F)
HYDRO-STONE Gypsum Cement	32	17-20	10,000	1,320	12-20 (at 120°F)

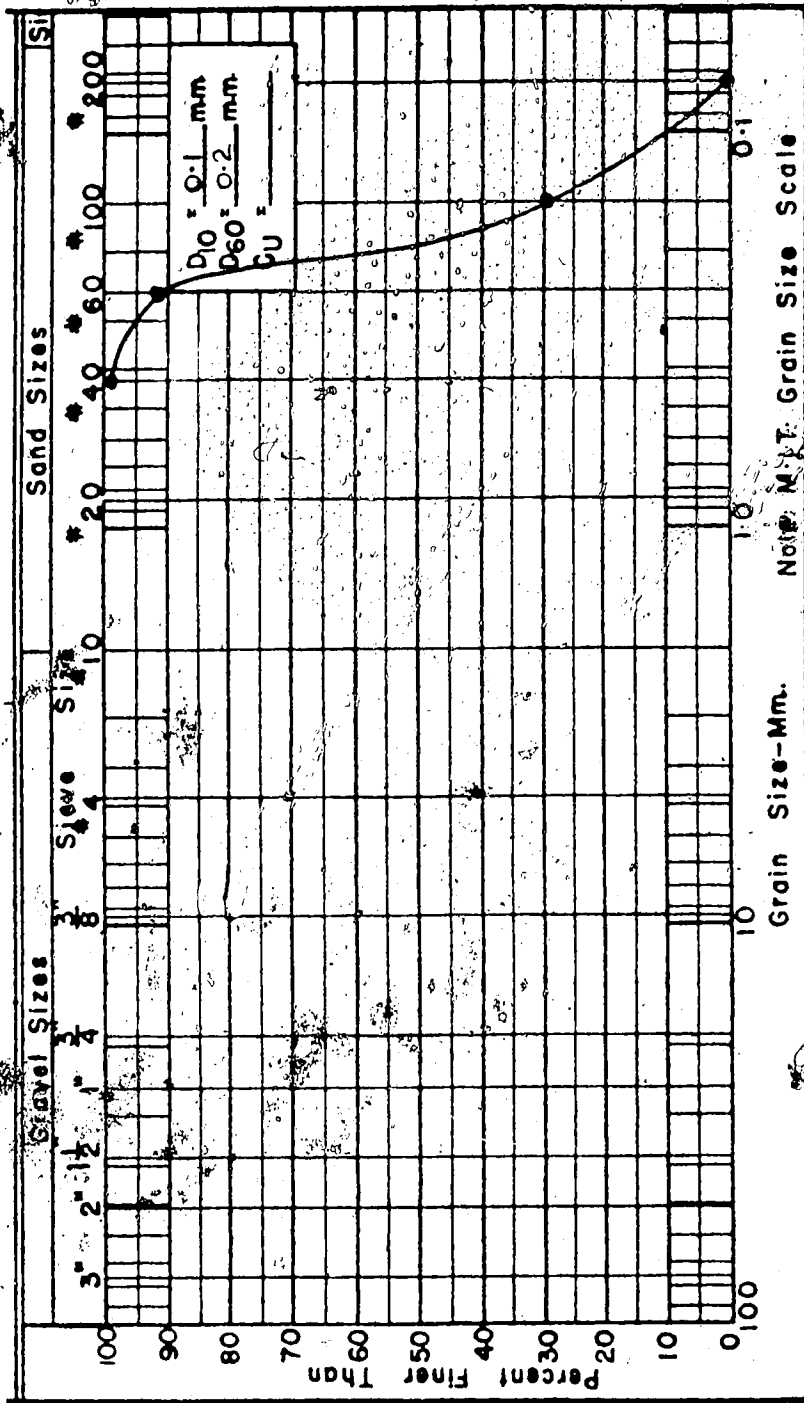


Figure F.1 Grading Curve of Fine Ottawa Sand

APPENDIX F2

Hardening and Curing of Gypstone

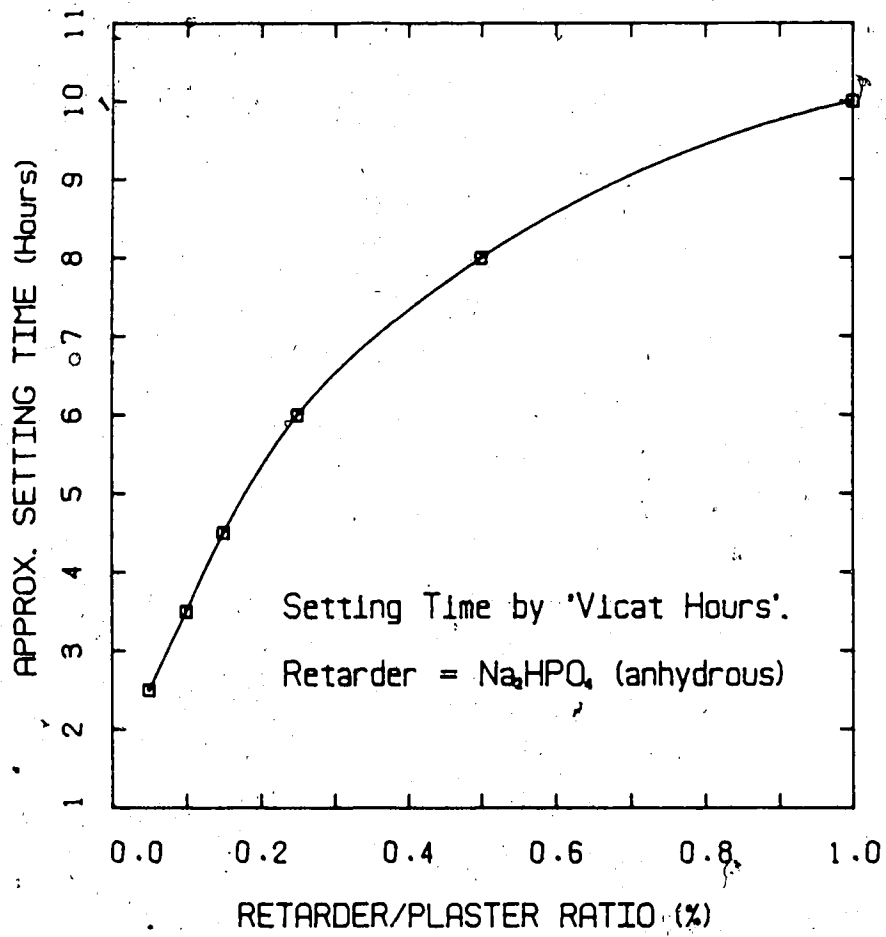


Figure F.2 Influence of Na_2HPO_4 on Setting Time of Gypstone

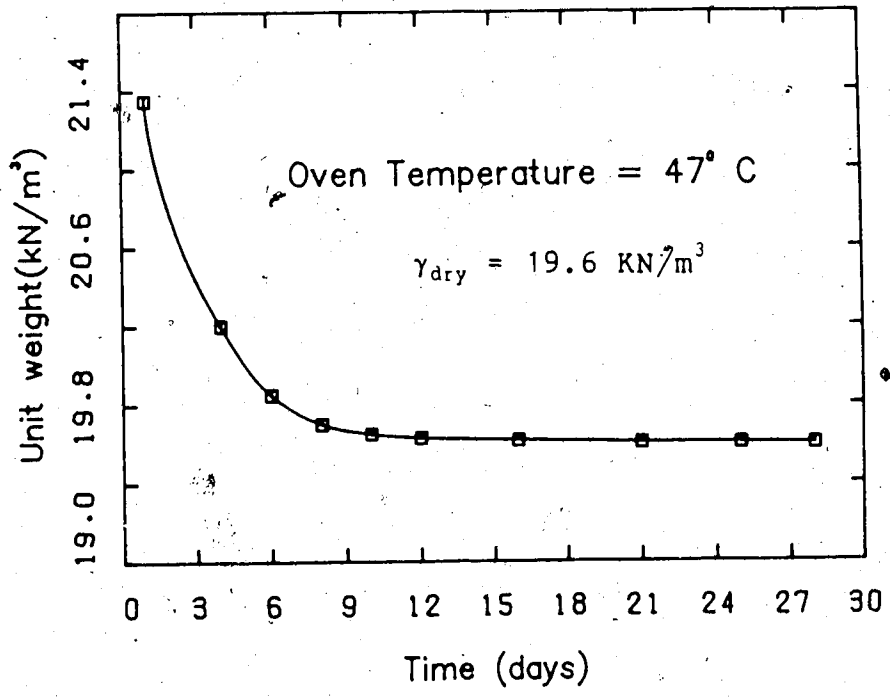


Figure F.3 Drying Curve of Gypstone Synthetic Rock

APPENDIX F3

Uniaxial Compression of Intact Gypstone Blocks

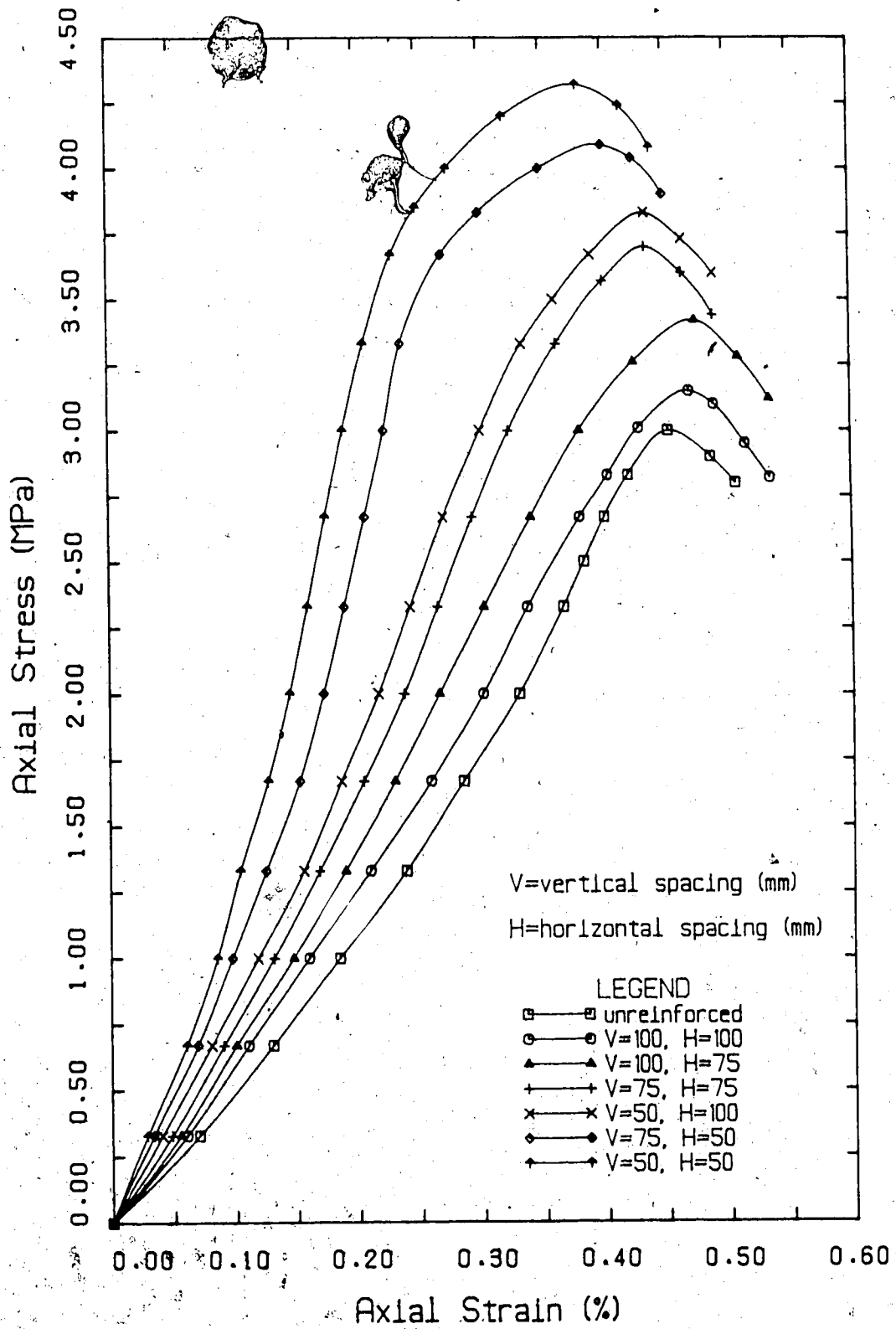


Figure F.4 Stress-Strain Behaviour of Intact Blocks

APPENDIX F4

Shear Box Tests on Hydrostone Joints

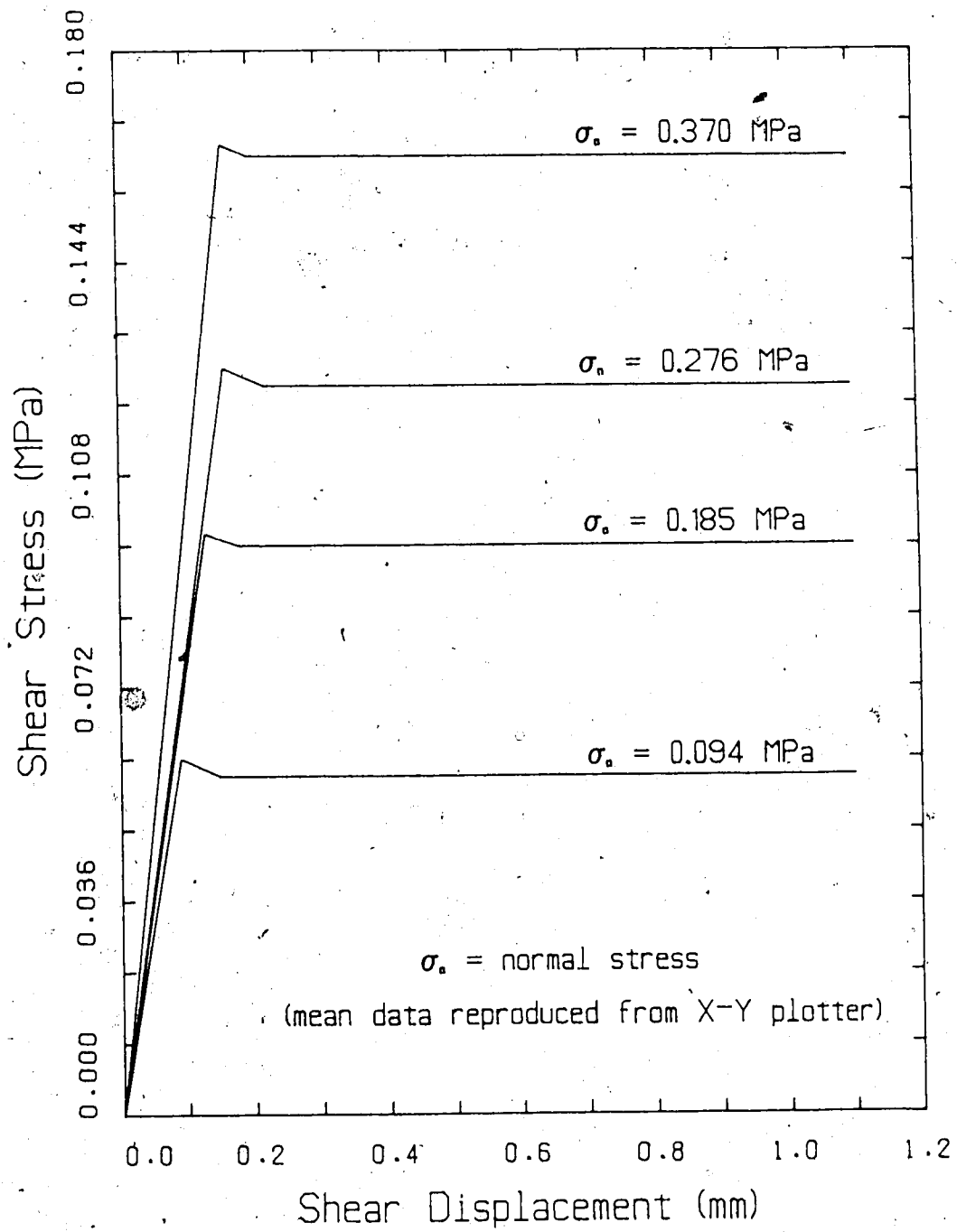


Figure F.5 Shear Behaviour of Synthetic Joints

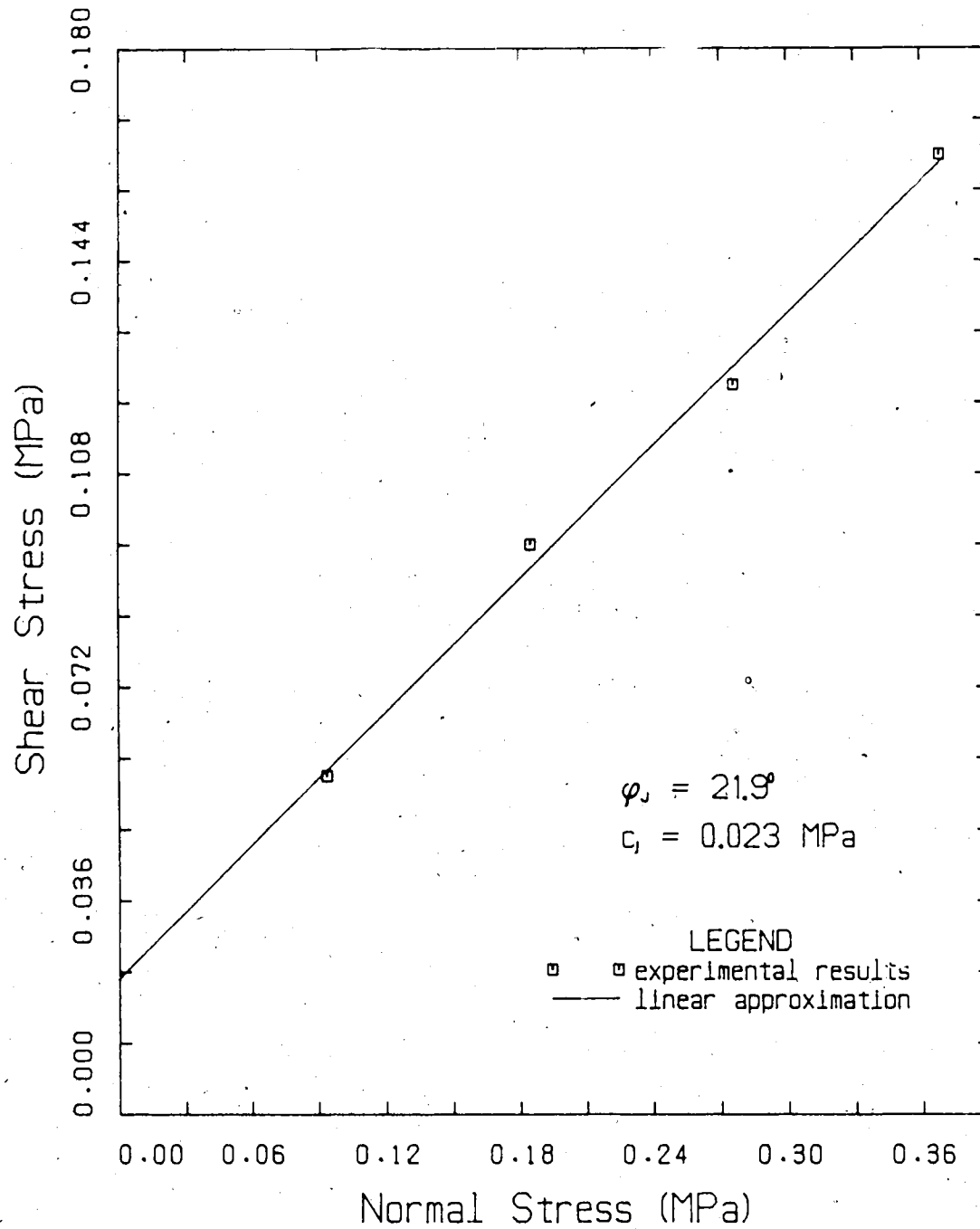


Figure F.6 Failure Envelope of Synthetic Joints

APPENDIX F5

Uniaxial Compression of Jointed Gypstone Blocks

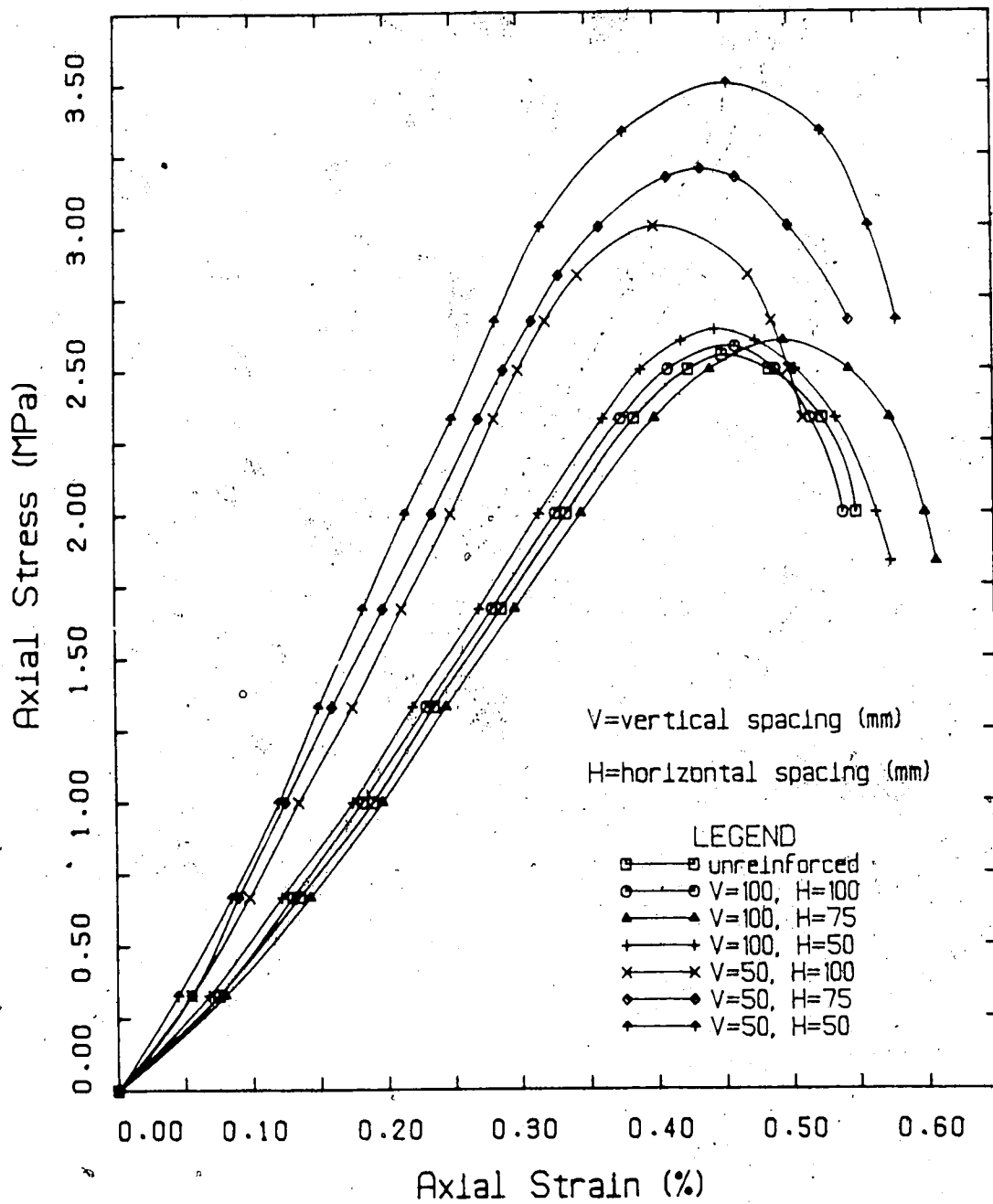


Figure F.7 Stress-Strain Behaviour of Jointed Blocks

APPENDIX F6

*Triaxial Compression of Jointed Gypstone Blocks in Plane
Strain*

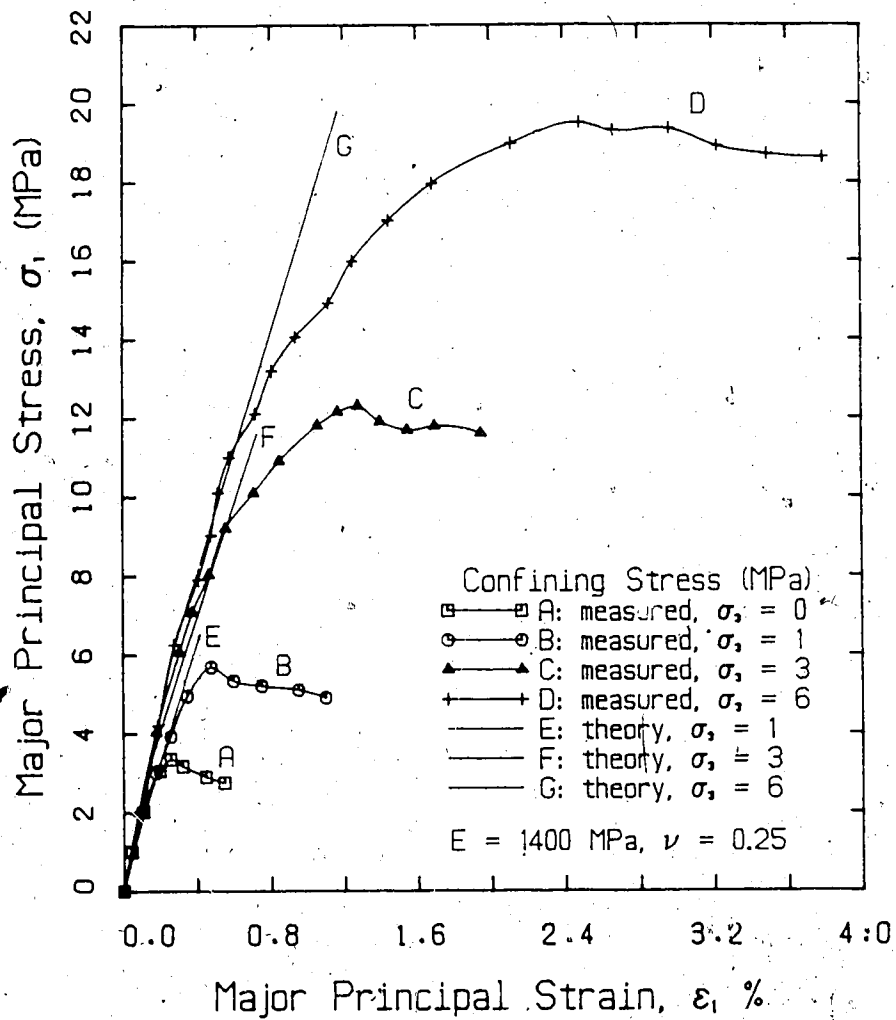


Figure F.8 Stress-Strain Behaviour of Jointed Blocks loaded in the PST apparatus

APPENDIX G

BEHAVIOUR OF REINFORCED OPENINGS (LONG BOLTS) IN AN INTACT MEDIUM

In this section, the variation of displacements and strains as a function of the applied field stress is illustrated for intact samples. The simulated tunnel is reinforced with 100 mm long bolts. The tunnel convergence, the field boundary displacement and the radial strains in both plastic and elastic regions have been measured by an assembly of LVDTs and extensometers. The measured results are plotted with the predicted data for comparison. The response of three different bolt densities ($\beta=0.073$, 0.220 and 0.291) are presented here. The behaviour corresponding to $\beta=0.145$ has been discussed in detail in Chapter 6.

The predicted behaviour was generally based on the following parameters: $E=1500$ MPa, $\nu=0.25$, $\sigma_c=3.5$ MPa, $\phi=32^\circ$ and $a=2.0$. The only exception was the higher values of E and σ_c (1650 and 4.0 MPa, respectively) assumed for one test sample ($\beta=0.073$), which may have been the result of slight over-compaction during casting.

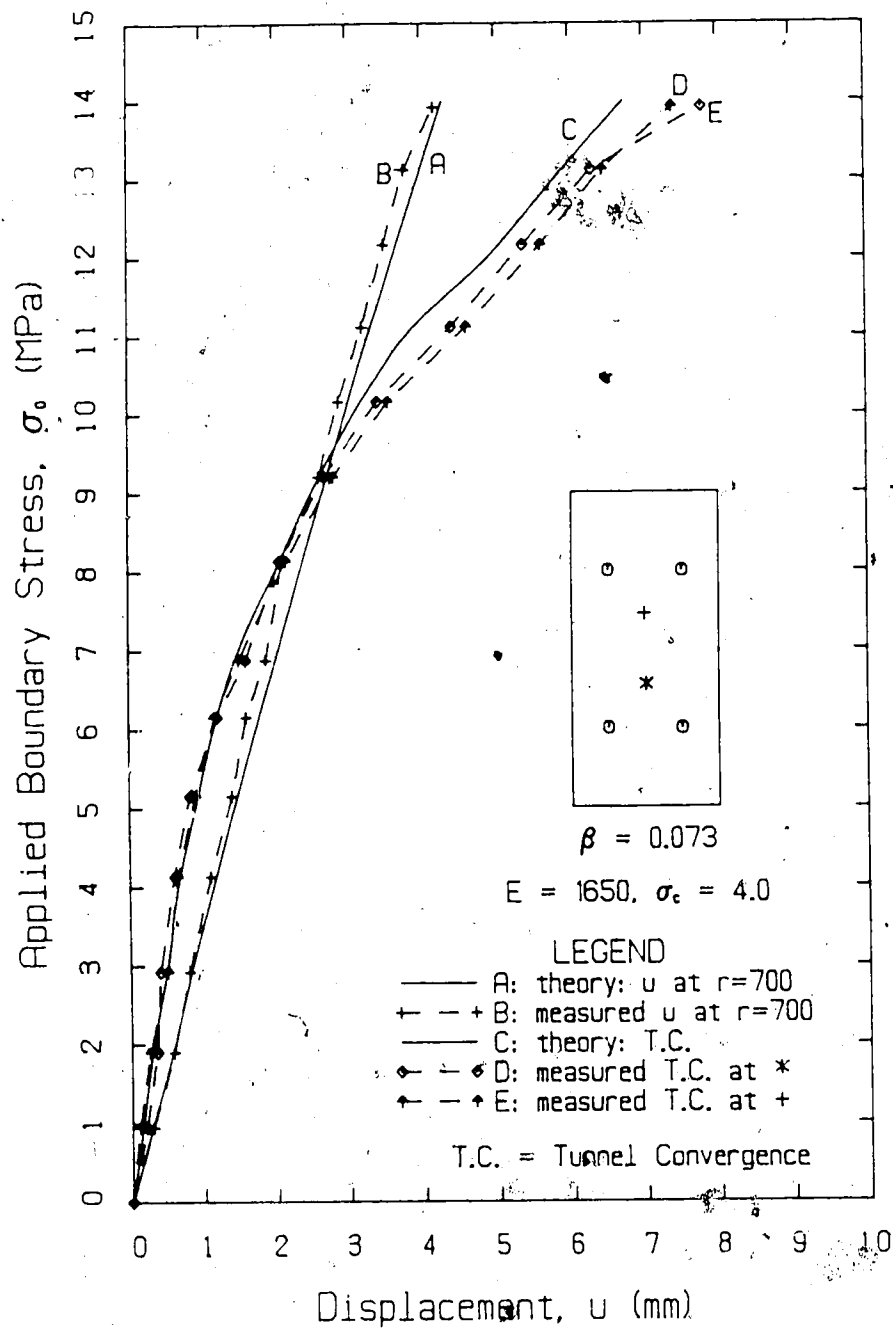


Figure G.1 Behaviour of Reinforced Opening for $\beta=0.073$,
 $L=100$

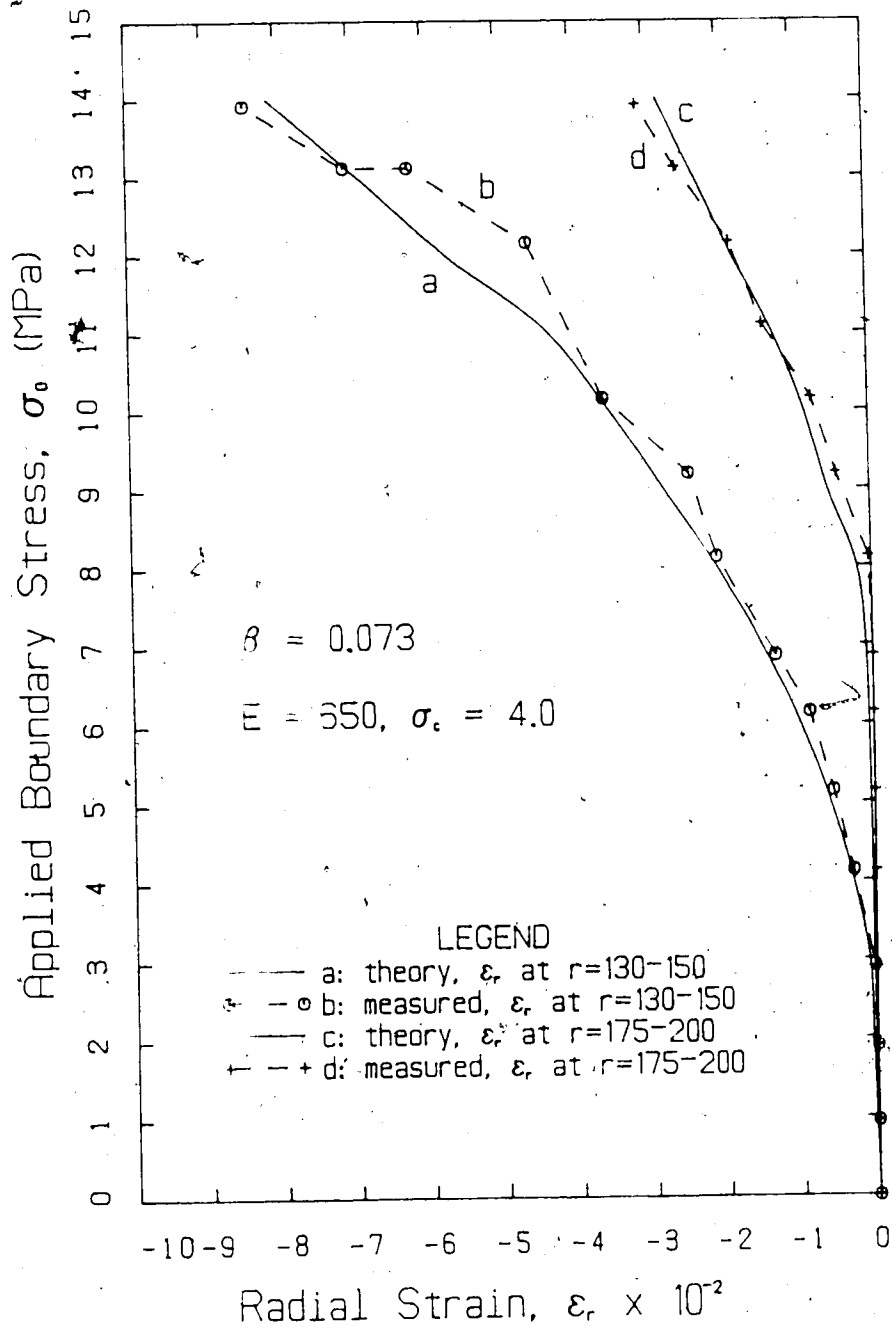


Figure G.2 Radial Strains near Tunnel Wall for $\beta=0.073$,

L=100

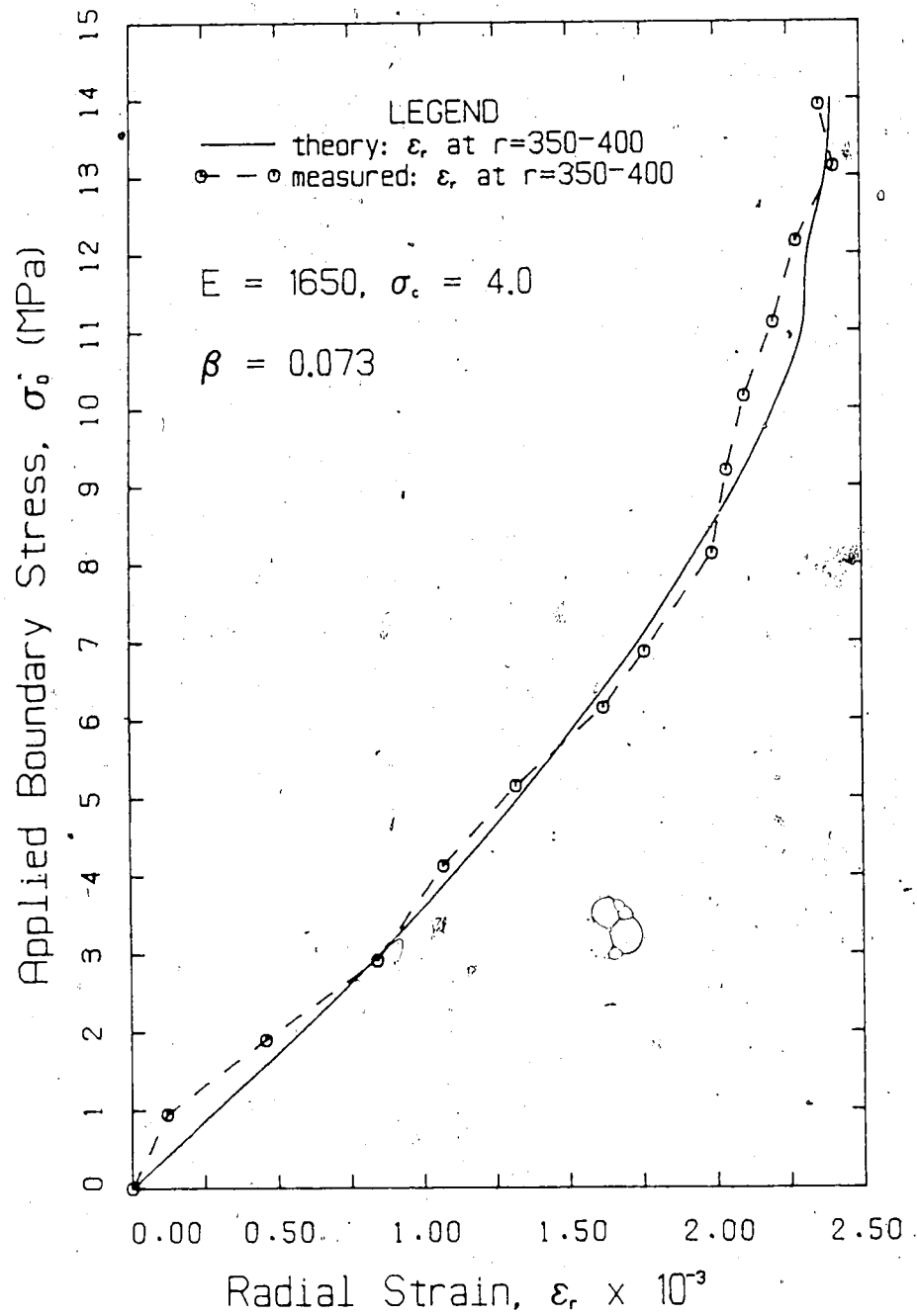


Figure G.3 Radial Strain in Elastic Zone for $\beta=0.073, L=100$

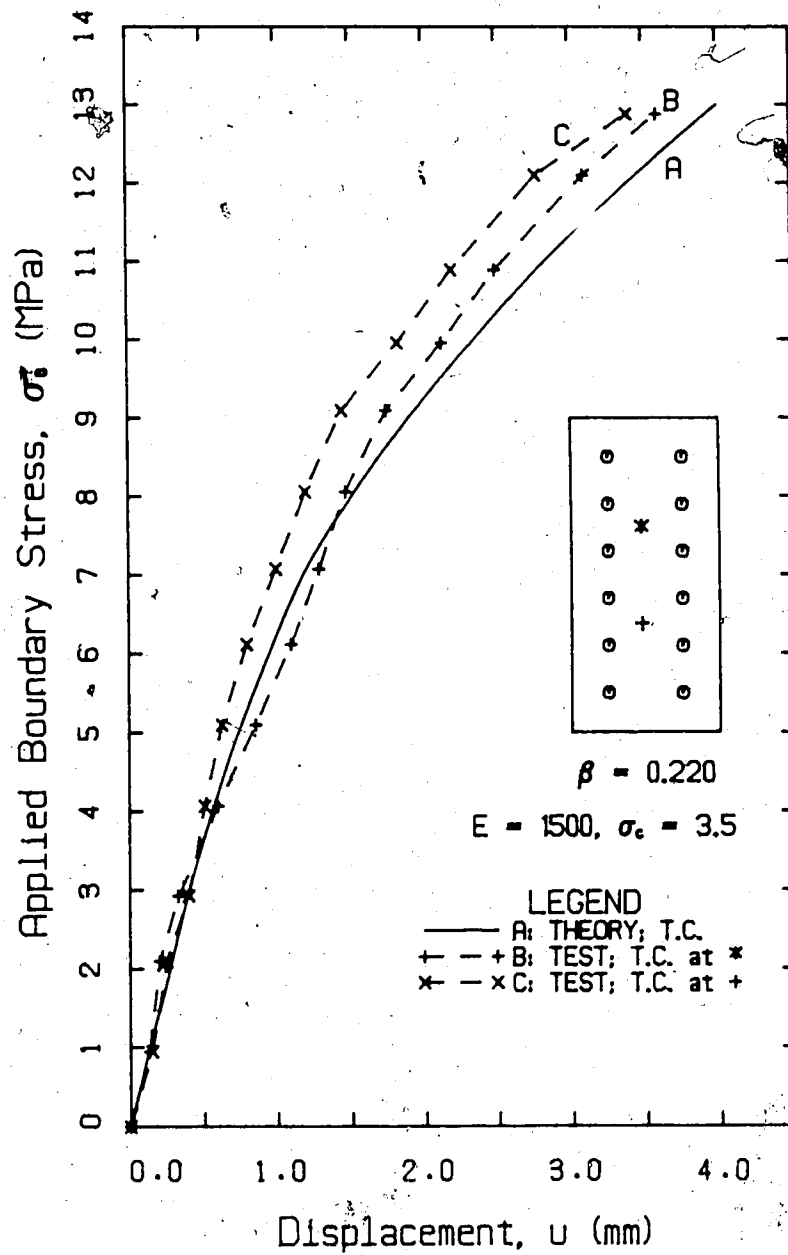


Figure G.4 Convergence of Reinforced Opening for $\beta=0.220$,

L=100

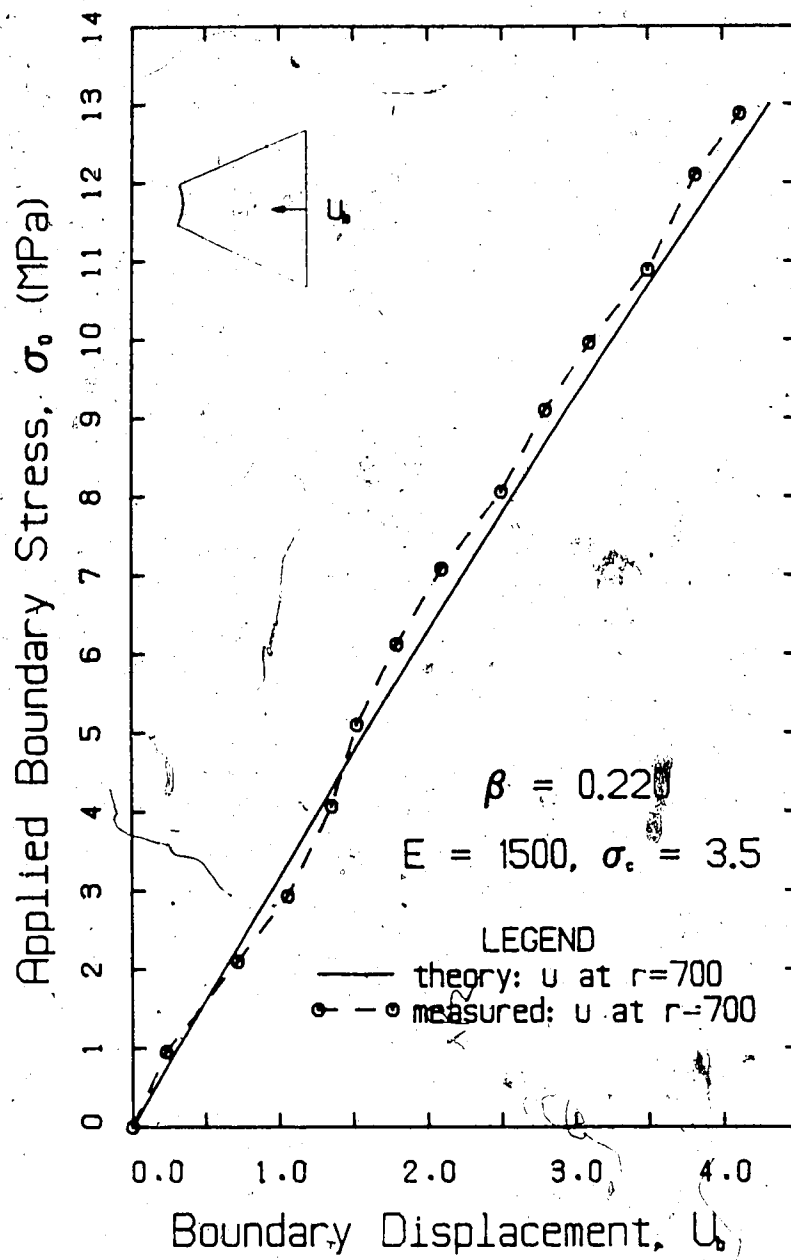


Figure G.5 Field Boundary Displacement for $\beta=0.220$, $L=100$

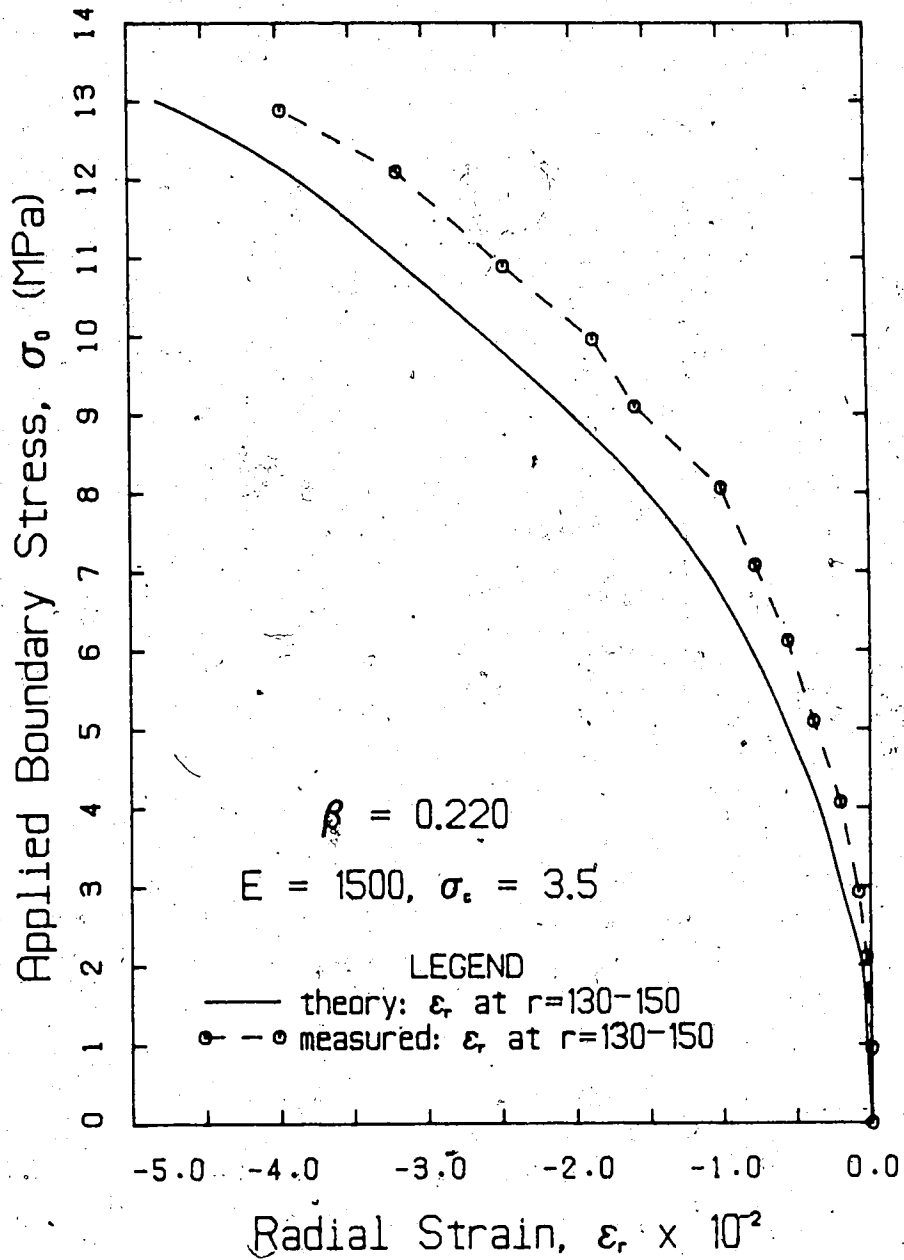


Figure G.6 Radial Strain at Tunnel Wall for $\beta=0.220$, $L=100$

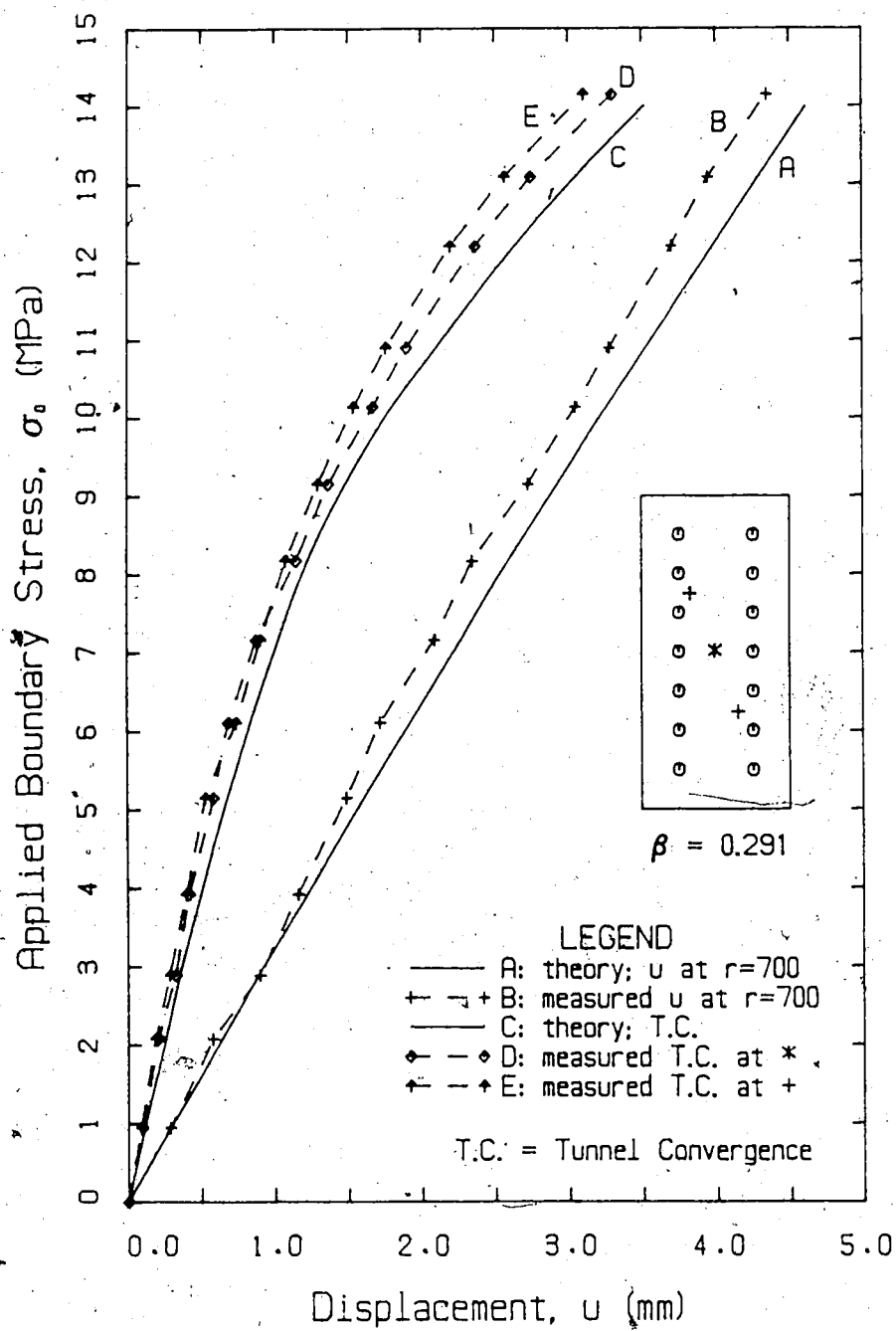


Figure G.7 Behaviour of Reinforced Opening for $\beta=0.291$,
 $L=100$

APPENDIX H

BEHAVIOUR OF REINFORCED OPENINGS (SHORT BOLTS) IN AN INTACT MEDIUM

In this section, the tunnel convergence, the field boundary displacement and the radial strain response in plastic and elastic zones are presented for intact samples. However, the model opening is reinforced with relatively short (50 mm) bolts. The response of two bolt densities ($\beta=0.145$ and 0.291) is illustrated. A summary of the convergence data has been given in Chapter 6. For the predicted curves, the same assumptions as in Appendix G were made.

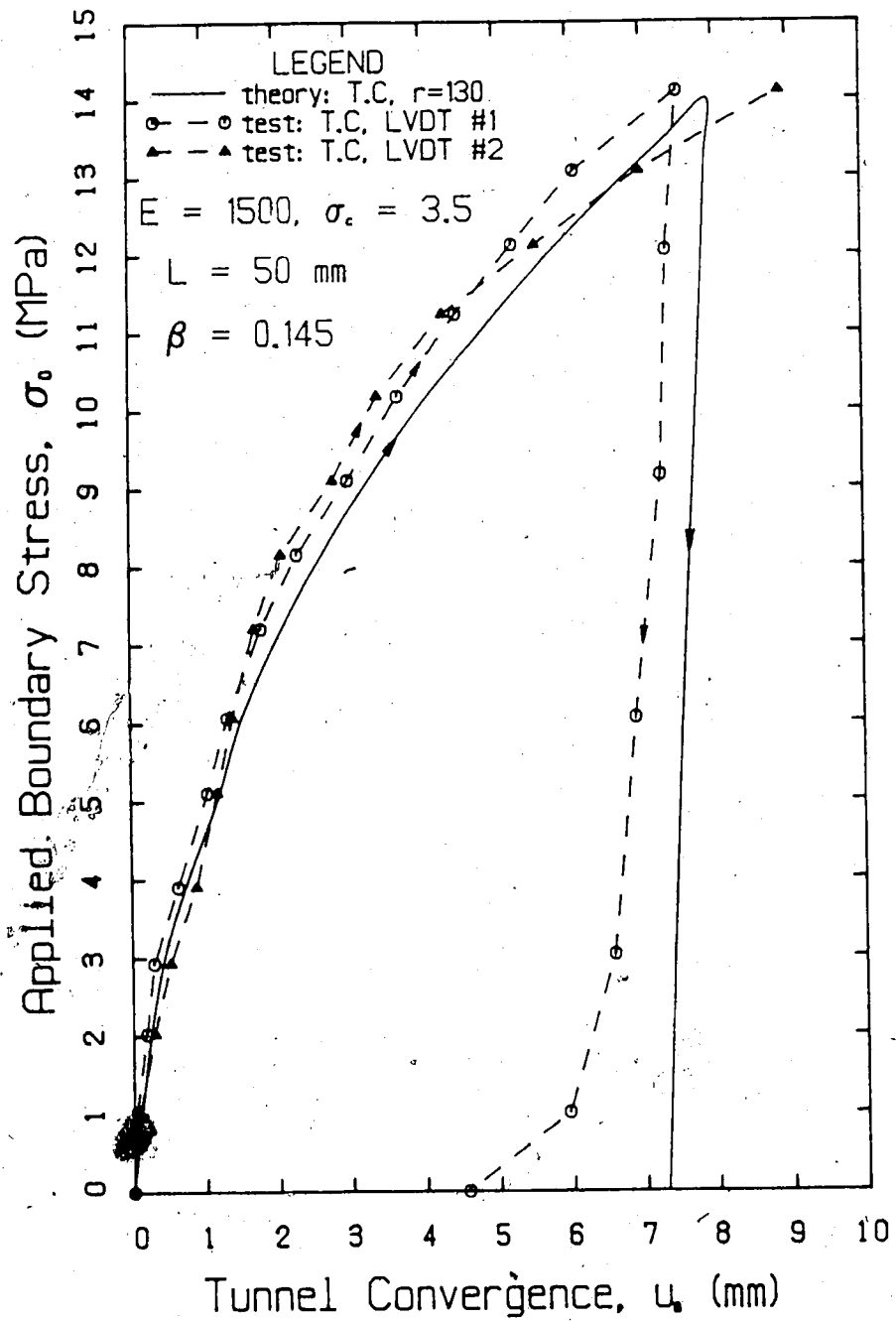


Figure H.1 Convergence of Reinforced Opening for $\beta=0.145$,
 $L=50$

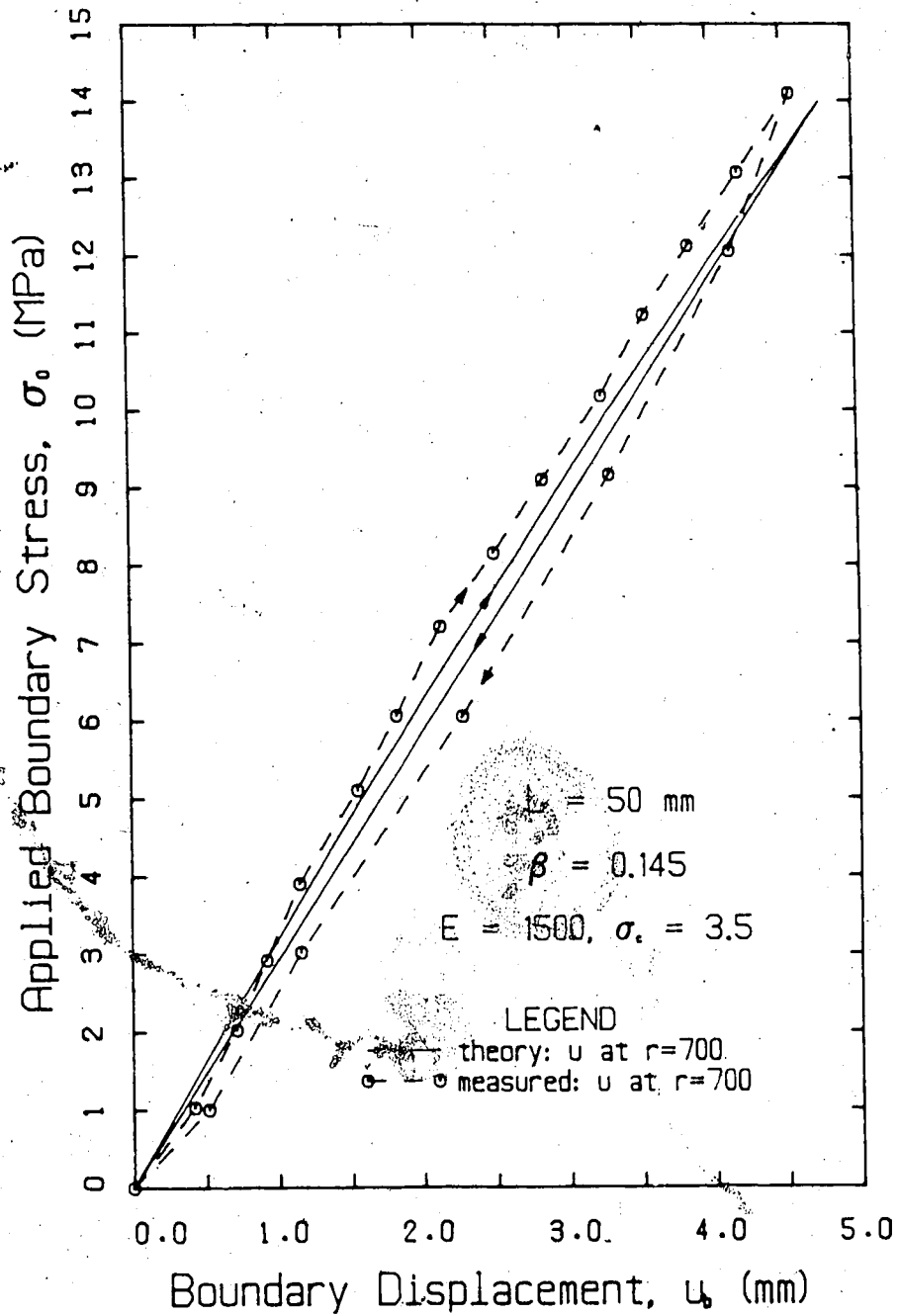


Figure H.2 Field Boundary Displacement for $\beta=0.145$, $r=50$.

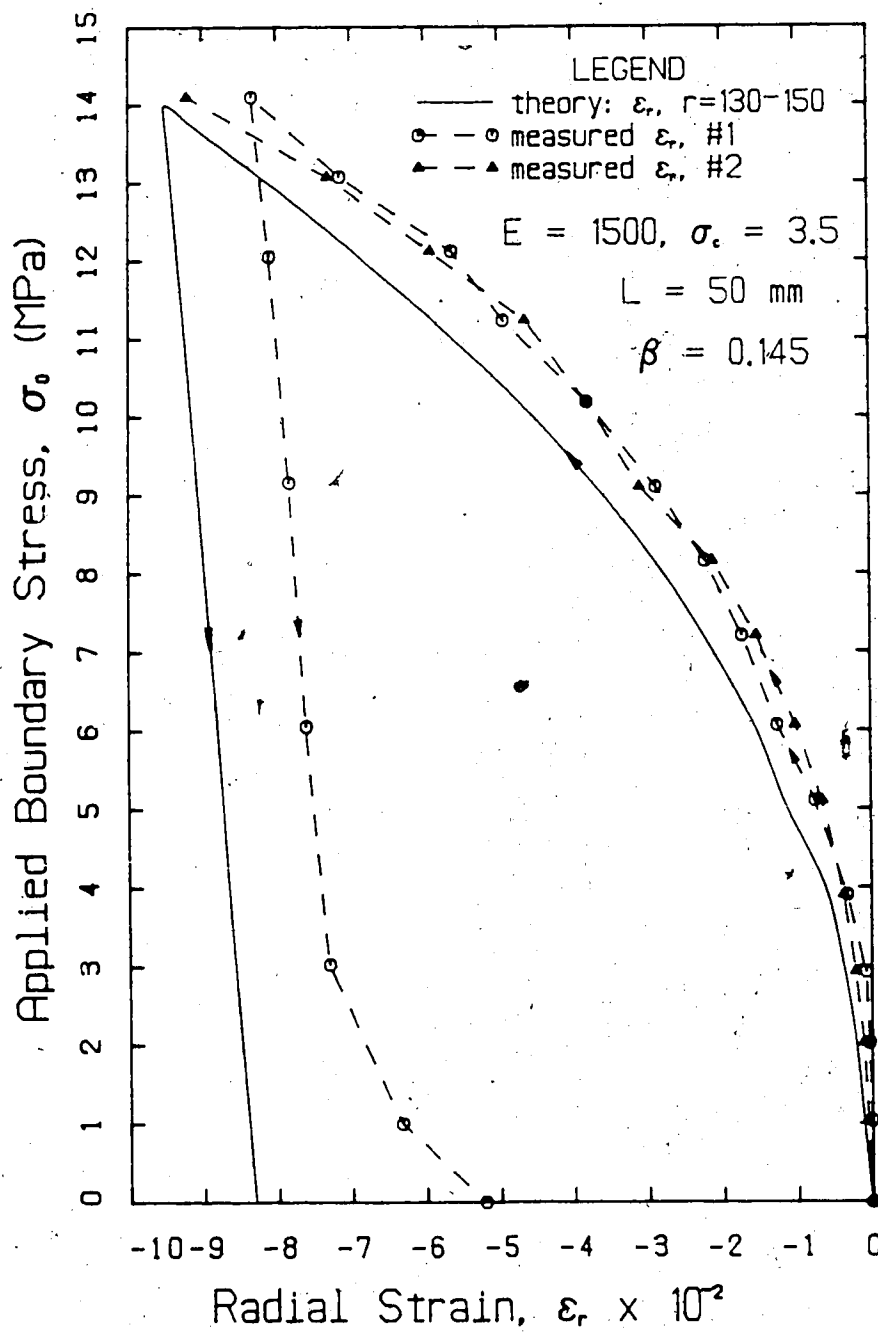


Figure H.3 Radial Strain at Tunnel Wall for $\beta=0.145$, $L=50$

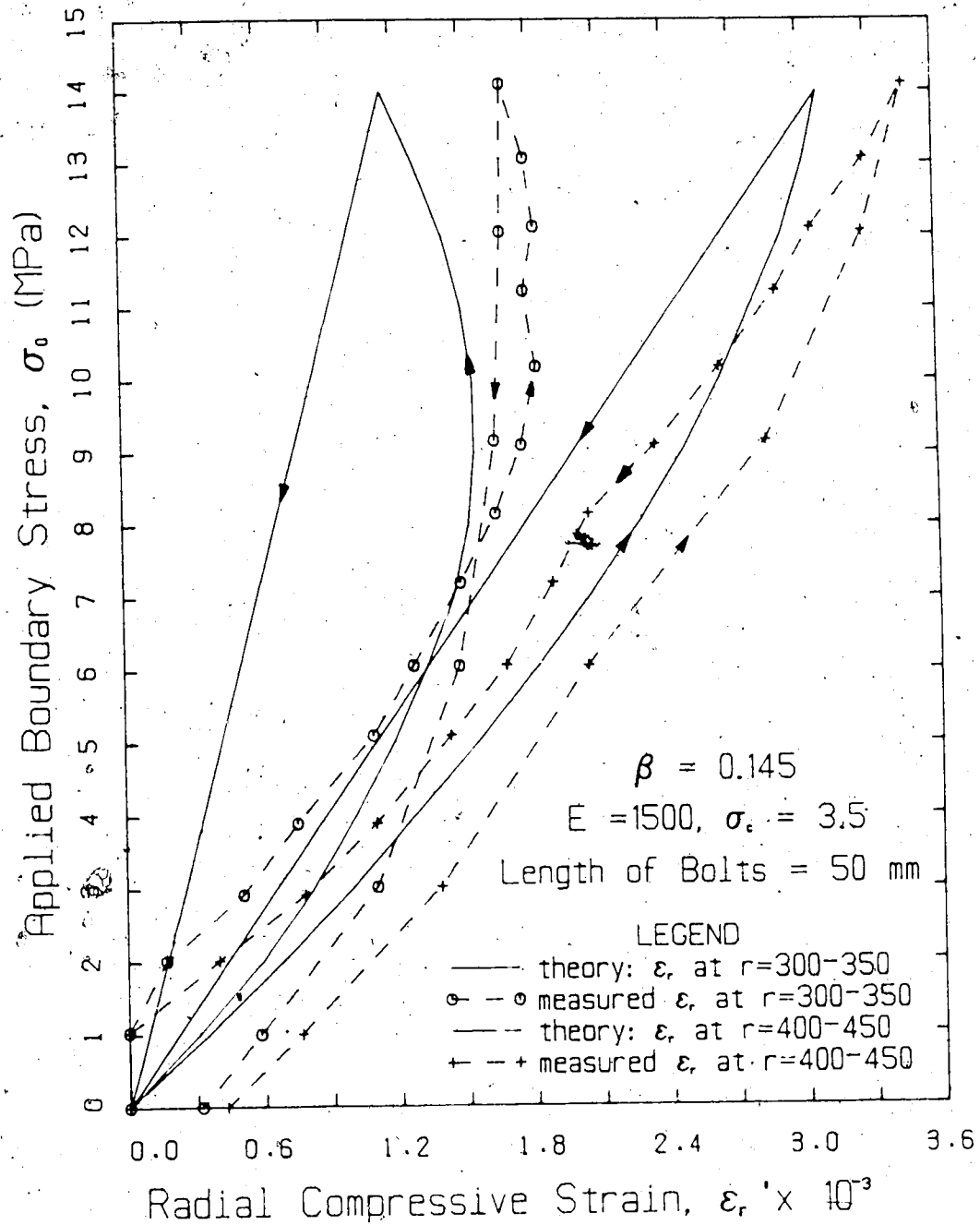


Figure H.4 Radial Strain in Elastic Zone for $\beta=0.145$, $L=50$

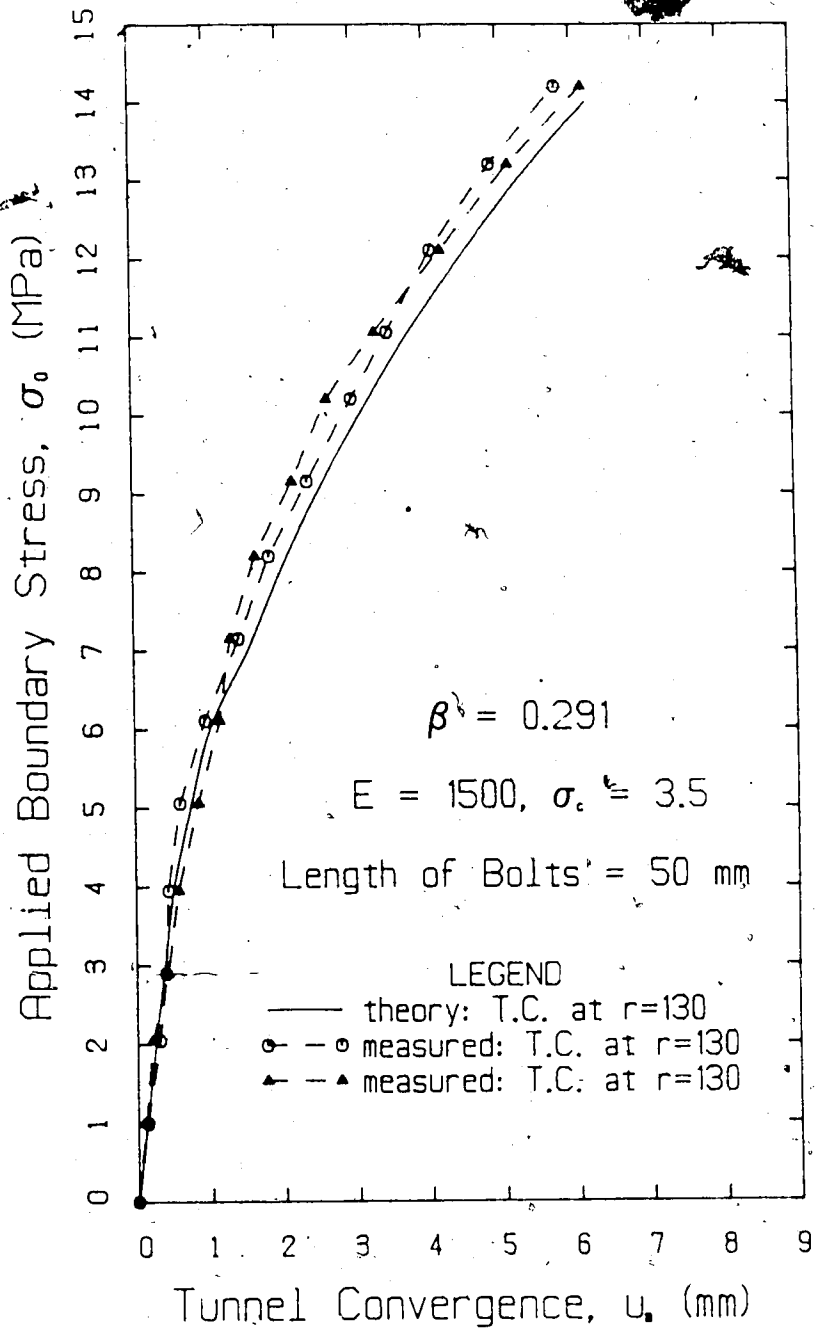


Figure H.5 Convergence of Reinforced Opening for $\beta=0.291$,
L=50

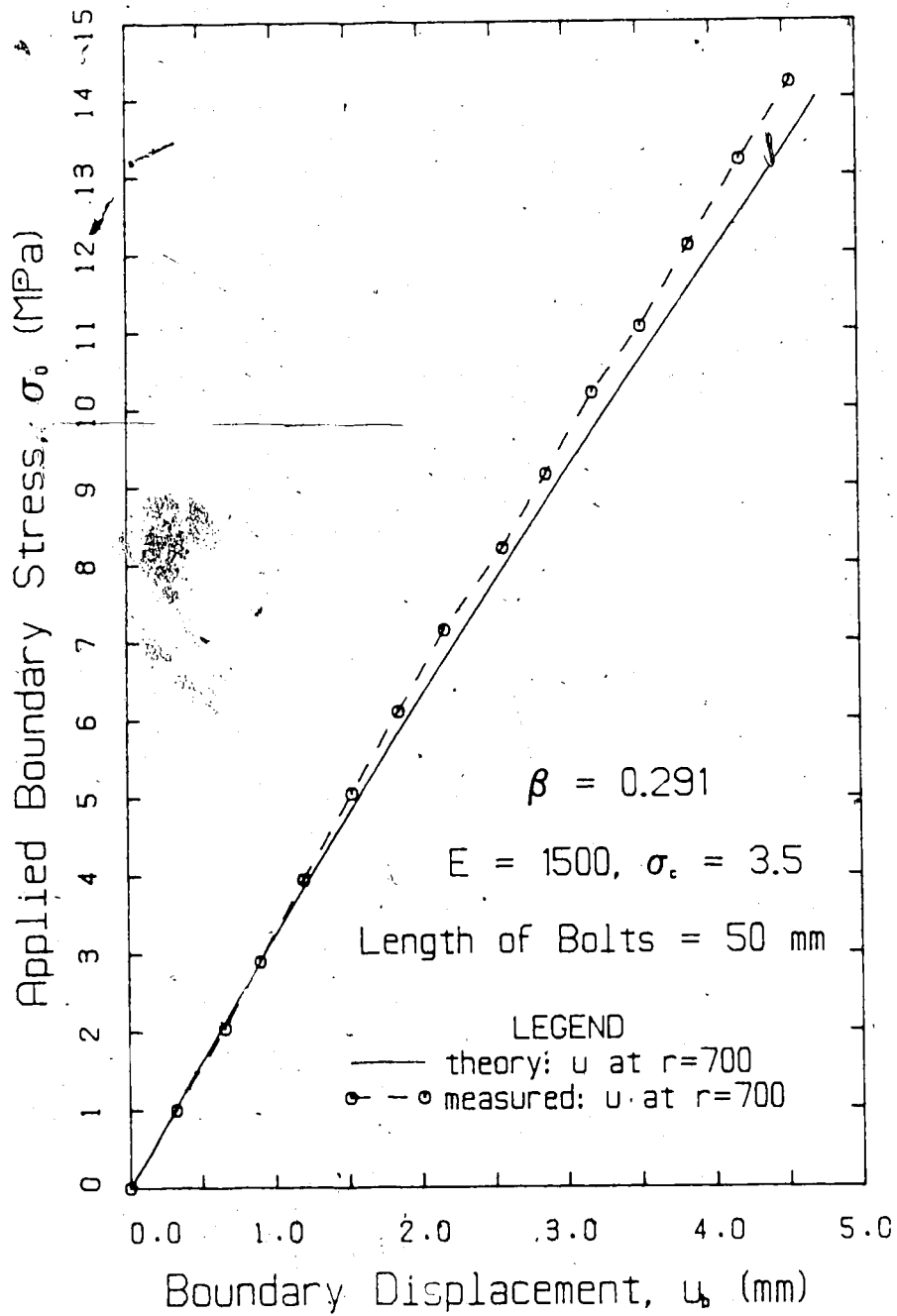


Figure H.6 Field Boundary Displacement for $\beta=0.291$, $L=50$

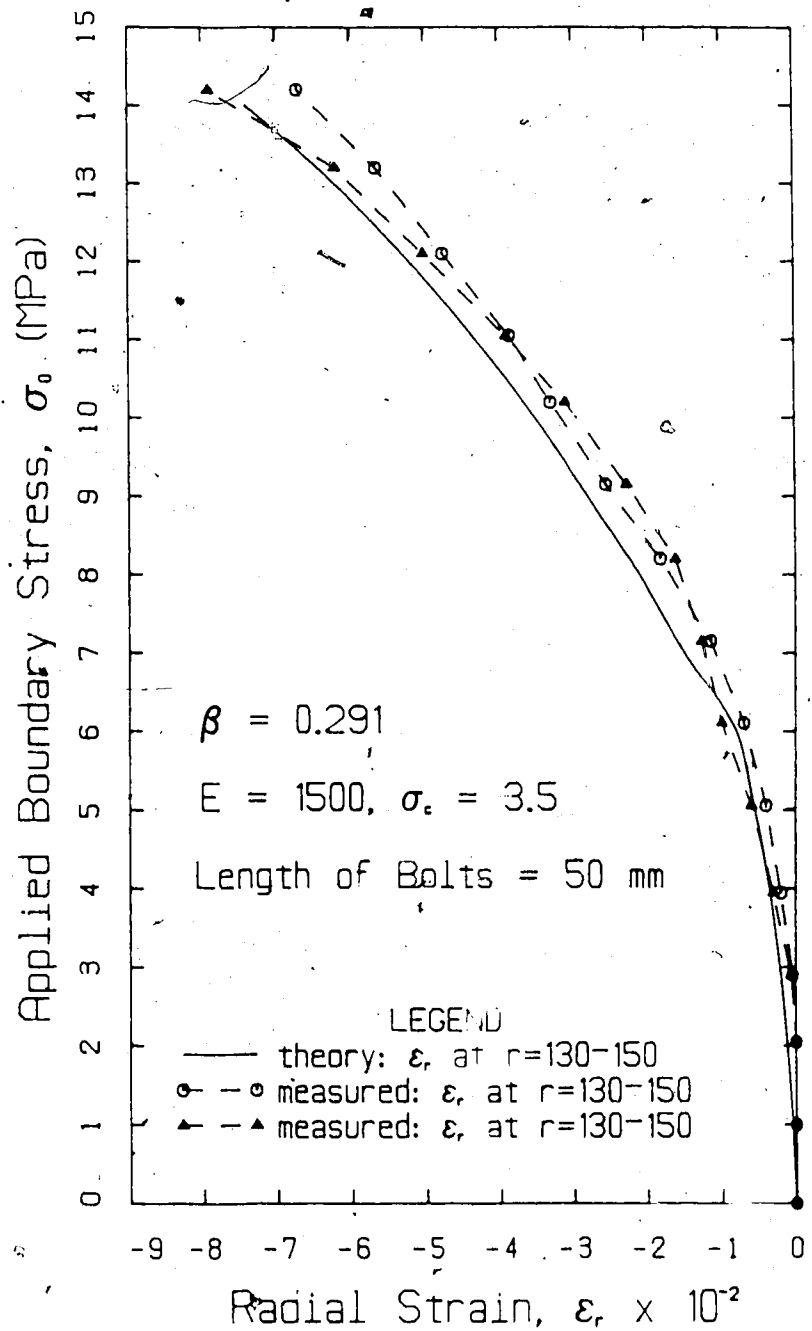


Figure H.7 Radial Strain at Tunnel Wall for $\beta=0.291, L=50$

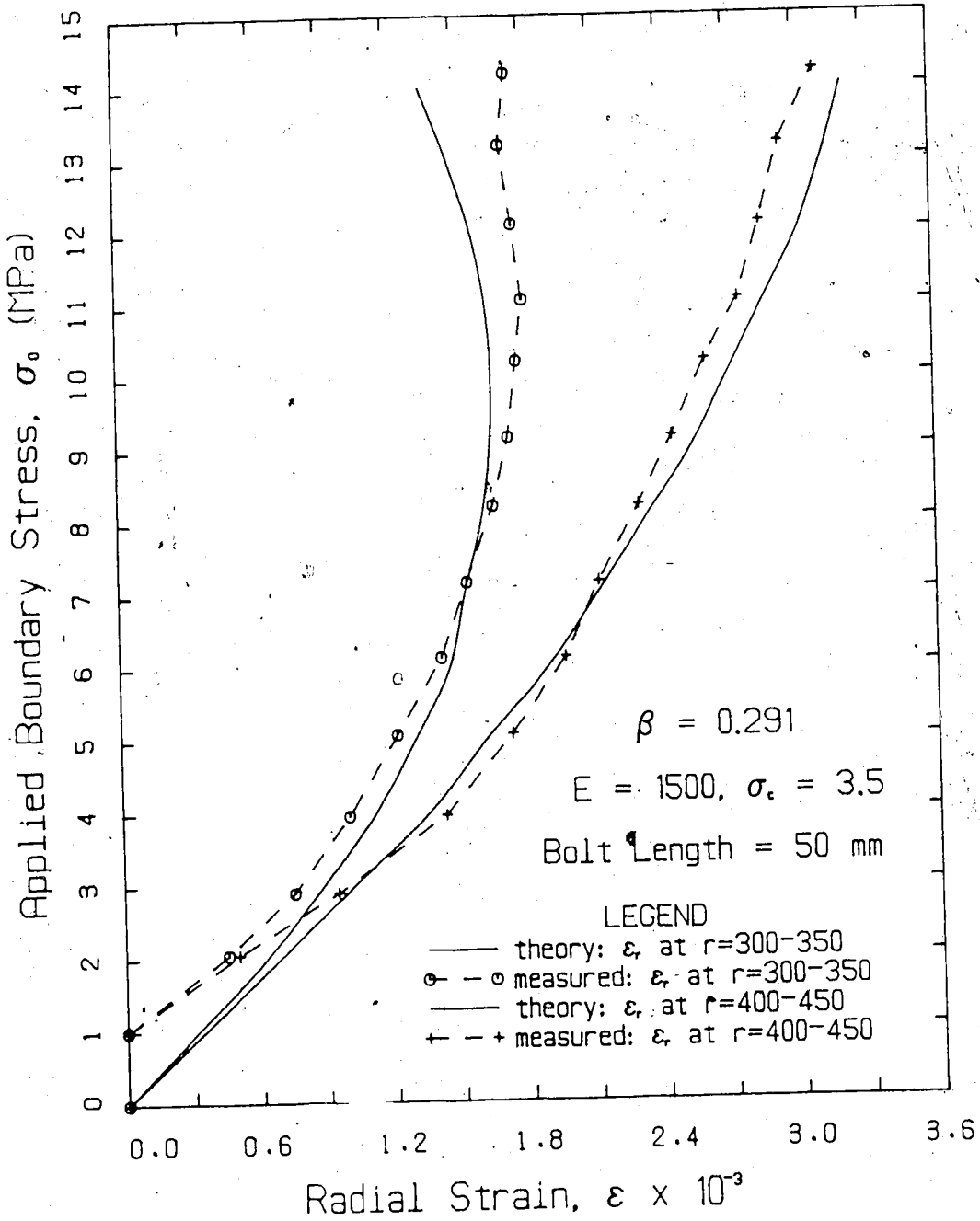


Figure H.8 Radial Strain in Elastic Zone for $\beta=0.291, L=50$

APPENDIX I

BEHAVIOUR OF REINFORCED OPENINGS (LONG BOLTS) IN A JOINTED MEDIUM

In this section, the tunnel convergence, the field boundary displacement and the radial strain response in plastic and elastic zones are presented for jointed samples. The behaviour of the unsupported opening is also presented, followed by the response of three bolt densities, $\beta=0.073$, 0.145 and 0.220. The model opening is reinforced with 100 mm long bolts. A summary of the convergence data has been discussed in Chapter 6. The predicted data was based on the following geotechnical parameters: $E=1400$ MPa, $\nu=0.25$, $\sigma_c=3.3$ to 3.4 MPa, $\phi=27.5^\circ$ to 28° and $a=2.0$.

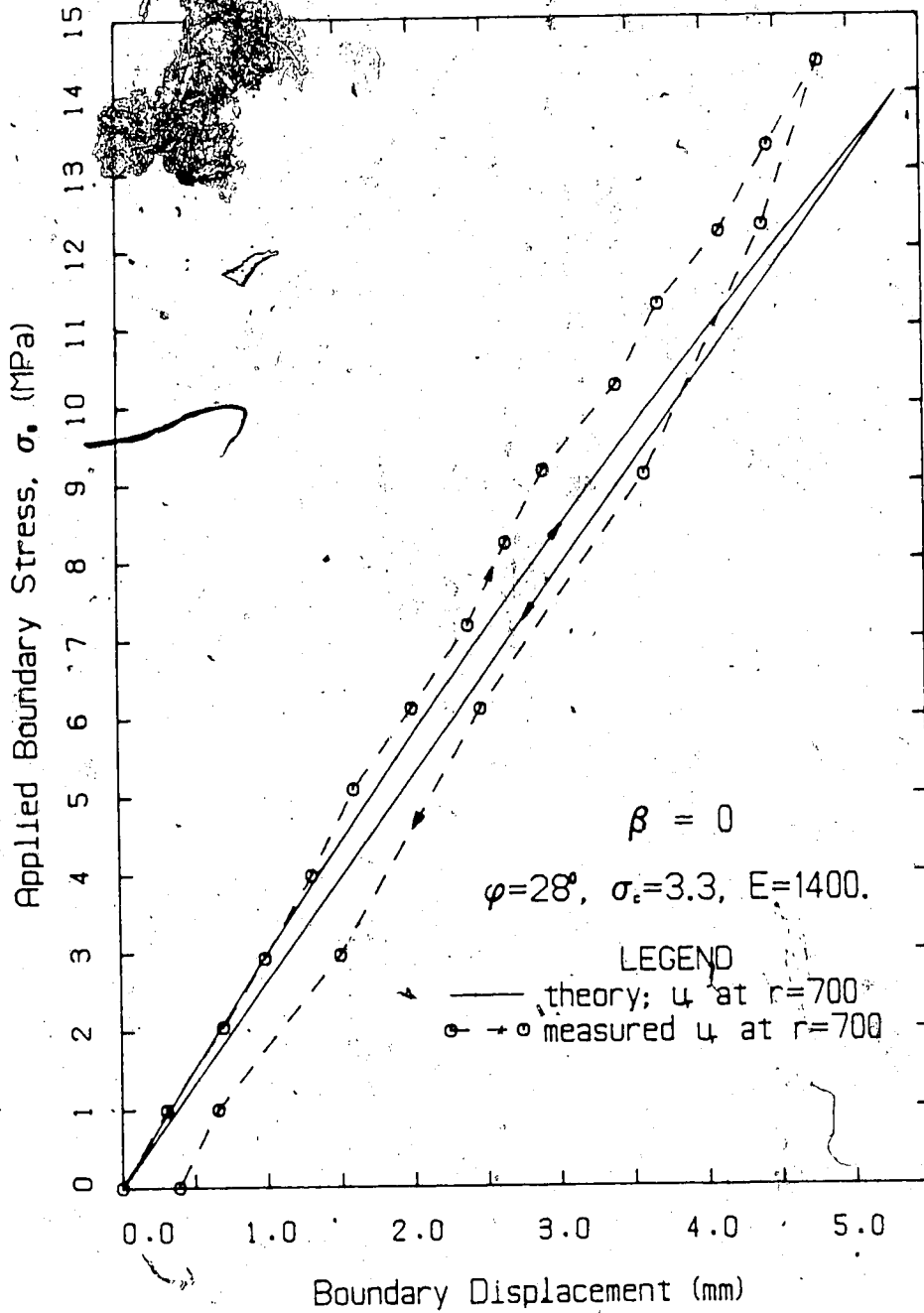


Figure I.1 Field Boundary Displacement (Jointed) for $\beta=0$

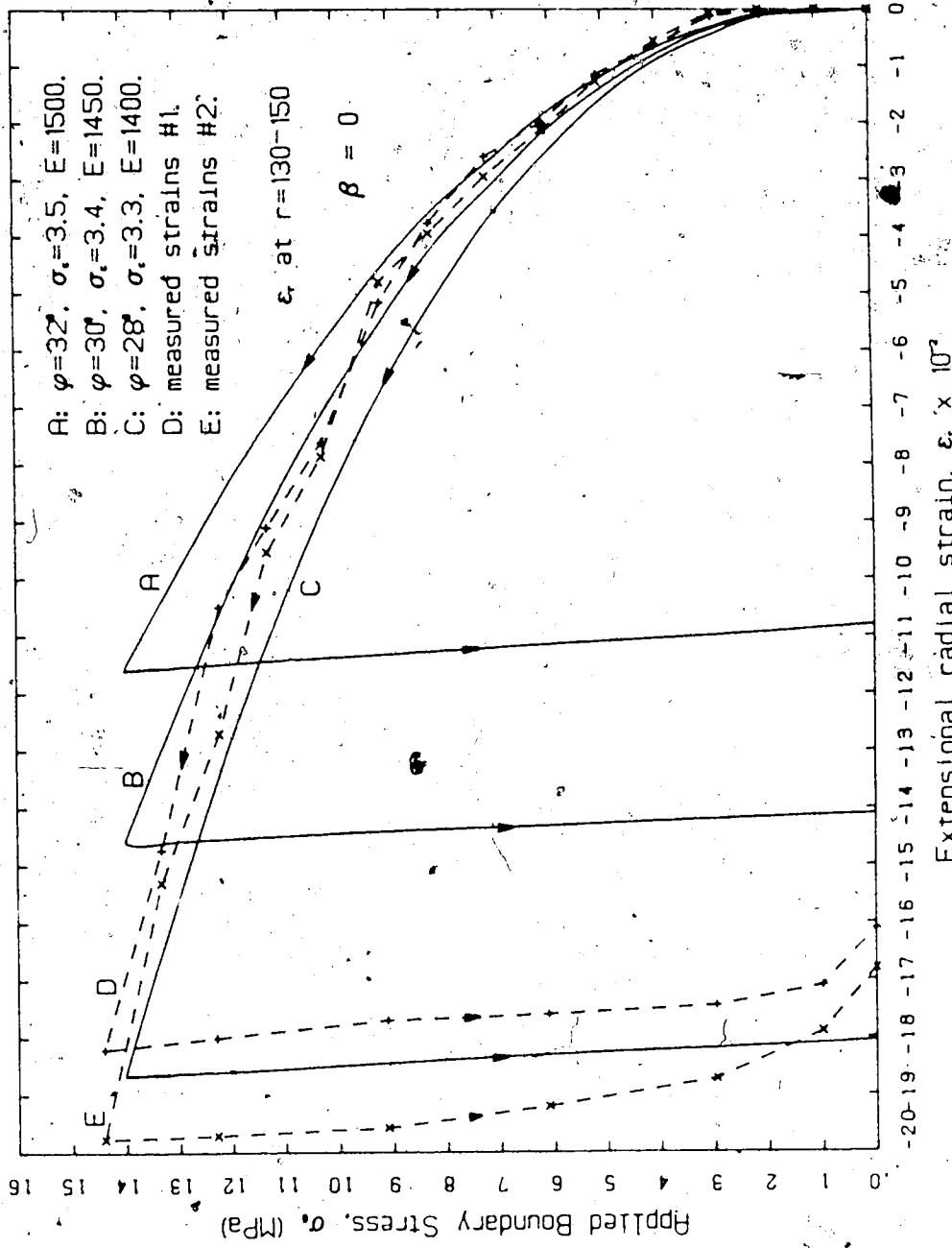


Figure I.2 Radial Strain at Tunnel Wall (Jointed) for $\beta=0$

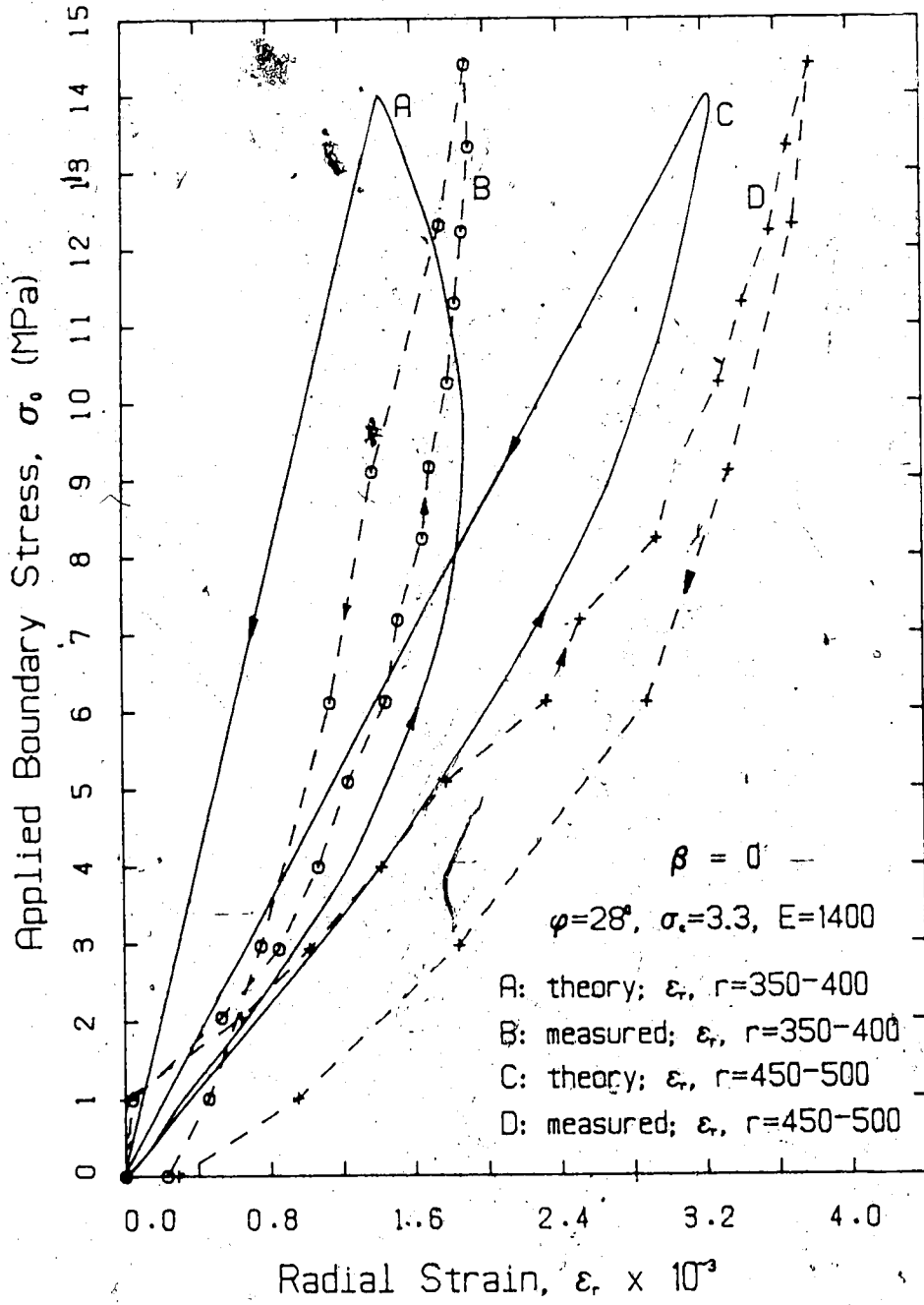


Figure I.3 Radial Strain in Elastic Zone (Jointed) for $\beta=0$

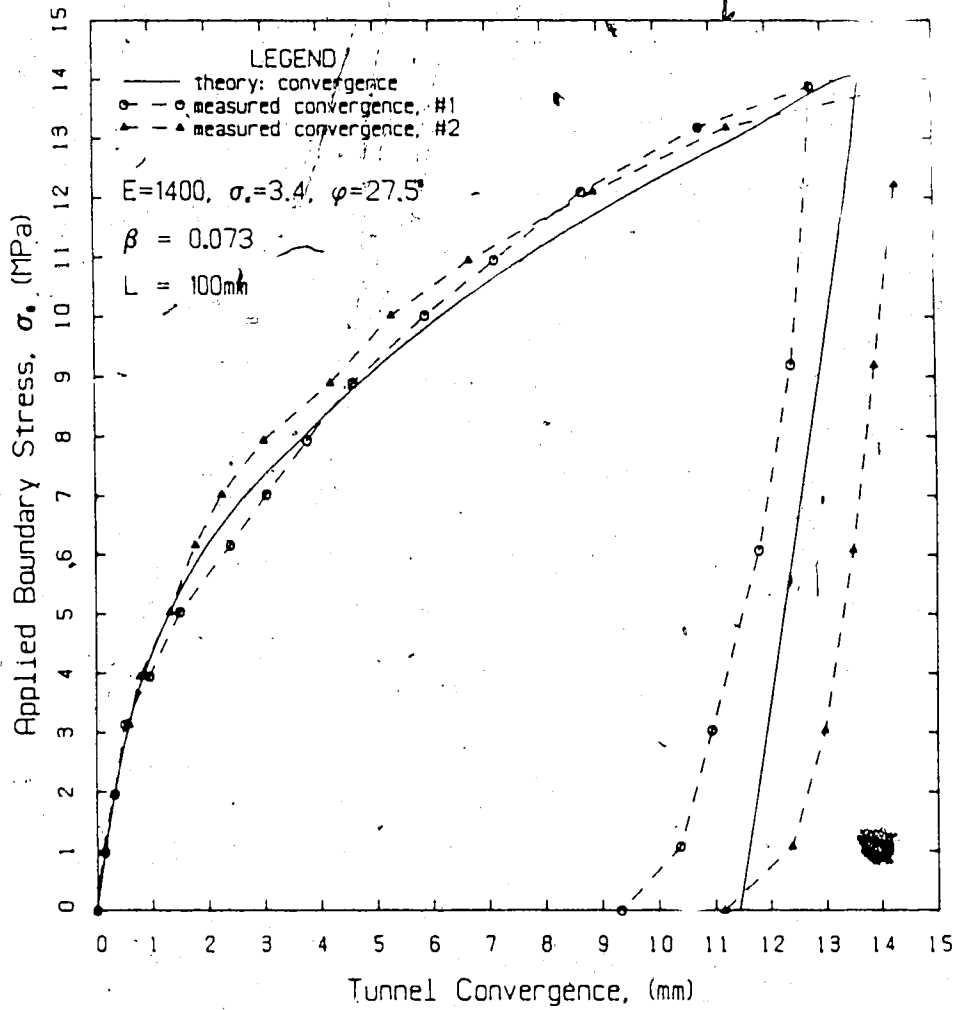


Figure I.4 Convergence of Opening in Jointed Medium for
 $\beta=0.073$, $L=100$

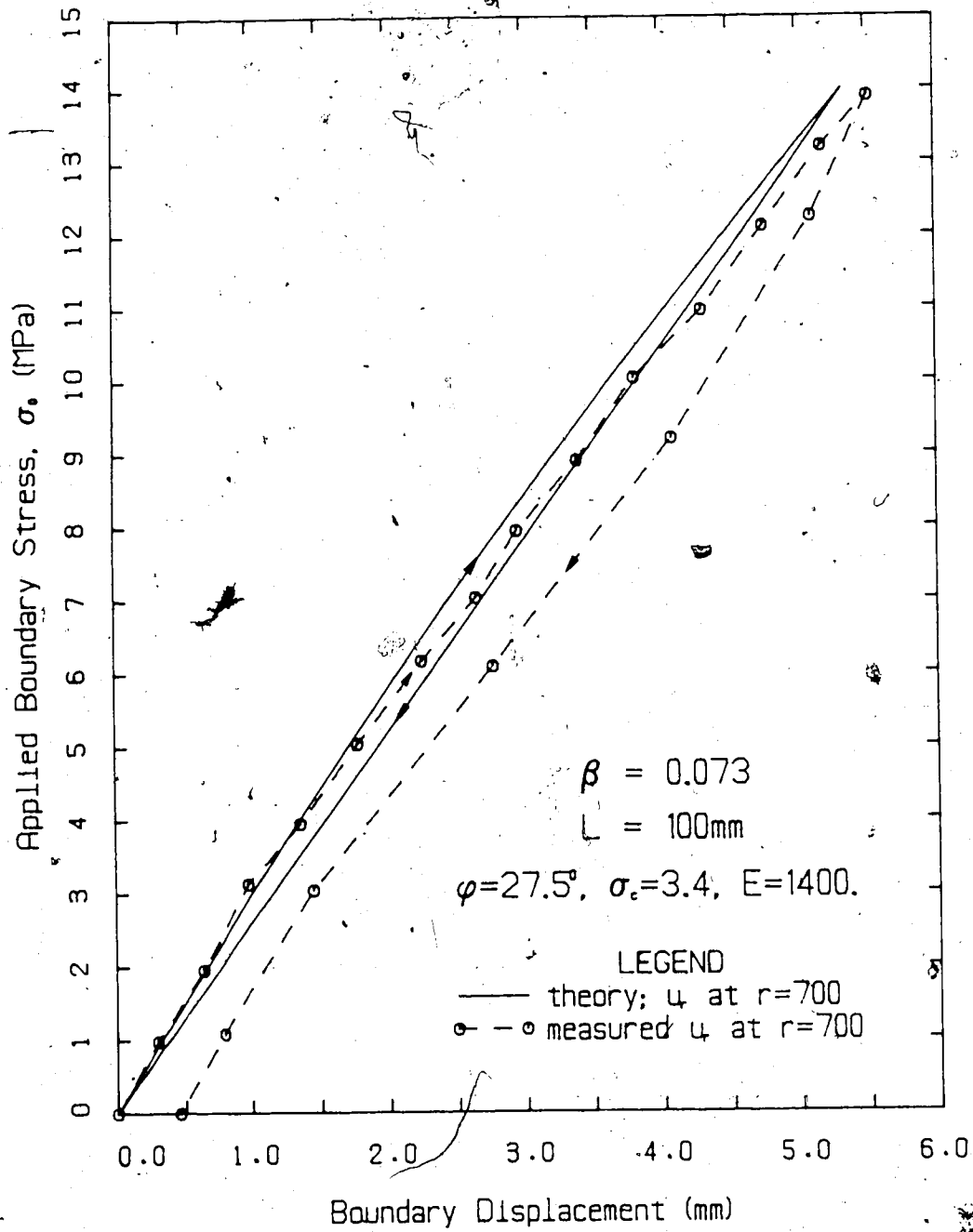


Figure I.5 Field Boundary Displacement (Jointed) for
 $\beta=0.073, L=100$

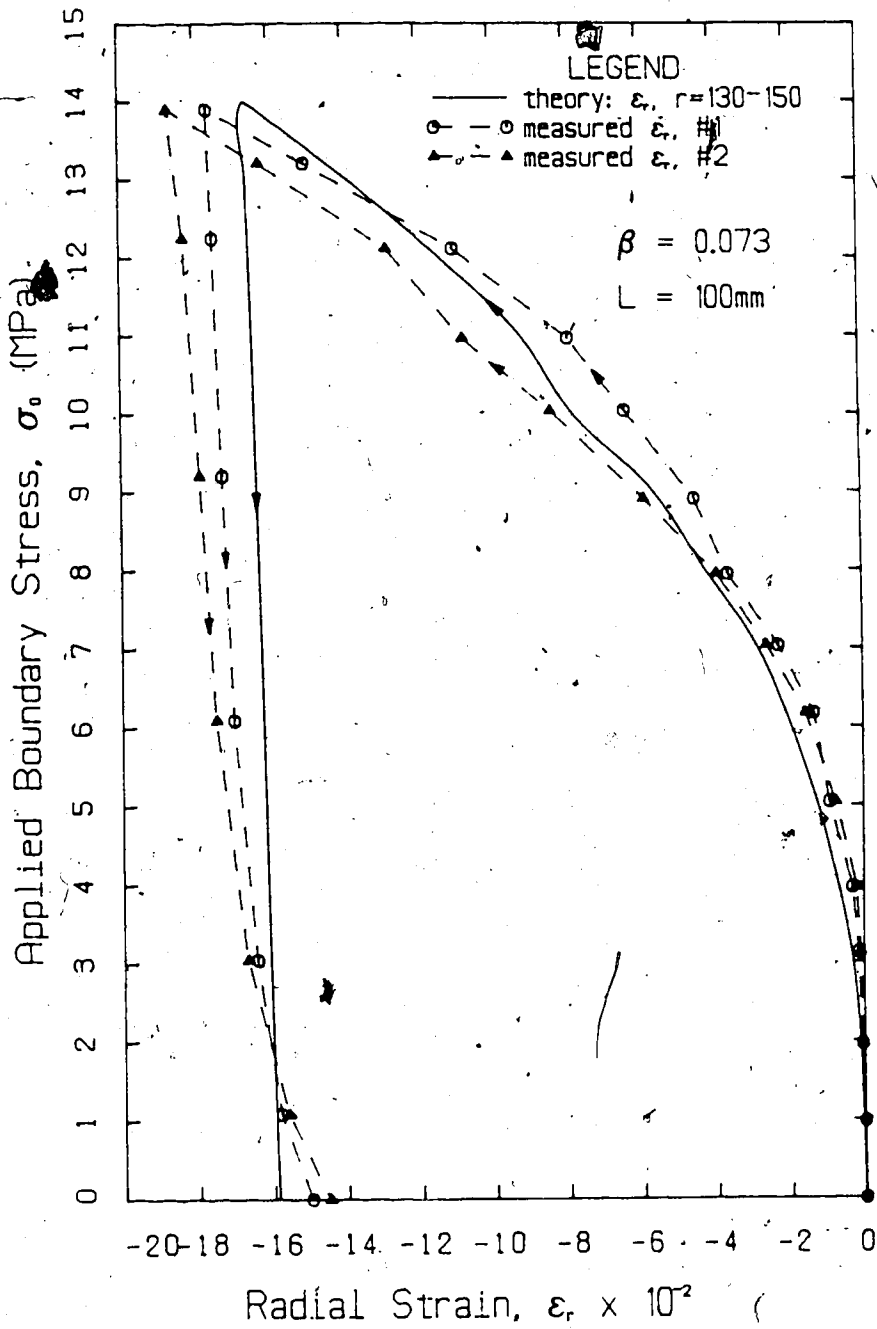


Figure 1.6 Radial Strain at Tunnel Wall (Jointed) for $\beta=0.073$, $L=100$

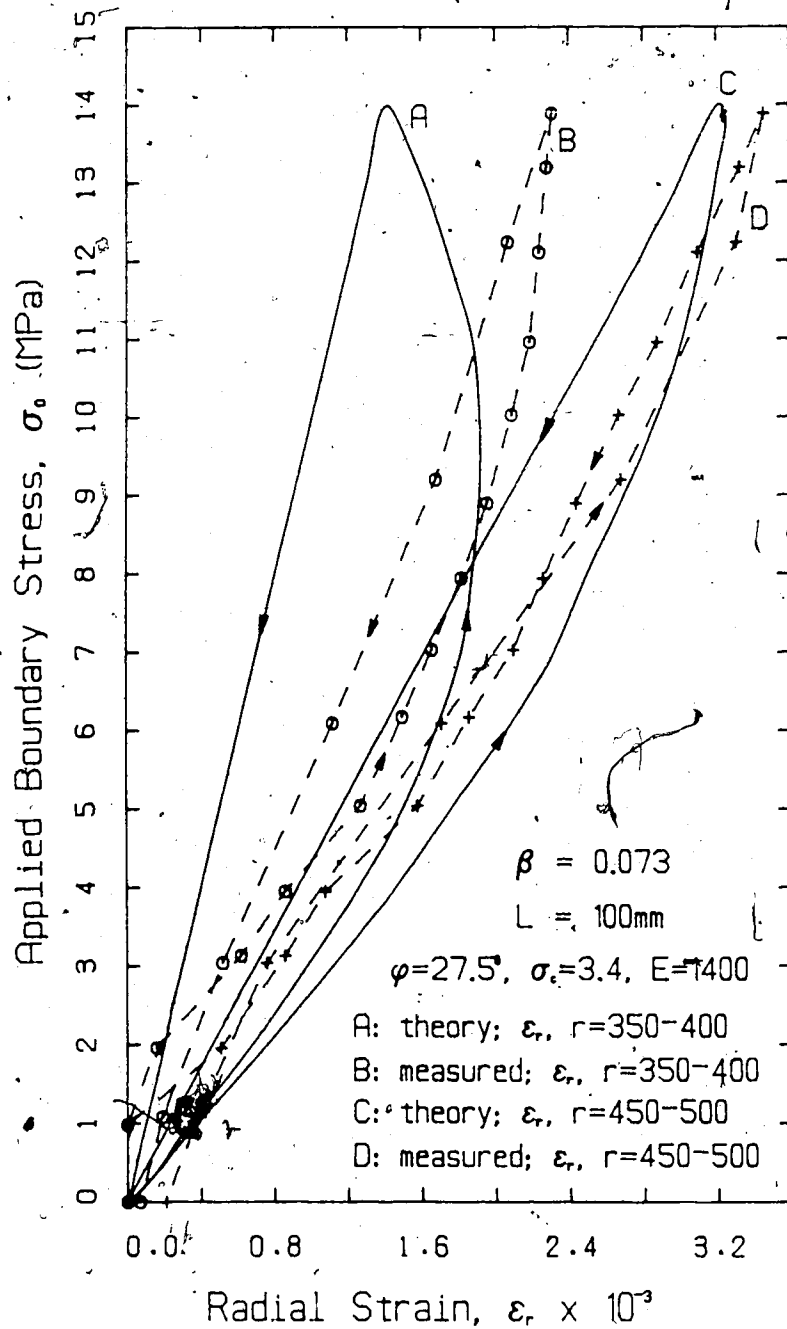


Figure I.7 Radial Strain in Elastic Zone (Jointed) for $\beta = 0.073, L = 100$

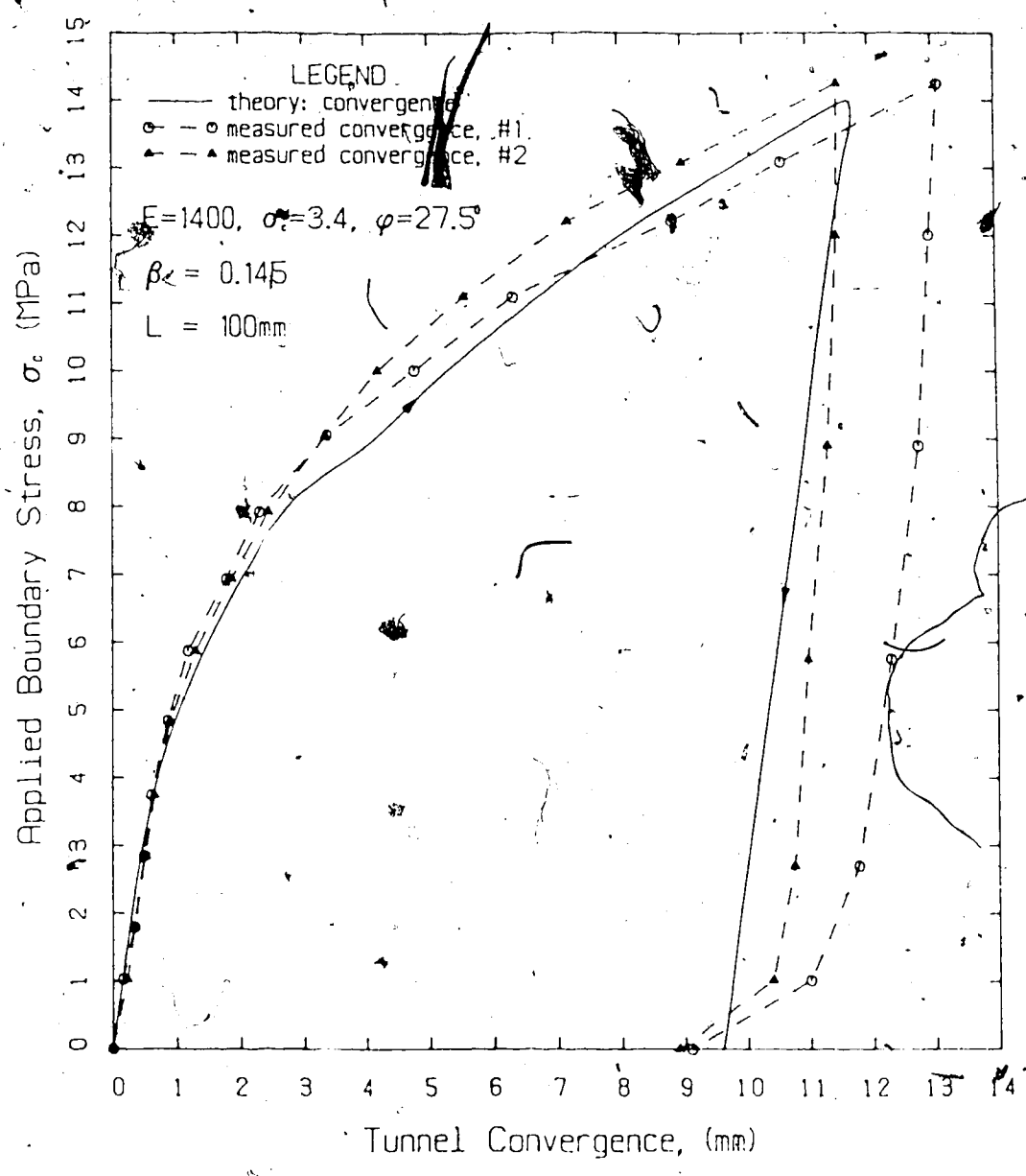


Figure I.8 Convergence of Opening in Jointed Medium for $\beta=0.145$, $L=100$

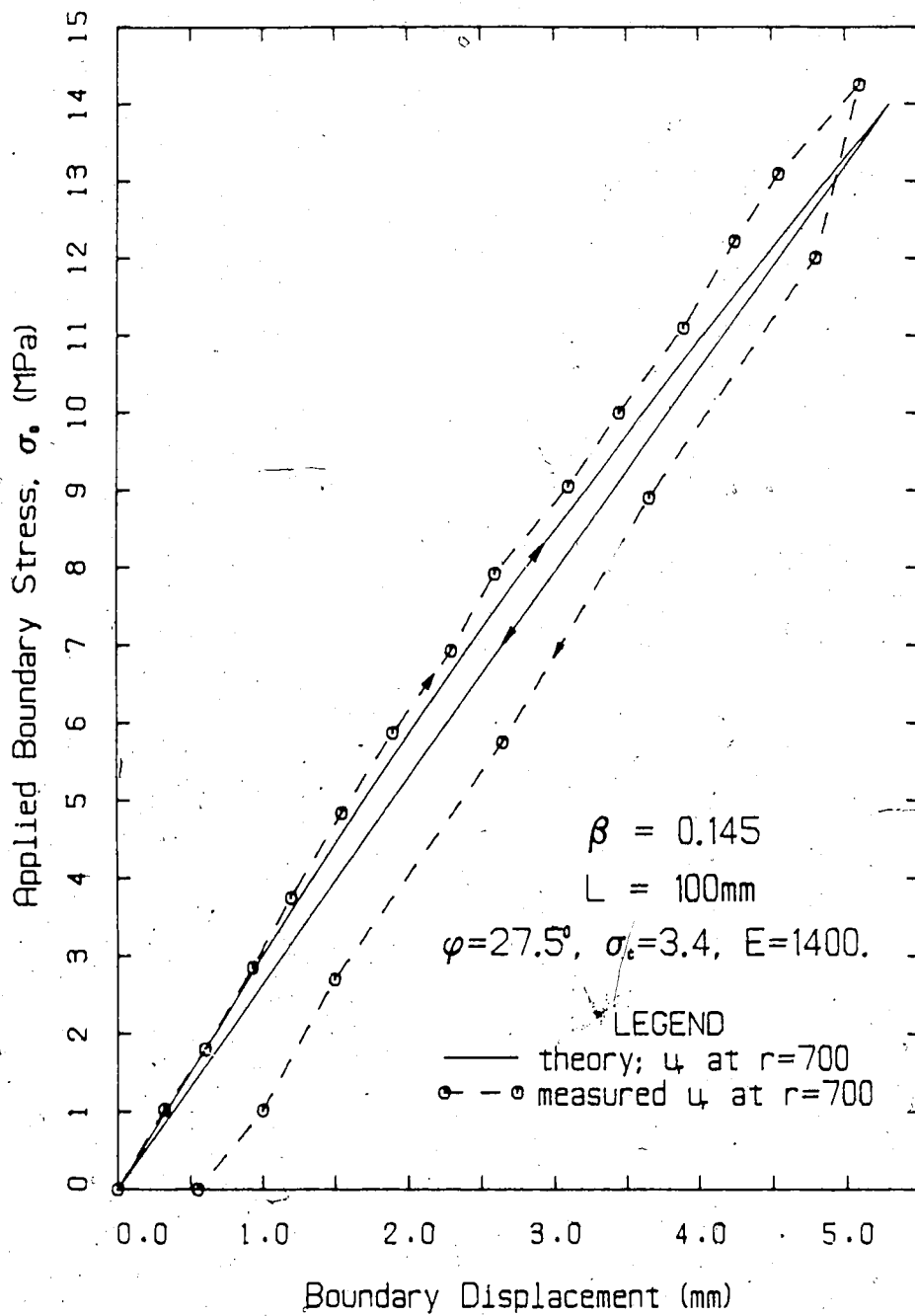


Figure I.9 Field Boundary Displacement (Jointed) for $\beta=0.145, L=100$

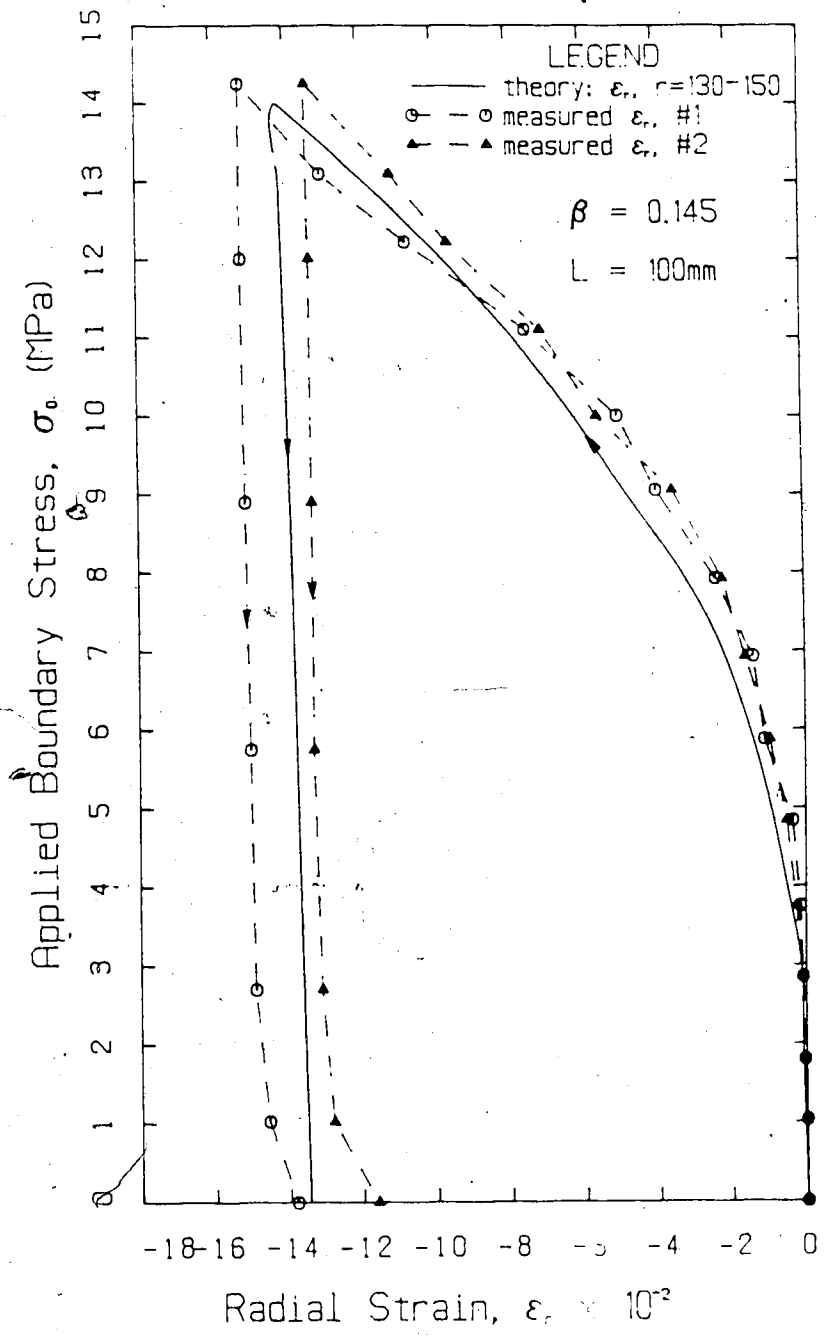


Figure I.10 Radial Strain at Tunnel Wall (Jointed) for $\beta=0.145$, $L=100$

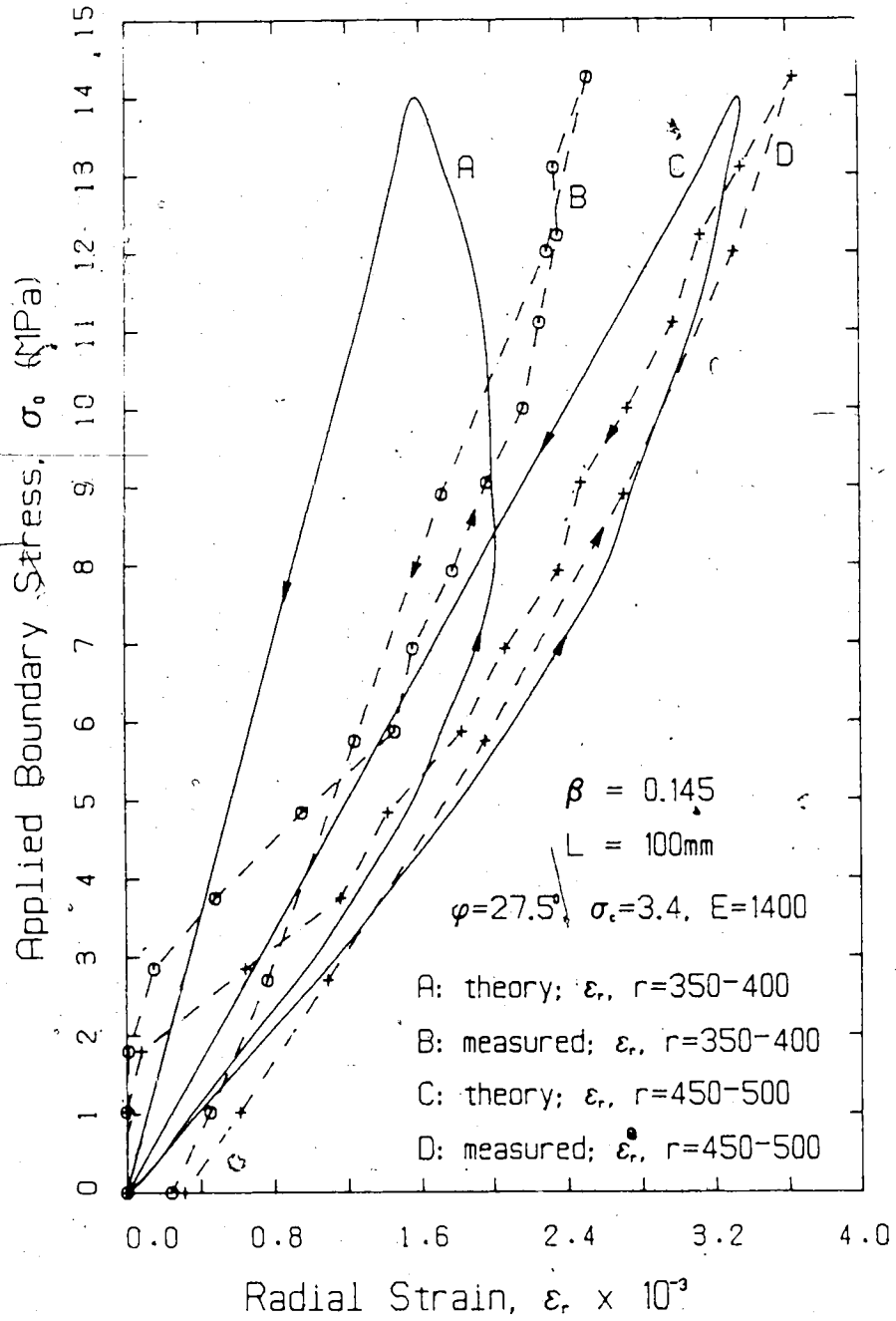


Figure I.11 Radial Strain in Elastic Zone (Jointed) for $\beta=0.145$, $L=100$

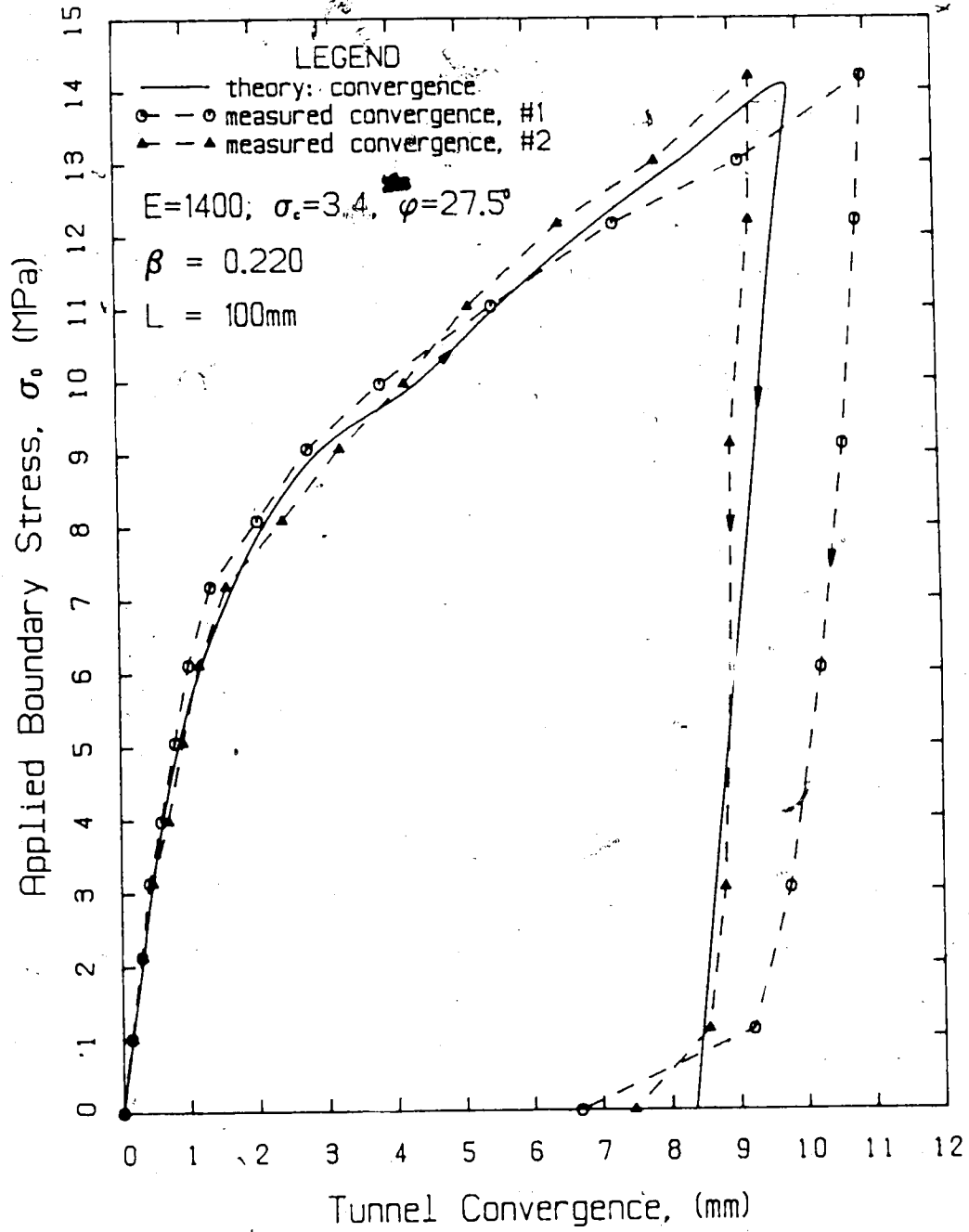


Figure I.12 Convergence of Opening in Jointed Medium for $\beta=0.220$, $L=100$

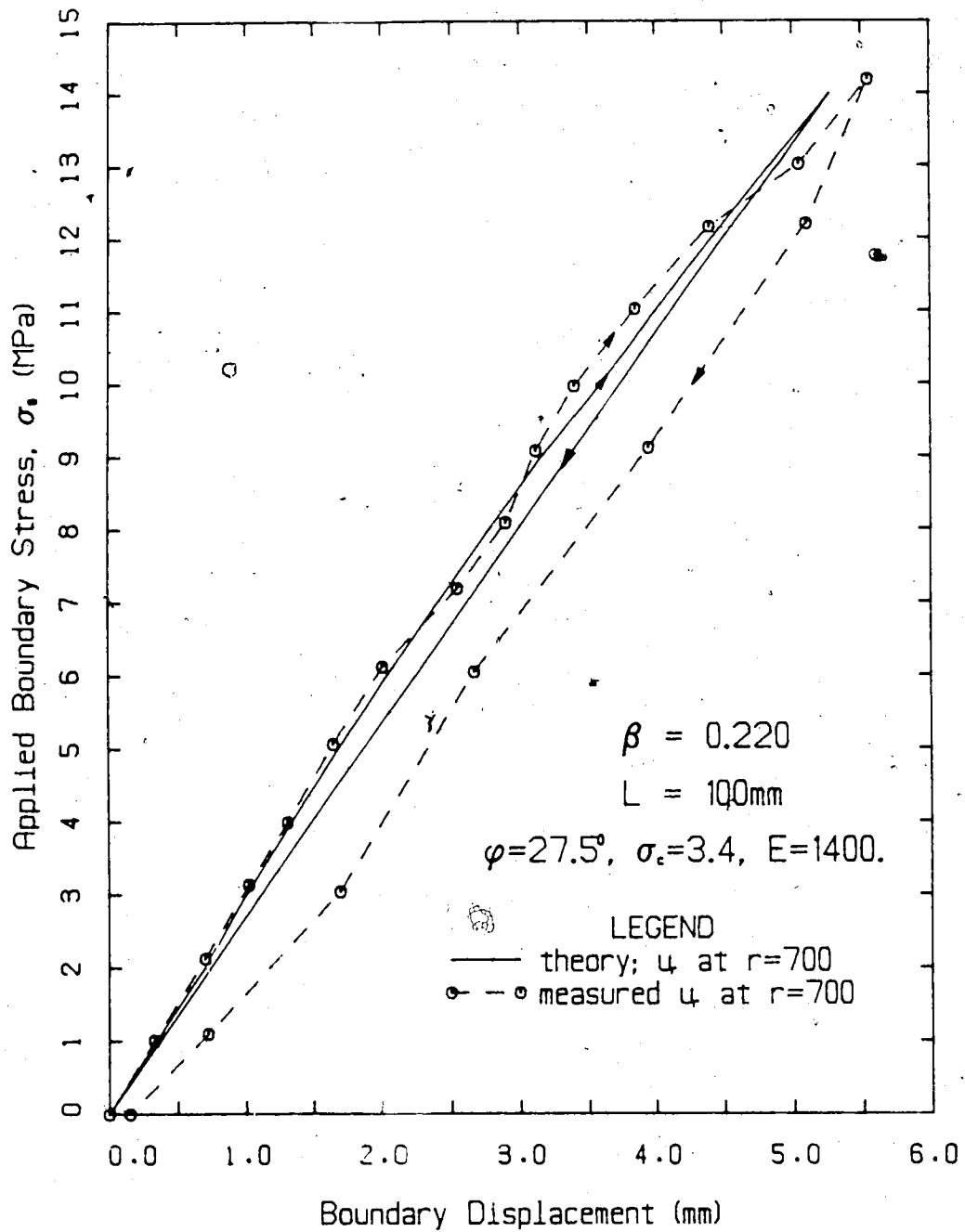


Figure 1.13 Field Boundary Displacement (Jointed) for $\beta=0.220, L=100$

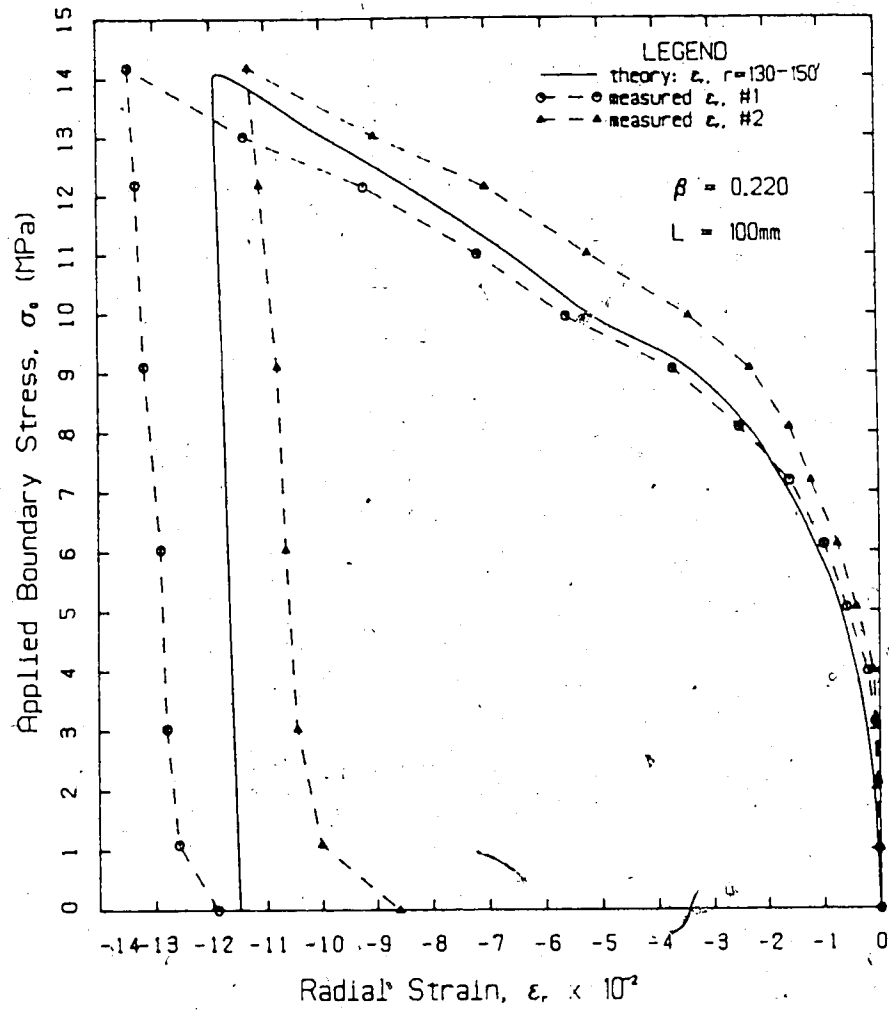


Figure I.14 Radial Strain at Tunnel Wall (Jointed) for $\beta=0.220$, $L=100$

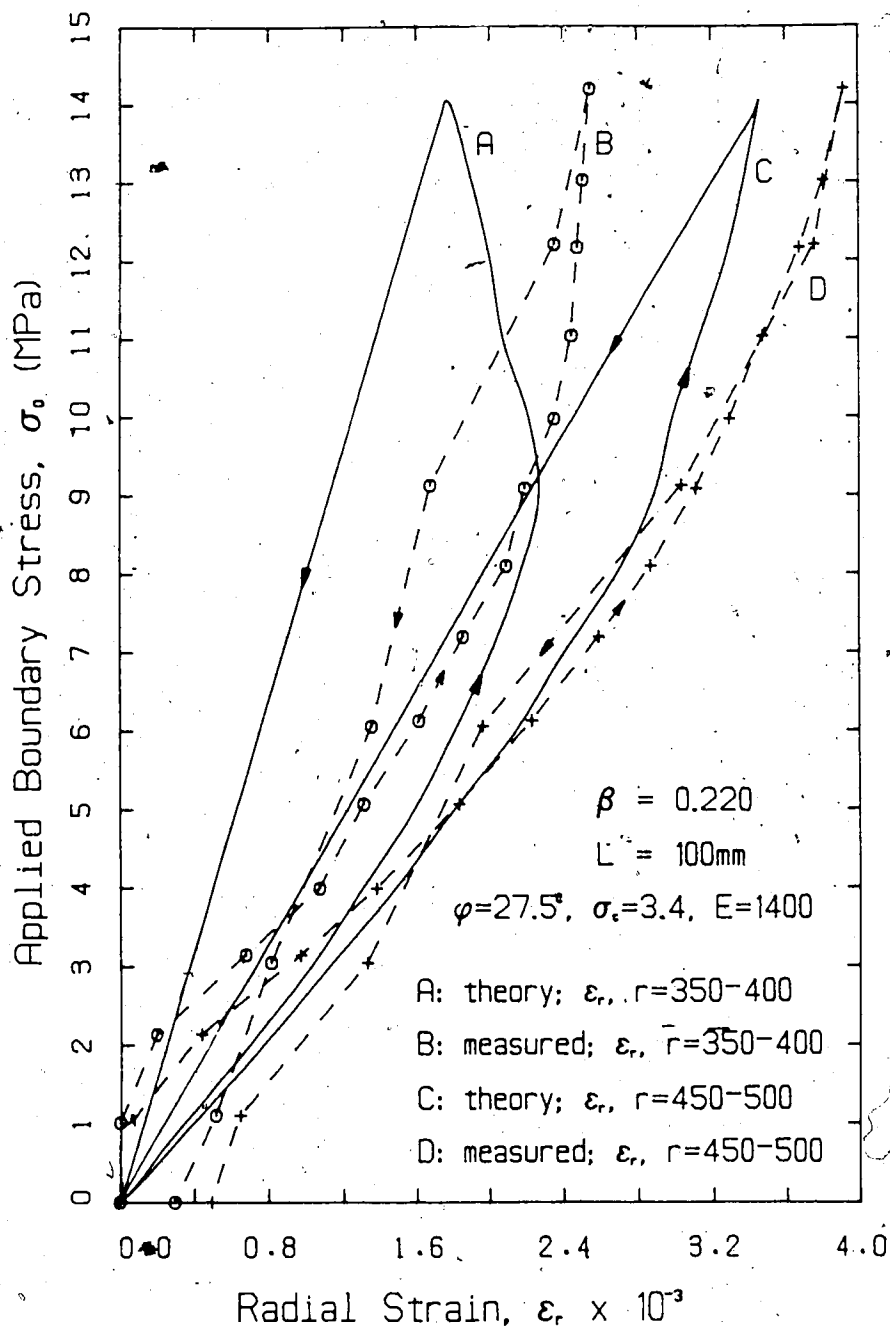


Figure I.15 Radial Strain in Elastic Zone (Jointed) for $\beta=0.220, L=100$